INFORMATION-GEOMETRIC METHOD FOR MULTIPLE NEURONAL SPIKE DATA ANALYSIS

YIMIN NIE
Master of Science, Peking University, 2005

A Thesis
Submitted to the School of Graduate Studies
of the University of Lethbridge
in Partial Fulfilment of the
Requirements for the Degree

DOCTOR OF PHILOSOPHY

Department of Neuroscience
University of Lethbridge
LETHBRIDGE, ALBERTA, CANADA

The University of Lethbridge

Preparation of thesis

Date of Defense: August, 05, 2014

Dr. M. Tatsuno Supervisor	Associate Professor	Ph.D.
Dr. B.L. McNaughton Thesis Examination Committee Member	Professor	Ph.D.
Dr. A. Gruber Thesis Examination Committee Member	Associate Professor	Ph.D.
Dr. D. Euston Internal Examiner	Assistant Professor	Ph.D.
Dr. T. Trappenberg External Examiner Dalhousie University Halifax, Nova Scotia	Professor	Ph.D.

DEDICATION

For my family

Jing and Anna

I would never have done it without your encouragement, support and love

ABSTRACT

This dissertation explores a novel statistical technique—information geometric method for theory and its application in analysis of multiple neuronal spike data. The previous studies have indicated that information-geometric method provides a powerful tool of estimating neuronal interactions from observed spiking data. However, these studies were conducted based on simplified neural network structure, which has limitations in the real brain. We systematically extended the previous studies by using intensive mathematical analysis and numerical simulations of realistic and complex neural network. The studies show that information geometric approach provide robust estimation for the sum of the connection weights between neuronal pairs in a complex recurrent network, providing a way of investigating the underlying network structures from neuronal spike data.

ACKOWLEDGEMENTS

First and foremost, I would like to thank my thesis advisor, Dr. Masami Tatsuno, who first introduced me to the fascinating area of computational neuroscience and statistical analysis for big data. I owe a lot to him. It has been an honor to be his first Ph.D. student. I am impressed by his deep knowledge and gracious personality. Dr. Tatsuno taught me how to do research and present multiple ideas, how to understand what the most important question is, how to expand the existing ideas, and how to write publications in convincing ways to general audiences. He also taught me how to organize massive scientific findings, which I found is extremely useful in my future career. He is a good teacher and a good friend. While working with him, he was always ready to discuss and answer questions with great enthusiasm, regardless they are deep or naïve, academic or non-academic. Without his patient instruction, it is impossible for me to complete this thesis with highly qualified publications. Dr. Tatsuno is more than just an academic advisor to me; he also taught me how to be a good speaker, a good listener, even a good person in my life.

I also would like to thank Dr. Bruce McNaughton, who leads the Polaris group at the department of neuroscience. His outstanding research facility provided me unique research environment in cluster computing, modeling and data analysis. I thank Dr. Artur Luczak, who provided me many opportunities for teaching assistant in programming and data analysis. I greatly benefited a lot from the collaboration with his excellent MATLAB programming and statistical analysis class.

For this dissertation I would like to thank my thesis defense committee members: Dr. Masami Tatsuno, Dr. Bruce McNaughton, Dr. Aaron Gruber, Dr. David Euston, and Dr. Thomas Trappenberg, for their precious time and insightful suggestions.

I sincerely thank my lab members and other collaborators, both inside the University of Lethbridge and out, for invaluable advice and ideas for my studies: Dr. Michael Eckert, Dr. Hendrik Steenland, Dr. Moritz Franosch, Vivek Trivedi, Ryan Rota, Karim Ali, LeAnna Kelvi, Paxman Eric, Klay Kurtz. I specially thank our secretaries: Mrs. Mauthe-Kaddoura, Amanda and Mrs. Naomi Cramer for every kind help and assistance for my research study. All of them made me feel at home. Whenever I had troubles, they were always willing to give me a hand.

Finally, my infinite thanks to my family for all their love and encouragement. Thanks for all of my loving, supportive, encouraging, and patient wife Jing and daughter Anna. Thanks my parents who raised me with love and support me in all my pursuits. Thank you!

Yimin Nie
The University of Lethbridge
August, 2014

Table of Contents

LIST OF FIGURES

Chapter 1 General overview: multiple spike data analysis

1.1 General introduction

The brain consists of billions of neurons, one of the elementary units for information processing. The brain cortex is a highly complex network that receives signals from thousands of neurons and projects their synapses to thousands of other neurons crossing multiple cortical regions. The neurons in the brain communicate each other in a highly parallel manner by emitting neuronal spikes. Over the past decades, electrophysiological recording techniques have been applied in order to observe the neuronal spiking activities in the brain from in *vitro* and in *vivo* experiments (Buzsaki, 2004; Chapin, et al., 1999; Davidson, et al., 2009; Dragoi and Tonegawa; Dragoi and Tonegawa, 2013; Euston, et al., 2007; Hoffman and McNaughton, 2002; Kudrimoti, et al., 1999; Laubach, et al., 2000; Peyrache, et al., 2009; Tatsuno, et al., 2006; Wilson and McNaughton, 1993). Among these recording techniques, intracellular recordings were employed to record the membrane potentials of individual neurons, extracellular recordings were used to record signals from one or more neurons. In recent years, EEG, MEG, or fMRI and other brain image methods (e.g. Ca^{2+} image, two-photon image) are widely applied to record brain activities from larger brain regions (Courchesne, 1975; Daw, 2005; Daw, 2011; Denk, 1990; Knutson, 2005; Meltzer J, 2008; Strobel, 2008). All these recording techniques reflect that assemble dynamics of neuronal interactions and the mechanisms of neural information processing play an important role in understanding how the brain processes complicated information.

One rudimentary way of investigating the neuronal interactions is to simultaneously record multi-neuronal firing activity from freely behaving animals using multiple electrodes, and analyze the correlations between individual recorded neurons (Buzsaki, 2004; Chapin, et al., 1999; Davidson, et al., 2009; Dragoi and Tonegawa; Dragoi and Tonegawa, 2013; Euston, et al., 2007; Hoffman and McNaughton, 2002; Kudrimoti, et al., 1999; Laubach, et al., 2000; Peyrache, et al., 2009; Tatsuno, et al., 2006; Wilson and McNaughton, 1993). Multiple electrode recording techniques make it possible to study the simultaneous neuron activity in a given or across different brain regions. Meanwhile, the neuronal data from multi-electrode studies present important analysis challenges which must be solved for optimal use of these neurophysiological measures, and answer the key questions of how the brain processes spatial-temporal sensory information. To this end, one can investigate the possible relationship between the external input stimulus and the individual or assemble responses from neurons in corresponding cortical regions. The stimulus can be physical in nature, such as light used to stimulate retinal or lateral geniculate neurons, or sound used to stimulate the auditory cortex, or the odor used to stimulate the olfactory cortex. It can also be abstract or cognitive, such as the random moving dots discrimination for decision making in prefrontal cortex (Wang, 2008). All these stimuli are represented in active brain as nonstationary and irregularly fired spiking patterns. Its considerable variability across the multiple tasks and the complex interplay of multiple time scales requires advanced statistical theories and methods to handle the drastically growing neural spike data.

In electrophysiology, spike sorting is an important step prior to spike data analysis. Individual spikes are not directly recorded, because the electrical voltage potential

recorded from any implanted electrodes represent the simultaneous activity from multiple neurons near the electrodes. One needs to identify the spike events for each neuron as well as the numbers of recorded neurons from these voltage traces. Therefore, prior to spike data analysis, spike sorting is the critical first step. It turns out that the accuracy of the spike sorting critically affects the accuracy of subsequent analysis (Harris, 2000). There are many algorithms used for spike sorting, and different algorithms applied to the same data set can yield different results. In present, there is no consensus as to which algorithms are the best. In reality, the model-based parametric algorithms are violated by the real clusters of voltage traces, which change over time as neuronal properties and experimental conditions evolve. A Monte-Carlo-based strategy has been proposed to identify the numbers of neurons in one voltage trace, but it has not been widely used (Nguyen, 2003). In addition, dual intracellular-extracellular recording studies have shown that spike sorting for large number of neurons has a non-zero error rate, because the probability distribution of spike shapes from different neurons share some degree of overlap (Harris, 2000). All these factors illustrate the many complexities of the spike train analysis. To overcome these problems in practice, one needs to develop and combine different machine learning algorithms such as feature analysis, Bayes methods (Bayesian clustering and classification), principle component analysis (PCA), independent component analysis (ICA). The detailed discussions for these spike sorting algorithms are beyond the scope of the present thesis. In the following, we review the main-stream methods for multiple neural data analysis based on sorted data.

This chapter is organized as follows. In section 1.2, we introduce the major approaches for multiple neuronal spike analysis in the level of neuronal interactions. We discuss the

methods which quantify single neuronal firing rate, pairwise correlations, higher-order neuronal interactions, and population coding based on information theory. Our aim is to discuss the advantage and disadvantage of these existing methods in practical neural data analysis. In section 1.3, we introduce the main work in the present thesis: information-geometric (IG) method. By presenting its solid mathematical basis and applications to spike data, we show that IG methods provide robust information for neuronal interactions from single neuronal firing rate to higher-order neuronal interactions in a hierarchical manner.

1.2 Neuronal spike data analysis: state-of-the-art

Solid data analysis is fundamental for the meaningful evaluation and reliable interpretation of experiments. Although the technologies of spike train analysis have been developed in the past decades (Abeles and Gerstein, 1988; Aertsen, et al., 1989; Amari, 2009; Brown, et al., 2004; Czanner, et al., 2005; Fellous, et al., 2004; Gerstein and Perkel, 1969; Gilestro, et al., 2009; Grun, et al., 2002; Grun, et al., 2002; Lopes-dos-Santos, et al., 2011; Panzeri and Schultz, 2001; Peyrache, et al., 2009; Shimazaki and Shinomoto, 2007; Shimokawa and Shinomoto, 2009; Zhang et al., 1998), they only recently gain the attention among electro-physiologists. In this section, we introduce several analytical approaches that are often used in neuroscience community and elucidate some aspect of brain function on the level of individual neurons and their interactions.

In section 1.2.1, we first give an overview for the methods of estimating single neuronal firing rate which becomes a well-defined statistical procedure. In section 1.2.2, we

concentrate on the pairwise correlation techniques of spike trains in time and frequency domain, and discuss their advantage and limitations. Section 1.2.3 discusses the higher-order neuronal interactions. We discuss the method to quantify the cumulant correlations as natural and intuitive higher-order generalization of the covariance, and the unitary event analysis for coincidence detection and evaluation. In section 1.2.4, we aim to introduce population-based analysis and information entropy methods for encoding and decoding of neuronal populations. Shannon information entropy and maximal entropy method will be discussed.

1.2.1 Analysis of single neuronal spike trains

In the experiments of living animals, neuron responses may vary considerably from trial to trial in temporal and spatial scales. Understanding the nature and origin of neural variability at the level of single neuronal firing is fundamental to our understanding of how the brain processes reliable information. The starting point to measure the variability of single neuron spike train is the interspike intervals (ISI) variability with the coefficient of variation (CV) and the trial-by-trial count variability with Fano Factor (FF), including the measure of the estimation bias within limited time window of observations, the measurement of rate-modulated spike trains, and the time-resolved analysis of variability dynamics.

In practice, we obtain independent measurements of action potentials during repeated experimental trails. We consider the empirical observation of a series of spike events within a finite time interval (a, b). Suppose that the spikes within this interval are marked

as $a < t_1 < t_2 < \cdots < t_i < \cdots < b$. The ISI *X* is defined as the time difference between two subsequent spike time ($X_i = t_{i+1} - t_i$) in each trial (Fig 1.1 A). The *CV* for a set of ISI generated by repeated experiments are typically defined as the standard deviation of interval lengths divided by the mean interval length: $CV = SD(X)/E(X)$, where $SD(X)$ is the standard deviation of ISI and $E(X)$ is the mean of ISI over the trials. Under the assumption that the neuronal firing is stationary, one can first compute the individual CV_j for each trail *j* individually, and then calculate the mean $CV = E(CV_j)$ across all trials.

The *CV* measures the dispersion of the spike interval distribution. It quantifies the irregularity of spike trains and allows us to describe the stochastic nature of the observed spike trains. The *CV* measure, however, has some limitations in practice. First, due to the finite length of the observation window, one cannot sample the full interval distribution, which introduces a bias of estimation of *CV*. Second, the *CV* is a useful measure only if the spike rate is constant and the variations of the spike intervals relatively follow the Gamma distribution (Fig 1.1B) (Nawrot, 2010). It is because under stationary conditions, the generic stochastic process has a constant rate which is all identical in all trials. This assumptions allows that $CV = \overline{CV}$. Whenever the neuronal firing is modulated by nonstationary firing in response to the sensory stimulus, the rate modulation will strongly affect the calculation of the *CV*. For example, the slow rate modulation compared to the mean ISI will increase the dispersion of the interval distribution, leading an increased *CV* which no longer reflects the stochastic nature of spike train.

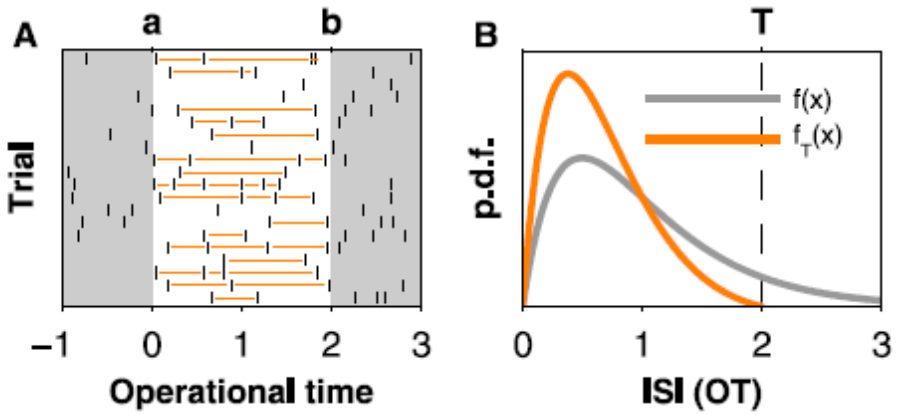

Figure 1.1: Bias of the CV analysis for a finite observed window

(A) Independent empirical observations (trials) of a Gamma process within the finite time window in operational time (0, 2]. Orange lines represent the ISI. Intervals larger than time window cannot be observed. (B) Gamma distribution. Grey curve represents the theoretical Gamma distribution with order $\alpha = 2$, and orange represents the distribution restricted within time interval. The mean and variance calculated within time window are different from theory (Adapted from Nawrot, 2010).

One remedy to this issue is that one can apply the method of time warping, which transfers nonstationary rate to a constant rate by changing the real spike time scale *t* to operational time t'(Fig 1.2), $t' = \int_0^T \lambda(s)ds$ which is estimated by the calculation of integral of instantaneous firing rate $\lambda(t)$ over the time interval [0,T]. In this way, one can transfer the experimental time axis to the operational time axis such that the firing rate modulation is compensated (Fig 1.2). It is shown that the transformation of spike times from the experimental time axis to the operational time axis can eliminate firing rate fluctuations in the spike train (Nawrot, 2006). The time warping method allows us to analyze the data using the *CV* method in operational time axis.

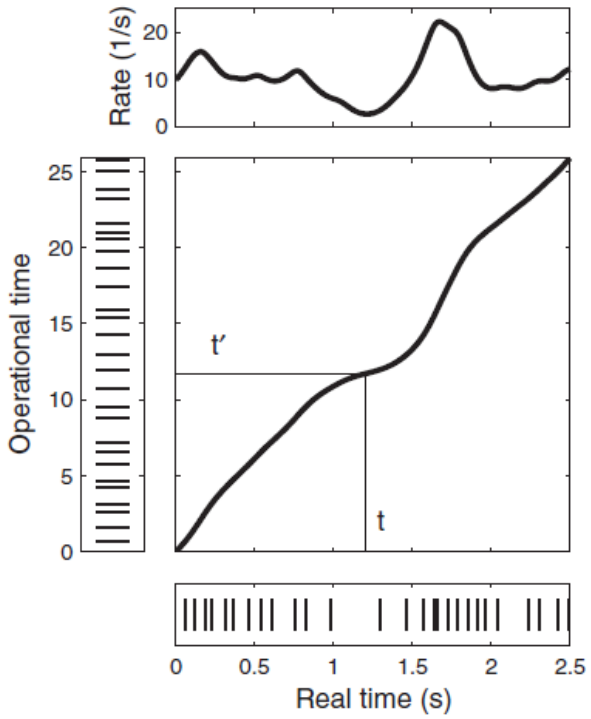

Figure 1.2: Transformation from experimental time to operational time.

A renewal process if unit rate is simulated in operational time (vertical panel). A spike event at time *t'* is translated into a spike event in real time *t* by the integral $t' = \int_0^T \lambda(s)ds$, where $\lambda(t)$ is an instant firing rate at time *t*.

The time warping method addresses the issue of rate modulation for CV analysis. However, it requires a reliable and accurate estimate of the firing rate from spike trains. In recent years, much effort has been made on developing approaches of estimating the neuronal firing rate from spiking data (Shimazaki, 2007; Shimazaki, 2009; Shimokawa, 2009). The promising methods for estimating the firing rate from spike train requires intensive study of machine learning algorithms and optimization principle. Any method for capturing the time varying nature of spikes needs to address the issue of controlling the jaggedness of the estimated rate, including the bin size of the time histogram or the bandwidth of the kernel smoother (Shimazaki, 2007; Shimokawa, 2009). The existing

standard methods for estimating firing rates include peri-stimulus time histogram (PSTH), kernel density estimation, or Bayes estimation, and maximum likelihood methods. Among these methods, PSTH is the most straightforward method which uses histogram to simply count the total spikes over the selected time bin size. In many physiological studies, people use the height of PSTH as the raw spike count per bin (Fig 1.3 C). An alternative method similar to PSTH is the kernel approach, with which a kernel density can be obtained by blurring each spike with a kernel function (Fig 1.3 D). In this scenario, the height of the density estimation measures the spike rate per trial, similar to the height of PSTH. People usually choose a Gaussian-like function as the kernel (Shimazaki, 2007). To obtain the reliable measurements and enhance the accuracy of estimating firing rate, researchers have already advanced these basic methods by optimizing the rate estimation based on the rule of least squared error and maximum likelihood based on Bayes theorem(Shimokawa, 2009). All these efforts to improve the reliability of estimating the firing rate reflect the complexities of statistic nature of spike data and the interdisciplinary mind from diverse fields inside and outside traditional neuroscience.

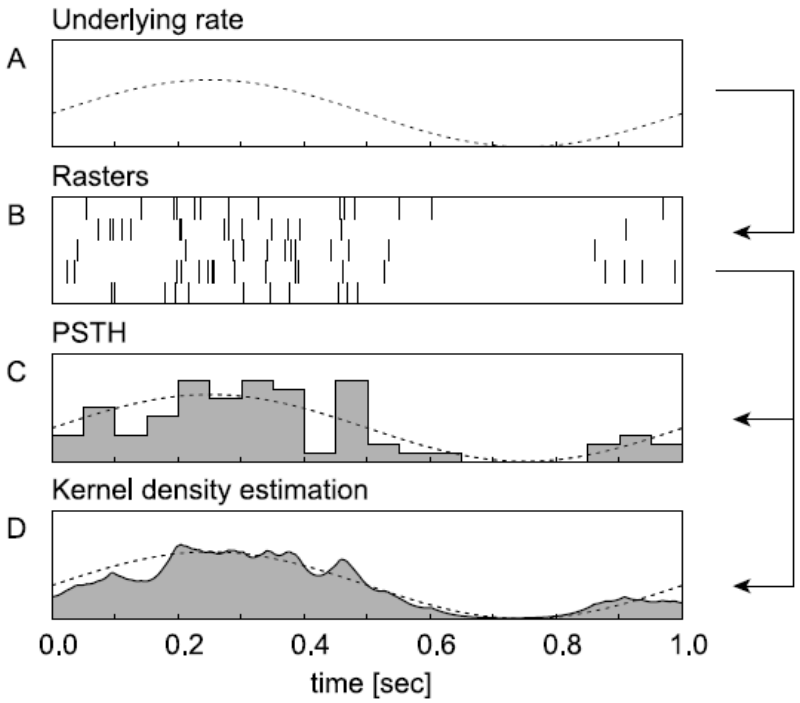

Figure 1.3: Methods of estimating instant firing rate.

(A) An underlying spike rate (B)sample spike raster for five trials (C) Peri-stimulus time histogram (PSTH) (D) A kernel density estimation (adapted from Shinomoto, 2010)

To better characterize the stochastic nature of spike train, it is also useful to combine ISI and count statistics. The Fano Factor (FF) is a well-established measure of count variability from trial to trial and has been repeatedly applied to quantify spike train variability (for review, see Nawrot, 2008). The empirical FF is defined as the ratio of the variance and the mean of the spike count N_j as measured within an observed time length T: $FF = Var(N_j)/E(N_j)$. Similarly, the finite time length T introduces the estimation bias from theoretical value of FF_∞, which is the limit when T approaches the infinity theoretically. It is suggested that one should use a longer observation windows to reduce

the bias, or use a fixed window in operational time to ensure a constant bias (Nawrot, 2010).

In summary, we discussed two standard methods for the analysis of single neuronal spike train: *CV* and *FF*. The most serious issue of applying these methods are due to the nonstationality of real spike train over time. In the typical experimental situation, we make repeated observations in time from trial to trial, which allows us to perform statistical analysis on the trial ensemble. This design is based on the assumption that the observed spike process is stationary in time and across the trials. This is not often true in reality. First, some experimental studies are not based on trial to trail measurements such as motor skill learning of rats' reaching tasks. One cannot obtain the repeated spike data over multiple trails. Second, neural system in animals' brain is nonstationary in most important behavioral tasks such as the theta oscillation during rats' navigation and Gamma rhythms during higher cognitive tasks (Bragin, 1995). Although the invention of time warping method compensates these disadvantages, it still needs advanced algorithms for estimating the firing rate reliably. Nevertheless, the methods developed for firing rate estimation is still widely used by neuroscientists to grasp the stochastic property of spike train at the level of single neuronal firing.

1.2.2 Methods for pairwise correlations of spike trains

The advancement of multineuronal recording techniques has enabled us to simultaneously record the spike activities of multiple single neurons. Therefore, the analysis of neuronal information processing is not necessarily only localized at the single neuron level. The

relationships and associations between pair of neurons have been widely investigated in recent years. In general, techniques which measure the association between two neural spike trains can be divided into time-domain and frequency-domain methods (Brown, 2004; Grun, 2010). Sometimes it is easier to see the effects in the time domain correlogram, and sometimes the frequency representation gives more insights about the neuronal correlations.

The most commonly used time-domain method for pairwise correlation between neurons is unnormalized cross-correlogram (CC) (Fig 1.4 A). After binning the spike times, the unnormalized cross-correlogram is calculated by the cross covariance between two neuronal spike trains *X* and *Y* at a series of time lags over *N* time bins

$$R(X,Y) = \frac{1}{N}\sum_{n=1}^{N} X(n)Y(n+k) \tag{1.1}$$

It analyzes the spike correlation between neuronal pairs by retrieving the probability for spike occurrence in spike train *X* relative to spike train *Y*, extracting the delayed and near coincidences (Grun et al, 2004). This method requires that the stochastic properties of two spike trains do not change in time.

Another often-used time domain method for pairwise correlation is the joint peri-stimulus time histogram (JPSTH), which is the logical extension of single neuron PSTH (Abeles, 1982; Abeles, 1988; Aertsen, 1989; Gerstein, 1969). Let us suppose that the spike activities of two cells *X* and *Y* are recorded simultaneously for a trial duration *T* over *K* trials. The average of the spike count over *K* trials for neuron *X* at certain time bin *t* is calculated by $E\big(X(t)\big) = (\sum_{k=1}^{K} \#spikes\ at\ time\ bin\ t)/K$, and the similar definition

holds for neuron *Y*. The goal of JPSTH is to provide a statistical measure which extracts the net degree of interdependence from joint probability $E(X(t)Y(t))$. Thus, the raw JPSTH is defined by $E(X(t_1)Y(t_2)) - E\big(X(t_1)\big)E\big(Y(t_2)\big)$. The JPSTH displays a two-dimensional histogram which shows the joint spike count per unit time at each time t_1 for neuron *X* and time t_2 for neuron *Y* (Fig 1.4 B). For each time *t*, the main diagonal of the JPSTH displays the observed rate where both neurons fire simultaneously. As the modified version of JPSTH, the normalized JPSTH subtracts from the joint firing rates which is expected under independence, and then divides by the normalization term, which is the product of the two standard deviations of the firing rates for two neurons *X* and *Y*. Mathematically, it is written by

$$r_{X,Y}(t_1, t_2) = \frac{E\big(X(t_1)Y(t_2)\big) - E\big(X(t_1)\big)E\big(Y(t_2)\big)}{\sqrt{E(X(t_1)^2) - \big(E(X(t_2))\big)^2}\sqrt{E(Y(t_1)^2) - \Big(E\big(Y(t_2)\big)\Big)^2}} \qquad (1.2)$$

This method corrects for the possibility that two independent neurons with jointly elevated firing rates can appear to be strongly associated. The normalized JPSTH $r_{X,Y}(t_1, t_2)$ is called Pearson correlation of the firing of neuron 1 at time t_1 and neuron 2 at time t_2. A related measurement, called the normalized cross-correlogram, can be calculated by summing the diagonals of the normalized JPSTH.

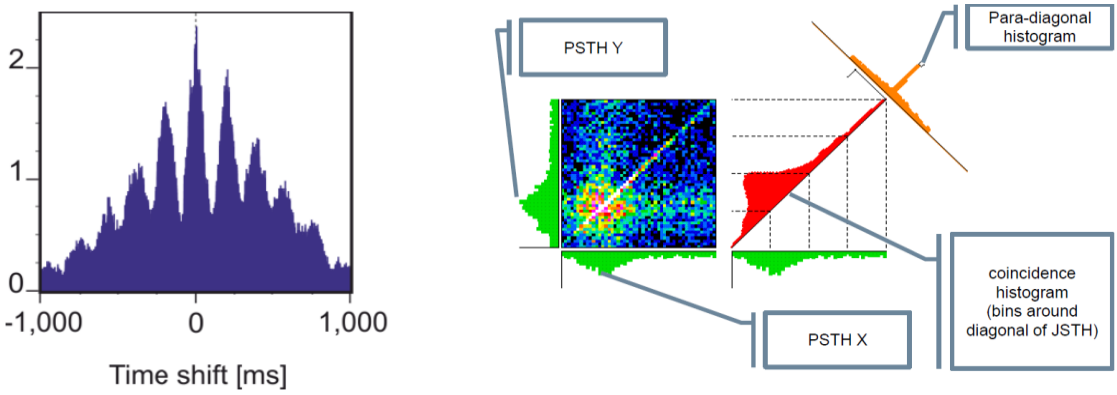

(A) (B)

Figure 1.4: Cross-correlogram and JPSTH.
(A) The cross correlogram with [-1000, 1000] time shift. (B)The PSTH of X and Y are represented by green histograms. The red histogram represents the coincidence histogram.

Although JPSTH and cross-correlogram are much-used easy methods by neuroscientists, they have some limitations. First, the Pearson correlation is only one of many possible measures of correlations, and different measures can produce different results. For instance, the way to normalize the JPSTH can be different from the standard way mentioned above (e.g., Aertsen's normalization) (Aertsen et al., 1989). Therefore, to find the proper normalization of JPSTH that reproduces the parameters in the designed neuron model, one needs to know the relationship between the JPSTH and the model parameters (for detail, see Ito et al., 2000). The accuracy of these methods depends on the underlying mechanism of producing the joint spiking activity. Moreover, if we start the analysis directly from experimental spike data without knowing the spike model, the model selected would no longer be unique, because there are other possible models generating

spike data with the same statistical structure as the given data. Thus, one may need a different normalization procedure to reproduce its parameter (Ito et al., 2000). Second, one can perform a statistical significance test in multiple ways such as least squared regression analysis and student's t test, which yield the various results depending on the assumptions and methods. Statisticians have developed an approach with smoothing procedures and bootstrap test to yield a batter statistical power (Kass, 2003) . Third, the normalized JPSTH and cross-correlogram assume that all trails are statistically indistinguishable. If there is detectable trial-to-trial variation in neuronal firing rates, this variation can appear artifactually as synchrony or time-lagged joint firing (Brody, 1999; Kass, 2003). Fourth, it is shown that the cross-correlogram has a limitation in analyzing a rapid change of the structure of interdependence due to averaging over the sample interval (Ito et al., 2000). Finally, a critical concern, which is related to all measurement methods, is that although all spike train analysis is predicated on good spike sorting, the accuracy of spike time information is particularly important when searching for synchrony or time-lagged joint firing. Therefore, the overlap of spikes, which are issues for most spike-sorting algorithms, can produce spurious correlations between neuronal pairs (Bar-Gad, 2001).

Besides the time-domain analysis, Frequency-domain analysis conducted by taking Fourier transform of the spike trains is used for processing continuous-valued ensemble spiking data under the assumption of stationarity (Brown, 2004). Using this method, the spectrum of individual spike trains or coherence between each spike train pair can be calculated (Brillinger, 1978; Brillinger, 1992). The coherence is a simple frequency-dependent correlation measure between two processes. Comparing to the time-domain

counterpart, the normalization of frequency power is not bin-size dependent, and it can be pooled across neuron pairs. It also allows for analysis of point process, continuous-valued process, and hybrid point and continuous-valued pairs using the same measure. Error estimates and confidence intervals can be calculated for spectra and coherence estimates from theoretical formula which are valid when the numbers of spikes in the spike trains are large, or from bootstrap procedures (Thomson, 1991).

As an important feature of neural spike train data, stimulus-driven non-stationarity may be analyzed using moving window estimates of spectra (spectrograms) and coherences (coherograms) (Brillinger, 1981). A key technical practical point for use of time-frequency spectral estimates, including moving window and wavelet-based estimates, is that they must obey the uncertainty principle ($\Delta f \Delta t \geq 1$), which puts a lower bound on the area of the point spread functions of these estimates at all points in the time-frequency plane (Brown, 2004). Moving window estimates calculated in the frequency domain are often less biased than the corresponding time-domain estimates. Thus, even time domain functions, such as the cross-correlogram and the PSTH, might be improvedby inverse Fourier-transforming the corresponding frequency-domain functions (Brown, 2004). One principle approach to estimating the frequency-domain quantities is to use multitaper techniques (Percival, 2002). These methods have also been proved useful in coherence estimation between spike trains and local field potentials (Pesaran, 2002).

1.2.3 Multiple neuronal interactions

It is suggested that understanding of the cooperative dynamics of populations of neurons is critical to obtain the insight into the nature of neuronal computation in the brain (Hebb, 1949; Gertein et al., 1989; Grun et al,. 2010). Recent advancement in electrophysiological and imaging techniques requires the measurement for higher order neuronal correlations beyond simple pairwise analysis (Staude et al., 2010). Except the classic view that the firing rates play a key role in neural coding, temporal organization of spike discharge within functional group of neurons, called neuronal assemblies, contributes to neural coding. Accordingly, synchronized spikes are considered a property of neuronal signals that can be detected and propagated by other neurons. In this section, we review two major approaches for multiple neuronal correlations: the cumulant correlations and the unitary event (UE) analysis. A novel statistical approach for multi-neuronal interactions —— information geometric method will be introduced separately in section 1.3.

There is evidence that cooperative computation characterize the neuronal interactions on various temporal and spatial scales (Salinas and Sejnowski, 2001; Lestienne, 2001; Womelsdorf and Fries, 2007; Kohn et al., 2009). Direct evidence shows that pairwise neuronal correlation analysis do not resolve such cooperative population dynamics (Martignon et al., 1995; Bohte et al., 2000; Kuhn et al., 2003). Figure 1.5 illustrates the limitation of only analyzing pairwise neuronal correlation on spike trains in a 3-neuron system. In this example, two types of external inputs generate triple-wise and pair-wise correlations (Fig 1.5 A and D). However, the cross- and auto- correlation analysis are identical in both cases (Fig 1.5 B and E), failing to show the difference between two neuronal population activities. Therefore, the apparent differences between two configurations are not captured by mere pairwise correlations. It is the higher-order

correlations which determine whether coincident spikes of two neurons are also coincident with the spikes of the third neuron.

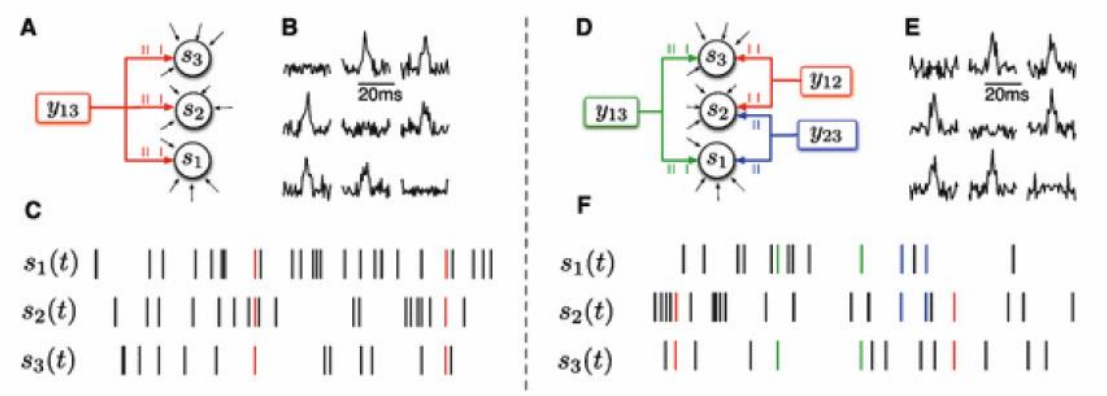

Figure 1.5: Signature of higher-order correlations.

Spike trains are generated from different inputs signals in a 3-neuron network. Connection diagrams (A, D), cross-and auto correlation functions (B, E), and raster plots (C, F) of two populations in a 3 –neuron system. Small black arrows represent independent background inputs. In A, the three neurons share one common external input y_{123}, inducing coordinated spikes in all three spike trains (red ticks in C). In D, only pairs of neurons receives correlated signals (y_{12}, y_{13}, y_{23}), which produce the correlated spikes (green, red, and blue colored ticks). The results based on cross- and auto- correlation analysis are almost identical (B and E), failing to show the triple-wise correlation (Adapted from Grun et al. 2010).

To study higher-order neuronal interactions, researchers have investigated cumulant-based correlation analysis (Staude et al., 2010). As discussed in the section 1.2.2, the common measure for dependence between two random variables *X* and *Y* is characterized by Pearson's correlation coefficient shown in Equation (1.2). As an extension, a straightforward generation of covariance as a measure of dependence among three random variables *X*, *Y* and *Z* can be expressed by

$$E(X,Y,Z) - E(X)E(Y)E(Z) \tag{1.3}$$

which calculates the probability of observing a coincident spike in all three neurons (first term) and subtracts from it the prediction that assumes complete independence (second term). However, the three neuronal interactions are far more complicated than pairwise interactions. For instance, if *X* and *Y* are correlated, but both are independent of *Z*, we have

$$E(X,Y,Z) = E(X,Y)E(Z) \neq E(X)E(Y)E(Z) \tag{1.4}$$

which shows a non-zero measure even if the dependence in the population is only pairwise without any triple wise correlations. To quantify triplet correlations, one needs to subtract from $E(X,Y,Z)$ not only the prediction of complete independence $E(X)E(Y)E(Z)$, but also the predictions that assume non-zero covariance between neuron pairs and independence of the third neuron. Thus, a measure called connected cumulant is defined by

$$\kappa_{1,1,1}(X,Y,Z) = E(X,Y,Z) - E(X)E(Y)E(Z) - Cov(X,Y)E(Z)$$

$$-Cov(X,Z)E(Y) - Cov(Y,Z)E(X)$$

$$= E(X,Y,Z) + 2E(X)E(Y)E(Z) - E(X,Y)E(Z) - E(X,Z)E(Y) - E(Y,Z)E(X) \tag{1.5}$$

The quantity $\kappa_{1,1,1}(X,Y,Z)$ is called the third-connected cumulant. It measures the dependence in the triplet (*X*, *Y*, *Z*) that is not contained in the pairwise correlations. In general, in an *N*-neuron system $\boldsymbol{S} = (S_1, S_2, \ldots S_N)$, we measure *k*th-order correlations by the *k*th-connected cumulants, which are defined in terms of the moments for random variable *S*

$$\kappa_{1,0.0,\ldots 0}(\boldsymbol{S}) = E(S_1)$$

$$\kappa_{1,1,0,\ldots,0}(\boldsymbol{S}) = E(S_1 S_2) - E(S_1)E(S_2) \tag{1.6}$$

$$\kappa_{1,1,1,0,\ldots,0}(\boldsymbol{S}) = E(S_1, S_2, S_3) + 2E(S_1)E(S_2)E(S_3) - E(S_1, S_2)E(S_3) - E(S_1, S_3)E(S_2) - E(S_2, S_3)E(S_1)$$

……

Since the higher-order expressions of cumulants become increasingly complex, the estimation of higher-order cumulant correlations suffers from some limitations. Obviously, the number of parameters grows exponentially with the size of the neuronal population. Consequently, appropriate sample size is required for the reliable estimation of higher-order correlations (Martignon et al., 1995). Researchers have recently studied some approaches to avoid the need for such large sample sizes. Rather than directly estimating these correlations, Staude et al. proposed the cumulant based inference of higher-order correlations (CuBIC)(Staude et al., 2009), providing a lower bound for the maximal order of correlation in a given data. This lower bound is inferred by investigating the constraining relations between correlations of different orders. Another method, called de-Poissonization, is not only to aim for lower bound, but also to estimate a quantity called compounded component rates (for detail, see Ehm et al,.2007) from the population spike count. The CuBIC method exploits only the first few cumulants of the population spike count, while the de-Poissonization method integrates the entire empirical characteristic function, which is determined by available data sample (for detail discussion see Ehm et al., 2007). Both methods are based on additive Poisson process, which assumes that the spike counting of multiple spike train can be decomposed by the linear combination of independent Poisson process (Grun, et al., 2010).

In addition to cumulant analysis, the unitary event (UE) analysis has been developed to detect coincident spike patterns between two or more simultaneously recorded spike trains and to assess the significance of the observation (Grun et al., 2002a). This method allows us to analyze correlations not only between neuronal pairs but also between multiple neurons by considering the various spike patterns among neurons. This method is designed to answer the questions of whether the simultaneously recorded neurons show correlations of their spike activity and how such correlations are related to subgroups of the neurons (Grun, et al., 2010). The first step of the UE analysis is to detect the joint spike events by setting up the appropriate time bin Δt (e.g., $\Delta\, t = 1ms$) such that spike trains can be expressed by binary vectors with $\vec{v}(i)$ =0 (no spike) or 1 (spike) for each neuron i. Under the assumption of stationarity of firing, the probability of observing spikes for neuron *i* is estimated by its spike frequency, which counts the rate of spikes within the observed time interval *T* ($p_i = c_i \Delta t/T$). Then one can compute the expected the joint probability of occurrence of pattern *k* over all neuronal spike trains based on null hypothesis by

$$P_{\exp}^{k} = \prod_{i=1}^{N} \varphi\left(\vec{v}(i)\right) \; with \; \varphi\left(\vec{v}(i)\right) = \begin{cases} p_i & if \; \vec{v}(i) = 1 \\ 1 - p_i & if \; \vec{v}(i) = 0 \end{cases} \tag{1.7}$$

The expected number of occurrence of pattern *k* is therefore given by

$$n_{\exp} = \; P_{\exp}^{k} \; \cdot \frac{T}{\Delta t} \tag{1.8}$$

The second step of UE analysis is to evaluate whether empirical coincidence counting significantly deviates from the expected value defined above. Grun et al., defined the

significance of the empirical number of coincidences n_{emp} as the *p*-value (joint *p*-value), which is given by

$$\mathrm{jp}\left(n_{\mathrm{exp}}\middle|n_{\mathrm{emp}}\right) = \sum_{n=n_{\mathrm{emp}}}^{\infty} \frac{{n_{\mathrm{exp}}}^{n}}{n!} \cdot \exp\left(-n_{\mathrm{exp}}\right) \tag{1.9}$$

If jp is smaller than a predefined significance level α, we infer excess synchrony, and if jp is larger than $1-\alpha$, we infer significantly missing coincidences. In practice, a logarithmical form of jp is used for better visualization because highly significant events are indicated by very small jp values (Grun et al., 2002a)

$$S(\mathrm{jp}) = \log\frac{1-\mathrm{jp}}{\mathrm{jp}} \tag{1.10}$$

This measure is zero for no deviation from expectation, positive if there are more coincidences than expected, and negative if the measurement is lower than the expected count.

The elementary method of UE analysis introduced above is based on the stationary firing. A time-resolved version of the UE analysis has been proposed using a sliding-window approach to capture time dependent changes of the correlations between neurons (Grun et al., 2002b). The underlying assumption is that the same neuronal computation is performed over the neural data across multiple trials. The data can be cut and aligned on the corresponding stimulus or behavioral events. Then one has to decide a window width T_W which is sliding along the data (Fig 1.6). The standard UE analysis is then carried out within this time window for all trails. The sliding-window UE method has been used for the analysis of neuronal populations from motor cortex of awake behaving monkey.

In practice, neuronal synchrony is modulated on a various time scales (Vaadia et al., 1995). The choice of time window size affects how one can appropriately capture such modulation. For example, the larger window generates more coincidences. The expected number of coincidences also increases with the window size. A critical analysis of injection model was used to find out the optimal window size (Grun et al., 2002b). Briefly, one needs to find the lower and upper bound value $T_{\min}$ and $T_{\max}$ such that $T_{\min} < T_W < T_{\max}$.

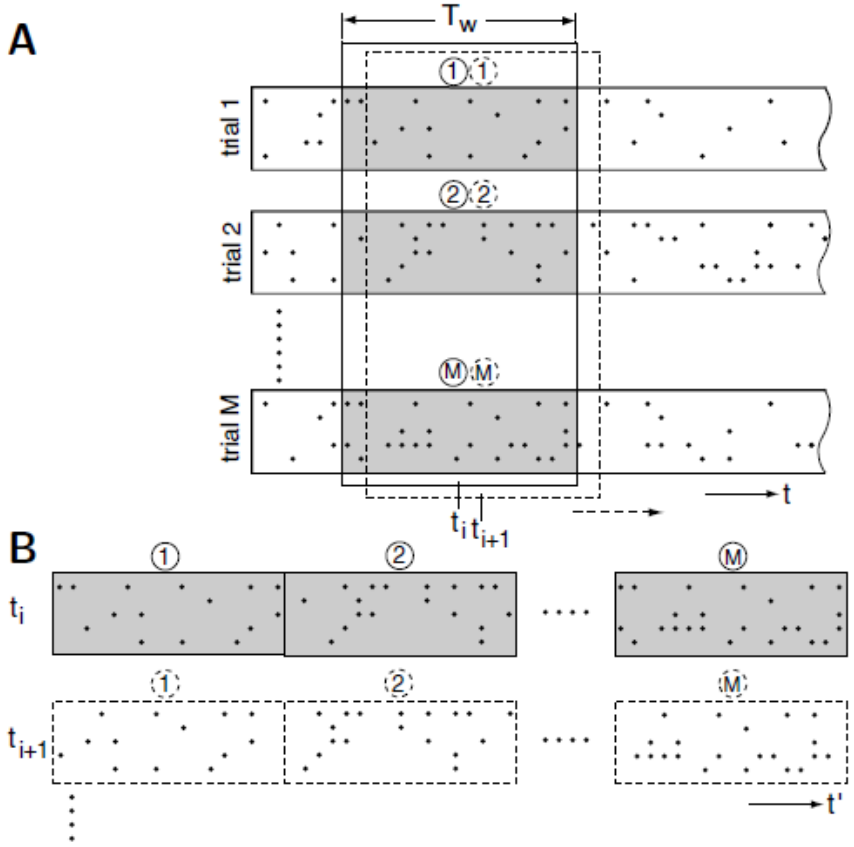

Figure 1.6: Sketch of the moving window analysis.

(A) Parallel spike trains of five neurons (marked as dots) for M trials of the same experiment. A window with width $T_W$centered at a given point in time t_i defines the segment of the data (shaded in grey). (B) From the data in each of such time segment, a new time axis t' is used to concatenate the windows from all trails. The UE analysis is then performed on this new process. The full data set is

analyzed by successively moving the window to the next point of time and repeating the above procedure (dashing frame). Typically, the window is shifted in steps of the time resolution of the data set.

The UE analysis allows us to analyze time-dependent spike correlations, providing important insights into principles of multi-neuronal information processing. It also allows us to examine the occurrence of excess spike synchrony within simultaneously recorded neurons and its relation to sensory stimulus. For instance, Riehle et al. found that neurons in monkey motor cortex synchronize their activity at the time when the monkey expects a "go" signal to initiate an arm movement, even if the signal does not occur. This demonstrates that cortical network is preparing for the upcoming events by activity of neuronal assemblies (Riehle et al., 1997).

In this section, we reviewed the two major approaches for multiple neuronal spike analysis. As the first method, the higher order neuronal interactions can be computed by *k*-th corrected cumulants correlation. The assumption of Poisson process for multiple spike trains provides a very intuitive relationship between cumulant correlations and above-chance coincident firing ("excess synchrony") in neuronal populations. This makes cumulant correlation analysis attractive for parallel spike train analysis. However, the calculation of cumulant correlation becomes increasingly complicated as the order of neuronal interaction increases, such that many parameters show up in the higher order cumulant. Several methods have been developed to obtain the lower bound of maximal order that needs to be considered. In the neuroscience literature, It has been shown that the role of higher order correlations rely almost on the higher-order parameters of an exponential log-linear family (Martignon et al., 1995, 2000; Shlens et al., 2006;

Schneidman et al., 2006; Montani et al., 2009; Shimazaki et al., 2009). The exponential log-linear family is the base of information geometric method, which is the main work in the present thesis. The detailed introduction of information geometric method will be presented in section 1.3 separately.

The second method, the UE analysis, provides a tool to analyze multiple parallel spike trains for time dependent synchrony, providing a way of correlating spike synchrony and behavioral context. The window-sliding UE analysis is used to analyze the time dependent spike trains, enabling the study of nonstationary neuronal spike trains. However, one has to carefully select the appropriate width of time window such that the excess synchrony can be evaluated properly.

1.2.4 Population approaches based on information theory

Information theory, initially proposed by Shannon (Shannon, 1948), determines the ultimate fidelity limits that communication and signal processing systems can achieve. The similarity between the communication system and the brain inspires neuroscientists to apply information theory on brain information processing. Although Shannon's original formulation of information theory is notoriously vague about how to deal with the communication between multiple channels in the real brain system (Doyle et al., 2007), it is useful to study a model of encoding and decoding in the similar way that a communication system does. From a neuroscience perspective, an information source produces an information-bearing signal, which can be either the stimulus in sensory system or an intended motion in motor system. In neuroscience, an encoder X represents

neural coding scheme: how the external stimulus is represented in the firing pattern of neurons. Then the encoded signal passes through the channels with noise such that the output signal *Y* cannot be fully determined by the input signal *X*. These channels represent the population of neurons, and thus, the output signal *Y* is spike train. Finally, a decoder is an estimate of the stimulus *X* given spike signal *Y*. In this theoretical scenario, the fundamental function of the brain is to calculate how much it can infer from observed noisy spike data. In probability theory, it needs to compute the likelihood $P(X|Y)$. Indeed, many of the same issues Shannon addressed have always been research issues in system neuroscience. How is information encoded and decoded? What is the fidelity of information represented in neural system? To address these questions, people use a fundamental model underlying classic information theory.

In information theory, a stochastic stimulus *s* is described by their probability distributions $P(s)$. For a discrete-valued stimulus $S = \{S_1, S_2, \dots, S_N\}$, the Shannon's information entropy is defined by

$$H(S) = -\sum_i P(S_i) \log_2 P(S_i) \tag{1.11}$$

which quantifies the uncertainty of the stimulus *S*.

Based on the Shannon entropy, the mutual information is used to quantify the relationships between input and output. Typically, the mutual information between two random variables *X* and *Y* is defined by

$$I(X;Y) = \sum_i P(X,Y) \log_2 \frac{P(X,Y)}{P(X)P(Y)} = H(Y) - H(Y|X) = H(X) - H(X|Y) \tag{1.12}$$

$I(X,Y) = 0$ when X and Y are statistically independent, and $I(X,Y)$ reaches the maximum when X is totally identical to Y. Mutual information completely characterizes the degree of similarity between the statistical properties of two random variables, making it a powerful measure of statistical dependence.

Based on the above theory, neuroscientists have developed population coding approach for neural information processing in recent years (Panzeri et al., 1999; Panzeri and Schultz, 2001; Pola et al., 2003; Schneidman, 2006; Tang et al., 2008). Population coding is the quantitative study of which algorithms or representations are used by the brain to combine together and evaluate the message carried by different neurons (Grun, 2010). In other words, population coding investigates how group of neurons resolve the ambiguity of the message carried within a single trial by individual neuron, because the responses of individual single neuron in the brain vary trial by trial. The brain itself is highly capable of making sense of the noisy responses of individual neurons by evaluating the activity of large neural populations such that it can process information and make decisions based on single events.

The population coding methods are mostly information-based approaches. In population coding, the Shannon's mutual information is used to quantify how well the presented external stimuli allow us to discriminate among the different stimuli. That is, it quantifies the reduction of uncertainty about the stimulus which can be gained from observation of a single trial of neural response. The general formula of mutual information introduced above can be written alternatively by conditional probability

$$I(\boldsymbol{S},\boldsymbol{R}) = H(\boldsymbol{R}) - H(\boldsymbol{R}|\boldsymbol{S}) = \sum_{s\in\boldsymbol{S}}\sum_{r\in\boldsymbol{R}} P(s)P(r|s)\log_2\frac{P(r|s)}{P(r)} \qquad (1.13)$$

where $P(r|s)$ is the conditional probability of observing response *r* when stimulus *s* is presented, $P(s)$ represents the probability of stimulus *s*, and $P(r)$ is the probability of observing *r* in response of any stimulus *s*.

The prototype of mutual information in Equation (1.13) has some limitations. For example, it only quantifies the overall information transmitted by the neuronal population activity, failing to tell us the contribution of specific correlations. It also fails to inform us whether correlations make the code redundant (Grun, 2010). To overcome these shortcomings, a method called "information breakdown", which decomposes the total mutual information $I(\boldsymbol{S}, \boldsymbol{R})$ into a number of components (Panzeri et al., 1999). Each of these components reflects a different way into which signal and noise correlation contribute to information transformation (Pola. G., 2003). More specifically, the total mutual information can be broke down into a linear component I_{lin}, the reduction of information generated by signal correlation $I_{sig-sim}$, and the contribution of noise correlation I_{cor}(Panzeri et al., 1999; Panzeri and Schultz, 2001; Pola et al., 2003).

$$I(\boldsymbol{S}, \boldsymbol{R}) = I_{lin} + I_{sig-sim} + I_{cor} = I_{lin} + I_{sig-sim} + \underbrace{I_{cor-ind} + I_{cor-dep}}_{I_{cor}} \qquad (1.14)$$

where I_{lin} represents the information that quantifies the independent information each neuron conveys, $I_{sig-sim}$ represents the reduction in total information due to signal correlation. The third term I_{cor} represents the overall effect of noise correlation, which contains two parts: $I_{cor-ind}$ denotes the effect of the average level of noise correlation over stimuli, $I_{cor-dep}$ denotes the contribution of dependence of noise correlation.

The linear term of mutual information I_{lin} gives the total amount of information conveyed by all the cells which share neither noise nor signal,

$$I_{lin} = \sum_{c} I_c \tag{1.15}$$

with $I_c = \sum_{s \in \boldsymbol{s}} \sum_{r_c} P(s)P(r_c|s) \log_2 \frac{P(r_c|s)}{P(r_c)}$. The difference between $I(S;R)$ and I_{lin} is called redundancy. The amount of redundancy produced by signal correlation such as the similarity of the stimulus modulation of individual neuron's response is defined by

$$I_{sig-sim} = \frac{1}{\ln 2} \sum_{r} P(r_c) \left\{ v(r) + \big(1 + v(r)\big) \ln \frac{1}{1 + v(r)} \right\} \tag{1.16}$$

where $v(r)$ quantifies the signal correlations ($v(r) = 0$ if there is no signal correlations). As for the third term I_{cor} , the first component $I_{cor-ind}$ reflects the contribution of stimulus-independent correlations

$$I_{cor-ind} = \sum_{r} \langle P(r|s)\gamma(r|s) \rangle_s \log_2 \frac{1}{1 + v(r)} \tag{1.17}$$

where the first multiplicative factor, with a noise correlation strength $\gamma(r|s)$, represents the effect of noise correlation averaged by stimuli; the second logarithmical factor depends on signal similarity. The second component $I_{cor-dep}$ measures the stimulus-dependent correlations

$$I_{cor-dep} = \sum_{r} \langle P(r|s)(1 + \gamma(r|s)) \log_2 \frac{\langle P(r|s') \rangle_{s'} (1 + \gamma(r|s))}{\langle P(r|s') \big(1 + \gamma(r|s')\big) \rangle_{s'}} \rangle_s \tag{1.18}$$

I_{cor}, the sum of Equation (1.17) and (1.18), therefore quantifies the total impact of noise correlation in information coding (Hatsopoulos et al., 1998), which also equals to the difference between the information in the presence of noise and the information without noise correlation.

The information breakdown method has been applied in the study the study of how the rat's somatosensory cortex encodes the identity of the deflected whisker (Petersen et al. 2001, 2002b). The whisker representation of rat's somatosensory cortex is organized by columns. To gain the insights of how such columnar organization may affect population code, Petersen et al. applied information breakdown method on the calculation of information of location of deflected whisker. They found that the stimulus-independent component $I_{cor-ind}$ was negative when pairs of neurons are both located in the same column, while the contribution of stimulus-dependent noise correlation $I_{cor-dep}$ was very small both for same column and different column neuron pairs. These results suggested that the neurons within the same column have similar stimulus selectivity (positive signal correlation) and positive noise correlations. While in different columns, $I_{cor-ind}$ is close to zero, showing that neurons in different columns have different stimulus preferences (weak signal correlation) and weak noise correlation (Petersen et al. 2001, 2002b). These studies suggested that cross-neuronal correlations limit the information encoding capacity of single cortical columns, and the noise correlations in somatosensory cortex can be ignored during decoding.

The advantage of this approach is that it allows a detailed characterization of how different aspects of neuronal population activity contribute to transmission of information on a single trials basis. The limitation is that it is relatively difficult to calculate the

accurate information with neuronal populations because it needs the large number of trials sample (Panzeri et al., 2007). Therefore, only the populations with small number of neurons (5-10) can be calculated accurately. Nevertheless, it is still useful to obtain some insights into the details of information processing in some networks.

In addition to population coding, an entropy-based approach, called the maximum entropy (MaxEnt) method, has attracted much attention recently (Schneidman et al., 2006; Tang et al., 2008; Tyler et al., 2012). The motivation of this study was to evaluate how given pairwise correlations say about the entire network which are mixed with higher-order interactions. To this end, they analyzed spike data from retina using a minimal model (the exponential family with the expansion up to pairwise interactions)

$$P_2(S_1, S_2, \dots, \dots S_N) = \frac{1}{Z} \exp\left[\sum_i h_i S_i + \frac{1}{2}\sum_{i \neq j} J_{ij} S_i S_j\right] \tag{1.19}$$

where h_i and J_{ij} are associated with the single neuronal firing and pairwise interactions, Z is the normalization factor. Using this model, they found that the pairwise correlations provide strikingly accurate predictions (>90%) of the collective effects of neuronal populations in retina (Schneidman et al., 2006). This study suggests that despite the existence of higher-order interactions, the MaxEnt model still captures more than 90% of the structure in the retina network. The success of this study provides us with the information that in real cortical network with weak neuronal correlations, only pairwise interactions provides an enormous simplification of the network. Interestingly, we will see that the MaxEnt method is equivalent to the 2nd-order information geometric measures, which will be discussed in the following sections.

In summary, information-based theory for neuronal population analysis gains a lot of attention by computational neuroscientists for the analysis of neural spike data. These include the entropy to quantify spike train variability, mutual information to measure the association between processes such as between two spike trains or between a spike train and a stimulus, information breakdown methods to further investigate the effect of specific signals and noise correlations, and MaxEnt model to capture the major contribution in population activity . These measures are applied extensively in the study of how much information multi-spike trains convey about a biological signal. The use of information measures is based on thinking about those parts of the nervous system, such as somatosensory system and visual pathways that may be modeled as communication channels. A major and important challenge for computational neuroscientists is to find ways to further extend the feasibility of performing information computations with large populations. This is the crucial step to enable us to gain better insights into how information is processed in complex brain network.

1.2.5 Summary

We have reviewed the often-used approaches for spike data analysis in the level of neuronal interactions. As the first step of spike data analysis, estimating the single neuronal firing rate and its variability plays an important role in understanding the stochastic nature of spike trains. In section 1.2.1, we presented the CV and FF analysis methods as a starting point to the empirical analysis and interpretation of the variability of the single neuronal spike trains. The original implementation of the CV method assumes

that the neuronal firing is stationary such that one can reliably compute the CV coefficient within a time period over all trials. Such approach, however, suffers from the problem due to the fact that the real neuronal data is often nonstationary. To overcome this difficulty, researchers have proposed time warping techniques that convert the real spike time into operational time. It ensures that the neuronal firing in operational time axis is relatively stationary, allowing us to apply the CV analysis in operational time axis. The appropriate implementation of time warping methods requires the advances of the methods of estimating firing rate. PSTH, kernel smoothing and the combination of likelihood principle and Bayes methods have been investigated by computational neuroscientists to improve the accuracy of estimating the firing rate from spike train data. In section 1.2.2, we discussed the methods for pairwise correlation analysis in the time and frequency domain. Two major methods, cross-correlogram and JPSTH were introduced. The importance of the analysis of pairwise correlations is that there is a unique relationship between known connectivity between two neurons and observed cross-correlation. The reverse, however, is not true unfortunately. A given cross-correlogram of two neurons' correlation can be result of the change of neuronal connectivity and the variability of external inputs on them. From the neural correlation analysis, one can only estimate the strength of neuronal interactions under certain assumptions with respect to the integration of neural input and the shape on the neuron's response curve, because the estimate of the peak neural correlation is very sensitive to the shape and the working point of the neuron's response curve (Melssen and Epping, 1987). Beyond the pairwise correlation analysis, section 1.2.3 introduced several approaches for higher order neuronal interactions based on connected cumulant calculation and the UE analysis. The *k*th connected cumulants quantify the *k*-th order neuronal correlations by

calculating the moment of firing probability. As the increase of the order of neuronal interactions, the calculation of cumulants becomes difficult. Therefore, one needs to evaluate the lower bound of maximal order from the given data. The UE analysis gives us the insight into how to evaluate the neuronal synchrony by calculating the joint *p*-value between the empirical and expected coincidences in neuronal populations. In other words, the UE analysis presents the tests for deviations from null hypothesis. In section 1.2.4, information-based population analysis was discussed. Inspired by the similarity between communication system and the brain, computational neuroscientists have applied Shannon information theory in the spike train encoding and decoding. An advanced version of information theory—information breakdown method has been proposed on quantifying the information from different signal sources. Finally, we briefly discussed the minimal model based on maximum entropy, which can be used to capture the majority of effect in population coding by only taking into account the pairwise neuronal correlations in real neuronal data.

Our ability to understanding such a complex brain system becomes impossible without advanced analysis approaches in the future. As the advancement of recording techniques in experimental neuroscience, novel statistical approaches for analyzing neuronal interactions at different level are necessary. Information geometric methods, based on differential geometry and information theory, gains increasing attention recently, providing a way of estimating neuronal interactions in hierarchical manner. Its theoretical investigation and potential application in neuronal data analysis constitutes the main work in the present thesis. In current work, we show that information geometric method provides a promising approach for the estimation of not only single and pair-wise

neuronal interactions, but also higher order neuronal interactions. It turns out that information geometric methods offers a power statistical tool for analyzing the neuronal network structure from observed spiking data. The applications of this method constitute the main text of this thesis. Before the detailed discussion of these applications, we first introduce its theoretical context and general mathematical treatment in probability space.

1.3 Information-Geometric method

Information geometry (IG) studies a family of probability distributions by using differential geometry. IG describes stochastic model of multiple spike trains by a family of probability distributions, providing not only intuitive understanding but also useful tools for the analysis of multiple spike data (Amari, 2001). By studying the geometrical structure of a family of probability distributions in curved space (Riemannian manifold), IG gives various relations among probability distributions such as divergence or discrepancies between two probability distributions, orthogonal property of two distributions (Amari, 2001; Amari, 2000). The most appealing property of IG is that it decomposes the joint probability distribution of multiple stochastic variables into hierarchical structures in orthogonal manner. In this section, we present the mathematical background for the analysis of multi-neuronal spike correlations from the point of view of IG theory.

Given a set of random variables $X_1, X_2, \dots, X_N$, interactions among them include not only pairwise correlations, but also triplewise and other higher order interactions, which forms

a hierarchical structure. Therefore, it is important to find an invariant orthogonal decomposition of this structure into pairwise, triplewise, and other higher order correlations. In information geometry, this structure can be established under the Riemannian manifold, which was first introduced by Rao (Rao., 1945). Chentsnov further developed Rao's idea and introduced new invariant affine connections in probability distribution manifold (Chentsnov, 1982). Later, IG theory was intensively studied by Nagaoka and Amari (Amari, 2000), who developed a theory of dual structures and unified all of these theories in the dual differential geometrical framework. IG has been widely applied so far not only to mathematical foundations of statistical inferences (Amari, 2000; Amari, 1997; Kass, 1997), but also to information theory (Amari, 2000; Campbell, 1985; Han, 1998), neural networks (Amari, 1992) , system theory (Ohara, 1996), statistical physics(Amari, 2000; Bhattacharyya, 2001; Tanaka.T., 2000) . In the following section, we briefly introduce the basic mathematical principle of IG theory, and then discuss how IG theory is generally used for the analysis of multiple neuronal spike data.

1.3.1 General theory

In this section, we present the information geometry theory developed by (Amari, 2001), which gives an answer of how to formulate an invariant decomposition of the hierarchical system of probability distributions. It turns out that this methodology leads to a new invariant decomposition of entropy and information. It can be further used to analyze the synchronous firing patterns of N-neuron system.

1.3.1.1 Manifold, Curve and Orthogonality

Let us assume a parameterized family of probability distributions $\boldsymbol{S} = \{p(x, \boldsymbol{\xi})\}$, where x is a random variable and $\boldsymbol{\xi} = (\xi_{\boldsymbol{1}}, \xi_{\boldsymbol{2}}, \ldots, \xi_{\boldsymbol{N}})$ is real vector parameter to specify a distribution. $\boldsymbol{S}$ represents an *N*-dimensional manifold with $\boldsymbol{\xi}$ as a coordinate system. The Fisher information matrix $G = (g_{ij})$ is then defined as

$$g_{ij} = E\left[\frac{\partial \log p(x, \boldsymbol{\xi})}{\partial \xi_{\boldsymbol{i}}} \frac{\partial \log p(x, \boldsymbol{\xi})}{\partial \xi_{\boldsymbol{j}}}\right]_x \tag{1.20}$$

where E denotes the expectation over variable *x*, the Fisher matrix G plays the role of a metric tensor in Riemannian space $\boldsymbol{S}$.

The distance between two distributions $p(x, \boldsymbol{\xi})$ and $p(x, \boldsymbol{\xi} + \boldsymbol{d\xi})$ in a curved Riemannian space is given by a quadratic form called geodesic distance

$$ds^2 = \sum g_{ij} d\xi_i d\xi_j \tag{1.21}$$

One can demonstrate that this squared distance has closer relationship with Kullback-Leibler (KL) divergence

$$ds^2 = 2KL[p(x, \boldsymbol{\xi}) : p(x, \boldsymbol{\xi} + \boldsymbol{d\xi})] \tag{1.22}$$

where

$$KL[p : q] = \int p(x) \log \frac{p(x)}{q(x)} dx \tag{1.23}$$

If we consider a curve $\dot{\boldsymbol{\xi}}(t)$ parameterized by *t* in manifold *S*. $\boldsymbol{\xi}(\boldsymbol{t})$ determined by

$$\dot{\boldsymbol{\xi}}(t)$$

$$= \frac{d}{dt}\log p(x, \boldsymbol{\xi}(\boldsymbol{t})) \qquad (1.24)$$

which is the

$$\langle \dot{\boldsymbol{\xi}}_1(t), \dot{\boldsymbol{\xi}}_2(t) \rangle = 0 \qquad (1.25)$$

That is, the two curves are not correlated.

1.3.1.2. Dually Flat Manifolds

We call a manifold $\boldsymbol{S}$ e-flat (exponential flat) when there exists a coordinate system parameterized by θ such that for all i, j, k

$$E\left[\frac{\partial^2}{\partial\theta_i\partial\theta_j}\log p(x, \boldsymbol{\theta})\frac{\partial}{\partial\theta_k}\log p(x, \boldsymbol{\theta})\right] = 0 \qquad (1.26)$$

Such parameters $\boldsymbol{\theta}$ are called *e*-affine coordinates. The curve $\boldsymbol{\theta}(\boldsymbol{t})$ is called an *e*-geodesic if $\boldsymbol{\theta}(\boldsymbol{t})$ is given by a linear function $\theta(t) = at + b$ in the θ coordinates, where a and b are constants.

A typical *e*-flat manifold is the well-known exponential family distributions

$$p(\boldsymbol{x}, \boldsymbol{\theta}) = \exp\left\{\sum \theta_i k_i(\boldsymbol{x}) - \psi(\theta)\right\} \qquad (1.27)$$

where $k_i(\boldsymbol{x})$ represents a given function and ψ is the normalization factor. A typical example of exponential family is Gaussian distribution

$p(x|\mu, \sigma) = \frac{1}{\sqrt{2\pi\sigma^2}}\exp(-\frac{(x-\mu)^2}{2\sigma^2})$, which can be expressed according to (1.27)

$$p(x|\mu,\sigma) = \exp\left\{\sum \theta_i k_i(\boldsymbol{x}) - \psi(\theta)\right\} \tag{1.28}$$

where

$$k(x) = \{x, x^2\}$$

$$\theta = \{\frac{\mu}{\sigma^2}, -\frac{1}{2\sigma^2}\}$$

$$\psi(\theta) = \frac{\mu}{\sigma^2} + \frac{\ln 2\pi}{2} + \ln\sigma$$

In the *e*-flat coordinates $\boldsymbol{\theta} = (\theta_i)$, the orthogonal relationship holds because

$$\frac{\partial^2}{\partial\theta_i\partial\theta_j}\log p = -\frac{\partial^2}{\partial\theta_i\partial\theta_j}\psi(\theta) \tag{1.29}$$

is independent of $\boldsymbol{x}$ and $E\left[\frac{\partial}{\partial\theta}\log p\right] = 0$.

Correspondingly, a manifold is said to be m-flat (mixture flat) when there is a coordinate system $\boldsymbol{\eta}$ such that

$$E\left[\frac{1}{p(x,\boldsymbol{\eta})}\frac{\partial^2}{\partial\eta_i\partial\eta_j}\log p(x,\boldsymbol{\eta})\frac{\partial}{\partial\eta_k}\log p(x,\boldsymbol{\eta})\right] = 0 \tag{1.30}$$

Here $\boldsymbol{\eta}$ is called m-affine coordinates. Similarly, a curve is called *m*-geodesic if it is represented by a linear function $\eta(t) = at + b$ in the m-affine coordinates.

In the theory of information geometry, it has been shown that an exponential family is automatically m-flat although it is not necessarily a mixture family(Amari, 2000). A mixture family is e-flat, although it is not in general an exponential family. The m-affine coordinates ($\boldsymbol{\eta}$-coordinates) of an exponential family are given by

$$\eta_i = E[k_i(x)] = \frac{\partial}{\partial \theta_i}\psi(\boldsymbol{\theta}) \tag{1.31}$$

which is known as the expectation parameters. The coordinate transformation between two coordinates $\boldsymbol{\theta}$ and $\boldsymbol{\eta}$ is given by the following rule

$$\theta_i = \frac{\partial \varphi(\boldsymbol{\eta})}{\partial \eta_i} \tag{1.32}$$

with the relationship $\varphi(\eta) = E[\log p(x, \eta)]$ and $\psi(\boldsymbol{\theta}) + \varphi(\boldsymbol{\eta}) + \boldsymbol{\theta} \cdot \boldsymbol{\eta} = 0$.

The tangent vectors of the coordinates curves θ_i: $e_i = \frac{\partial}{\partial \theta_i}\log p(x, \boldsymbol{\theta})$ and the tangent vectors of the coordinates curves η_j:$e_j^* = \frac{\partial}{\partial \theta_j}\log p(x, \boldsymbol{\eta})$ are orthogonal at any point

$$\langle e_i, e_j^* \rangle = \delta_{ij} \tag{1.33}$$

where δ_{ij} is the Kronecker delta.

1.3.1.3 Flat hierarchical structures

We have briefly introduced the basic concept of information geometry and the geometrical features of dually flat families of probability distributions. In this subsection, we extend them to the geometry of flat hierarchical structures, which is the key idea of information geometry.

A. e-flat structures

Let $\boldsymbol{T}$ be a submanifold of a dually flat manifold $\boldsymbol{S}$. it is called an e-flat submanifold if T has the linear subspace in the e-affine coordinates $\boldsymbol{\theta}$ in S. It is called an m-flat submanifold if it is linear in the m-affine coordinates $\boldsymbol{\eta}$ in **S.** Let us consider a nested

series of *e*-flat submanifolds $E_1 \subset E_2 \subset E_3 \cdots \subset E_n$ where every E_k is an e-flat submanifold of E_{k+1}. Each E_k is automatically dual flat, but is not an *m*-flat manifold. We call such a nested series an e-flat hierarchical structure, or *e*-structure (Amari, 2000). A typical example of the *e*-structure is the following exponential probability distributions:

$$p(\boldsymbol{x}, \boldsymbol{\theta}) = \exp\{\sum \boldsymbol{\theta}_i \cdot \boldsymbol{g}_i(x) - \psi(\boldsymbol{\theta})\} \tag{1.34}$$

where $\boldsymbol{\theta} = (\theta_1, \theta_2, \theta_3, \ldots \theta_n)$ is parameter set.

The expectation parameter in the above equation is correspondingly given by

$$\eta_i = E_\theta[g_i(\boldsymbol{x})], i = 1,2,3, \ldots n \tag{1.35}$$

where $E_\theta[\cdot]$ is the expectation with respect to $p(\boldsymbol{x}, \boldsymbol{\theta})$.

B. Orthogonal structures

It is convenient that we consider a new coordinate system called the k-cut mixed ones, which is the mixture of $\boldsymbol{\theta}$ and $\boldsymbol{\eta}$ coordinates**:**

$$\boldsymbol{\xi}_k = (\eta_1, \eta_2, \ldots, \eta_k; \theta_{k+1}, \ldots, \theta_n) \tag{1.36}$$

This new coordinate $\boldsymbol{\xi}$ consists of a pair of complementary parts of $\boldsymbol{\theta}$ and $\boldsymbol{\eta}$**.** Let us assume two subsets $\boldsymbol{\eta}_{k^-} = (\eta_1, \eta_2, \ldots, \eta_k)$ and $\boldsymbol{\theta}_{k^+} = (\theta_{k+1}, \ldots, \theta_n)$. According to the orthogonality rule, the two subsets are orthogonal in the sense that submanifolds $\boldsymbol{M}_k$ and $\boldsymbol{E}_k$ are complementary and orthogonal at any point in the manifold $\boldsymbol{S}$.

C. Orthogonal Decomposition

The exponential family distribution $p(\boldsymbol{x}, \boldsymbol{\theta})$ needs to be singled out in terms of *k*-th order effects. It is shown that the amount of effect of order k is given by the KL divergence

$$D_k = D\left[p^{(k)}: p^{(k-1)}\right] \tag{1.37}$$

This is called Pythagoras decomposition in curved Riemannian space. In flat Euclidean space, let *a*, *b*, *c* are three points of a rectangle triangle, then the Pythagoras theorem gives $\overline{ac}^2 = \overline{ab}^2 + \overline{bc}^2$. In curved probability space, consider a nested series

$\{p_0\} = E_0 \subset E_1 \subset E_2 \subset E_3 = \{p\}$ as an example, the corresponding Pythagoras in the language of information divergence gives

$$D[p: p_0] = D\left[p: p^{(2)}\right] + D\left[p^{(2)}: p^{(1)}\right] + D\left[p^{(1)}: p^{(0)}\right] \tag{1.38}$$

which holds under the following coordinates system

$$\begin{aligned} p: \theta &= (\theta_1, \theta_2, \theta_3), \eta = (\eta_1, \eta_2, \eta_3) \\ p^{(2)}: \theta &= (\overline{\theta_1}, \overline{\theta_2}, 0), \eta = (\eta_1, \eta_2, \overline{\eta_3}) \\ p^{(1)}: \theta &= (\overline{\overline{\theta_1}}, 0, 0), \eta = (\eta_1, \overline{\overline{\eta_2}}, \overline{\overline{\eta_3}}) \end{aligned} \tag{1.39}$$

1.3.2 Information-geometric measures for multi-spike data analysis

One promising application of information geometry is multi-spike data analysis in neuroscience research. Information-geometric (IG) measures refer to the measure for

neuronal interactions using the hierarchical structure introduced in section 1.3.1. IG measures has been demonstrated as a promising novel statistical method for the estimation of neural network structures, and it gains a lot of attention by neuroscientists recently. One of the central challenges in neuroscience is to understand how information is carried and processed by a population of neural firing patterns in the brain (Georgopoulos, Schwartz et al., 1986; Abeles, 1991; Aertsen and Arndt, 1993; Singer and Gray, 1995; Deadwyler and Hampson, 1997; Parker and Newsome, 1998). The single neuronal mean firing rate is the most-commonly-studied quantity for brain information processing. Many experimental studies show that the mean firing rate of each neuron can be modulated by experimental control and thereby carry information about these experimental conditions. However, information conveyed by neuronal population maybe not only the single neuronal mean firing rate, but also higher order interactions that cannot be directly controlled and estimated. Indeed, growing attention has been paid to the coincidence firing, triplewise correlations, and other higher-order neuronal correlations when analyzing the statistical structures embedded in the neural firing (Gerstein et al., 1989; Engel, Konig et al., 1992; Wilson and McNaughton, 1993; Zohary et al., 1994; Vaadia et al., 1995; Nicolelis et al., 1997; Riehle et al., 1997; Lisman, 1997; Zhang et al., 1998; Maynard et al., 1999; Nadasdy et al., 1999; Kudrimoti et al., 1999; Oram et al., 1999; Nawrot et al., 1999; Baker and Lemon, 2000; Reinagel and Reid, 2000; Steinmetz et al., 2000; Laubach et al., 2000; Salinas and Sejnowski,
2001; Oram et al., 2001, Abeles and Gerstein, 1988; Aertsen, et al., 1989; Amari, 2009; Brown, et al., 2004; Czanner, et al., 2005; Fellous, et al., 2004; Gerstein and Perkel, 1969; Gilestro, et al., 2009; Grun, et al., 2002; Grun, et al., 2002; Lopes-dos-Santos, et al., 2011; Panzeri and Schultz, 2001; Peyrache, et al., 2009; Shimazaki and Shinomoto, 2007;

Shimokawa and Shinomoto, 2009). One popular research topic towards this purpose is to investigate a significant coincident firing between two neurons, which is highly related to learning induced synaptic change. In general, however, it is not easy to only test a pairwise correlation of neural firing if there are be triplewise and higher-order correlations that are mixed into pairwise correlations. For instance, three neurons in a neural network may not be independent in general even when they are pairwise independent. Therefore, we need to build a new analysis method to distinguish these neuronal interactions in different correlation level.

Information geometry decomposes a joint probability distribution into hierarchical structures, which can be applied in the analysis of neural firing patterns by taking into account not only the second-order (pairwise interactions) but also higher order interactions among neurons. As shown previously, information geometry provides useful tools and concepts for this purpose. Using information geometry, complex neuronal interactions in a large neuronal system are singled out by purely pairwise, triplewise, and higher-order correlations. In this section, we discuss some applications of information geometry in multiple neural spike data by showing several examples. As discussed in the previous section, the orthogonality of the natural and expectation parameters in the exponential family of probability distributions and the hierarchical structure methodology provide the key ideas.

1.3.2.1 Information-geometric (IG) measures in spike train analysis

We first present the concept of IG measures. We focus on analyzing the probability distribution in an N-neuron network. The firing patterns of a neuron can be represented by binary random vector such that the overall probability distribution of the neural network can be explicitly expanded by a log-linear model. Let us assume $X = (X_1, X_2, X_3, \dots X_N)$ be the states of *N* neurons, and $p = p(\boldsymbol{x}) = p(x_1, x_2, \dots x_N)$ be their joint probability distribution. The state of each neuron $x_i = 0\ or\ 1$ represents firing or silence, respectively. Hence, $p(\boldsymbol{x})$ is given by $2^N - 1$ possible distributions, forming a $2^N - 1$ dimensional manifold $\boldsymbol{S}$

$$p(x_1, x_2, \dots x_N) = \text{Prob}\{x_1 = i_1, x_2 = i_2, \dots, x_N = i_N\} \tag{1.40}$$

where $i_k = 0\ or\ 1$.

According to information geometry theory, one can choose parameters $\boldsymbol{\eta}$ as the coordinates for expectation, which are written by

$$\eta_i = E[x_i] = \text{Prob}\{x_i = 1\}$$

$$\eta_{ij} = E[x_i x_j] = \text{Prob}\{x_i = x_j = 1\} \tag{1.41}$$

$$\eta_{12,\dots n} = E[x_1 x_2, \dots x_n] = \text{Prob}\{x_1 = x_2 = x_3 = \cdots = x_n = 1\}$$

Accordingly, $p(\boldsymbol{x})$ can also be given by the natural coordinates $\boldsymbol{\theta}$,

$$\log p(\boldsymbol{x}) = \sum \theta_i x_i + \sum \theta_{ij} x_i x_j + \sum \theta_{ijk} x_i x_j x_k + \cdots + \theta_{123\dots N} x_1 x_2 \dots x_n - \psi$$

(1.42)

where $\boldsymbol{\theta} = \{\theta_i, \theta_{ij}, \theta_{ijk}, \dots, \theta_{123\dots N}\}$ are IG measures and ψ represent a normalization factor. All $2^n - 1$ $\boldsymbol{\theta}$ forms an *e*-flat structure in $\boldsymbol{S}$.

The finding of information geometry shows that the η and θ coordinates are dual flat and mutually orthogonal.

Let us first consider how to present pairwise neuronal interaction under this framework. For simplicity, a two neuron system with joint probability $p(x_1, x_2)$ expands four probabilities $\{p_{00}, p_{01}, p_{10}, p_{11}\}$ constrained by $p_{00} + p_{01} + p_{10} + p_{11} = 1$. $p(x_1, x_2)$ is then decomposed into marginal and pairwise correlational components. In η-coordinate, $\eta_i = E[x_i]$ and $\eta_{12} = E[x_1 x_2] = p_{12}$. The covariance of x_1 and x_2 is then expressed by

$$\text{Cov}\,[X_1, X_2] = \eta_{12} - \eta_1 \eta_2 \tag{1.43}$$

In IG measure method, we use mixed coordinates $(\eta_1, \eta_2; \theta)$ such that θ is always orthogonal to η_1 and η_2. In the 2-neuron system, given the log-linear expansion

$$\log p(x_1, x_2) = \theta_1 x_1 + \theta_2 x_2 + \theta_{12} x_1 x_2 - \psi \tag{1.44}$$

Where

$$\theta_1 = \log \frac{p_{10}}{p_{00}}, \theta_2 = \log \frac{p_{01}}{p_{00}}, \theta_{12} = \log \frac{p_{11} p_{00}}{p_{01} p_{10}} \tag{1.45}$$

It has been shown that θ_{12} is orthogonal to η_1 and η_2.The importance here is that the quantity θ_{12} is related the pairwise correlations between two neurons, and θ_1, θ_2corresponds to the single firing rate of neuron 1 and 2, respectively. In this simplest 2-neuro system, $\boldsymbol{\theta} = (\theta_1, \theta_2, \theta_{12})$ is called IG measures for single neuronal firing of each neuron and their pair-wise correlation.

For a 3-neuron system in a manifold $\boldsymbol{S}_3 = \{p(\boldsymbol{x})\}, \boldsymbol{x} = (x_1, x_2, x_3)$, similarly we can again write down the log-linear expansion as

$$\log p(\boldsymbol{x}) = \sum \theta_i x_i + \sum \theta_{ij} x_i x_j + \theta_{123} x_1 x_2 x_3 - \psi \qquad (1.46)$$

with 7-coefficients:

$$\theta_1 = \log \frac{p_{100}}{p_{000}}, \theta_2 = \log \frac{p_{010}}{p_{000}}, \theta_3 = \log \frac{p_{001}}{p_{000}}$$

$$\theta_{12} = \log \frac{p_{110} p_{000}}{p_{100} p_{010}}, \theta_{23} = \log \frac{p_{011} p_{000}}{p_{010} p_{001}}, \theta_{13} = \log \frac{p_{101} p_{000}}{p_{100} p_{001}}$$

$$\theta_{123} = \log \frac{p_{111} p_{100} p_{010} p_{001}}{p_{110} p_{101} p_{011} p_{000}}$$

$$\psi = -\log p_{000} \qquad (1.47)$$

The canonical or *e*-affine coordinates are $\boldsymbol{\theta} = (\theta_1, \theta_2, \theta_3; \theta_{12}, \theta_{23}, \theta_{31}; \theta_{123})$ .The corresponding *m*-affine coordinates are given by $\boldsymbol{\eta} = (\eta_1, \eta_2, \eta_3; \eta_{12}, \eta_{13}, \eta_{23}; \eta_{123})$ where

$$\eta_i = E[x_i] = \text{Prob}\{x_i = 1\}$$

$$\eta_{ij} = E[x_i x_j] = \text{Prob}\{x_i = x_j = 1\} \qquad (1.48)$$

$$\eta_{123} = E[x_1 x_2 x_3] = \text{Prob}\{x_1 = x_2 = x_3 = 1\}$$

The quantity θ_{123} represents the pure triplewise interaction in the sense that it is orthogonal to any changes in the single and pairwise marginal in the mixture coordinates $(\eta_1, \eta_2, \eta_3; \eta_{12}, \eta_{13}, \eta_{23}; \theta_{123})$.

1.3.2.2 The application of IG measure on neural spiking data analysis

In this subsection, we describe one example for the application of IG measures on neural spike data from Nakahara and Amari (2002). Using modeling techniques, they studied the pairwise and triplewise neural correlations. Figure 8 shows the example of detecting the significant triplewise interaction in a 3-neuron system. The spikes of three neurons were generated such that the probability of finding a spike in each time bin (1ms bin width) was determined in each simulation trials, given an assumed probability ($\eta_1, \eta_2, \eta_{12}$) in each period *a*-*c*. Each period was simulated by specifying the firing rates within 100ms. To estimate the probabilities from sampled data, they calculated averaged values in each time bin over all trials. This study shows that during the control period when all neurons were weakly correlated. The calculation of correlation coefficient (COR) is almost zero in this period, while COR in periods *b* and *c* are almost the same as each other but both were different from zero. Interestingly, when the pairwise correlations between any neuronal pairs were calculated more carefully using IG measures ($\theta_{ij}$for all pairwise correlations and $\theta_{123}$for triplewise correlation); one can see that the nature of the interaction is largely different between period *b* and *c*.

This modeling study also showed the advantage of taking into accounting IG measures as hierarchical structure. IG measures provide a separate measure for all-order neuronal interactions which the traditional COR calculation is not capable of. Figure 1.7 (C)

indicates that 0-400ms (period *a* and *b*) is the purely pairwise correlation period, because the triplewise interaction θ_{123} is nearly zero in this period, as shown in (D). However, period d is not purely pairwise correlation since θ_{123} is negative, which indicates that purely triplewise interactions exists in this period. These comparisons cannot be realized only by calculating the correlation coefficient.

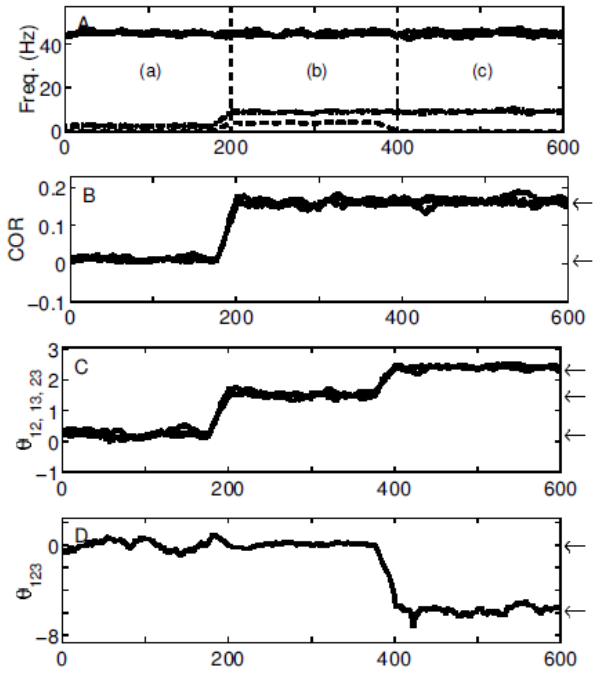

Figure 1.7: Example of detecting the interactions in a 3-neuron system.

(A) The firing frequency in each period *a-c.* (B) Correlation coefficients of three pairs of neuronal firing. (C) The second order (pair-wise) IG measures ($\theta_{ij} = (\theta_{12}, \theta_{23}, \theta_{13})$). (D) The third-order (triple-wise) IG measure θ_{123}. (Adapted from (Nakahara, 2002))

Instead, by fully considering all the IG measures ($\theta_{ij}, \theta_{123}$), we are able to determine and separate the neuronal interactions at the different level from multiple neuronal spiking data.

In section 1.3, we have presented the theoretical framework of IG measures and discussed example for the application of IG approach on detecting pairwise and triple wise neuronal correlations separately. The solid mathematical foundation of IG method makes it a promising analytical method on the analysis of multiple neuronal spike data. However, the understanding of IG approach is far from being well although many studies have been conducted previously (Tanaka.T., 2000; Tatsuno, 2009; Tatsuno, 2004). Previous studies showed that IG measures provide robust measures for neuronal connection weights, indicating that IG methods enable us to estimate the sum of the connection weights $(J_{ij} + J_{ji})$ by computing the second-order IG measures for neuron pairs *i* and *j* ($\theta_{ij} \propto J_{ij} + J_{ji}$) (Tatsuno, 2009). This conclusion, however, only holds when a network receives uncorrelated external input signals. The relationship between θ_{ij} and $J_{ij} + J_{ji}$ is violated when correlated external inputs are imposed on a network. Additionally, how IG measures for higher-order neuronal interactions are characterized is still poorly understood. Furthermore, existing theoretical studies on IG methods rely on the assumption of stationarity of network firing, which is also unrealistic in practical spike train analysis. Therefore, further investigations in more complicated and realistic situations are necessary and interesting research topics for the IG methods. The following chapters 2, 3 and 4 constitute the main part of our present work. In chapter 2, we investigated how IG methods can be applied to estimate the pairwise correlations in a network that receives correlated external inputs by mathematical analysis and computer simulations. In chapter 3, we systematically studied the properties of higher-order IG measures for higher-order neuronal interactions by theoretical analysis and numerical simulations. In chapter 4, we studied how IG measures estimate the network structures

under oscillatory networks by numerical simulations. By the simulations using simple and biologically plausible neuronal models, we confirmed that IG measures provide a promising way of estimating neuronal connection strength even under oscillatory networks, suggesting that IG measures can be a good candidate for multiple neuronal spike train analysis in neuroscience research.

Chapter 2 Information-Geometric Measures for Estimation of Connection Weight under Correlated Inputs

Preface

This chapter is based on *Nie, Y. and Tatsuno, M., Information-Geometric Measures for Estimation of Connection Weight under Correlated Inputs, Neural Computation (2012)*. This study demonstrated that information-geometric measures with higher-order log linear expansion provide a robust estimation of synaptic connection weights in an asymmetrically connected recurrent neural network receiving correlated external inputs.

Abstract

The brain processes information in a highly parallel manner. Determination of the relationship between neural spikes and synaptic connections plays a key role in the analysis of electrophysiological data. Information geometry (IG) has been proposed as a powerful analysis tool for multiple spike data, providing useful insights into the statistical interactions within a population of neurons. Previous work has demonstrated that IG measures can be used to infer the connection weight between two neurons in a neural network. This property is useful in neuroscience because it provides a way to estimate learning-induced changes in synaptic strengths from extracellular neuronal recordings. A previous study has shown, however, that this property would hold only when inputs to neurons are not correlated. Since neurons in the brain often receive common inputs, this would hinder the application of the IG method to real data. We investigated the two-neuron-IG measures in higher-order log-linear models to overcome this limitation. First, we mathematically showed that the estimation of uniformly connected synaptic weight

can be improved by taking into account higher-order log-linear models. Second, we numerically showed that the estimation can be improved for more general asymmetrically connected networks. Considering the estimated number of the synaptic connections in the brain, we showed that the two-neuron-IG measure calculated by the fourth- or fifth- order log-linear model would provide an accurate estimation of connection strength within approximately a ten percent error. These studies suggest that the two-neuron-IG measure with higher-order log-linear expansion is a robust estimator of connection weight even under correlated inputs, providing a useful analytical tool for real multi-neuronal spike data.

2.1 Introduction

Information processing in the brain is carried out by a large number of connected neurons via action potentials. To understand how information is represented and processed in the brain, it is important to record simultaneously from as many neurons as possible from behaving animals. To this end, multiple electrode recording techniques have been developed and widely used in many electrophysiological research studies (Buzsaki, 2004; Chapin, et al., 1999; Davidson, et al., 2009; Dragoi and Tonegawa, 2011; Euston, et al., 2007; Hampson, et al., 1999; Hoffman and McNaughton, 2002; Kudrimoti, et al., 1999; Laubach, et al., 2000; Peyrache, et al., 2009; Riehle, et al., 1997; Tatsuno, et al., 2006; Wilson and McNaughton, 1993). At the same time, the theory of neuron population activity has advanced the understanding of neural information processing by studying pair-wise and higher-order correlations (Abeles and Gerstein, 1988; Aertsen, et al., 1989; Amari, 2009; Brown, et al., 2004; Czanner, et al., 2005; Fellous, et al., 2004; Gerstein and

Perkel, 1969; Grun, et al., 2002; Grun, et al., 2002; Lopes-dos-Santos, et al., 2011; Panzeri and Schultz, 2001; Peyrache, et al., 2009; Shimazaki and Shinomoto, 2007; Shimokawa and Shinomoto, 2009; Zhang, et al., 1998). Among these theoretical approaches, information geometry (IG), based on the theory of differential geometry, has been proposed as a powerful tool for analyzing neuronal activity (Amari, 2001; Amari and Nagaoka, 2000; Amari, et al., 2003; Eleuteri, et al., 2005; Ikeda, 2005; Ince, et al., 2010; Miura, et al., 2006; Nakahara and Amari, 2002; Nakahara, et al., 2006; Ohiorhenuan and Victor, 2011; Shimazaki, et al., 2012; Tatsuno, et al., 2009; Tatsuno and Okada, 2004). One of the advantages of the IG approach is that it provides an orthogonal decomposition of higher-order interactions (Amari, 2001; Amari, 2009; Nakahara and Amari, 2002). Another advantage is the direct relationship between IG measures and synaptic connection strengths (Tatsuno, et al., 2009; Tatsuno and Okada, 2004). This latter property is useful for neuroscience because it allows an experimenter to estimate the connection strength from extracellulary recorded spike data. However, the previous investigations showed that the robust estimation of synaptic connection strengths is possible only when the external inputs are not correlated (Tatsuno, et al., 2009). Since neurons in the brain often receive common inputs, this would impede the application of IG to real data.

To overcome this difficulty, we extended the IG approach by considering higher-order log-linear expansion. First, we analytically showed that the two-neuron IG measure calculated with higher-order neural interactions provides a robust estimation of connection strengths under correlated inputs. For this analytical calculation, we assumed uniformly connected networks and obtained a recursive relationship for the parameters

necessary for calculating the IG measures. Exact solutions up to a ten-neuron network were obtained and were used to evaluate the estimation accuracy of connection weight under correlated inputs. Second, we numerically showed that the two-neuron-IG measure with higher-order neural interactions is robust for more general asymmetrically connected neural networks. From the simulation of different network sizes, we estimated the order of the log-linear model that would be necessary for obtaining accurate estimations of connection strength within approximately a ten percent error.

The outline of this paper is as follows. In Section 2, we provide a brief introduction of IG theory. In Section 3, we introduce the model of neurons, its stochastic dynamics and the method to calculate the IG measures. In Section 4, we provide the recursive relationship and analytical solution for uniformly connected networks. In Section 5, we provide numerical results for asymmetrically connected networks. In Section 6, we summarize our results and discuss future directions for research.

2.2 Information-Geometric Measures

We briefly introduce the IG approach for neural spikes. Amari (Amari, 2001) proposed a novel approach for analysis of neural data by a hierarchical decomposition of probability distribution of neuronal activities on Riemannian manifold. Generally, the spike trains can be represented by binary random variables. As the simplest example, let us consider the case of a two-neuron system. Let x_1 and x_2 be two binary variables where $x_i = 1, 0$ $(i = 1, 2)$ represents neuronal firing or silence respectively. Their joint firing probability is given by $p_{x_1 x_2} = \text{prob}(x_1 = i; x_2 = j) \geq 0,\ i, j = 0,1$ with the

constraint $p_{00} + p_{01} + p_{10} + p_{11} = 1$. In the IG approach, the logarithm of joint probability distribution, $\log p_{x_1 x_2}$, is expanded by a polynomial of x_1 and x_2,

$$\log p_{x_1 x_2} = \theta_1^{(2,2)} x_1 + \theta_2^{(2,2)} x_2 + \theta_{12}^{(2,2)} x_1 x_2 - \psi^{(2,2)}, \tag{2.1}$$

where $\psi^{(2,2)}$ is a normalization parameter and the first and second part of superscript (2,2) represent the order of the log-linear model and the number of neurons in the network, respectively. The coefficients and the normalization parameter can be obtained exactly by solving for p_{00}, p_{01}, p_{10} and p_{11}. The result is given by

$$\begin{aligned} \theta_1^{(2,2)} &= \log \frac{p_{10}}{p_{00}}, \ \theta_2^{(2,2)} = \log \frac{p_{01}}{p_{00}}, \\ \theta_{12}^{(2,2)} &= \log \frac{p_{11} p_{00}}{p_{01} p_{10}}, \\ \psi^{(2,2)} &= -\log p_{00}. \end{aligned} \tag{2.2}$$

Here we call $\boldsymbol{\theta}^{(2,2)} = (\theta_1^{(2,2)}, \ \theta_2^{(2,2)}; \ \theta_{12}^{(2,2)})$ the information geometric (IG) measures (Tatsuno and Okada, 2004). They represent the first and second order interactions, respectively. Specifically, we call $\theta_{12}^{(2,2)}$ the two-neuron IG measure because it represents a pair-wise interaction. The two-neuron IG measure provides correlation information similar to that of other correlation measures such as the correlation coefficient. However, note that the advantage of the two-neuron IG measure is its statistical independence from the change in the marginal firing distributions of neurons (Amari, 2001; Amari, 2009; Nakahara and Amari, 2002).

Another advantage of the IG approach is that the IG measures of any order can be calculated in a straightforward manner. For example, let us consider a three-neuron system. The joint firing probability $p_{x_1x_2x_3}$ of the system is represented as

$$\log p_{x_1x_2x_3} = \theta_1^{(3,3)}x_1 + \theta_2^{(3,3)}x_2 + \theta_3^{(3,3)}x_3 + \theta_{12}^{(3,3)}x_1x_2 + \theta_{13}^{(3,3)}x_1x_3 + \theta_{23}^{(3,3)}x_2x_3 + \theta_{123}^{(3,3)}x_1x_2x_3 - \psi^{(3,3)}. \quad (2.3)$$

By solving the equation for $p_{000}, p_{001}, p_{010}, p_{011}, p_{100}, p_{101}, p_{110}$ and p_{111}, we obtain

$$\theta_1^{(3,3)} = \log\frac{p_{100}}{p_{000}}, \quad \theta_2^{(3,3)} = \log\frac{p_{010}}{p_{000}}, \quad \theta_3^{(3,3)} = \log\frac{p_{001}}{p_{000}},$$

$$\theta_{12}^{(3,3)} = \log\frac{p_{110}p_{000}}{p_{100}p_{010}}, \quad \theta_{23}^{(3,3)} = \log\frac{p_{011}p_{000}}{p_{010}p_{001}}, \quad \theta_{13}^{(3,3)} = \log\frac{p_{101}p_{000}}{p_{100}p_{001}}, \quad (2.4)$$

$$\theta_{123}^{(3,3)} = \log\frac{p_{111}p_{100}p_{010}p_{001}}{p_{110}p_{101}p_{011}p_{000}},$$

$$\psi^{(3,3)} = -\log p_{000}.$$

$\boldsymbol{\theta}^{(3,3)} = (\theta_i^{(3,3)}; \theta_{ij}^{(3,3)}; \theta_{ijk}^{(3,3)})$ represents the single, pair-wise and triple-wise interactions among neurons x_1, $x_2$and x_3, respectively. Here, note the difference between $\theta_{ij}^{(2,2)}$ in

equation 2.2 and $\theta_{ij}^{(3,3)}$ in equation 2.4. They both represent a pair-wise interaction between neurons i and j, but $\theta_{ij}^{(2,2)}$ is calculated from the second-order log-linear model of the two-neuron network while $\theta_{ij}^{(3,3)}$ is calculated from the third-order log-linear model of the three-neuron network. Previous work (Tatsuno and Okada, 2004) showed that if the number of neurons *N* in the network is known, the log-linear model of the same order *N* provides a more accurate estimation of the connection strength. That is, for the three-neuron system discussed above, $\theta_{12}^{(3,3)}$ in equation 2.4 provides a more accurate estimation of connection weight than the second-order two-neuron IG measure, $\theta_{12}^{(2,3)}$,

$$\theta_{12}^{(2,3)} = \log \frac{p_{11*} p_{00*}}{p_{01*} p_{10*}}, \tag{2.5}$$

where '$*$' represents the marginalization over the third (hidden) neuron and therefore, $p_{x_1 x_{2^*}}$ represents the marginal distribution of x_1 and x_2. Note that we use the notation $\theta_i^{(k,N)}$ or $\theta_{ij}^{(k,N)}$ to denote the general case that the IG measure partly expanded up to the *k*th order in an N-neuron network ($N \geq k$).

Generally, the full log-linear expansion for an N-neuron system is given by

$$\log p_{x_1 x_2 \ldots x_N} = \sum_i \theta_i^{(N,N)} x_i + \sum_{i<j} \theta_{ij}^{(N,N)} x_i x_j + \sum_{i<j<k} \theta_{ijk}^{(N,N)} x_i x_j x_k + \cdots$$
$$+ \cdots + \theta_{12,\ldots N}^{(N,N)} x_1 x_2 \ldots x_N - \psi^{(N,N)}, \tag{2.6}$$

where $\theta_{12,\dots l}^{(N,N)}$ is the lth-order neuronal correlation. The first few terms of the IG measure $\boldsymbol{\theta}^{(N,N)}$ and $\psi^{(N,N)}$ in equation 2.6 are expressed as

$$\theta_i^{(N,N)} = \log \frac{p_{x_1=0,\dots,x_i=1,\dots,x_N=0}}{p_{x_1=0,\dots,x_N=0}},$$

$$\theta_{ij}^{(N,N)} = \log \frac{p_{x_1=0,\dots,x_i=1,\dots,x_j=1,\dots,x_N=0} p_{x_1=0,\dots,x_N=0}}{p_{x_1=0,\dots,x_i=1,\dots,x_j=0,\dots,x_N=0} p_{x_1=0,\dots,x_i=0,\dots,x_j=1,\dots,x_N=0}},$$

… … …

$$\psi^{(N,N)} = -\log p_{x_1=0,\dots,x_N=0}, \tag{2.7}$$

where $1 \le i < j < k \le N$.

In practice, the estimates of $\boldsymbol{\theta}$s are obtained by maximum likelihood estimates of $p_{x_1 x_2,\dots,x_N}$, given by

$$p_{x_1 x_2,\dots,x_N} = \frac{c_{x_1 x_2,\dots,x_N}}{\sum_{x_1 x_2,\dots,x_N} c_{x_1 x_2,\dots,x_N}}, \tag{2.8}$$

where $c_{x_1 x_2,\dots,x_N}$ is the number of counts in which the event $(X_1 = x_1, X_2 = x_2, \dots, X_N = x_N)$ occurs.

In real experiments, however, it is not possible to specify the total number of neurons in the network. Furthermore, because the number of $\boldsymbol{\theta}^{(N,N)}$ parameters in the log-linear model increases as $2^N - 1$, it is difficult to obtain a robust estimation of all the parameters for a large *N*. To overcome this difficulty, the previous study (Tatsuno, et al., 2009) proposed to use the second-order log-linear model regardless of the number of neurons *N* in the network,

$$\log p_{x_1 x_2 * \ldots *} = \theta_1^{(2,N)} x_1 + \theta_2^{(2,N)} x_2 + \theta_{12}^{(2,N)} x_1 x_2 - \psi^{(2,N)}, \tag{2.9}$$

where the superscript (2, *N*) represents that the second-order log-linear model was used for an *N*-neuron system. Note that interactions with other *N-2* neurons were included in the equation implicitly. The IG measures are then given by

$$\theta_1^{(2,N)} = \log \frac{p_{10*\ldots*}}{p_{00*\ldots*}},\ \theta_2^{(2)} = \log \frac{p_{01*\ldots*}}{p_{00*\ldots*}},\ \theta_{12}^{(2)} = \log \frac{p_{11*\ldots*} p_{00*\ldots*}}{p_{01*\ldots*} p_{10*\ldots*}},$$

$$\psi^{(2,N)} = -\log p_{00*\ldots*}, \tag{2.10}$$

where '$* \ldots *$' represents the marginalization over the other *N-2* neurons. In general, the IG measures partly expanded up to the *k*th order in an *N*-neuron network are given by

$$\theta_i^{(k,N)} = \log \frac{p_{x_1=0,\ldots,x_i=1,\ldots,x_k=0,*\ldots*}}{p_{x_1=0,\ldots,x_k=0,*\ldots*}},$$

$$\theta_{ij}^{(k,N)} = \log \frac{p_{x_1=0,\ldots,x_i=1,\ldots,x_j=1,\ldots,x_k=0,*\ldots*} p_{x_1=0,\ldots,x_k=0,*\ldots*}}{p_{x_1=0,\ldots,x_i=1,\ldots,x_j=0,\ldots,x_k=0,*\ldots*} p_{x_1=0,\ldots,x_i=0,\ldots,x_j=1,\ldots,x_k=0,*\ldots*}},$$

… … …

$$\psi^{(k,N)} = -\log p_{x_1=0,\ldots,x_k=0,*\ldots*}, \tag{2.11}$$

where '$*$ ... $*$' represents the marginalization over the other *N*-*k* neurons.

With assumption of random asymmetric connections, Tatsuno et al. (Tatsuno, et al., 2009) showed that the two-neuron IG measures and the network parameters are related as

$$\theta_i^{(2,N)} \propto h_i + O\left(\frac{1}{N}\right),$$
$$\theta_{ij}^{(2,N)} \propto \left(J_{ij} + J_{ji}\right) + O\left(\frac{1}{N}\right), \tag{2.12}$$

where h_i is an external input to a neuron i and J_{ij} (J_{ji}) is a connection weight from a pre-synaptic neuron j (i) to a post-synaptic neuron i (j). Equation 12 suggests that the two-neuron IG measures can estimate an external input and connection strength separately. For symmetric connections, $J_{ij} = J_{ji}$, the two-neuron IG measure reduces to

$$\theta_{ij}^{(2,N)} \propto 2J_{ij} + O\left(\frac{1}{N}\right). \tag{2.13}$$

These relationships are very useful for neuroscience because they can provide a tool to estimate the changes of underlying neural network parameters from extracellularly recording data. However, it also can be shown that this separation of external input and connection strength does not hold true if external inputs are correlated. Therefore, in the following section, we investigated how to overcome this difficulty by taking into account higher order neural interactions.

2.3 Model

To investigate the relationship between the IG measures and underlying neural architectures mathematically, we adopt a simple model neuron with stochastic dynamics (Ginzburg and Sompolinsky, 1994). Briefly, $S_j(t)$, the state of the *j*-th neuron at time *t* takes a binary value, 0 or 1, corresponding to a quiescent and active state, respectively. The total input to the *i*th neuron at time *t* is given as

$$u_i(t) = \sum_j J_{ij} S_j(t) + h_i. \tag{2.14}$$

The response of the model neuron depends on the total input u_i and is determined stochastically. The transition rate *w* between the binary states is written as,

$$w(S_i = 0 \to S_i = 1) = \frac{g(u_i)}{\tau_0},$$
$$w(S_i = 1 \to S_i = 0) = \frac{1 - g(u_i)}{\tau_0}, \tag{2.15}$$

$$w(S_i = 0 \to S_i = 0) = 1 - w(0 \to 1),$$

$$w(S_i = 1 \to S_i = 1) = 1 - w(1 \to 0),$$

where τ_0 is a microscopic characteristic time, and $g(u_i)$ is a sigmoidal activation function whose value is bounded in the interval [0, 1]. The probability of finding the system in a state $\boldsymbol{S^{(N)}} = (S_1, \dots, S_N, t)$ at time *t* is characterized by the following master equation

$$\frac{d}{dt}P\left(S^{(N)}; t\right) = -\sum_i w\left(S_i \to (1 - S_i)\right)P\left(S^{(N)}; t\right) + \sum_i w((1 - S_i) \to S_i)P\left(S_i^{(N)}; t\right). \quad (2.16)$$

where $\boldsymbol{S_i^{(N)}} = (S_1, \dots (1 - S_i), \dots, S_N, t)$.

Using the master equation above, the marginal distribution of a neuronal state variable, $\langle S_i(t)\rangle = p_{*\dots*,x_i=1,*\dots*}$, is shown to obey

$$\tau_0 \frac{d}{dt}\langle S_i(t)\rangle = -\langle S_i(t)\rangle + \langle g(u_i(t))\rangle. \quad (2.17)$$

Similarly, the coincident firing of the ith and jth neurons, $\langle S_i(t)S_j(t)\rangle = p_{*\dots*,x_i=1,*\dots*,x_j=1,*\dots*}$, is expressed as

$$\tau_0 \frac{d}{dt}\langle S_i(t)S_j(t)\rangle = -2\langle S_i(t)S_j(t)\rangle + \langle S_i(t)g(u_j(t))\rangle + \langle S_j(t)g(u_i(t))\rangle. \quad (2.18)$$

In general, the coincident firing of N neurons, $\langle S_1(t)S_2(t) \dots S_N(t)\rangle = p_{x_1=1,x_2=1,\dots,x_N=1}$, is written

$$\begin{aligned}\tau_0 \frac{d}{dt}\langle S_1(t)S_2(t) \dots S_N(t)\rangle = &-N\langle S_1(t)S_2(t) \dots S_N(t)\rangle \\ &+\langle S_2(t)S_3(t) \dots S_{N-1}(t)S_N(t)g(u_1(t)\rangle \\ &+\langle S_1(t)S_3(t) \dots S_{N-1}(t)S_N(t)g(u_2(t)\rangle \\ &+ \dots + \langle S_1(t)S_2(t) \dots S_{N-2}(t)S_{N-1}(t)g(u_N(t)\rangle \quad (2.19)\end{aligned}$$

In this paper, we investigate the properties of the IG measures when the network is in the equilibrium state. From equations 2.17, 2.18 and 2.19, the marginal, two-neuron coincident firing, and the *N*-neuron coincident firing at the equilibrium state obey

$$\langle S_i\rangle = \langle g(u_i)\rangle, \quad (2.20)$$

$$\langle S_iS_j\rangle = \tfrac{1}{2}\big(\langle S_ig(u_j)\rangle + \langle S_jg(u_i)\rangle\big), \quad (2.21)$$

$$\begin{aligned}\langle S_1S_2 \dots S_N\rangle = \frac{1}{N}(&\langle S_2(t)S_3(t) \dots S_{N-1}(t)S_N(t)g(u_1(t)\rangle \\ &+\langle S_1(t)S_3(t) \dots S_{N-1}(t)S_N(t)g(u_2(t)\rangle \\ &+ \dots + \langle S_1(t)S_2(t) \dots S_{N-2}(t)S_{N-1}(t)g(u_N(t)\rangle). \quad (2.22)\end{aligned}$$

To calculate the IG measures, we use the relationship between the probability of each event, $p_{x_1x_2}, p_{x_1x_2x_3} \ldots, p_{x_1x_2\ldots x_N}$ and the marginal and coincident firings in the equilibrium state, $\langle S_i \rangle, \langle S_i S_j \rangle, \ldots, \langle S_1 S_2 \ldots S_N \rangle$ (Tatsuno and Okada, 2004). For example, the IG measures, $\boldsymbol{\theta}^{(\mathbf{2,2})} = (\theta_1^{(2,2)}, \theta_2^{(2,2)};\ \theta_{12}^{(2,2)})$, for a two-neuron system in equation 2.2 can be calculated from

$$
\begin{aligned}
p_{00} &= 1 - \langle S_1 \rangle - \langle S_2 \rangle + \langle S_1 S_2 \rangle, \\
p_{01} &= \langle S_2 \rangle - \langle S_1 S_2 \rangle, \\
p_{10} &= \langle S_1 \rangle - \langle S_1 S_2 \rangle, \\
p_{11} &= \langle S_1 S_2 \rangle.
\end{aligned} \tag{2.23}
$$

Similarly, the IG measures, $\boldsymbol{\theta}^{(\mathbf{3,3})} = (\theta_i^{(3,3)};\ \theta_{ij}^{(3,3)};\ \theta_{ijk}^{(3,3)})$, for the three-neuron system in equation 2.4 can be obtained from

$$
\begin{aligned}
p_{000} &= 1 - \langle S_1 \rangle - \langle S_2 \rangle - \langle S_3 \rangle + \langle S_1 S_2 \rangle + \langle S_2 S_3 \rangle + \langle S_1 S_3 \rangle - \langle S_1 S_2 S_3 \rangle, \\
p_{100} &= \langle S_1 \rangle - \langle S_1 S_2 \rangle - \langle S_1 S_3 \rangle + \langle S_1 S_2 S_3 \rangle, \\
p_{010} &= \langle S_2 \rangle - \langle S_1 S_2 \rangle - \langle S_2 S_3 \rangle + \langle S_1 S_2 S_3 \rangle, \\
p_{001} &= \langle S_3 \rangle - \langle S_1 S_3 \rangle - \langle S_2 S_3 \rangle + \langle S_1 S_2 S_3 \rangle, \\
p_{110} &= \langle S_1 S_2 \rangle - \langle S_1 S_2 S_3 \rangle, \\
p_{011} &= \langle S_2 S_3 \rangle - \langle S_1 S_2 S_3 \rangle, \\
p_{101} &= \langle S_1 S_3 \rangle - \langle S_1 S_2 S_3 \rangle, \\
p_{111} &= \langle S_1 S_2 S_3 \rangle.
\end{aligned} \tag{2.24}
$$

For a general *N*-neuron system, the IG measures, $\boldsymbol{\theta}^{(\boldsymbol{N},\boldsymbol{N})} = (\theta_i^{(N,N)};\ \theta_{ij}^{(N,N)};\ldots;\ \theta_{12,\ldots,N}^{(N,N)})$, in equation 2.7 are obtained by

$$p_{0,\ldots,0} = 1 - \sum_i \langle S_i\rangle + \sum_{i<j}\langle S_iS_j\rangle - \sum_{i<j<k}\langle S_iS_jS_k\rangle + \cdots \pm \langle S_1S_2\ldots S_N\rangle,$$

$$p_{0,\ldots 0,x_l=1,0\ldots,0} = \langle S_l\rangle - \sum_{i<j}\langle S_iS_j\rangle + \sum_{i<j<k}\langle S_iS_jS_k\rangle - \cdots \mp \langle S_1S_2\ldots S_N\rangle,$$

$$p_{0,\ldots 0,x_l=1,0\ldots 0,x_m=1,0\ldots,0} = \langle S_lS_m\rangle - \sum_{i<j<k}\langle S_iS_jS_k\rangle + \cdots \pm \langle S_1S_2\ldots S_N\rangle, \qquad (2.25)$$

where an upper sign (lower sign) at the last term on the right-hand side is taken when *N* is an even (odd) number.

For the partly expanded IG measures, $\boldsymbol{\theta}^{(\boldsymbol{k},\boldsymbol{N})} = (\theta_i^{(k,N)};\ \theta_{ij}^{(k,N)};\ldots;\ \theta_{12,\ldots,k}^{(k,N)})$, in equation 2.11, we have the following formula,

$$p_{x_1=0,\ldots,x_k=0,*\ldots*} = 1 - \sum_{i=1}^{k}\langle S_i\rangle + \sum_{i=1}^{k-1}\sum_{j=i+1}^{k}\langle S_iS_j\rangle - \cdots \pm \langle S_1S_2\ldots S_k\rangle,$$

$$p_{x_1=0,\ldots,x_l=1,\ldots,x_k=0,*\ldots*} = \langle S_l\rangle - \sum_{i=1,i\neq l}^{k}\langle S_lS_i\rangle + \sum_{i=1,i\neq l}^{k-1}\sum_{j=i+1,j\neq l}^{k}\langle S_lS_iS_j\rangle - \cdots \mp \langle S_1S_2\ldots S_k\rangle,$$

$$p_{x_1=0,\ldots,x_l=1,\ldots,x_m=1,\ldots,x_k=0,*\ldots*} = \langle S_lS_m\rangle - \sum_{i=1,i\neq l,m}^{k}\langle S_lS_mS_i\rangle + \cdots \pm \langle S_1S_2\ldots S_k\rangle \qquad (2.26)$$

where an upper sign (lower sign) at the last term on the right-hand side is taken when *k* is an even (odd) number.

2.4 Analytical calculations of information-geometric measures for small neural networks

In this section, we first calculated the two-neuron-IG measures for several small networks to obtain insight into how the IG measures are affected by correlated inputs. Next, we derived a polynomial expansion of a sigmoidal gain function to calculate the IG measures for a larger network. Using the polynomial expansion, we then calculated the two-neuron IG measures for a ten-neuron network and showed that the estimation errors for the connection weight can be reduced by taking into account higher-order neuronal interactions.

For mathematical clarity, we considered a neural network with a simple structure. The network consists of a layer of recurrently connected *N* neurons n_i $(i = 1, \dots, N)$, where a connection strength from a pre-synaptic neuron *j* to a post-synaptic neuron *i* is represented by J_{ij}. Each neuron in the layer receives a common input from a single neuron n_0. For simplicity, we assumed that a connection from n_0 to any neuron n_i is uniform, and represent it by *W*. The activity of the neuron n_0 can be modulated by an external input *h* to it.

Under these conditions, the total inputs to the *i*th neuron in the layer and to n_0 are written

$$u_i = \sum_{j \neq i} J_{ij} S_j(t) + W S_0,$$

$$u_0 = h, \tag{2.27}$$

respectively. The state of neurons changes following the transition rate in (2.15). For a sigmoidal activation function, we used,

$$g(u_i) = \frac{1 + \tanh(u_i - m)}{2} \tag{2.28}$$

where m is a parameter controlling the firing probability of a model neuron. To demonstrate that the IG method is robust in a wide range of firing activity, we investigated the IG measures in two representative parameter values. The first parameter value,$m = 0$, was used as a high firing example. It corresponds to a firing probability of 0.7 in a 1000 neuron network. The second parameter value, $m = 1$, was used as a low firing example. It corresponds to a firing probability of 0.1 in a 1000 neuron network.

The focus of the present study is to mathematically investigate the relationship between the two-neuron IG measures $\theta_{ij}^{(k,N)}$ of a pair of neurons n_i and n_j in the layer and the sum of their connection strengths $(J_{ij} + J_{ji})$ when they receive correlated inputs from n_0 by a connection weight *W*.

2.4.1 Calculations of $\theta_{ij}^{(2,2)}$, $\theta_{ij}^{(3,3)}$ and $\theta_{ij}^{(4,4)}$ by fully expanded two, three, and four-neuron log-linear models

To obtain explicit analytical results, we first focused on the two-neuron IG measures of simple networks consisting of two, three and four neurons (see Figure 1.1). For mathematical convenience we treat a case that all recurrent connections are uniform: $J_{ij} = J$. A more general neural network structure with asymmetric connections ($J_{ij} \neq J_{ji}$) will be discussed in the following section. In the following, we represent the two-neuron IG measure using the neurons one and two because any two-neuron IG measures are identical due to uniform assumption.

For the simplest two-neuron network (Figure 1.1A), by plugging equation 2.27 into equations 2.20, 2.21 and 2.22, the marginal distribution $\langle S_i \rangle$, the two-neuron coincident firing $\langle S_i S_j \rangle$ and the three-neuron coincident firing $\langle S_i S_j S_k \rangle$ of S_1, S_2 and S_0 are obtained as

$$\langle S_1 \rangle = \langle S_2 S_0 \rangle [g(J+W) - g(J) - g(W) + g(0)]$$

$$+ \langle S_2 \rangle [g(J) - g(0)] + g(h)[g(W) - g(0)] + g(0),$$

$$\langle S_2 \rangle = \langle S_1 S_0 \rangle [g(J+W) - g(J) - g(W) + g(0)]$$

$$+ \langle S_1 \rangle [g(J) - g(0)] + g(h)[g(W) - g(0)] + g(0),$$

$$\langle S_0 \rangle = g(h),$$

$$2\langle S_1 S_2 \rangle = (\langle S_1 S_0 \rangle + \langle S_2 S_0 \rangle)[g(J+W) - g(J)] + (\langle S_1 \rangle + \langle S_2 \rangle) g(J), \qquad (2.29)$$

$$2\langle S_1 S_0 \rangle = \langle S_2 S_0 \rangle [g(J+W) - g(W)] + \langle S_1 \rangle g(h) + g(W) g(h),$$

$$2\langle S_2 S_0 \rangle = \langle S_1 S_0 \rangle [g(J+W) - g(W)] + \langle S_2 \rangle g(h) + g(W) g(h),$$

$$3\langle S_1 S_2 S_0 \rangle = \langle S_1 S_2 \rangle g(h) + 2\langle S_1 S_0 \rangle g(J+W).$$

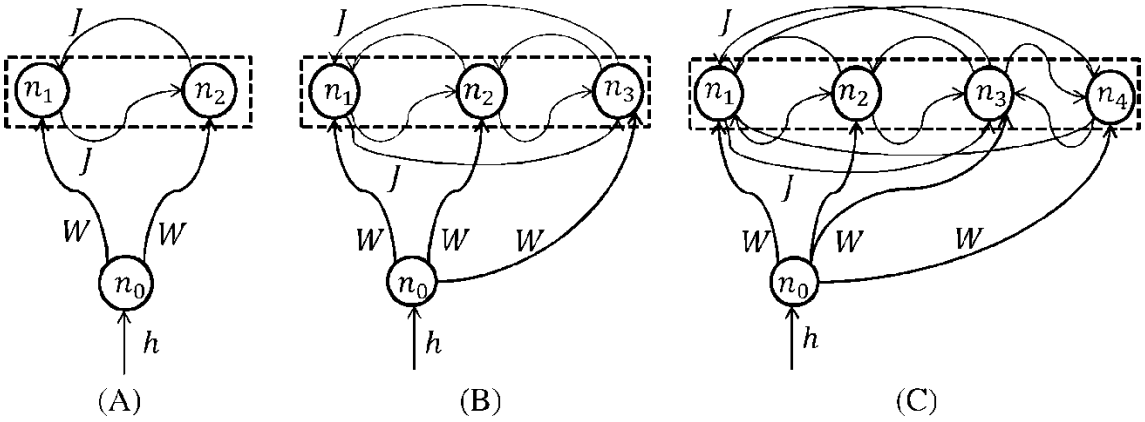

Figure 2.1: Schematic of neural network architecture.
For mathematical simplicity, neurons in the upper layer, $n_i (i = 1, 2, 3, 4)$, are connected uniformly by connection weight J. A single neuron n_0 sends a common signal to the neurons in the upper layer by connection weight W. Activity of n_0 can be modulated by an input h. Note that due to the uniform connection assumption, all two-neuron IG measures θ_{ij} between neurons in the upper layer are identical. (A) A two-neuron network. (B) A three-neuron network. (C) A four-neuron network.

By solving equation 2.29 simultaneously, $\langle S_i \rangle$, $\langle S_i S_j \rangle$ and $\langle S_i S_j S_k \rangle$ can be expressed by the neural network parameters *J*, *W* and *h*. To calculate the two-neuron IG measure $\theta_{12}^{(2,2)}$, we use $\langle S_1 \rangle$, $\langle S_2 \rangle$ and $\langle S_1 S_2 \rangle$. By equations 2.2, 3.10 and 2.29 and after some algebra we obtain,

$$\theta_{12}^{(2,2)} = 2J + \log\left(\frac{A_2 B_2}{C_2^2}\right). \tag{2.30}$$

The explicit form of A_2, B_2 and C_2 is provided in Appendix A. In equation 2.30, the second logarithmic term on the right hand side was induced by a correlated input by W. In other words, in the absence of common input *W*, $\theta_{12}^{(2,2)}$ reduces to 2*J*.

Figures 2(A) and 2(D) show how the IG measure $\theta_{12}^{(2,2)}$ deviates from the correct estimation 2*J* with the increase of *W*, for $m = 0$ and $m = 1$, respectively. Defining the maximum relative estimation error by

$$\delta_{max}^{(N,N)} = \frac{\max |\, \theta_{12}^{(N,N)} - 2J|}{2J}, \tag{2.31}$$

we see that the maximum error can get larger than 2. This demonstrates that under correlated input, $\theta_{12}^{(2,2)}$ is not a good estimator of connection strength. Note that, however, when the common input is zero ($W = 0$), $\theta_{12}^{(2,2)}$ recovers the appropriate relationship $\theta_{12}^{(2,2)} = 2J$ as was expected from the previous work (Tatsuno, et al., 2009).

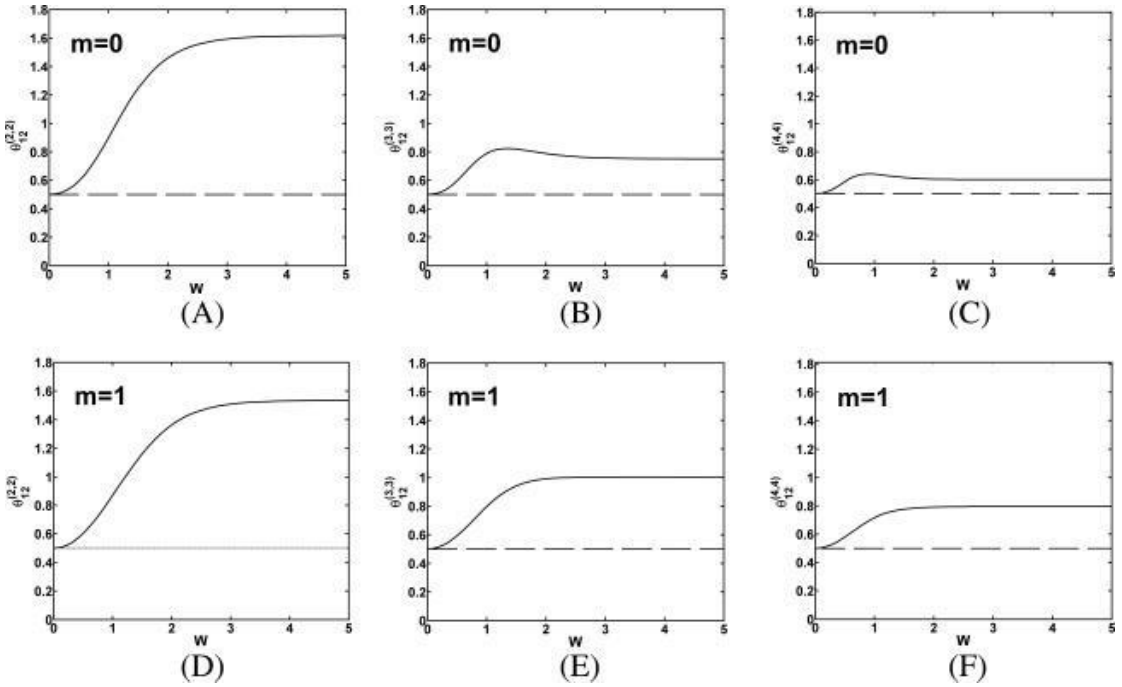

Figure 2.2: **Relationship between the two-neuron IG measure, $\theta_{12}^{(N,N)}$ and a correlated input *W* for *N* = 2, 3 and 4.**
The network parameters are set as $J = 1/4$ and $h = 0.50$. *W* is modified in the range of $[0, 20J]$. (A)-(C) and (D)-(F) correspond a high firing case ($m = 0$) and a low firing case ($m = 1$), respectively. (A) The two-neuron IG measure, $\theta_{12}^{(2,2)}$, for the two neuron network (Figure 1(A)). The horizontal dashed line represents $2J = 0.50$. Note that $\theta_{12}^{(2,2)} = 2J$ when no correlated input exists ($W = 0$). The maximum relative estimation error, $\delta_{max}^{(2,2)}$, is approximately (1.6-0.5)/0.5=2.20 (220%). (B) The two-neuron IG measure, $\theta_{12}^{(3,3)}$, for the three neuron network (Figure 1(B)). $\delta_{max}^{(3,3)}$ is approximately (0.85-0.50)/0.50=0.70 (70%). (C) The two-neuron IG measure, $\theta_{12}^{(4,4)}$, for the four-neuron network (Figure 1(C)). $\delta_{max}^{(4,4)}$ is approximately (0.65-0.50)/0.50=0.30 (30%). (D) The two-neuron IG measure, $\theta_{12}^{(2,2)}$. $\delta_{max}^{(2,2)}$, is approximately (1.53-0.5)/0.5=2.05 (205%). (E) The two-neuron IG measure, $\theta_{12}^{(3,3)}$. $\delta_{max}^{(3,3)}$ is approximately (1.00-0.50)/0.50=1.00 (100%). (F) The two-neuron IG measure, $\theta_{12}^{(4,4)}$. $\delta_{max}^{(4,4)}$ is approximately (0.80-0.50)/0.50=0.60 (60%).

To investigate how the estimation error changes as the network size increases, we further calculated $\theta_{12}^{(3,3)}$ in the three-neuron network under correlated inputs (Figure 2.1(B)).

Following the same procedure as $\theta_{12}^{(2,2)}$, we obtained the two-neuron IG parameters $\theta_{12}^{(3,3)}$. The result is summarized as

$$\theta_{12}^{(3,3)} = 2J + \log\left(\frac{A_3 B_3}{C_3^2}\right). \tag{2.32}$$

See Appendix A for the form of A_3, B_3 and C_3, and see Appendix B for detailed derivation. Similarly, we also obtained the IG measure $\theta_{12}^{(4,4)}$ for the four-neuron network (Figure 2.1(C)),

$$\theta_{12}^{(4,4)} = 2J + \log\left(\frac{A_4 B_4}{C_4^2}\right). \tag{2.33}$$

See Appendix A for the form of A_4, B_4 and C_4, and see Appendix C for detailed derivation.

Figures 2.2(B) and 2.2(E) show the relationship between the two-neuron IG measure $\theta_{12}^{(3,3)}$ and the amplitude of common input W, for $m = 0$ and $m = 1$, respectively. Figures 2.2(C) and 2.2(F) show the relationship between $\theta_{12}^{(4,4)}$ and W, for $m = 0$ and $m = 1$, respectively. As was the case for $\theta_{12}^{(2,2)}$, the IG measures are affected by a correlated input. However, as a promising observation, the relative error decreases as the network size increases. At the same time, we also encountered the increase of complexity of equations (see Appendices A, B, and C). Thus, in the next section, we developed a systematic approach to calculate the IG measures for more neurons.

2.4.2 Polynomial expansion of the sigmoid function and recursive relationship

Generally, it is difficult to write down the relationship among all coincident firings explicitly for a large number of neurons. However, for uniformly connected networks, we found that the sigmoid gain function in an N-neuron network has the following general polynomial relationship,

$$\langle g(u_i)\rangle = \langle g\left(J\sum_{j\neq i} S_j + WS_0\right)\rangle$$

$$= a_0 + a_1 C_{N-1}^1\langle S\rangle + a_2 C_{N-1}^2\langle S^{(2)}\rangle + \cdots + a_{N-1}C_{N-1}^{N-1}\langle S^{(N-1)}\rangle$$

$$+b_0\langle S_0\rangle + b_1 C_{N-1}^1\langle S_0 S\rangle + b_2 C_{N-1}^2\langle S_0 S^{(2)}\rangle + \cdots + b_{N-1}C_{N-1}^{N-1}\langle S_0 S^{(N-1)}\rangle, \quad (2.34)$$

where C_N^k is a binomial constant. Here, we use the notation $S^{(k)} \coloneqq \langle S_1 S_2 \ldots S_k\rangle$ to represent the kth-order coincident firing of all possible combinations of k neurons in the recurrent layer and $\langle S_0 S^{(k)}\rangle \coloneqq \langle S_0 S_1 S_2 \ldots S_k\rangle$ to represent a coincident firing of an input neuron n_0 and all possible kth-order firing in the layer. The coefficients are given by the following recursive relationships

$$a_0 = g(0),$$

$$b_0 = g(W) - a_0,$$

… …

$$a_n = g(nJ) - \sum_{k=0}^{n-1} C_n^k a_k\,, \qquad n \geq 1$$

$$b_n = g(nJ + W) - \sum_{k=0}^{n} C_n^k a_k - \sum_{k=0}^{n-1} C_n^k b_k\,. \qquad n \geq 1 \tag{2.35}$$

Using equation 2.35, the marginal distribution is then given by

$$\begin{aligned}\langle S\rangle \; &= a_0 + a_1 C_{N-1}^1 \langle S\rangle + a_2 C_{N-1}^2 \langle S^{(2)}\rangle + a_3 C_{N-1}^3 \langle S^{(3)}\rangle + \cdots \\ &+ b_0 g(0) + b_1 C_{N-1}^1 \langle S_0 S\rangle + b_2 C_{N-1}^2 \langle S_0 S^{(2)}\rangle + b_3 C_{N-1}^3 \langle S_0 S^{(3)}\rangle + \cdots \end{aligned} \tag{2.36}$$

Similarly, the several higher-order coincident firings are written as

$$\begin{aligned}\langle S^{(2)}\rangle &= (a_0 + a_1)\langle S\rangle + C_{N-2}^1 (a_1 + a_2)\langle S^{(2)}\rangle + C_{N-2}^2 (a_2 + a_3)\langle S^{(3)}\rangle + \cdots \\ &+ (b_0 + b_1)\langle S_0 S\rangle + C_{N-2}^1 (b_1 + b_2)\langle S_0 S^{(2)}\rangle + C_{N-2}^2 (b_2 + b_3)\langle S_0 S^{(3)}\rangle + \cdots \end{aligned}$$

$$\begin{aligned}\langle S^{(3)}\rangle &= (a_0 + 2a_1 + a_2)\langle S^{(2)}\rangle + C_{N-3}^1 (a_1 + 2a_2 + a_3)\langle S^{(3)}\rangle + \cdots \\ &+ (b_0 + 2b_1 + b_2)\langle S_0 S^{(2)}\rangle + C_{N-3}^1 (b_1 + 2b_2 + b_3)\langle S_0 S^{(3)}\rangle + \cdots \end{aligned}$$

… … …

$$2\langle S_0 S\rangle = S g(h) + (a_0 + b_0)\langle S_0\rangle + C_{N-1}^1 (a_1 + b_1)\langle S_0 S\rangle + C_{N-1}^2 (a_2 + b_2)\langle S_0 S^{(2)}\rangle$$

$$+C_{N-1}^{3}(a_2+b_3)\langle S_0S^{(3)}\rangle \ldots$$

$$3\langle S_0S^{(2)}\rangle = S^{(2)}g(h) + 2[(a_0+b_0+a_1+b_1)\langle S_0S\rangle$$
$$+C_{N-2}^{1}(a_1+b_1+a_2+b_2)\langle S_0S^{(2)}\rangle + C_{N-1}^{2}(a_2+b_2+a_2+b_3)\langle S_0S^{(3)}\rangle$$
$$+\cdots]$$

$$4\langle S_0S^{(3)}\rangle = S^{(3)}g(h) + 3[(a_0+b_0+2a_1+2b_1+a_2+b_2)\langle S_0S^{(2)}\rangle$$
$$+C_{N-3}^{1}(a_1+b_1+2a_2+2b_2+a_3+b_3)\langle S_0S^{(3)}\rangle+\cdots] \qquad (2.37)$$

… … …

Using the polynomial expansions above, we can systematically write down the relationship among all orders of firings. We can then solve equations simultaneously and represent the firings of all orders by network parameters *J*, *W* and *h*. By plugging them into equations 2.11 and 2.13, we can calculate the two-neuron IG measures, $\theta_{ij}^{(k,N)}$ for an arbitrary N-neuron network.

2.4.3 Calculations of the two-neuron IG measure for a ten-neuron network

By using the recursive formula developed in the previous section, we calculated all orders of the two-neuron-IG measures for a ten-neuron network, from $\theta_{12}^{(2,10)}$ to $\theta_{12}^{(10,10)}$. Here, $\theta_{12}^{(2,10)}$ represents the two-neuron IG measure considering only two neurons out of ten neurons. It corresponds to the coefficient of the term x_1x_2 of the following two-neuron log-linear model,

$$\log p_{x_1x_2} = \theta_1^{(2,10)}x_1 + \theta_2^{(2,10)}x_2 + \theta_{12}^{(2,10)}x_1x_2 - \psi^{(2,10)}. \quad (2.38)$$

Similarly, $\theta_{12}^{(3,10)}$ represents the IG measure considering three neurons out of ten neurons (two neurons of interest and one additional neuron). It corresponds to the coefficient of the term x_1x_2 of the three-neuron log linear model,

$$\log p_{x_1x_2x_3} = \theta_1^{(3,10)}x_1 + \theta_2^{(3,10)}x_2 + \theta_3^{(3,10)}x_3 + \theta_{12}^{(3,10)}x_1x_2 + \theta_{13}^{(3,10)}x_1x_3 + \theta_{23}^{(3,10)}x_2x_3 + \theta_{123}^{(3,10)}x_1x_2x_3 - \psi^{(3,10)}. \quad (2.39)$$

Note that all coefficients of the second order terms, $\theta_{12}^{(3,10)}$, $\theta_{13}^{(3,10)}$ and $\theta_{23}^{(3,10)}$, are identical due to uniform connection. The remaining higher-order IG measures, $\theta_{12}^{(4,10)}$ to $\theta_{12}^{(10,10)}$, can be treated in the same manner.

Figures 2.3(A) and 2.3(B) summarize how the two-neuron-IG measures of different orders are affected by a common input W, for $m = 0$ and $m = 1$, respectively. First, by comparing the fully expanded IG measures $\theta_{12}^{(10,10)}$ and $\theta_{12}^{(2,2)}$, $\theta_{12}^{(3,3)}$ and $\theta_{12}^{(4,4)}$ in Figure 2, we confirmed that the relative estimation error further decreased as the network size increased; for $m = 0$ (high firing probability), the error decreases from 220% of the two-neuron network (Figure 2.2(A)), 70% of the three-neuron network (Figure 2.2(B)), 30% of the four-neuron network (Figure 2.2(C)), and to 10% of the ten-neuron network (Figure 2.3(A)). For $m = 1$ (low firing probability), the error decreases from 205% of

the two-neuron network (Figure 2.2(D)), 100% of the three-neuron network (Figure 2.2(E)), 60% of the four-neuron network (Figure 2.2(F)), and to 40% of the ten-neuron network (Figure 2.3(B)). This suggests that if a neuron is connected to a large number of other neurons, like in the real brain, the estimation of connection strength by the IG measures would approach the correct value.

Second, the relative estimation error also decreased when the order of the log-linear model increased from 2 to 10; for $m = 0$ (high firing probability), the error decreased from 530% for $\theta_{12}^{(2,10)}$ to 10% for $\theta_{12}^{(10,10)}$ (Figure 2.3(A)). For $m = 1$ (low firing probability), the error decreased from 570% for $\theta_{12}^{(2,10)}$ to 40% for $\theta_{12}^{(10,10)}$ (Figure 2.3(B)). This suggests that the estimation can be improved by taking into account the activity of other neurons. Note, however, that the estimation of higher-order two-neuron IG measures gets increasingly more difficult as the number of neurons involved increases. As was shown in equation 2.8, $p_{x_1 x_2,\ldots,x_N}$ is obtained by maximum likelihood estimates. Therefore, a reliable estimate of $p_{x_1 x_2,\ldots,x_{10}}$ (necessary for calculation of $\theta_{12}^{(10,10)}$) is much more difficult than that of $p_{x_1 x_2,***}$ (necessary for $\theta_{12}^{(2,10)}$).

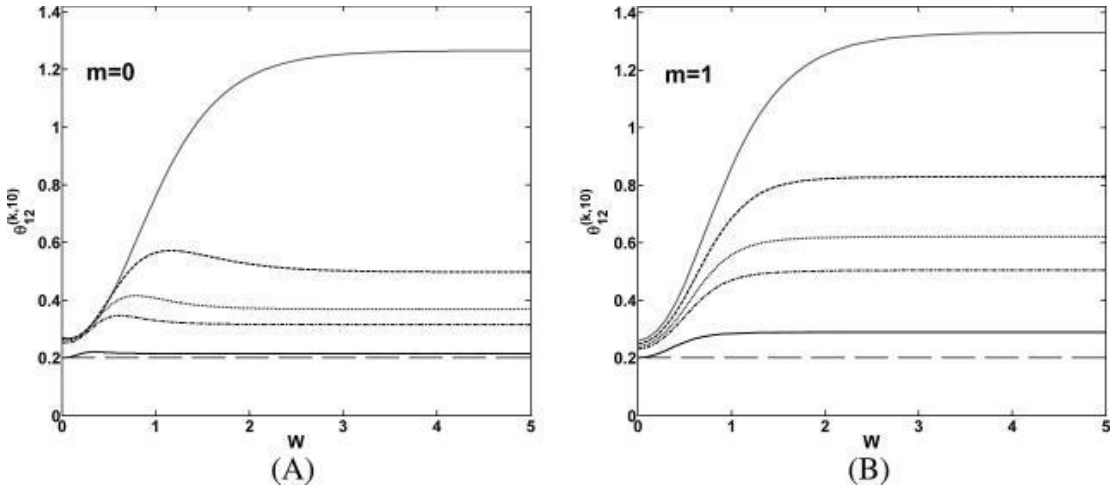

Figure 2.3: Relationship between the two-neuron IG measure, $\theta_{12}^{(k,10)}$ and a correlated input *W* for a ten-neuron network.
The network parameters are set as $J = 1/10$ and $h = 0.50$. *W* is modified in the range of $[0, 50J]$. The horizontal dashed line represents $2J = 0.20$. The curves (from top to bottom) represent $\theta_{12}^{(2,10)}$, $\theta_{12}^{(3,10)}$, $\theta_{12}^{(4,10)}$, $\theta_{12}^{(5,10)}$ and $\theta_{12}^{(10,10)}$, respectively. Estimation error decreases monotonically when higher-order log-linear expansion is taken into account. Note that $\theta_{12}^{(10,10)} = 2J$ when no correlated input exists ($W = 0$). (A) The IG measures correspond to a high firing case ($m = 0$). (B) The IG measures correspond to a low firing case ($m = 1$).

In the real brain, neurons are connected to many other neurons. For example, the number of synaptic connections of pyramidal neurons in the cortex is estimated in the order of 10^3 to 10^4 (Braitenberg and Schuz, 1999). In other words, *N* in the log-linear model can be 10^3 to 10^4. Inspired by the above theoretical insights that the relative estimation error decreases when *N* becomes large, we speculated that lower-order two-neuron IG measures, such as $\theta_{12}^{(4,N)}$ or $\theta_{12}^{(5,N)}$, can be a good estimator of the connection weight for large *N*. In the following section, we numerically investigate this possibility by increasing the network size to a comparable size of the real brain. Also, we investigate the property of IG measures for more general asymmetric connections.

2.5 Numerical simulations

We performed numerical simulations using the Ginzburg and Sompolinsky network (Ginzburg and Sompolinsky, 1994). Our aim was to obtain a minimum order of *k* of log-linear expansion,

$$\log p_{x_1 x_2 \ldots x_k * \ldots *} = \sum_i \theta_i^{(k,N)} x_i + \sum_{i<j} \theta_{ij}^{(k,N)} x_i x_j + \sum_{i<j<k} \theta_{ijk}^{(k,N)} x_i x_j x_k$$
$$\ldots + \theta_{12,\ldots k}^{(k,N)} x_1 x_2 \ldots x_k - \psi^{(k,N)}, \quad (2.40)$$

such that the maximum relative estimation error

$$\delta_{max}^{(k,N)} = \frac{\max |\theta_{12}^{(k,N)} - 2J|}{2J}, \quad (2.41)$$

can be in a reasonably low range, such as ten percent. We simulated neural networks with the size of N=10, 50, 100, 500 and 1000 neurons. Weights of recurrent connections were adjusted to the order of $1/N$ to prevent saturation of neural activity. For uniformly connected networks, the connection weight was set as $J = 1/N$. For asymmetrically connected networks, the connection weight was set as $J_{ij} = 1/N + \varepsilon_{ij}$ at each trial, where a bias term ε_{ij} is a random variable following normal distribution with the mean value 0 and the standard deviation $1/\sqrt{N}$.

For each trial, an initial network state was selected randomly with an equal probability of a neuronal state of 1 or 0. A network was then updated asynchronously by Ginzburg and Sompolinsky dynamics (Ginzburg and Sompolinsky, 1994). To show that the equilibrium states are reached quickly regardless of the initial firing values, Figure 2.4 shows an example of time evolution of firing probability averaged over 1000 asymmetrically connected neurons. The network started from three different initial states (0.1, 0.5 and 0.9) and converged to three equilibrium states (0.1, 0.4 and 0.7) that were realized by setting $m = 1, 0.6$ and 0 in equation (2.28), respectively. The figure confirms that the equilibrium states were reached quickly regardless of the initial firing values, typically within 100 updates. The initial 5000 updates were discarded from the analysis to ensure that the network was in the equilibrium state. We then updated the network 10^6 times to calculate $\theta_{12}^{(2,N)}$, $\theta_{12}^{(3,N)}$, $\theta_{12}^{(4,N)}$ and $\theta_{12}^{(5,N)}$. Note that multiple $\theta_{12}^{(3,N)}$s, $\theta_{12}^{(4,N)}$s and $\theta_{12}^{(5,N)}$s can be calculated from a single simulation trial because they require one or more neuronal activities from *N-2* other neurons. In this study, the number of simultaneously estimated $\theta_{12}^{(3,N)}$, $\theta_{12}^{(4,N)}$ and $\theta_{12}^{(5,N)}$ was [*N-2*], [*(N-2)/2*] and [*(N-2)/3*], respectively. Gauss's symbol [*x*] represents the greatest integer that is less than or equal to *x*. The final value of $\theta_{12}^{(3,N)}$, $\theta_{12}^{(4,N)}$ and $\theta_{12}^{(5,N)}$ from a single simulation trial was obtained by averaging those individual estimations. We repeated 100 simulation trials to calculate the mean, the standard deviation, and the standard error. For the strength of a common input *W*, we considered the range that can be observed in the real brain. For example, the mossy-fiber from the dentate gyrus to the CA3 region of the hippocampus is known to make a very strong synaptic connection. The strength has been estimated five to ten fold compared to

the intrinsic recurrent connection in CA3 (Urban, et al., 2001). Therefore, we varied the strength of a common input W within the range of $[0, 10J]$.

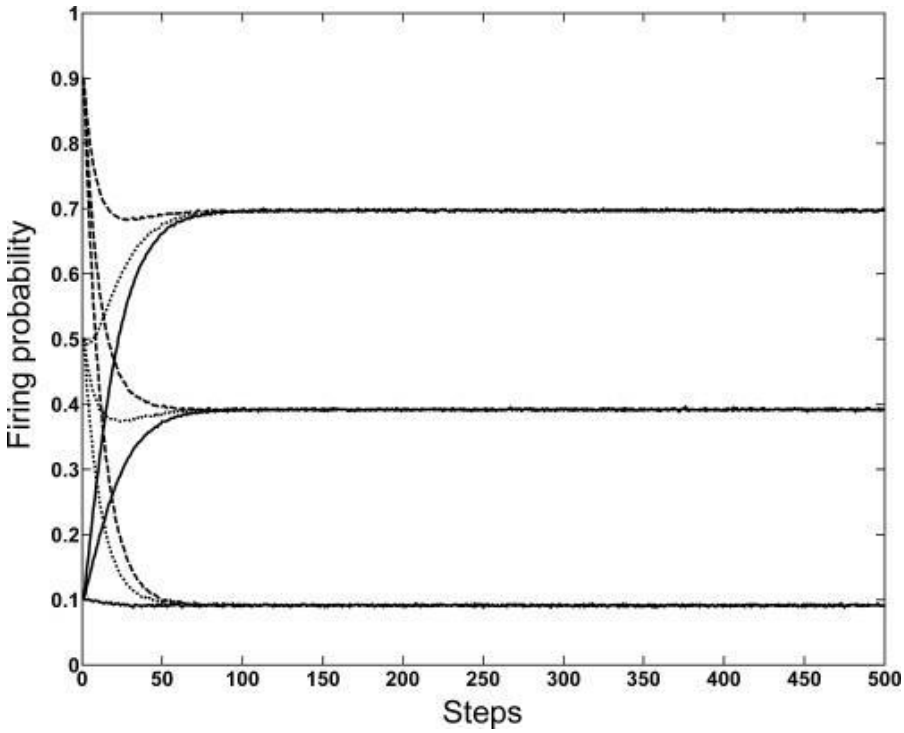

Figure 2.4: **An illustration of the time evolution of firing probability into the equilibrium states.**
Three initial conditions corresponding to low, intermediate, and high firing probability (0.1, 0.5 and 0.9) were plotted by solid, dotted and dashed lines, respectively. The three equilibrium firing probabilities (0.1, 0.4 and 0.7) were realized by setting the m parameter in equation (4.2) as (1, 0.6 and 0), respectively. The network consists of 1000 neurons whose connection is distributed subject to $N(m, \sigma^2)$ where $m = 1/1000$ and $\sigma^2 = 1/1000$, respectively. The strength of a common input *W* was set at *5J* but variation of *W* does not affect the behavior. A network state was updated according to equation (3.2). The equilibrium states were quickly reached, typically within 100 steps, regardless of initial firing probabilities.

Figures 2.5 and 2.6 show how $\theta_{12}^{(4,N)}$ is affected by common input W when the network size N is increased. Here, we selected $\theta_{12}^{(4,N)}$ as a representative example because it was expected to achieve the estimation accuracy within ten percent at the network size comparable to the real brain (more details in Figure 2.7). Figures 2.5(A) and 2.5(B), high

firing activity ($m = 0$) and low firing activity ($m = 1$) respectively, compare the theoretically calculated $\theta_{12}^{(4,10)}$ (filled diamond, taken from Figure 2.3) and numerically obtained $\theta_{12}^{(4,10)}$ (gray solid line) for a uniformly connected ten-neuron network as a function of a common input *W*. The error bar represents the standard deviation. The result shows that the numerical simulation has a strong agreement with the theoretical calculation, especially a more realistic low firing case ($m = 1$), ensuring that the numerical simulation can be used for investigation of the estimation errors for larger networks. Figures 2.5(C) and 2.5(D), high firing activity ($m = 0$) and low firing activity ($m = 1$) respectively, compare the numerically obtained $\theta_{12}^{(4,10)}$ by uniformly connected (gray solid line) and asymmetrically connected networks (dashed line). The error bar is the standard deviation. These figures show that $\theta_{12}^{(4,10)}$s calculated from uniform and asymmetric networks behave similarly. Therefore, the figures also suggest that the theoretical calculation using uniform connection in the previous section will be valid for a random asymmetric connection case.

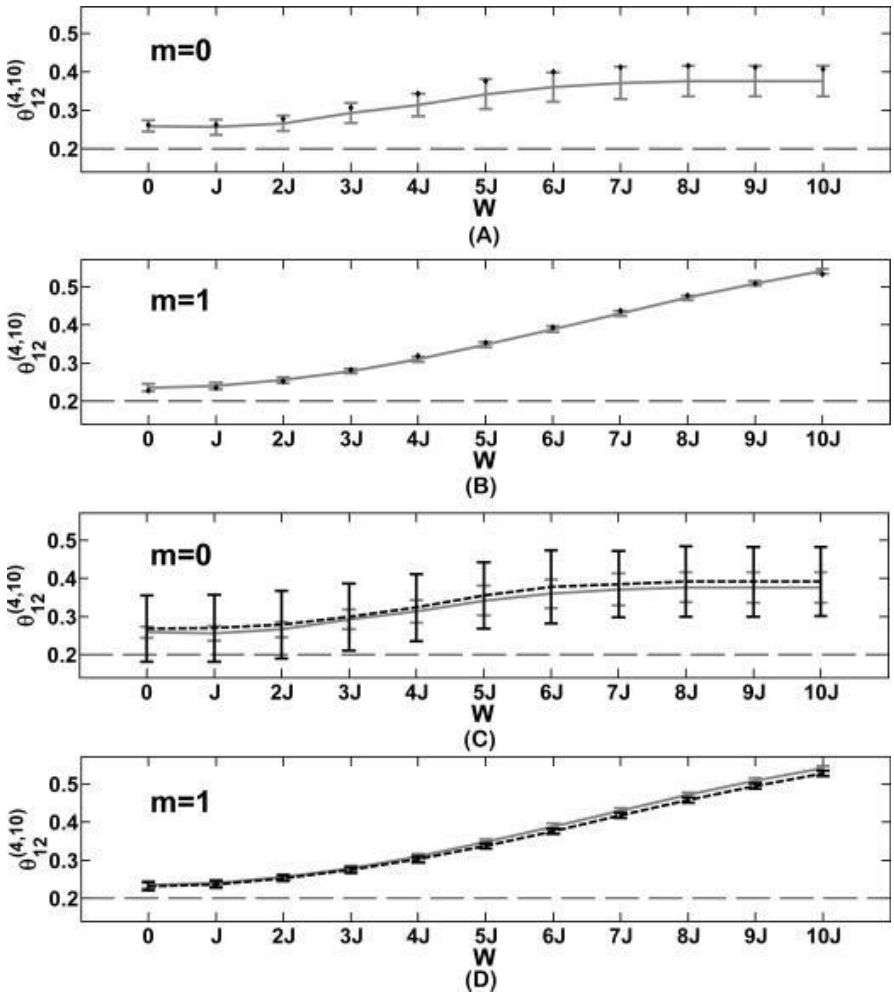

Figure 2.5: Effect of a common input *W* on the two-neuron IG measure, $\boldsymbol{\theta_{12}^{(4,10)}}$ for a ten-neuron network.

(A) Comparison between analytical solution (filled diamond) and numerical simulation (gray line) for a high firing case ($m = 0$). An error bar represents the standard deviation. The network parameters were set $J = 1/10$ and $h = 0.50$, and a common input W was varied between 0 and *10J*. The accurate estimation value is $2J = 0.20$ (dotted horizontal line). Theoretical values are always within a range of the single standard deviation of the numerical simulation, suggesting that simulation and theory have a strong agreement. (B) Comparison between analytical solution (filled diamond) and numerical simulation (gray line) for a low firing case ($m = 1$). There is a very strong agreement between theory and simulation. (C) Comparison between numerical simulation by uniform connection (gray line) and asymmetric connection (dashed line) for a high firing case ($m = 0$). An error bar represents the standard deviation. The input parameter to S_0 is set $h = 0.50$. The connection parameters are selected as $J = 1/10$ for a uniform connection, and $J_{ij} = 1/10 + \varepsilon_{ij}$ for an asymmetric connection where ε_{ij} is a random number drawn from the normal distribution $N(m, \sigma^2)$ with the mean $m = 0$ and variance $\sigma^2 = 1/10$, respectively. Two simulations have a strong

agreement. (D) Comparison between numerical simulation by uniform connection (gray line) and asymmetric connection (dashed line) for a low firing case ($m = 1$). Two simulations have a strong agreement.

Figure 2.6 shows the numerical results of $\theta_{12}^{(4,N)}$ for 50-neuron networks (Figure 2.6(A) for $m = 0$ and Figure 6(E) for $m = 1$), 100-neuron networks (Figure 2.6(B) for $m = 0$ and Figure 2.6(F) for $m = 1$), 500-neuron networks (Figure 2.6(C) for $m = 0$ and Figure 2.6(G) for $m = 1$), and 1000-neuron networks (Figure 2.6(D) for $m = 0$ and Figure 2.6(H) for $m = 1$) as a function of a common input W. The gray line and dashed line are uniformly and asymmetrically connected networks, respectively. The error bar represents the standard error. The results indicate that the relative error of $\theta_{12}^{(4,N)}$ decreases as the size of the network increases; for N=500 and 1000, the correct value (dashed line) is within the standard error. We also observe that for larger networks (N=500 and 1000), the estimation error becomes independent from the strength of a common input W. Furthermore, the IG estimation also becomes independent from the difference of firing activity ($m = 0$ or $m = 1$) as the network size is increased. This result is also consistent with the finding that the IG measure is statistically independent from firing rate modulation (Amari, 2001; Amari, 2009).

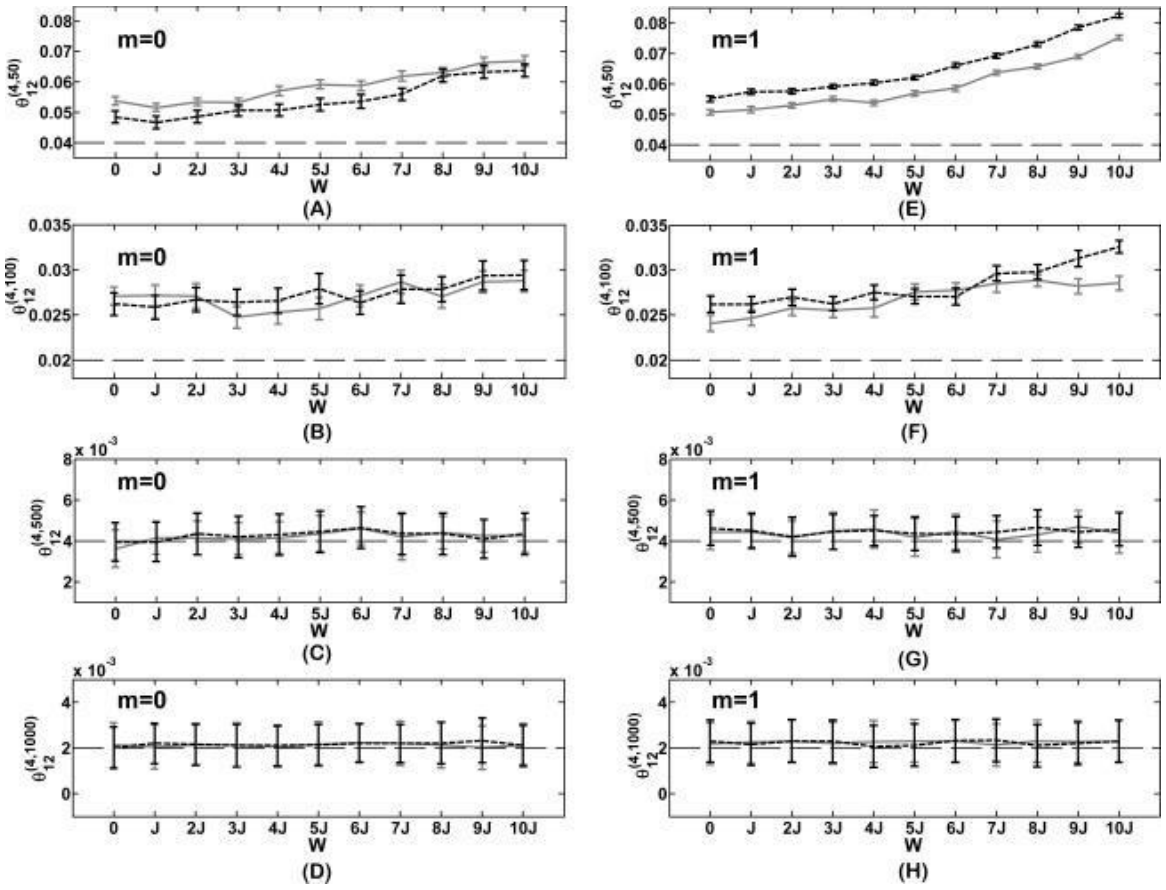

Figure 2.6: Effect of a common input *W* on the two-neuron IG measure, $\theta_{12}^{(4,N)}$, for $N = 50, 100, 500$ and 1000 neurons.

The input parameter to S_0 is set as $h = 0.50$. The connection parameters are selected as $J = 1/N$ for a uniform connection, and as $J_{ij} = 1/N + \varepsilon_{ij}$ for an asymmetric connection where ε_{ij} is a random number drawn from the normal distribution $\mathrm{N}(m, \sigma^2)$ with the mean $m = 0$ and variance $\sigma^2 = 1/N$, respectively. A common input W was varied between 0 and 10J. A uniform connection and an asymmetric connection are shown by gray line and dashed line, respectively. An error bar represents the standard error. The accurate estimation value is $2J = 2(1/N)$ (dotted horizontal line).]. (A)-(D) and (E)-(H) correspond to a high firing case ($m = 0$) and a low firing case ($m = 1$), respectively. (A) The two-neuron IG measure $\theta_{12}^{(4,50)}$ for a 50-neuron network. (B) The two-neuron IG measure $\theta_{12}^{(4,100)}$ for a 100-neuron network. (C) The two-neuron IG measure $\theta_{12}^{(4,500)}$ for a 500-neuron network. (D) The two-neuron IG measure $\theta_{12}^{(4,1000)}$ for a 1000-neuron network. (E) The two-neuron IG measure $\theta_{12}^{(4,50)}$ for a 50-neuron network. (F) The two-neuron IG measure $\theta_{12}^{(4,100)}$ for a 100-neuron network. (G) The two-neuron IG measure $\theta_{12}^{(4,500)}$ for a 500-neuron network. (H) The two-neuron IG measure $\theta_{12}^{(4,1000)}$ for a 1000-neuron network.

In order to summarize how the maximum relative estimation error $\delta_{max}^{(k,N)}$ for the different order of the two-neuron IG measures $\theta_{12}^{(2,N)}$, $\theta_{12}^{(3,N)}$, $\theta_{12}^{(4,N)}$ and $\theta_{12}^{(5,N)}$ changes with the network size, we plotted the $\delta_{max}^{(k,N)}$ as a function of the network size in Figure 2.7. The value of $\delta_{max}^{(k,N)}$ was taken from the numerical simulation of asymmetrically connected networks. The nonlinear curves represent the fitting to the data points. Figure 2.7(A), corresponding to high firing probability ($m = 0$), suggest that $\theta_{12}^{(4,N)}$ and $\theta_{12}^{(5,N)}$ would achieve the estimation accuracy of five to ten percent for the number of connections that can be found in the brain (10^3-10^4), respectively. Figure 2.7(B), corresponding to low firing probability ($m = 1$), suggests that $\theta_{12}^{(3,N)}$, $\theta_{12}^{(4,N)}$ and $\theta_{12}^{(5,N)}$ would achieve the estimation accuracy of ten to twenty percent for 10^3-10^4 connections, respectively. However, note that for $m = 1$, the data points of $\theta_{12}^{(4,N)}$ (filled circle) and $\theta_{12}^{(5,N)}$ (filled diamond) for larger networks (N=500 and 1000) were clustered around ten percent, therefore undershooting the fitted curve significantly. This observation indicates that the estimation accuracy for a low firing case would be smaller than the fitted curve and be similar to a high firing case. Based on these findings, we have concluded that $\theta_{12}^{(4,N)}$ and $\theta_{12}^{(5,N)}$ can be used as a robust estimator of connection weight under the existence of common inputs.

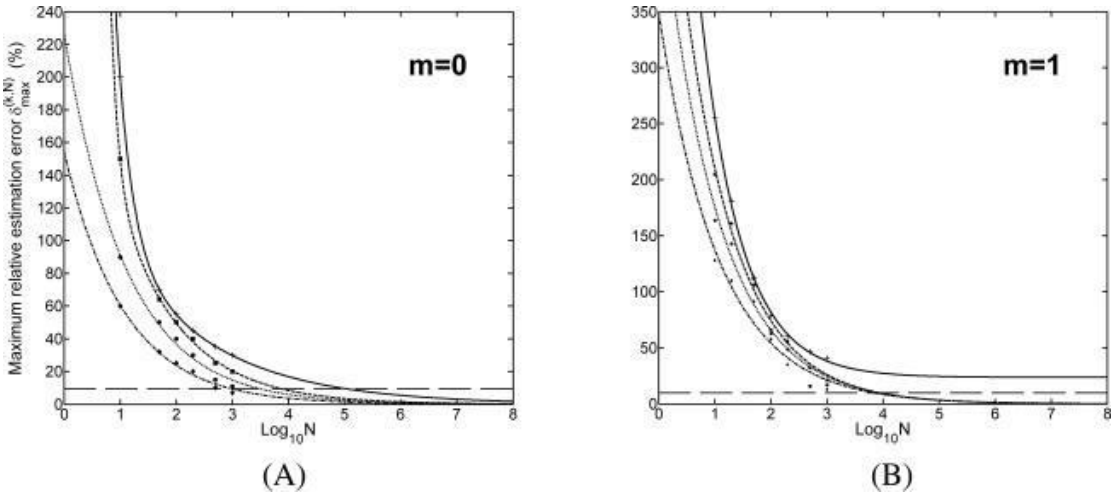

Figure 2.7: Comparison of the maximum relative estimation error of the two-neuron IG measure, $\boldsymbol{\delta_{max}^{(k,N)}}$, as a function of the network size.
The data points (plus, filled square, filled circle and filled diamond) corresponds to the IG measures ($\theta_{12}^{(2,N)}, \theta_{12}^{(3,N)}, \theta_{12}^{(4,N)}, \theta_{12}^{(5,N)}$), respectively. They were obtained by the numerical simulation of 10, 50, 100, 200, 500 and 1000-neuron networks. The corresponding maximum relative estimation errors, $\delta_{max}^{(k,N)}$, are represented in percentages. The curve represents a nonlinear fitting for each order of the IG measure. (A) and (B) correspond a high firing case ($m = 0$) and a low firing case ($m = 1$), respectively. (A) For the network size of $10^3 - 10^4$ neurons, $\theta_{12}^{(4,N)}$ and $\theta_{12}^{(5,N)}$ are expected to achieve five to ten percent accuracy. (B) For the network size of $10^3 - 10^4$ neurons, the fitted curves indicate that $\theta_{12}^{(3,N)}$, $\theta_{12}^{(4,N)}$ and $\theta_{12}^{(5,N)}$ are expected to achieve ten to twenty percent accuracy. Note that $\theta_{12}^{(4,N)}$ and $\theta_{12}^{(5,N)}$ for larger networks such as N=500 and N=1000 are well below the fitted curves. This observation indicates that actual accuracy would be better than the fitted curve.

Finally, we also investigated the minimum difference of connection weights that the IG method is able to distinguish. Note that the current framework of the IG approach estimates the sum of connection weights, $(J_{ij} + J_{ji})$, not an individual weight. We simulated a network of 1000 neurons for which the connection was distributed subject to $N(1/N, 1/N)$ where $N = 1000$. We modified the sum of connection weights $(J_{12} + J_{21})$ from -7/N (-7J) to 12/N (12J) in a discrete step size of 1/N, while allowing asymmetry

between J_{12} and J_{21}. Figure 2.8 shows the distribution of $\theta_{ij}^{(4,1000)}$ and $\theta_{ij}^{(5,1000)}$ as the function of discrete increment of $(J_{12} + J_{21})$. Figures 2.8(A) and 2.8(B) are examples for high firing probability ($m = 0$). Figures 2.8(C) and 2.8(D) are examples for low firing probability ($m = 1$). The solid line and error bar represent the mean and the standard error, respectively. The dotted line represents the correct value. Firstly, we observed that the mean is very close to the correct value, showing that the estimation of the sum of connection weights is accurate over the wide range of modulation. Secondly, comparison of the standard error of neighboring distributions suggests that if the sum of connection weights is different three-four times or more, the IG measures will be able to distinguish the connection weights. To verify this observation, we performed Wilcoxon's rank sum test for two samples and obtained the following results. For the distributions separated by three times, such as 1/N (J) and 3/N (3J), 16.7% (Figure 2.8(A)), 16.7% (Figure 2.8(B)), 5.56% (Figure 2.8(C)) and 5.56% (Figure 2.8(D)) of those distributions can be distinguished ($p<0.05$). For the distributions separated by four times, such as 1/N (J) and 4/N (4J), 88.2% (Figure 2.8(A)), 88.2% (Figure 2.8(B)), 82.4% (Figure 2.8(C)) and 76.5% (Figure 2.8(D)) of those distributions can be distinguished ($p<0.05$). For the distributions separated by five times, such as 1/N (J) and 5/N (5J) the IG measures were able to distinguish all of them ($p<0.05$). These results suggest that the sum of connection weights $(J_{12} + J_{21}) = 1/N$ and $(J_{34} + J_{43}) = 4/N$ or *5/N*, where *N* is the number of neurons in the network can be distinguished reliably. All these findings show that the IG approach is a very useful measure for the estimation of connection weights from the observation of spiking activity.

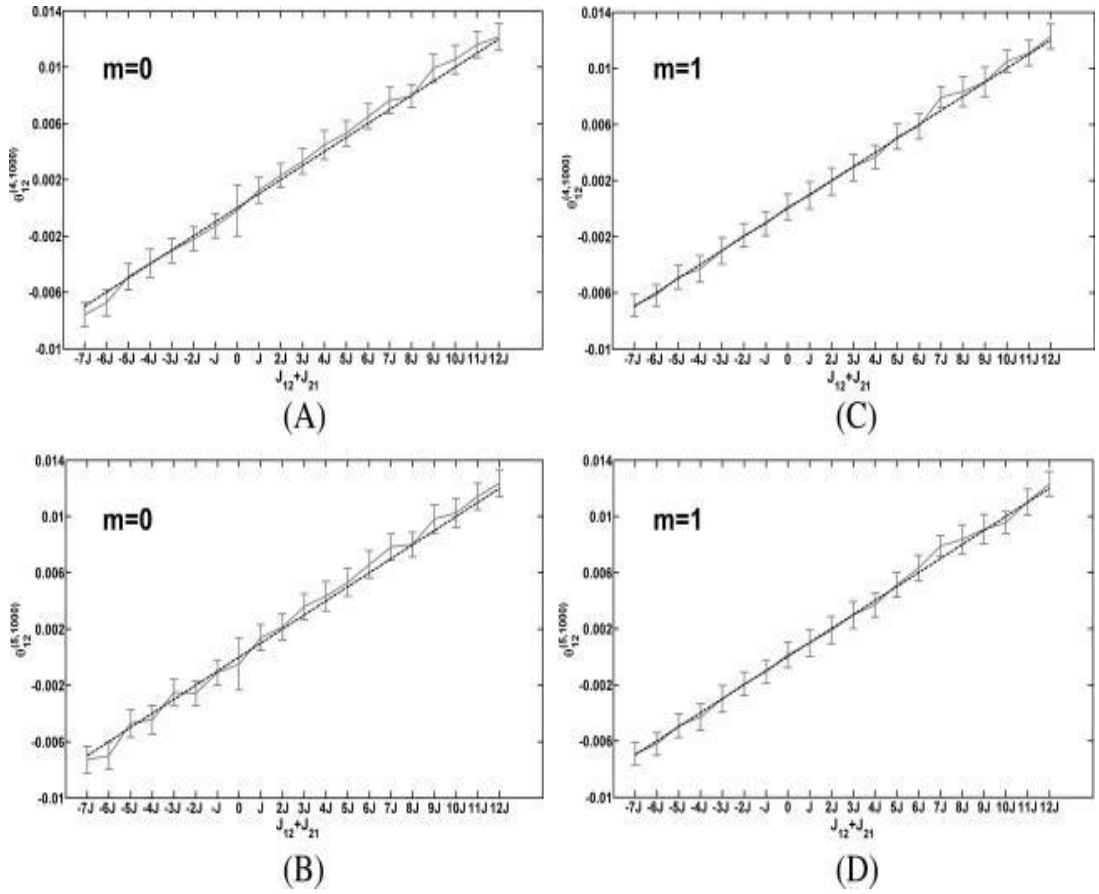

Figure 2.8: The minimum difference of the sum of connection weights $(J_{ij} + J_{ji})$ that can be distinguished by the IG measures.
A network consists of 1000 asymmetrically connected neurons whose connections are distributed subject to $N(m, \sigma^2)$ where $m = 1/1000$ and $\sigma^2 = 1/1000$, respectively. The strength of a common input *W* was set to *5J*, but variation of *W* does not affect the result. The solid line and error bar represent the mean and the standard error, respectively. The dotted line represents the correct value. (A) $\theta_{12}^{(4,1000)}$ for a high firing case ($m = 0$). (B) $\theta_{12}^{(5,1000)}$ for a high firing case ($m = 0$). (C) $\theta_{12}^{(4,1000)}$ for a low firing g case ($m = 1$) (D) $\theta_{12}^{(5,1000)}$ for a low firing case ($m = 1$). The sum of connection weights $(J_{ij} + J_{ji})$ can be distinguished if they are different by four times or more.

2.6 Discussion

In this study, we investigated how to estimate connection weight under the influence of correlated inputs. Our goal was to develop a robust and experimentally applicable

measure by which one can infer the synaptic connection strength between any pair of neurons from extracellularly recorded spike trains. To this end, we extended the previously proposed information geometric approach (Tatsuno, et al., 2009) by taking into account higher log-linear expansion.

Using a simple neural network with stochastic dynamics, we analytically showed that the IG measure, by fully expanded log-linear model, $\theta_{12}^{(N,N)}$, is severely influenced by correlated input when *N* is small ($N = 2, 3, 4$). With the aid of a recursive formula, we successfully calculated $\theta_{12}^{(k,N)}$ for $N = 10$ and $2 \leq k \leq 10$, and showed that the estimation error due to a common input decreases as the network size and the order of the log-linear model increase. To investigate the property of $\theta_{12}^{(k,N)}$ in a more realistic condition, including asymmetric connections and larger network size that can be observed in the real brain (10^3-10^4 connections), we performed numerical simulations. The results suggest that $\theta_{12}^{(4,N)}$ or $\theta_{12}^{(5,N)}$ would provide a robust and accurate estimation of connection strength with approximately a ten percent error. In other words, we found that the two-neuron IG measures taking into account two ($\theta_{12}^{(4,N)}$) or three ($\theta_{12}^{(5,N)}$) additional neural activities provide a good estimation of connection strength even under the influence of a common input. In addition, we also showed that the IG estimation is not dependent on the firing probability and that $\theta_{12}^{(4,N)}$ and $\theta_{12}^{(5,N)}$ can distinguish the sum of connection weights if they are different by four times or more. All these results suggest that the IG method is a promising approach for multi-neuronal spike trains.

In the present study, we investigated the property of the IG measure in an equilibrium state. In real electrophysiological experiments, however, neural firing changes dynamically over time. To analyze such non-stationary data, it is vital to extend the IG approach to a time-dependent situation (Shimazaki, et al., 2012). In addition, the present study focuses on coincident firings only. This corresponds to the lag-zero bin of a cross correlation function. Therefore, it is interesting to consider extension of the IG measures to lagged bins so that a directed connection can be estimated more directly.

Another interesting extension of the present research includes using realistic neuronal models to investigate more detailed properties of the IG measure. Previously, we investigated the performance of the IG method using the Hodgkin-Huxley (HH) model (Hines and Carnevale, 1997; Hodgkin and Huxley, 1952; Lipa, et al., 2006; Lipa, et al., 2007). Under uncorrelated noisy inputs, we showed that the IG measure was linearly related to the sum of connection weights that were measured as the probability of firing of a postsynaptic neuron by a presynaptic spike. We have not conducted an investigation with correlated noisy inputs, but it is a very important question that needs to be answered in future research. Also, it would be worth considering the extension of the IG approach to analog signals such as EEG and local field potentials (LFP).

The proposed IG method relies on successful binary representation by binning spike trains. One way to select bin size is to use a small enough bin, such as a few milliseconds, so that no more than one spike falls in the same bin. Another option would be to calculate interspike interval histograms of all recorded neurons and use the minimal interspike interval as the bin size of all neurons. One of the authors (Tatsuno) has also conducted a

preliminary study on mild violation of binary requirement (allowing a couple of spikes in a single bin and converting them into a single spike), and found that it did not affect the IG result significantly. In principle, binary representation can be obtained by using a small enough bin size. However, in the limit of infinitesimally small bin size, no coincident firing will occur and correlation analyses including the IG method will fail. Therefore, the size of the bin would need to be selected not only by the requirement of binary representation, but also by considering a biologically important time-scale. For example, a bin size of a few milliseconds would be appropriate if one wants to study fine timescale, possibly mono-synaptic interactions. A larger bin size, within the mild violation of binary requirement, would be appropriate if one wants to investigate influences of more poly-synaptic interactions. The size of a bin is an important parameter for the application of the IG approach to real data. The authors suggest that an appropriate bin size should be selected by considering both binary restriction and the time scale of interest. The authors also consider that analysis with different bin sizes should be conducted because it would provide more insights into correlation structures.

To advance our understanding of how the brain works according to neuronal population dynamics, further theoretical and experimental research would be inevitable. In this paper, we showed that the information-geometric approach is a promising analytical tool for spike trains and that it will provide useful information about a possible change of the underlying networks. We hope that an effort for developing a novel analysis method presented here or elsewhere would lead to a break-through finding in neuroscience.

Appendix A

In equations 4.4, 4.6 and 4.7, the second logarithmic terms for high firing probability (m=0) are given by

$$A_2 = 2 + 7e^{2h} + 5e^{4h} + 2e^{2h+2J} + 3e^{4h+2J} + 3e^{2W} + 3e^{2h+2W} + e^{2J+2W} + 3e^{2h+2J+2W} + e^{2h+2J+4W} + 2e^{2J+4W},$$

$$B_2 = 2 + e^{2h} + 3e^{2W} + 5e^{2h+2W} + 5e^{4h+4W} + e^{2J+2W} + e^{2h+2J+2W} + 5e^{2h+2J+4W} + 4e^{2h+4W} + 2e^{2J+4W} + 3e^{4h+2J+4W},$$

$$C_2 = 2 + 2e^{2h} + e^{2h+2J} + 3e^{2W} + 8e^{2h+2W} + e^{2J+2W} + 2e^{2h+2J+2W} + 3e^{4h+2J+2W} + 5e^{4h+2W} + 3e^{2h+2J+4W} + 2e^{2J+4W}$$

$$A_3 = 6 + 30e^{2h} + 42e^{4h} + 18e^{6h} + 12e^{2h+2J} + 8e^{4h+4J} + 8e^{6h+6J} + 28e^{4h+2J} + \cdots + 4e^{4h+6J+4W} + 4e^{2h+4J+4W} + 7e^{2h+6J+6W} + 2e^{4h+6J+6W},$$

$$B_3 = 6 + 9e^{2h} + 3e^{4h} + e^{4h+4J} + 2e^{2h+4J} + 12e^{2W} + 30e^{2h+2W} + 33e^{4h+4W} + \cdots + 6e^{4h+4J+6W} + 6e^{2h+4J+4W} + 14e^{2h+6J+6W} + 6e^{6h+4J+4W} + 8e^{4h+6J+6W},$$

$$C_3 = 6 + 12e^{2h} + 6e^{4h} + 4e^{2h+2J} + 2e^{4h+4J} + 4e^{4h+2J} + 2e^{2h+4J} + \cdots + 7e^{2h+6J+4W} + 8e^{4h+6J+4W} + 10e^{4h+4J+4W} + 11e^{2h+6J+6W} + 4e^{4h+6J+6W}.$$

$$A_4 = 24 + 156e^{2h} + 324e^{4h} + 276e^{6h} + 84e^{8h} + 80e^{2h+2J} + 55e^{4h+4J} + 233e^{6h+6J}$$
$$+ \cdots + 6e^{6h+12J+8W} + 50e^{2h+4J+4W} + 145e^{2h+6J+6W} + 115e^{4h+6J+6W},$$

$$B_4 = 24 + 60e^{2h} + 48e^{4h} + 12e^{6h} + 15e^{4h+4J} + \cdots + 60e^{2W} + 204e^{2h+2W} + 228e^{4h+4W}$$
$$+ \cdots + 15e^{6h+12J+8W} + 60e^{2h+4J+4W} + 213e^{2h+6J+6W} + 65e^{6h+4J+4W} + 249e^{4h+6J+6W},$$

$$C_4 = 24 + 72e^{2h} + 72e^{4h} + 24e^{6h} + 20e^{2h+2J} + \cdots + 60e^{2W} + 20e^{2J+2W}$$
$$+ \cdots + 10e^{2h+12J+4W} + 85e^{2h+4J+4W} + 175e^{2h+6J+6W} + 35e^{6h+4J+4W} + 165e^{4h+6J+6W}.$$

Similarly, the corresponding term for lower firing probability (m=1) are given by

$$A_2 = 2e^{8} + 3e^{2h+4} + 4e^{2h+6} + 3e^{4h+2} + 2e^{4h+4} + e^{2h+2J+2} + e^{2h+2J+4} + 2e^{4h+2J}$$
$$+e^{4h+2J+2} + 3e^{2h+2W+4} + e^{2J+2W+6} + 2e^{2h+2J+2W+2} + e^{2h+2J+2W+4}$$
$$+e^{2h+2J+4W+2} + e^{2J+4W+4} + 3e^{2W+6},$$

$$B_2 = 2e^{8} + e^{2h+6} + 2e^{4h+4W+4} + 3e^{2h+2W+4} + 2e^{2h+2W+6} + e^{2W+2J+6} + e^{2h+2J+2W+4}$$
$$+3e^{2W+6} + 3e^{2h+2J+4W+2} + e^{2h+2J+4W+4} + 3e^{2h+4W+4} + e^{2h+4W+6}$$
$$+3e^{4h+4W+2} + 2e^{2J+4W+4} + 2e^{2J+4W+4h} + e^{4h+2J+4W+2},$$

$$C_2 = 2e^{8} + 2e^{2h+6} + e^{2h+2J+4} + 6e^{2h+2W+4} + 2e^{2h+2W+6} + e^{2J+2W+6} +$$

$$2e^{2h+2W+2J+2}$$

$$+2e^{4h+2J+2W} + 2e^{4h+2J+2W+2} + 3e^{2W+6} + 3e^{4h+2W+2} + 2e^{4h+2W+4}$$

$$+2e^{4h+2J+2W+2} + e^{2h+2J+4W+4} + 2e^{2J+4W+4},$$

$$A_3 = 6e^{12} + 18e^{2h+10} + 12e^{2h+8} + 24e^{4h+6} + 18e^{4h+8} + 12e^{6h+4} + 6e^{6h+6} + \cdots$$

$$+12e^{6h+2J+2} + 2e^{6h+4J+4} + 4e^{4J+4W+8} + 4e^{2J+2W+10} + 6e^{6J+6W+6} + \cdots$$

$$+e^{4h+6J+4W+4} + 7e^{2h+6J+6W+4} + 2e^{4h+6J+6W+2},$$

$$B_3 = 6e^{12} + 9e^{2h+10} + 3e^{4h+8} + 2e^{2h+4J+8} + e^{4h+4J+6} + 12e^{2W+10} + 9e^{4h+4W+8}$$

$$+ \cdots$$

$$+4e^{4h+4J+2W+4} + 2e^{4h+4J+2W+6} + 2e^{4h+6J+2W+4} + 36e^{4h+2J+4W+4} + \cdots$$

$$+2e^{2h+6J+6W+6} + 2e^{6h+4J+4W+4} + 2e^{2h+4J+4W+8},$$

$$C_3 = 6e^{12} + 12e^{2h+10} + 6e^{4h+8} + 4e^{2h+2J+8} + 4e^{4h+2J+6} + 2e^{2h+4J+8} +$$

$$2e^{4h+4J+6} \ldots$$

$$+24e^{4h+6J+2W+4} + 2e^{4h+4J+2W+6} + 2e^{4h+8J+2W+4} + 36e^{4h+2J+4W+4} + \cdots$$

$$+3e^{2h+6J+6W+6} + 3e^{6h+4J+4W+4} + 2e^{2h+4J+4W+8},$$

$$A_4 = 24e^{16} + 144e^{4h+12} + 60e^{2h+12} + 96e^{2h+14} + 180e^{4h+10} + 180e^{6h+8}$$

$$+ 96e^{6h+10}$$

$$+ \cdots + 70e^{6h+6J+6} + 25e^{4h+4J+8} + 60e^{2h+2J+10} + 20e^{2J+2h+12} + 60e^{2J+4h+10}$$

$$+\cdots+24e^{12J+8W+8}+6e^{6h+12J+8W+2}+115e^{4h+6J+6W+6},$$

$$B_4 = 24e^{16}+48e^{2h+12}+60e^{2h+14}+12e^{6h+10}+10e^{2h+4J+12}+6e^{2W+10}$$
$$+9e^{4h+4W+8}$$
$$+\cdots+4e^{4h+4J+2W+4}+2e^{4h+4J+2W+6}+2e^{4h+6J+2W+4}+36e^{4h+2J+4W+4}$$
$$+\cdots+3e^{2h+6J+6W+12}+15e^{6h+4J+4W+8}+10e^{2h+4J+4W+12},$$

$$C_4 = 24e^{16}+72e^{4h+12}+72e^{2h+14}+24e^{6h+10}+15e^{6h+6J+6}+20e^{2h+2J+12}$$
$$+\cdots+52e^{6h+12J+2W+2}+24e^{8h+16J+2W}+6e^{8h+12J+2W+2}+60e^{8h+2W+6}$$
$$+\cdots+140e^{4h+6J+6W+6}+10e^{6h+4J+4W+8}+10e^{2h+4J+4W+12}.$$

Appendix B

We provide all orders of the coincident firings for the three-neuron network in Figure 1(B). They can be derived from equations 3.7, 3.8, 3.9 and 4.1 in the same manner with the two-neuron case.

$$\langle S_1\rangle = \langle S_2\rangle = \langle S_3\rangle$$
$$= a_0 + b_0 g(h) + 2a_1\langle S_1\rangle + a_2\langle S_1S_2\rangle + 2b_1\langle S_1S_0\rangle + b_2\langle S_1S_2S_0\rangle,$$
$$\langle S_0\rangle = g(h),$$
$$\langle S_1S_2\rangle = \langle S_2S_3\rangle = \langle S_1S_3\rangle$$
$$= (a_0+a_1)\langle S_1\rangle + (a_1+a_2)\langle S_1S_2\rangle + (b_0+b_1)\langle S_1S_0\rangle + (b_1+b_2)\langle S_1S_2S_0\rangle$$
$$\langle S_1S_2S_3\rangle = (a_0+2a_1+a_2)\langle S_1S_2\rangle + (b_0+2b_1+b_2)\langle S_1S_2S_0\rangle \quad \text{(B. 1)}$$
$$2\langle S_1S_0\rangle = 2\langle S_2S_0\rangle = 2\langle S_3S_0\rangle$$

$$= (a_0 + b_0 + \langle S_1 \rangle) g(h) + 2(a_1 + b_1)\langle S_1 S_0 \rangle + (a_2 + b_2)\langle S_1 S_2 S_0 \rangle,$$

$$3\langle S_1 S_2 S_0 \rangle = 3\langle S_1 S_3 S_0 \rangle = 3\langle S_2 S_3 S_0 \rangle$$

$$= \langle S_1 S_2 \rangle g(h) + 2(a_0 + b_0 + a_1 + b_1)\langle S_1 S_0 \rangle + 2(a_0 + b_0 + a_1 + b_1)\langle S_1 S_2 S_0 \rangle.$$

$$4\langle S_1 S_2 S_3 S_0 \rangle = \langle S_1 S_2 S_3 \rangle g(h) + 3(a_0 + b_0 + 2a_1 + 2b_1 + a_2 + b_2)\langle S_1 S_2 S_0 \rangle,$$

where

$$a_0 = g(0),$$

$$b_0 = g(W) - g(0),$$

$$a_1 = g(J) - g(0),$$

$$b_1 = g(J + W) - g(J) - g(W) - g(0), \qquad \text{(B. 2)}$$

$$a_2 = g(2J) - 2g(J) + g(0),$$

$$b_2 = g(2J + W) - 2g(J + W) - g(2J) + 2g(J) + g(W) - g(0).$$

Appendix C

We provide all orders of the coincident firings for the four-neuron network in Figure 1(C). They can be derived from equations 3.7, 3.8, 3.9 and 4.1 in the same manner with the two- and three-neuron cases.

$$\langle S_1 \rangle = \langle S_2 \rangle = \langle S_3 \rangle = \langle S_4 \rangle$$

$$= a_0 + b_0 g(h) + 3a_1\langle S_1 \rangle + 3a_2\langle S_1 S_2 \rangle + a_3\langle S_1 S_2 S_3 \rangle$$

$$+3b_1\langle S_1 S_0 \rangle + 3b_2\langle S_1 S_2 S_0 \rangle + b_3\langle S_1 S_2 S_3 S_0 \rangle,$$

$$\langle S_0\rangle = g(h),$$

$$\langle S_1S_2\rangle = \langle S_2S_3\rangle = \langle S_1S_3\rangle = \langle S_1S_4\rangle = \langle S_2S_4\rangle = \langle S_3S_4\rangle$$
$$= (a_0 + a_1)\langle S_1\rangle + 2(a_1 + a_2)\langle S_1S_2\rangle + (a_2 + a_3)\langle S_1S_2S_3\rangle$$
$$+(b_0 + b_1)\langle S_1S_0\rangle + 2(b_1 + b_2)\langle S_1S_2S_0\rangle + (b_1 + b_2)\langle S_1S_2S_0\rangle$$
$$+ (b_2 + b_3)\langle S_1S_2S_3S_0\rangle,$$

$$\langle S_1S_2S_3\rangle = \langle S_1S_2S_4\rangle = \langle S_2S_3S_4\rangle = \langle S_1S_3S_4\rangle$$
$$= (a_0 + 2a_1 + a_2)\langle S_1S_2\rangle + (a_1 + 2a_2 + a_3)\langle S_1S_2S_3\rangle$$
$$+(b_0 + 2b_1 + b_2)\langle S_1S_2S_0\rangle + (b_1 + 2b_2 + b_3)\langle S_1S_2S_3S_0\rangle \qquad \text{(C. 1)}$$

$$\langle S_1S_2S_3S_4\rangle = (a_0 + 3a_1 + 3a_2 + a_3)\langle S_1S_2S_3\rangle + (b_0 + 3b_1 + 3b_2 + b_3)\langle S_1S_2S_3S_0\rangle$$

$$2\langle S_1S_0\rangle = 2\langle S_2S_0\rangle = 2\langle S_3S_0\rangle = 2\langle S_4S_0\rangle$$
$$= (a_0 + b_0 + \langle S_1\rangle)g(h) + 3(a_1 + b_1)\langle S_1S_0\rangle + 3(a_2 + b_2)\langle S_1S_2S_0\rangle$$
$$+(a_3 + b_3)\langle S_1S_2S_3S_0\rangle,$$

$$3\langle S_1S_2S_0\rangle = 3\langle S_1S_3S_0\rangle = 3\langle S_2S_3S_0\rangle = 3\langle S_1S_4S_0\rangle = 3\langle S_2S_4S_0\rangle = 3\langle S_3S_4S_0\rangle$$
$$= \langle S_1S_2\rangle g(h) + 2(a_0 + b_0 + a_1 + b_1)\langle S_1S_0\rangle$$
$$+4(a_1 + b_1 + a_2 + b_2)\langle S_1S_2S_0\rangle + 2(a_2 + b_2 + a_3 + b_3)\langle S_1S_2S_3S_0\rangle.$$

$$4\langle S_1S_2S_3S_0\rangle = 4\langle S_1S_3S_4S_0\rangle = 4\langle S_1S_2S_4S_0\rangle = 4\langle S_2S_3S_4S_0\rangle$$
$$= \langle S_1S_2S_3\rangle g(h) + 3(a_0 + b_0 + 2a_1 + 2b_1 + a_2 + b_2)\langle S_1S_2S_0\rangle$$
$$+3(a_1 + b_1 + 2a_2 + 2b_2 + a_3 + b_3)\langle S_1S_2S_3S_0\rangle$$

$$5\langle S_1S_2S_3S_4S_0\rangle$$
$$= \langle S_1S_2S_3S_4\rangle g(h)$$
$$+ 4(a_0 + b_0 + 3a_1 + 3b_1 + 3a_2 + 3b_2 + a_3 + b_3)\langle S_1S_2S_3S_4S_0\rangle.$$

where

$$a_0 = g(0),$$

$$b_0 = g(W) - g(0),$$

$$a_1 = g(J) - g(0),$$

$$b_1 = g(J + W) - g(J) - g(W) - g(0), \tag{C.2}$$

$$a_2 = g(2J) - 2g(J) + g(0),$$

$$b_2 = g(2J + W) - 2g(J + W) - g(2J) + 2g(J) + g(W) - g(0),$$

$$a_3 = g(3J) - 3g(2J) + 3g(J) - g(0),$$

$$b_3 = g(3J + W) - 3g(2J + W) + 3g(J + W) - g(W) - g(3J) + 3g(2J) - 3g(J) + g(0).$$

Chapter 3 Influence of external inputs and asymmetry of connections on information-geometric measures involving up to ten neuronal interactions

Preface

This chapter refers *Nie, Y. Fellous. J.M. and Tatsuno, M., Influence of External Inputs and Asymmetry of Connections on Information-geometric Measures involving up to Ten-neuronal Interactions, in pressing in Neural Computation, 2014*. This work is the extension of chapter 2, which investigated how information-geometric methods are affected by the combination of uncorrelated and correlated external inputs. The higher order interaction, rather than only pair-wise correlations, among neurons in large neuronal network were systematically studied by both mathematical analysis and numerical simulations. This paper is the first investigation of information-geometric methods involving up to ten-neuronal interactions.

Abstract

The investigation of neural interactions is crucial for understanding information processing in the brain. Recently, an analysis method based on information geometry (IG) has gained increased attention, and the property of the pairwise IG measure has been studied extensively in relation to the two-neuron interaction. However, little is known about the property of IG measures involving more neuronal interactions. In this study, we systematically investigated the influence of external inputs and the asymmetry of connections on the IG measures in cases ranging from one-neuron to ten-neuron interactions. First, the analytical relationship between the IG measures and external inputs

was derived for a network of ten neurons with uniform connections. Our results confirmed that the single and pairwise IG measures were good estimators of the mean background input and of the sum of the connection weights, respectively. For the IG measures involving three to ten neuronal interactions, we found that the influence of external inputs was highly non-linear. Second, by computer simulation, we extended our analytical results to asymmetric connections. For a network of ten neurons, the numerical simulation showed that the behavior of the IG measures in relation to external inputs was similar to the analytical solution obtained for a uniformly connected network. When the network size was increased to one-thousand neurons, the influence of external inputs almost disappeared. This result suggests that all IG measures from one-neuron to ten-neuron interactions are robust against the influence of external inputs. In addition, we also investigated how the strength of asymmetry influenced the IG measures. By simulation with a one-thousand-neuron network, we found that that all the IG measures were robust against the modulation of asymmetry of connections. Our results provide further support for an information-geometric approach, and provide useful insights when these IG measures are applied to real experimental spike data.

3.1. Introduction

The interaction between neurons plays a key role in information processing in the brain. A number of attempts at understanding the contribution of correlations to information processing have been made by studying pairwise and higher-order neural correlations (Abeles and Gerstein, 1988; Aertsen, et al., 1989; Amari, 2009; Brown, et al., 2004; Czanner, et al., 2005; Fellous, et al., 2004; Gerstein and Perkel, 1969; Grun, et al., 2002;

Grun, et al., 2002; Lopes-dos-Santos, et al., 2011; Panzeri and Schultz, 2001; Peyrache, et al., 2009; Shimazaki and Shinomoto, 2007; Shimokawa and Shinomoto, 2009; Zhang, et al., 1998). Recently, information geometry (IG) has provided an information-theoretic approach based on differential geometry, and has been used as a powerful tool for analyzing neuronal activity patterns (Amari, 2001; Amari and Nagaoka, 2000; Amari, et al., 2003; Eleuteri, et al., 2005; Ikeda, 2005; Ince, et al., 2010; Miura, et al., 2006; Nakahara and Amari, 2002; Nakahara, et al., 2006; Nie and Tatsuno, 2012; Ohiorhenuan and Victor, 2011; Shimazaki, et al., 2012; Tatsuno, et al., 2009; Tatsuno and Okada, 2004). The advantages of the IG approach include an orthogonal decomposition of higher-order interactions (Amari, 2001; Amari, 2009; Nakahara and Amari, 2002) and the direct relationship between IG measures and connection weights (Nie and Tatsuno, 2012; Tatsuno, et al., 2009; Tatsuno and Okada, 2004).

Many of the previous theoretical studies, including information geometry, have focused on the pairwise interaction or relatively low orders of interactions. However, since the brain may process information with highly coordinated neural activity, the development of a correlation measure that is capable of estimating interactions with more neurons is important. The IG measures are ideal for this purpose because they can be extended to higher-order interactions in a straightforward manner (Amari, 2001). However, a systematic investigation of the relationship between different orders of IG measures and their dependency on network parameters has not yet been conducted. In this study, we investigated how the IG measures up to ten-neuronal interactions were influenced by a correlated input, a background input, and the asymmetry of connections. First, we derived the analytical relationship between the IG measures and external inputs using a network

of ten neurons that were connected by uniform weights. Second, we extended our investigation to an asymmetrically connected neural network by computer simulation. We investigated how the IG measures were influenced by external inputs and the level of asymmetry of connections.

This study is organized as follows: in Section 2, we introduce information geometry, a model network, and a recursive formula for analytically calculating the IG measures; in Section 3, we describe the analytical relationship between the IG measures and the external inputs for ten neurons that are uniformly connected; in Section 4, we show the numerical results for an asymmetrically connected neural network for up to one-thousand neurons; and in Section 5, we summarize the results and discuss the limitations of the present work and direction for future studies.

3.2. Information geometry, model network, and a recursive formula for analytically calculating the IG measures

3.2.3 Information Geometry

In this section, we describe an information-geometric approach (for further details see (Amari and Nagaoka, 2000). x_i is a binary variable that represents the state of the i-th neuron in cases where it is silent ($x_i = 0$) or has a spike ($x_i = 1$). $p_{x_1 x_2 \dots x_N}$ is the probability of an *N*-neuron system where we assume $p_{x_1 x_2 \dots x_N} > 0$. The full *N*-th order log-linear model (LLM) of an *N*-neuron system is given by:

$$\log p_{x_1 x_2 \ldots x_N} = \sum_i \theta_i^{(N,N)} x_i + \sum_{i<j} \theta_{ij}^{(N,N)} x_i x_j + \cdots$$

$$+ \sum_{i<j<\cdots<m} \theta_{ij,\ldots,m}^{(N,N)} x_i x_j \ldots x_m + \cdots + \theta_{12,\ldots N}^{(N,N)} x_1 x_2 \ldots x_N - \psi(\boldsymbol{\theta})^{(N,N)}, \quad (3.1)$$

where $\theta_{ij,\ldots,m}^{(N,N)}$ $(1 \leq m \leq N)$ represents the m-neuron interaction and $\psi(\boldsymbol{\theta})^{(N,N)}$ is the normalizing factor so that $\sum p_{x_1,x_2,\ldots,x_N} = 1$ (Amari and Nagaoka, 2000). The first and second superscripts represent the order of LLM and the number of neurons in the system, respectively. We call $\theta_{ij,\ldots m}^{(N,N)}$ the m–neuron IG measure of the fully expanded LLM (Tatsuno and Okada, 2004). For simplicity, we also refer to the one-neuron IG measure as the single IG measure, and the two-neuron IG measure as the pairwise IG measure. The first few IG measures and the normalizing factor are expressed as:

$$\theta_i^{(N,N)} = \log \frac{p_{x_1=0,\ldots,x_i=1,\ldots,x_N=0}}{p_{x_1=0,\ldots,x_N=0}},$$

$$\theta_{ij}^{(N,N)} = \log \frac{p_{x_1=0,\ldots,x_i=1,\ldots,x_j=1,\ldots,x_N=0}\, p_{x_1=0,\ldots,x_N=0}}{p_{x_1=0,\ldots,x_i=1,\ldots,x_j=0,\ldots,x_N=0}\, p_{x_1=0,\ldots,x_i=0,\ldots,x_j=1,\ldots,x_N=0}},$$

$$\theta_{ijk}^{(N,N)} = \log \frac{p_{x_i=1,x_j=1,x_k=1;x_{N-i,j,k}=0} p_{x_i=1;x_{N-i}=0} p_{x_j=1;x_{N-j}=0} p_{x_k=1;x_{N-k}=0}}{p_{x_i=1,x_j=1;x_{N-i,j}=0} p_{x_j=1,x_k=1;x_{N-j,k}=0} p_{x_i=1,x_k=1;x_{N-i,k}=0} p_{x_{1:N}=0}},$$

$$\theta_{ijkl}^{(N,N)}$$

$$= \log \left(\frac{p_{x_i=1,x_j=1,x_k=1,x_l=1;x_{N-i,j,k,l}=0} p_{x_i=1,x_j=1;x_{N-i,j}=0} p_{x_i=1,x_k=1;x_{N-i,k}=0}}{p_{x_i=1,x_j=1,x_k=1;x_{N-i,j,k}=0} p_{x_i=1,x_j=1,x_l=1;x_{N-i,j,l}=0} p_{x_i=1,x_k=1,x_l=1;x_{N-i,k,l}=0}} \right.$$

$$\times \frac{p_{x_i=1,x_l=1;x_{N-i,l}=0} p_{x_j=1,x_k=1;x_{N-j,k}=0} p_{x_j=1,x_l=1;x_{N-j,l}=0} p_{x_k=1,x_l=1;x_{N-k,l}=0}}{p_{x_j=1,x_k=1,x_l=1;x_{N-j,k,l}=0} p_{x_i=1;x_{N-i}=0} p_{x_j=1;x_{N-j}=0} p_{x_k=1;x_{N-k}=0}}$$

$$\times \frac{p_{x_{1:N}=0}}{p_{x_l=1;x_{N-l}=0}}\Bigg),$$

… … …

$$\psi(\boldsymbol{\theta})^{(N,N)} = -\log p_{x_1=0,\ldots,x_N=0}, \tag{3.2}$$

where $1 \le i < j < k < l \le N$. Note that for $\theta_{ijk}^{(N,N)}$ and $\theta_{ijkl}^{(N,N)}$, we used the following form of representation:

$$p_{x_i=1,x_j=1,x_k=1;x_{N-i,j,k}=0} = p_{x_1=0,\ldots,x_i=1,\ldots,x_j=1,\ldots,x_k=1,\ldots,x_N=0}$$

$$p_{x_i=1,x_j=1,x_k=1,x_l=1;x_{N-i,j,k,l}=0} = p_{x_1=0,\ldots,x_i=1,\ldots,x_j=1,\ldots,x_k=1,\ldots,x_l=1,\ldots,x_N=0} \tag{3.3}$$

In general terms, the partially expanded *k*-th order LLM of an *N*-neuron system is expressed by:

$$\log p_{x_1 x_2 \ldots x_{k*\ldots*}} = \sum_i \theta_i^{(k,N)} x_i + \sum_{i<j} \theta_{ij}^{(k,N)} x_i x_j + \cdots$$

$$+ \sum_{i<j<\cdots<m} \theta_{ij,\ldots,m}^{(k,N)} x_i x_j \ldots x_m + \cdots + \theta_{12,\ldots k}^{(k,N)} x_1 x_2 \ldots x_k - \psi(\boldsymbol{\theta})^{(k,N)}, \tag{3.4}$$

where $\theta_{12,\ldots m}^{(k,N)}$ $(1 \le m \le k \le N)$ is the m-neuron IG measure of the partially expanded *k*-th order LLM. The first few terms and normalizing factor are given as follows:

$$\theta_i^{(k,N)} = \log \frac{p_{x_1=0,\ldots,x_i=1,\ldots,x_k=0,*\ldots*}}{p_{x_1=0,\ldots,x_k=0,*\ldots*}},$$

$$\theta_{ij}^{(k,N)} = \log \frac{p_{x_1=0,\ldots,x_i=1,\ldots,x_j=1,\ldots,x_k=0,*\ldots*} p_{x_1=0,\ldots,x_k=0,*\ldots*}}{p_{x_1=0,\ldots,x_i=1,\ldots,x_j=0,\ldots,x_k=0,*\ldots*} p_{x_1=0,\ldots,x_i=0,\ldots,x_j=1,\ldots,x_k=0,*\ldots*}},$$

$$\theta_{ijq}^{(k,N)} = \log \frac{p_{x_i=1,x_j=1,x_q=1;x_{k-i,j,q}=0;*} p_{x_i=1;x_{k-i}=0;*} p_{x_j=1;x_{k-j}=0;*} p_{x_q=1;x_{k-q}=0;*}}{p_{x_i=1,x_j=1;x_{k-i,j}=0;*} p_{x_j=1,x_q=1;x_{k-j,q}=0;*} p_{x_i=1,x_q=1;x_{k-i,q}=0;*} p_{x_{1:k}=0;*}},$$

$$\theta_{ijqr}^{(k,N)}$$

$$= \log \left(\frac{p_{x_i=1,x_j=1,x_q=1,x_r=1;x_{k-i,j,q,r}=0;*} p_{x_i=1,x_j=1;x_{k-i,j}=0;*} p_{x_i=1,x_q=1;x_{k-i,q}=0;*}}{p_{x_i=1,x_j=1,x_q=1;x_{k-i,j,q}=0;*} p_{x_i=1,x_j=1,x_r=1;x_{k-i,j,r}=0;*} p_{x_i=1,x_q=1,x_r=1;x_{k-i,q,r}=0;*}} \right.$$

$$\times \frac{p_{x_i=1,x_r=1;x_{k-i,r}=0;*} p_{x_j=1,x_q=1;x_{k-j,q}=0;*} p_{x_j=1,x_r=1;x_{k-j,r}=0;*} p_{x_q=1,x_r=1;x_{k-q,r}=0;*}}{p_{x_j=1,x_q=1,x_r=1;x_{k-j,q,r}=0;*} p_{x_i=1;x_{k-i}=0;*} p_{x_j=1;x_{k-j}=0;*} p_{x_q=1;x_{k-q}=0;*}}$$

$$\left. \times \frac{p_{x_{1:k}=0;*}}{p_{x_r=1;x_{k-r}=0;*}} \right),$$

$$\ldots \ldots \ldots$$

$$\psi(\boldsymbol{\theta})^{(k,N)} = -\log p_{x_1=0,\ldots,x_k=0,*\ldots*}, \tag{3.5}$$

where '$* \ldots *$' represents the marginalization over the (*N-k)* neurons. Also note that for $\theta_{ijq}^{(k,N)}$ and $\theta_{ijqr}^{(k,N)}$, we used the following form of representation:

$$p_{x_i=1,x_j=1,x_q=1;x_{k-i,j,q}=0;*} = p_{x_1=0,\ldots,x_i=1,\ldots,x_j=1,\ldots,x_q=1,\ldots,x_k=0,*\ldots*}$$

$$p_{x_i=1,x_j=1,x_q=1,x_r=1;x_{k-i,j,q,r}=0;*} = p_{x_1=0,\ldots,x_i=1,\ldots,x_j=1,\ldots,x_q=1,\ldots,x_r=1,\ldots,x_k=0,*\ldots*} \quad (3.6)$$

Both $\theta_{ij,\ldots m}^{(N,N)}$ (the IG measure from the full model) and $\theta_{ij,\ldots m}^{(k,N)}$ (the IG measure from the *k*-th order partial model) represent the *m*-neuron interactions. However, note the difference between them; $\theta_{ij,\ldots m}^{(N,N)}$ is calculated from the full information of all *N* neurons. By contrast, $\theta_{ij,\ldots m}^{(k,N)}$ is calculated from the partial information of *k* neurons by marginalizing (*N-k)* neurons. It has been shown that $\theta_{ij,\ldots N}^{(N,N)}$ is statistically orthogonal to any $\langle x_i \rangle$ where $\langle x_i \rangle$ represents the expectation of x_i. On the other hand, $\theta_{ij,\ldots k}^{(k,N)}$ is orthogonal to $\langle x_i \rangle$ for *i* that is included in the *k* neurons (Amari, 2001; Nakahara and Amari, 2002).

To calculate the IG measures, it is often convenient to use the relationship between the marginal and coincident firings ($\langle x_i \rangle, \langle x_i x_j \rangle, \ldots, \langle x_1 x_2 \ldots x_N \rangle$) and the probability of events ($p_{x_1 x_2}, p_{x_1 x_2 x_3} \ldots, p_{x_1 x_2 \ldots x_N}$). For the IG measures with the full LLM, by extending the previous study (Nie and Tatsuno, 2012), we have

$$p_{x_1=0,\ldots,x_N=0} = 1 - \sum_i \langle x_i \rangle + \sum_{i<j} \langle x_i x_j \rangle - \sum_{i<j<k} \langle x_i x_j x_k \rangle + \cdots \pm \langle x_1 x_2 \ldots x_N \rangle,$$

$$p_{0,\ldots 0,x_q=1,0\ldots,0} = \langle x_q \rangle - \sum_{i \neq q} \langle x_q x_i \rangle + \sum_{i,j \neq q} \langle x_q x_i x_j \rangle - \cdots \mp \langle x_1 x_2 \ldots x_N \rangle,$$

$$p_{0,\ldots 0,x_q=1,0\ldots 0,x_r=1,0\ldots,0} = \langle x_q x_r \rangle - \sum_{i \neq q,r} \langle x_q x_r x_i \rangle + \cdots \pm \langle x_1 x_2 \ldots x_N \rangle,$$

$$p_{0,\dots 0,x_q=1,0\dots 0,x_r=1,0\dots,0,x_s=1,0\dots 0} = \langle x_q x_r x_s \rangle - \sum_{i\neq q,r,s} \langle x_q x_r x_s x_i \rangle + \cdots \mp \langle x_1 x_2 \dots x_N \rangle,$$

… … …

$$p_{x_1=1,\dots,x_N=1} = \langle x_1 x_2 \dots x_N \rangle \tag{3.7}$$

where an upper sign (lower sign) at the last term on the right-hand side is taken when *N* is an even (odd) number. Similarly, for the partly expanded *k*-th order IG measures, the formula becomes

$$p_{x_1=0,\dots,0,x_k=0,*\dots*} = 1 - \sum_{i=1}^{k} \langle x_i \rangle + \sum_{i=1}^{k-1} \sum_{j=i+1}^{k} \langle x_i x_j \rangle - \cdots \pm \langle x_1 x_2 \dots x_k \rangle,$$

$$p_{x_1=0,\dots,0,x_q=1,0\dots 0,x_k=0,*\dots*}$$

$$= \langle x_q \rangle - \sum_{i=1,i\neq q}^{k} \langle x_q x_i \rangle + \sum_{i=1,i\neq q}^{k-1} \sum_{j=i+1,j\neq q}^{k} \langle x_q x_i x_j \rangle - \cdots \mp \langle x_1 x_2 \dots x_k \rangle,$$

$$p_{x_1=0,\dots,0,x_q=1,0\dots 0,x_r=1,0\dots 0,x_k=0,*\dots*} = \langle x_q x_r \rangle - \sum_{i=1,i\neq q,r}^{k} \langle x_q x_r x_i \rangle + \cdots \pm \langle x_1 x_2 \dots x_k \rangle$$

$$p_{x_1=0,\dots,0,x_q=1,0\dots 0,x_r=1,0\dots 0,x_s=1,0\dots 0,x_k=0,*\dots*}$$

$$= \langle x_q x_r x_s \rangle - \sum_{i=1,i\neq q,r,s}^{k} \langle x_q x_r x_s x_i \rangle + \cdots \mp \langle x_1 x_2 \dots x_k \rangle$$

… … …

$$p_{x_1=1,\dots,x_k=1,*\dots*} = \langle x_1 x_2 \dots x_k \rangle \tag{3.8}$$

where an upper sign (lower sign) at the last term on the right-hand side is taken when k is an even (odd) number.

In summary, the probability of events ($p_{x_1x_2}, p_{x_1x_2x_3}, \dots, p_{x_1x_2\dots x_k}, \dots, p_{x_1x_2\dots x_N}$) can be calculated from the marginal and coincident firings ($\langle x_i \rangle, \langle x_i x_j \rangle, \dots, \langle x_1 x_2 \dots x_k \rangle, \dots, \langle x_1 x_2 \dots x_N \rangle$) using equation 3.7 for the full LLM, and using equation 3.8 for the partially expanded LLM. The IG measures with any neuronal interactions can be then calculated with equation 3.2 for the full LLM, and with equation 3.5 for the partially expanded LLM. However, performing these calculations for large N is difficult. In addition, obtaining the relationship between ($\langle x_i \rangle, \langle x_i x_j \rangle, \dots, \langle x_1 x_2 \dots x_k \rangle, \dots, \langle x_1 x_2 \dots x_N \rangle$) and network parameters such as external inputs for an arbitrary network structure is not straightforward. Therefore, in the analytical part of this study, we focused on a uniformly connected network of ten neurons. Our goal was to obtain an insight into how the IG measures of up to ten-neuron interactions were related to external inputs. We also expanded the study to include asymmetric connections and a network with more neurons through the use of computer simulation. In the next section, we describe the structure and dynamics of the neural network that we used in this study.

3.2.2 Model Network

3.2.2.1 General Description

We begin with a general description of a network (see Figure 3.1). The network consists of a layer of recurrently connected N neurons n_i $(i = 1, \dots, N)$, where a connection strength from a pre-synaptic neuron (j) to a post-synaptic neuron (i) is represented by J_{ij}. Each neuron in the layer receives a correlated input from a single up-stream neuron n_0 with a connection strength represented by W_{i0}. It also receives a background input h_i. The up-stream neuron n_0 receives a background input h_0. We assume that a background input is a random variable $h_i \sim N(m_i, \sigma_i)$ where $N(m_i, \sigma_i)$ is the normal distribution with the mean (m_i) and variance (σ_i^2). If we let $x_i(t)$ be the state of the i-th neuron at time *t*, the binary value, 0 or 1, correspond to a quiescent and active state, respectively. Under these conditions, the total input to the i-th neuron n_i in the layer and to the up-stream neuron n_0 are written as follows:

$$u_i(t) = \sum_{j \neq i} J_{ij} x_j(t) + W_{i0} x_0(t) + h_i(t), \tag{3.9}$$

$$u_0(t) = h_0(t), \tag{3.10}$$

The first term on the right-hand side of equation 3.9 represents inputs from the neurons in the same layer. The second and third terms on the right-hand side of equation 3.9 represent a correlated input from the up-stream neuron n_0 and uncorrelated background input, respectively.

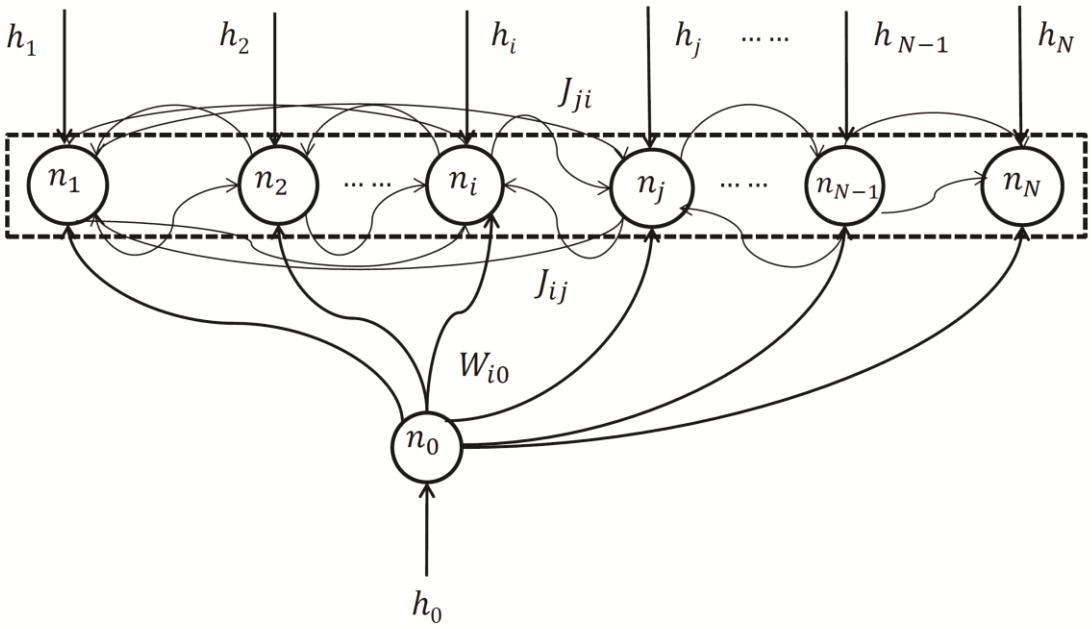

Figure 1

Figure 3.1: Schematic of a network.

Neurons in the upper layer $n_i (i = 1, \dots, N)$ are connected by the connection weight J_{ij} from a pre-synaptic neuron (j) to a post-synaptic neuron (i). Each neuron in the layer receives a correlated input from a single up-stream neuron n_0 with a connection strength represented by W_{i0}. It also receives a background input h_i. The up-stream neuron n_0 receives a background input h_0. A background input is a random variable $h_i \sim N(m_i, \sigma_i)$ where $N(m_i, \sigma_i)$ is the normal distribution with the mean (m_i) and variance (σ_i^2).

The response of the model neuron is stochastic, depending on the total input u_i.

Following the work of Ginzburg and Sompolinsky (1994), the transition rate w between the binary states is written as:

$$w\big(x_i \to (1 - x_i)\big) = \frac{1}{2\tau_0}\{1 - (2x_i - 1)[2g(u_i) - 1]\} \tag{3.11}$$

where τ_0 is a microscopic characteristic time and $g(u_i)$ is a monotonically increasing sigmoidal function whose value is bounded in the interval [0, 1]. The firing probability of a neuronal state variable $\langle x_i(t)\rangle$ is:

$$\tau_0 \frac{d}{dt}\langle x_i(t)\rangle = -\langle x_i(t)\rangle + \langle g(u_i(t))\rangle. \tag{3.12}$$

Note that

$$\langle x_i(t)\rangle = p_{*\ldots*x_i(t)=1*\ldots*} \tag{3.13}$$

is the marginal probability distribution of $x_i(t)$ where the *i*-th neuron takes the value 1, while all the other *N-1* neurons take arbitrary values (0 or 1). Similarly, the coincident firing of the i-th and j-th neurons, $\langle x_i(t)x_j(t)\rangle = p_{*\ldots*,x_i(t)=1,*\ldots*,x_j(t)=1,*\ldots*}$, is expressed as:

$$\tau_0 \frac{d}{dt}\langle x_i(t)x_j(t)\rangle = -2\langle x_i(t)x_j(t)\rangle + \langle x_i(t)g(u_j(t))\rangle + \langle x_j(t)g(u_i(t))\rangle. \tag{3.14}$$

The coincident firing of N neurons, $\langle x_1(t)x_2(t)\ldots x_N(t)\rangle = p_{x_1(t)=1,x_2(t)=1,\ldots,x_N(t)=1}$, is written as:

$$\begin{aligned}\tau_0 \frac{d}{dt}\langle x_1(t)x_2(t)\ldots x_N(t)\rangle = &-N\langle x_1(t)x_2(t)\ldots x_N(t)\rangle \\ &+\langle x_2(t)x_3(t)\ldots x_{N-1}(t)x_N(t)g(u_1(t))\rangle \\ &+\langle x_1(t)x_3(t)\ldots x_{N-1}(t)x_N(t)g(u_2(t))\rangle \\ &+\cdots+\langle x_1(t)x_2(t)\ldots x_{N-2}(t)x_{N-1}(t)g(u_N(t))\rangle\end{aligned} \tag{3.15}$$

For mathematical clarity, we investigate neural interactions when the network is in the equilibrium state. Equations 2.12, 2.14, and 2.15 then reduce to

$$\langle x_i \rangle = \langle g(u_i) \rangle. \tag{3.16}$$

$$\langle x_i x_j \rangle = \frac{1}{2}\big(\langle x_i g(u_j) \rangle + \langle x_j g(u_i) \rangle\big), \tag{3.17}$$

$$\begin{aligned}\langle x_1 x_2 \dots x_N \rangle = \frac{1}{N}(&\langle x_2 x_3 \dots x_{N-1} x_N g(u_1) \rangle \\ &+ \langle x_1 x_3 \dots x_{N-1} x_N g(u_2) \rangle \\ &+ \dots + \langle x_1 x_2 \dots x_{N-2} x_{N-1} g(u_N) \rangle).\end{aligned} \tag{3.18}$$

Note that $\langle x_i \rangle = p_{*\dots*,x_i=1,*\dots*}$, $\langle x_i x_j \rangle = p_{*\dots*,x_i=1,*\dots*,x_j=1,*\dots*}$ and $\langle x_1 x_2 \dots x_N \rangle = p_{x_1=1,x_2=1,\dots,x_N=1}$ do not depend on t.

3.2.2.2 Simplified Network

Our goal for the analytical part of this study is to find the explicit relationship between $(\langle x_i \rangle, \langle x_i x_j \rangle, \dots, \langle x_1 x_2 \dots x_N \rangle, \dots, \langle x_1 x_2 \dots x_N \rangle)$ in equations 3.16, 3.17, and 3.18 and external inputs (a correlated input W_{i0} and a background input h_i). To help facilitate the analytical investigation, we set all recurrent connections to be equal (uniform): $J_{ij} = J$. In addition, for mathematical clarity, we assumed that a connection weight from the up-stream neuron (n_0) to a neuron (n_i) is uniform, and that the background input to a neuron (n_i) has the same mean (h) and variance σ^2 $(h_i \sim N(h, \sigma))$. These assumptions simplified equation 2.9 as follows:

$$u_i(t) = J\sum_{j\neq i} x_j(t) + Wx_0(t) + h_i(t). \tag{3.19}$$

For a sigmoidal activation function $g(u_i)$, we used:

$$g(u_i) = \frac{1+\tanh(u_i - m)}{2} \tag{3.20}$$

where m is a parameter controlling the firing probability of a model neuron.

In the equilibrium limit, the influence of the background input is characterized by its mean value h. In the following section, we investigate how the strength of a correlated input (W) and the mean of a background input (h) influence the IG measures.

3.2.3 Derivation of System Equations in the Equilibrium Limit

3.2.3.1 Two-neuron System

Before we investigate the ten-neuron network, it is instructive to consider a simpler case where the layer contains only two neurons. In the equilibrium limit, equation 3.16 for the two neurons in the layer is written as:

$$\langle x_1\rangle = \langle g(u_1)\rangle = \langle g(Jx_2 + Wx_0 + h)\rangle \tag{3.21}$$

$$\langle x_2 \rangle = \langle g(u_2) \rangle = \langle g(Jx_1 + Wx_0 + h) \rangle \tag{3.22}$$

By taking advantage of the relationship

$$g\big(Jx_j + Wx_0 + h\big) = x_0 x_j g(J + W + h) + x_j(1 - x_0)g(J + h) + \big(1 - x_j\big)x_0 g(W + h) + \big(1 - x_j\big)(1 - x_0)g(h), \tag{3.23}$$

and considering $\langle x_1 \rangle = \langle x_2 \rangle, \langle x_0 x_1 \rangle = \langle x_0 x_2 \rangle$, equations 3.21 and 3.22 reduce to one equation,

$$\langle x_1 \rangle = \langle x_0 x_1 \rangle \big\{ g(J + W + h) - g(W + h) - \big(g(J + h) - g(h)\big) \big\} + \langle x_1 \rangle \{ g(J + h) - g(h) \} + \langle x_0 \rangle \{ g(W + h) - g(h) \} + g(h) \tag{3.24}$$

For an up-stream neuron x_0, we have

$$\langle x_0 \rangle = g(h_0) \tag{3.25}$$

For the joint firing of two neurons, equation 3.17 becomes:

$$\langle x_1 x_2 \rangle = \frac{1}{2} [(\langle x_0 x_1 \rangle + \langle x_0 x_2 \rangle) \{ g(J + W + h) - g(J + h) \} + (\langle x_1 \rangle + \langle x_2 \rangle) g(J + h)], \tag{3.26}$$

$$\langle x_0 x_1 \rangle = \frac{1}{2} [\langle x_0 x_2 \rangle \{ g(J + W + h) - g(W + h) \} + \langle x_0 \rangle g(W + h) + \langle x_1 \rangle g(h)],$$

(3.27)

$$\langle x_0 x_2 \rangle = \frac{1}{2}[\langle x_0 x_1 \rangle \{g(J + W + h) - g(W + h)\} + \langle x_0 \rangle g(W + h) + \langle x_2 \rangle g(h)].$$

(3.28)

Considering $\langle x_1 \rangle = \langle x_2 \rangle, \langle x_0 x_1 \rangle = \langle x_0 x_2 \rangle$, equations 3.27 and 3.28 become identical. Therefore, equations 3.26, 3.27, and 3.28 reduce to two equations,

$$\langle x_1 x_2 \rangle = \langle x_1 x_0 \rangle \{g(J + W + h) - g(J + h)\} + \langle x_1 \rangle g(J + h), \quad (3.29)$$

$$\langle x_0 x_1 \rangle = \frac{1}{2}[\langle x_0 x_1 \rangle \{g(J + W + h) - g(W + h)\} + \langle x_0 \rangle g(W + h) + \langle x_1 \rangle g(h)].$$

(3.30)

For the coincident firing of three neurons, equation 3.18 translates to:

$$\langle x_0 x_1 x_2 \rangle = \frac{1}{3}[(\langle x_0 x_1 \rangle + \langle x_0 x_2 \rangle) g(J + W + h) + \langle x_1 x_2 \rangle g(h_0)]$$

$$= \frac{1}{3}[2\langle x_0 x_1 \rangle g(J + W + h) + \langle x_1 x_2 \rangle g(h_0)]. \quad (3.31)$$

Note that we used $\langle x_0 x_1 \rangle = \langle x_0 x_2 \rangle$ from the first to the second lines on the right-hand side of the equation.

We now have five equations (3.24, 3.25, 3.29, 3.30, and 3.31) for five marginal and coincident firings ($\langle x_0 \rangle$, $\langle x_1 \rangle$, $\langle x_0 x_1 \rangle$, $\langle x_1 x_2 \rangle$ and $\langle x_0 x_1 x_2 \rangle$). By solving these equations simultaneously, we represent the marginal and coincident firings in terms of the network

parameters J, W, h, h_0 and m. We then use these parameters in equations 3.7 or 3.8 to obtain the probability of events such as $p_{x_0}, p_{x_0x_1}, \ldots, p_{x_0x_1x_2}$. Finally, the IG measures for the full LLM are calculated by using equation 3.2 and the IG measures for the partially expanded LLM are calculated by using equation 3.5.

In the following section, we use a simplified notation such as $\langle x_1x_2 \rangle$ for $\langle x_ix_j \rangle$ and $\theta_{12}^{(k,N)}$ for $\theta_{ij}^{(k,N)}$ because all IG measures of the same order in the layer are identical due to the uniform connection assumption.

3.2.3.2 Ten-neuron System

The equations for a ten-neuron system can be obtained by expanding the procedure in the previous section. Therefore, we solved twenty-one equations simultaneously for the following twenty-one marginal and coincident firings: $\langle x_0 \rangle$, $\langle x_1 \rangle$, $\langle x_0x_1 \rangle$, $\langle x_1x_2 \rangle$, $\langle x_0x_1x_2 \rangle$, $\langle x_1x_2x_3 \rangle$, $\langle x_0x_1x_2x_3 \rangle$, $\langle x_1x_2x_3x_4 \rangle$, $\langle x_0x_1x_2x_3x_4 \rangle$, $\langle x_1x_2x_3x_4x_5 \rangle$, $\langle x_0x_1x_2x_3x_4x_5 \rangle$, $\langle x_1x_2x_3x_4x_5x_6 \rangle$, $\langle x_0x_1x_2x_3x_4x_5x_6 \rangle$, $\langle x_1x_2x_3x_4x_5x_6x_7 \rangle$, $\langle x_0x_1x_2x_3x_4x_5x_6x_7 \rangle$, $\langle x_1x_2x_3x_4x_5x_6x_7x_8 \rangle$, $\langle x_0x_1x_2x_3x_4x_5x_6x_7x_8 \rangle$, $\langle x_1x_2x_3x_4x_5x_6x_7x_8x_9 \rangle$, $\langle x_0x_1x_2x_3x_4x_5x_6x_7x_8x_9 \rangle$, $\langle x_1x_2x_3x_4x_5x_6x_7x_8x_9x_{10} \rangle$ and $\langle x_0x_1x_2x_3x_4x_5x_6x_7x_8x_9x_{10} \rangle$. Since space does not allow us to write all twenty-one equations, we provide an equation for the first-order marginal $\langle x_1 \rangle$ as an example in the Appendix.

Next, we analytically calculated the IG measures with all possible neuronal interactions: the one-neuron IG ($\theta_1^{(1,10)}$ - $\theta_1^{(10,10)}$), the two-neuron IG ($\theta_{12}^{(2,10)}$ - $\theta_{12}^{(10,10)}$), the three-

neuron IG ($\theta_{123}^{(3,10)}$ - $\theta_{123}^{(10,10)}$), the four-neuron IG ($\theta_{1234}^{(4,10)}$ - $\theta_{1234}^{(10,10)}$), the five-neuron IG ($\theta_{12345}^{(5,10)}$ - $\theta_{12345}^{(10,10)}$), the six-neuron IG ($\theta_{123456}^{(6,10)}$ - $\theta_{123456}^{(10,10)}$), the seven-neuron IG ($\theta_{1234567}^{(7,10)}$ - $\theta_{1234567}^{(10,10)}$), the eight-neuron IG ($\theta_{12345678}^{(8,10)}$ - $\theta_{12345678}^{(10,10)}$), the nine-neuron IG ($\theta_{123456789}^{(9,10)}$ - $\theta_{123456789}^{(10,10)}$), and the ten-neuron IG ($\theta_{12345678910}^{(10,10)}$). To this end, we took advantage of a simplified network structure where equation 2.2 for the full LLM reduces to:

$$\theta_{123\ldots(2s)}^{(N,N)} = \log \frac{p_{\underbrace{1\ldots1}_{2s}\cdot\underbrace{0\ldots0}_{N-2s}} \cdot p_{\underbrace{1\ldots1}_{2s-2}00\cdot\underbrace{0\ldots0}_{N-2s}}^{\binom{2s}{2}} \cdot p_{\underbrace{1\ldots1}_{2s-4}0000\cdot\underbrace{0\ldots0}_{N-2s}}^{\binom{2s}{4}} \cdots p_{\underbrace{0\ldots0}_{N}}}{p_{\underbrace{1\ldots1}_{2s-1}0\cdot\underbrace{0\ldots0}_{N-2s}}^{\binom{2s}{1}} \cdot p_{\underbrace{1\ldots1}_{2s-3}000\cdot\underbrace{0\ldots0}_{N-2s}}^{\binom{2s}{3}} \cdots p_{1\underbrace{0\ldots0}_{2s-1}\cdot\underbrace{0\ldots0}_{N-2s}}^{\binom{2s}{1}}}, \quad (3.32)$$

$$\theta_{123\ldots(2s+1)}^{(N,N)} = \log \left(\frac{p_{\underbrace{1\ldots1}_{2s+1}\cdot\underbrace{0\ldots0}_{N-(2s+1)}} \cdot p_{\underbrace{1\ldots1}_{2s-1}00\cdot\underbrace{0\ldots0}_{N-(2s+1)}}^{\binom{2s+1}{2}}}{p_{\underbrace{1\ldots1}_{2s}0\cdot\underbrace{0\ldots0}_{N-(2s+1)}}^{\binom{2s+1}{1}} p_{\underbrace{1\ldots1}_{2s-2}000\cdot\underbrace{0\ldots0}_{N-(2s+1)}}^{\binom{2s+1}{3}}} \times \frac{p_{\underbrace{1\ldots1}_{2s-3}0000\cdot\underbrace{0\ldots0}_{N-(2s+1)}}^{\binom{2s+1}{4}} \cdots p_{1\underbrace{0\ldots0}_{2s}\cdot\underbrace{0\ldots0}_{N-(2s+1)}}^{\binom{2s+1}{1}}}{p_{\underbrace{1\ldots1}_{2s-4}000\cdot\underbrace{0\ldots0}_{N-(2s+1)}}^{\binom{2s+1}{5}} \cdots p_{\underbrace{0\ldots0}_{N}}} \right), \quad (3.33)$$

where s is the integer and $\binom{n}{k}$ represents a binomial coefficient. Note that $p_{x_1\ldots x_{2s+1}\cdot x_{2s+2}\ldots x_N}^{\binom{2s+1}{i}}$ expresses possible combinations on the first $(2s+1)$ variables. Similarly, equation 2.5 for the partial LLM reduces to:

$$\theta^{(k,N)}_{123\ldots(2s)} = \log\left(\frac{p_{\underbrace{1\ldots1}_{2s}\cdot\underbrace{0\ldots0}_{k-2s}\cdot\underbrace{*\ldots*}_{N-k}} \cdot p_{\underbrace{1\ldots1}_{2s-2}00\cdot\underbrace{0\ldots0}_{k-2s}\cdot\underbrace{*\ldots*}_{N-k}}^{\binom{2s}{2}}}{p_{\underbrace{1\ldots1}_{2s-1}0\cdot\underbrace{0\ldots0}_{k-2s}\cdot\underbrace{*\ldots*}_{N-k}}^{\binom{2s}{1}} \cdot p_{\underbrace{1\ldots1}_{2s-3}000\cdot\underbrace{0\ldots0}_{k-2s}\cdot\underbrace{*\ldots*}_{N-k}}^{\binom{2s}{3}}} \right.$$

$$\left. \times \frac{p_{\underbrace{1\ldots1}_{2s-4}0000\cdot\underbrace{0\ldots0}_{k-2s}\cdot\underbrace{*\ldots*}_{N-k}}^{\binom{2s}{4}} \cdots p_{\underbrace{0\ldots0}_{k}\cdot\underbrace{*\ldots*}_{N-k}}}{p_{\underbrace{1\ldots1}_{2s-5}000\cdot\underbrace{0\ldots0}_{k-2s}\cdot\underbrace{*\ldots*}_{N-k}}^{\binom{2s}{5}} \cdots p_{1\underbrace{0\ldots0}_{2s-1}\cdot\underbrace{0\ldots0}_{k-2s}\cdot\underbrace{*\ldots*}_{N-k}}^{\binom{2s}{1}}} \right), \qquad (2.34)$$

$$\theta^{(k,N)}_{123\ldots(2s+1)} = \log\left(\frac{p_{\underbrace{1\ldots1}_{2s+1}\cdot\underbrace{0\ldots0}_{k-(2s+1)}\cdot\underbrace{*\ldots*}_{N-k}} \cdot p_{\underbrace{1\ldots1}_{2s-1}00\cdot\underbrace{0\ldots0}_{k-(2s+1)}\cdot\underbrace{*\ldots*}_{N-k}}^{\binom{2s+1}{2}}}{p_{\underbrace{1\ldots1}_{2s}0\cdot\underbrace{0\ldots0}_{k-(2s+1)}\cdot\underbrace{*\ldots*}_{N-k}}^{\binom{2s+1}{1}} \cdot p_{\underbrace{1\ldots1}_{2s-2}000\cdot\underbrace{0\ldots0}_{k-(2s+1)}\cdot\underbrace{*\ldots*}_{N-k}}^{\binom{2s+1}{3}}} \right.$$

$$\left. \times \frac{p_{\underbrace{1\ldots1}_{2s-3}0000\cdot\underbrace{0\ldots0}_{k-(2s+1)}\cdot\underbrace{*\ldots*}_{N-k}}^{\binom{2s+1}{4}} \cdots p_{1\underbrace{0\ldots0}_{2s}\cdot\underbrace{0\ldots0}_{k-(2s+1)}\cdot\underbrace{*\ldots*}_{N-k}}^{\binom{2s+1}{1}}}{p_{\underbrace{1\ldots1}_{2s-4}000\cdot\underbrace{0\ldots0}_{k-(2s+1)}\cdot\underbrace{*\ldots*}_{N-k}}^{\binom{2s+1}{5}} \cdots p_{\underbrace{0\ldots0}_{k}\cdot\underbrace{*\ldots*}_{N-k}}} \right). \qquad (3.35)$$

In the next section, we describe how W (the strength of a correlated input to neurons in the layer) and h (the mean of a background input to the neurons in the layer) influence the IG measures using a simplified ten-neuron network.

3.3. Analytical Study of IG Measures by Uniformly Connected Ten Neurons

In the analytical study in this section, we vary the strength of the correlated input W between *0* and *50J* where *J* is the strength of the intrinsic connection between neurons in a layer. *J* is set to *1/10* following the general scaling rule of $J = 1/N$ where *N* is the number of neurons. The range of values is chosen to cover the strength of correlated inputs that could be observed in the brain. For example, the mossy-fiber from the dentate gyrus to the CA3 region of the hippocampus is known to make a very strong synaptic connection. This strength has been estimated to be five to ten fold of the intrinsic recurrent connections in CA3 (Urban, et al., 2001). Therefore, $W = [0, 50J]$ is wide enough to cover the vast majority of correlated inputs that could be observed experimentally. The strength of the mean background input h is varied between *0* and *5J*. The difference of the range between W and h comes from the different implementation of these inputs. While the correlated input W was modeled with an up-stream neuron n_0, the background input h was implemented as a direct input to each neuron in a layer (see equation 3.19). This was done so that the model was consistent with previous studies (Ginzburg and Sompolinsky, 1994; Nie and Tatsuno, 2012; Tatsuno, et al., 2009; Tatsuno and Okada, 2004). The parameter m that controls the firing probability of a model neuron in equation 3.24 was set to 1. It corresponds to the firing probability of approximately 0.15 when the network receives the weakest inputs ($W = 0, h = 0$), and approximately 0.64 when the network receives the maximum inputs ($W = 50J, h = 5J$).

In the following section, we summarize the results in four categories of the IG measures: the IG measure for a single neuron ($\theta_1^{(k,10)}$), the IG measure for a two-neuron interaction ($\theta_{12}^{(k,10)}$), the IG measures for three to five-neuron interactions ($\theta_{123}^{(k,10)}$, $\theta_{1234}^{(k,10)}$, $\theta_{12345}^{(k,10)}$), and the IG measures for six to ten-neuron interactions ($\theta_{123456}^{(k,10)}$, $\theta_{1234567}^{(k,10)}$, $\theta_{12345678}^{(k,10)}$, $\theta_{123456789}^{(k,10)}$, $\theta_{12345678910}^{(10,10)}$).

3.3.1 The IG Measure for a Single Neuron Interaction, $\boldsymbol{\theta_1^{(k,10)}}$

The IG measure for a single neuron is the coefficient $\theta_i^{(N,N)}$ in the full LLM (equation 3.1) and $\theta_i^{(k,N)}$ in the partially expanded LLM (equation 3.4). Under the condition that there is no correlated input ($W = 0$), a previous study (Tatsuno, et al., 2009) showed that $\theta_i^{(2,N)}$ can be related to an uncorrelated background input h_i such as:

$$\theta_i^{(2,N)} \propto 2(h_i - m) + O\left(\frac{1}{N}\right). \tag{3.36}$$

Below, we investigate the influence of a correlated input W and the mean of a background input h to $\theta_i^{(k,N)}$ where k is systematically varied from one to ten. For a simplified ten-neuron network, $\theta_i^{(k,N)}$ reduces $\theta_1^{(k,N)}$, and is given by:

$$\theta_1^{(N,N)} = \log\frac{p_{1\cdot 000000000}}{p_{0\cdot 000000000}}, \qquad (Full\ LLM) \tag{3.37}$$

$$\theta_1^{(k,N)} = \log \frac{p_{1\cdot \underbrace{0\ldots0}_{k-1}\cdot \underbrace{*\ldots*}_{10-k}}}{p_{0\cdot \underbrace{0\ldots0}_{k-1}\cdot \underbrace{*\ldots*}_{10-k}}}. \qquad (Partial\ LLM) \qquad (3.38)$$

Figures 3.2A shows how $\theta_1^{(k,10)}$ is influenced by a correlated input W in the absence of a background input h (data with a background input was not shown because the overall tendency was the same). The calculation shows that $\theta_1^{(k,10)}$ is linearly related to the strength of W initially, but that it becomes insensitive to it (asymptotic flat line). In addition, the influence of W was decreased with the increase of the order of LLM. In contrast, we found that a background input h was related to $\theta_1^{(k,10)}$ linearly regardless of the existence of W(Figure 3.2B for $W = 0$. Data where $W \neq 0$ was not shown because the overall tendency was same). Furthermore, the figures showed that the linear relationship between $\theta_1^{(k,10)}$ and h described in equation 3.1 holds stronger for the higher-order LLM; the exact relationship $\theta_1^{(10,10)} = 2(h - m)$ being obtained at $k = 10$ (full LLM, Figure 3.2B). In summary, the analytical calculation shows that the single IG measure $\theta_1^{(k,10)}$ is not sensitive to the strength of a correlated input W, but that it is linearly related to the strength of the background input h. In practice, this property could be useful to estimate the relative amount of background input that a neuron receives.

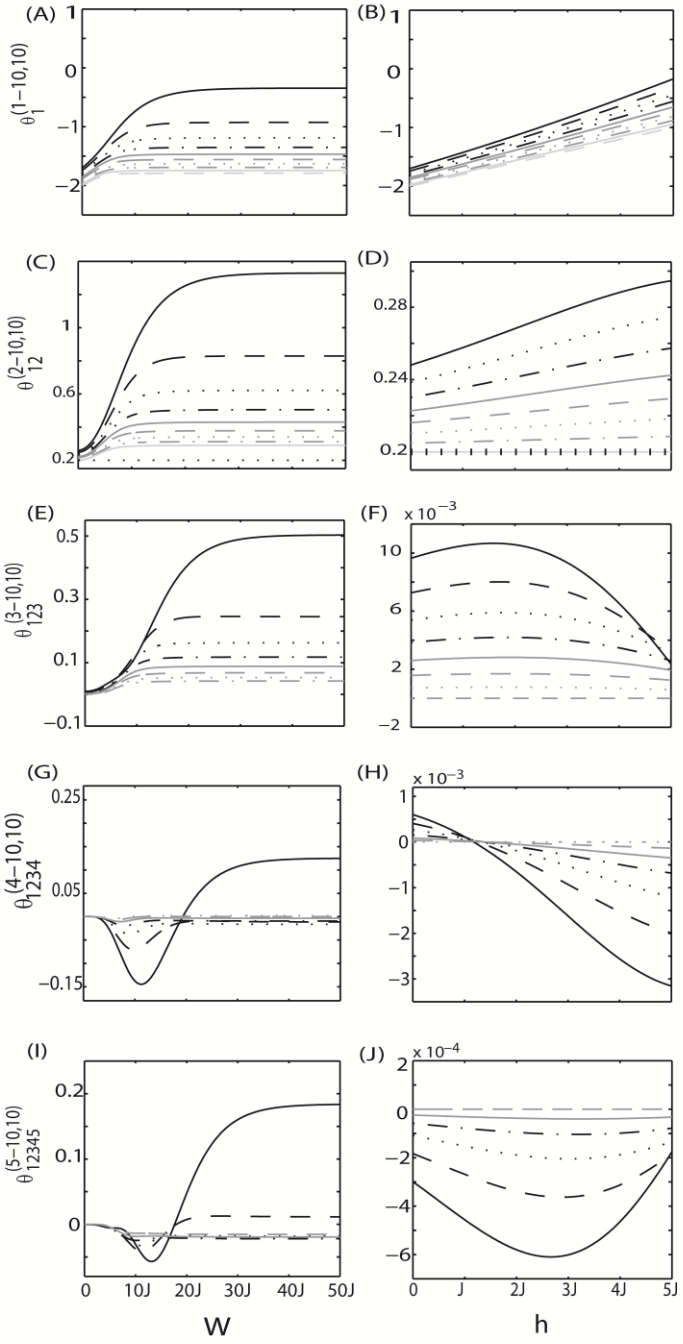

Figure 2

Figure 3.2: Relationship between the IG measures ($\boldsymbol{\theta_1^{(k,10)}}$, $\boldsymbol{\theta_{12}^{(k,10)}}$, $\boldsymbol{\theta_{123}^{(k,10)}}$, $\boldsymbol{\theta_{1234}^{(k,10)}}$, $\boldsymbol{\theta_{12345}^{(k,10)}}$), a correlated input ($\boldsymbol{W}$), and a background input ($\boldsymbol{h}$) for a ten-neuron uniformly connected network

The network parameters are set as $J = 1/10$ and $h_0 = 0.5$. W is modified in the range of $[0, 50J]$ and h is modified in the range of $[0, 5J]$. (A) $\theta_1^{(k,10)}$ when a

correlated input (W) is varied in the absence of a background input ($h = 0$). (B) $\theta_1^{(k,10)}$ when background input (h) is varied in the absence of a correlated input ($W = 0$). $\theta_1^{(1,10)}$, $\theta_1^{(2,10)}$, $\theta_1^{(3,10)}$, $\theta_1^{(4,10)}$, $\theta_1^{(5,10)}$, $\theta_1^{(6,10)}$, $\theta_1^{(7,10)}$, $\theta_1^{(8,10)}$, $\theta_1^{(9,10)}$, and $\theta_1^{(10,10)}$ are represented by a black solid line, a black dashed line, a black dotted line, a black dash-dot line, a gray solid line, a gray dashed line, a gray dotted line, a gray dash-dot line, a light-gray solid line, and a light-gray dashed line. (C) $\theta_{12}^{(k,10)}$when a correlated input (W) is varied in the absence of a background input ($h = 0$). (D) $\theta_{12}^{(k,10)}$ when a background input (h) is varied in the absence of a correlated input ($W = 0$). $\theta_{12}^{(2,10)}$, $\theta_{12}^{(3,10)}$, $\theta_{12}^{(4,10)}$, $\theta_{12}^{(5,10)}$, $\theta_{12}^{(6,10)}$, $\theta_{12}^{(7,10)}$, $\theta_{12}^{(8,10)}$, $\theta_{12}^{(9,10)}$, and $\theta_{12}^{(10,10)}$ are represented by a black solid line, a black dashed line, a black dotted line, a black dash-dot line, a gray solid line, a gray dashed line, a gray dotted line, a gray dash-dot line, and a light-gray solid line. (E) $\theta_{123}^{(k,10)}$when a correlated input (W) is varied in the absence of a background input ($h = 0$). (F) $\theta_{123}^{(k,10)}$ when a background input (h) is varied in the absence of a correlated input ($W = 0$). $\theta_{123}^{(3,10)}$, $\theta_{123}^{(4,10)}$, $\theta_{123}^{(5,10)}$, $\theta_{123}^{(6,10)}$, $\theta_{123}^{(7,10)}$, $\theta_{123}^{(8,10)}$, $\theta_{123}^{(9,10)}$, and $\theta_{123}^{(10,10)}$ are represented by a black solid line, a black dashed line, a black dotted line, a black dash-dot line, a gray solid line, a gray dashed line, a gray dotted line, and a gray dash-dot line. (G) $\theta_{1234}^{(k,10)}$ when a correlated input (W) is varied in the absence of a background input ($h = 0$). (H) $\theta_{1234}^{(k,10)}$ when a background input (h) is varied in the absence of a correlated input ($W = 0$). $\theta_{1234}^{(4,10)}$, $\theta_{1234}^{(5,10)}$, $\theta_{1234}^{(6,10)}$, $\theta_{1234}^{(7,10)}$, $\theta_{1234}^{(8,10)}$, $\theta_{1234}^{(9,10)}$, and $\theta_{1234}^{(10,10)}$ are represented by a black solid line, a black dashed line, a black dotted line, a black dash-dot line, a gray solid line, a gray dashed line, and a gray dotted line. (I) $\theta_{12345}^{(k,10)}$ when a correlated input (W) is varied in the absence of a background input ($h = 0$). (J) $\theta_{12345}^{(k,10)}$ when a background input (h) is varied in the absence of a correlated input ($W = 0$). $\theta_{12345}^{(5,10)}$, $\theta_{12345}^{(6,10)}$, $\theta_{12345}^{(7,10)}$, $\theta_{12345}^{(8,10)}$, $\theta_{12345}^{(9,10)}$, and $\theta_{12345}^{(10,10)}$ are represented by a black solid line, a black dashed line, a black dotted line, a black dash-dot line, a gray solid line, and a gray dashed line.

3.3.2 The IG Measure for a Two-neuron Interaction, $\boldsymbol{\theta_{12}^{(k,10)}}$

The IG measure for a two-neuron interaction $\theta_{ij}^{(k,N)}$ has been extensively studied because it represents an interaction between two neurons (Amari, 2001). It has been shown that the measure is statistically independent from firing rate modulation (Amari, 2009;

Nakahara and Amari, 2002). Under the assumption that there is no correlated input ($W = 0$), it has also been shown that it is directly related to the sum of connection weights (Tatsuno, et al., 2009),

$$\theta_{ij}^{(2,N)} \propto \left(J_{ij} + J_{ji}\right) + O\left(\frac{1}{N}\right), \qquad (Asymmetric\ connection) \quad (3.39)$$

$$\theta_{ij}^{(2,N)} \propto 2J_{ij} + O\left(\frac{1}{N}\right). \qquad (Symmetric\ connection) \quad (3.40)$$

Furthermore, even under the influence of a correlated input W, it has been shown that the pairwise measure with the fourth or fifth-order LLM, $\theta_{ij}^{(4,N)}$ or $\theta_{ij}^{(5,N)}$, is able to estimate the connection weight provided that the size of the network is sufficiently large ($N = 10^3 - 10^4$) (Nie and Tatsuno, 2012).

For the simplified ten-neuron network, the pairwise IG measure is calculated as:

$$\theta_{12}^{(N,N)} = \log\frac{p_{11\cdot 00000000}\, p_{00\cdot 00000000}}{p_{10\cdot 00000000}\, p_{01\cdot 00000000}}, \qquad (Full\ LLM) \qquad (3.41)$$

$$\theta_{12}^{(k,N)} = \log\frac{p_{11\cdot \underbrace{0\ldots0}_{k-2}\cdot \underbrace{*\ldots*}_{10-k}}\, p_{00\cdot \underbrace{0\ldots0}_{k-2}\cdot \underbrace{*\ldots*}_{10-k}}}{p_{10\cdot \underbrace{0\ldots0}_{k-2}\cdot \underbrace{*\ldots*}_{10-k}}\, p_{01\cdot \underbrace{0\ldots0}_{k-2}\cdot \underbrace{*\ldots*}_{10-k}}}. \qquad (Partial\ LLM) \qquad (3.42)$$

Here, we analytically investigated the influence of a correlated input W and a background input h on $\theta_{12}^{(k,10)}$ where k was systematically varied from two to ten. When W was modified, $\theta_{12}^{(k,10)}$ was affected but to a lesser extent for higher-order k of the LLM (see

Figure 2C). Interestingly, when a background input existed, $\theta_{12}^{(k,10)}$ was less likely affected by the correlated input (data not shown). Note that $\theta_{12}^{(k,10)} = 0.2 = 2J$ is the correct answer for estimating the sum of the connection weights (a horizontal dashed line). When h was modified, $\theta_{12}^{(k,10)}$ was weakly affected when there was no correlated input (see Figure 4.2D). For the full LLM ($k = 10$), $\theta_{12}^{(k,10)}$ was completely independent from the modulation of h, providing the correct answer of 0.2 ($2J = 0.2$, the horizontal dashed line). When a correlated input existed, the value of $\theta_{12}^{(k,10)}$ was affected more severely, especially when the order of LLM k was low (data not shown).

In summary, the analysis shows that the pairwise IG measure $\theta_{12}^{(k,10)}$ is a good estimator of the sum of connection weights, even under the influence of both a correlated input W and a background input h. This is especially true if the order of LLM k is high. In practice, the calculation of $\theta_{12}^{(10,10)}$ might not be easy to obtain because of the limited size of experimental data. However, as we previously discussed, $\theta_{12}^{(4,N)}$ or $\theta_{12}^{(5,N)}$ would provide a reasonable estimation of connection weights provided that the size of the network is large (for example, N=1000) (Nie and Tatsuno, 2012). Therefore, $\theta_{12}^{(k,N)}$ could be a useful measure for estimating the sum of connection weights in electrophysiological recordings.

3.3.3 The IG Measures for Three to Five-Neuron Interactions, ($\boldsymbol{\theta}_{\mathbf{123}}^{(\boldsymbol{k},\mathbf{10})}$, $\boldsymbol{\theta}_{\mathbf{1234}}^{(\boldsymbol{k},\mathbf{10})}$, $\boldsymbol{\theta}_{\mathbf{12345}}^{(\boldsymbol{k},\mathbf{10})}$)

To investigate whether the brain processes information with higher-order neural interactions, several studies have started using the IG measures with a couple of neuronal interactions (Ganmor, et al., 2011; Ohiorhenuan, et al., 2010; Shimazaki, et al., 2012). Therefore, it is important to understand how the IG measures at these interaction levels are influenced by correlated and background inputs. For the simplified ten-neuron network, they are calculated as:

$$\theta_{123}^{(10,10)} = \log\frac{p_{111\cdot 0000000}\,p_{001\cdot 0000000}\,p_{010\cdot 0000000}\,p_{100\cdot 0000000}}{p_{011\cdot 0000000}\,p_{101\cdot 0000000}\,p_{110\cdot 0000000}\,p_{000\cdot 0000000}}, \quad (Full\ LLM) \qquad (3.43)$$

$$\theta_{123}^{(k,10)} = \log\frac{p_{111\cdot\underbrace{0\ldots0}_{k-3}\cdot\underbrace{*\ldots*}_{10-k}}\,p_{001\cdot\underbrace{0\ldots0}_{k-3}\cdot\underbrace{*\ldots*}_{10-k}}\,p_{010\cdot\underbrace{0\ldots0}_{k-3}\cdot\underbrace{*\ldots*}_{10-k}}\,p_{100\cdot\underbrace{0\ldots0}_{k-3}\cdot\underbrace{*\ldots*}_{10-k}}}{p_{011\cdot\underbrace{0\ldots0}_{k-3}\cdot\underbrace{*\ldots*}_{10-k}}\,p_{101\cdot\underbrace{0\ldots0}_{k-3}\cdot\underbrace{*\ldots*}_{10-k}}\,p_{110\cdot\underbrace{0\ldots0}_{k-3}\cdot\underbrace{*\ldots*}_{10-k}}\,p_{000\cdot\underbrace{0\ldots0}_{k-3}\cdot\underbrace{*\ldots*}_{10-k}}}, \quad (Partial\ LLM) \qquad (3.44)$$

$$\theta_{1234}^{(10,10)} = \log\frac{p_{1111\cdot 000000}\cdot p_{0011\cdot 000000}\cdot p_{0000\cdot 000000}^{\binom{4}{2}}}{p_{0111\cdot 000000}^{\binom{4}{1}}\cdot p_{0001\cdot 000000}^{\binom{4}{1}}}, \qquad (Full\ LLM) \qquad (3.45)$$

$$\theta_{1234}^{(k,10)} = \log\frac{p_{1111\cdot\underbrace{0\ldots0}_{k-4}\cdot\underbrace{*\ldots*}_{10-k}}\cdot p_{0011\cdot\underbrace{0\ldots0}_{k-4}\cdot\underbrace{*\ldots*}_{10-k}}^{\binom{4}{2}}\cdot p_{0000\cdot\underbrace{0\ldots0}_{k-4}\cdot\underbrace{*\ldots*}_{10-k}}}{p_{0111\cdot\underbrace{0\ldots0}_{k-4}\cdot\underbrace{*\ldots*}_{10-k}}^{\binom{4}{1}}\cdot p_{0001\cdot\underbrace{0\ldots0}_{k-4}\cdot\underbrace{*\ldots*}_{10-k}}^{\binom{4}{1}}}, \quad (Partial\ LLM) \qquad (3.46)$$

$$\theta_{12345}^{(10,10)} = \log\frac{p_{11111\cdot 00000}\cdot p_{00111\cdot 00000}^{\binom{5}{2}}\cdot p_{00001\cdot 00000}^{\binom{5}{1}}}{p_{01111\cdot 00000}^{\binom{5}{1}}\cdot p_{00011\cdot 00000}^{\binom{5}{2}}\cdot p_{00000\cdot 00000}}, \quad (Full\ LLM) \qquad (3.47)$$

$$\theta_{12345}^{(k,10)}$$

$$= \log \frac{p_{11111\cdot\underbrace{0\ldots0}_{k-5}\cdot\underbrace{*\ldots*}_{10-k}}{}^{\binom{5}{2}} \cdot p_{00111\cdot\underbrace{0\ldots0}_{k-5}\cdot\underbrace{*\ldots*}_{10-k}}{}^{\binom{5}{1}} \cdot p_{00001\cdot\underbrace{0\ldots0}_{k-5}\cdot\underbrace{*\ldots*}_{10-k}}}{p_{01111\cdot\underbrace{0\ldots0}_{k-5}\cdot\underbrace{*\ldots*}_{10-k}}{}^{\binom{5}{1}} \cdot p_{00011\cdot\underbrace{0\ldots0}_{k-5}\cdot\underbrace{*\ldots*}_{10-k}}{}^{\binom{5}{2}} \cdot p_{00000\cdot\underbrace{0\ldots0}_{k-5}\cdot\underbrace{*\ldots*}_{10-k}}}, \quad (Partial\ LLM) \quad (3.48)$$

Note that $\binom{m}{i}$ represents a binomial coefficient and that $p_{x_1\ldots x_m\cdot x_{m+1}\ldots x_{10}}{}^{\binom{m}{i}}$ runs over the possible combinations on the first m variables.

The analytical results for $\theta_{123}^{(k,10)}$, $\theta_{1234}^{(k,10)}$ and $\theta_{12345}^{(k,10)}$ are plotted from Figures 4.2E to 4.2J. When a correlated input W is 0, all the measures are zero regardless of the existence of a background input h (see Figures 4.2E, 4.2G and 4.2I). Since the network reduces to a Hopfield-type network where $W = 0$, the result is consistent with the finding that the energy function has terms only up to the second order. For $W > 0$, the IG measures deviate from 0 because a non-zero W introduces higher-order interactions. The analytical calculation shows that $\theta_{123}^{(k,10)}$ is affected monotonically by W (see Figure 4.2E) while $\theta_{1234}^{(k,10)}$ and $\theta_{12345}^{(k,10)}$ are influenced in a non-linear manner (see Figures 4.2G and 4.2I). Interestingly, $\theta_{123}^{(k,10)}$ was less affected by W if there was a background input h (data not shown), as was the case for the pairwise IG measure $\theta_{12}^{(k,10)}$. This tendency was not obvious for the other IG measures $\theta_{1234}^{(k,10)}$ and $\theta_{12345}^{(k,10)}$. For all the IG measures investigated here, the values approach zero when the order of LLM k increases. When a background input h is varied, the IG measures stay very close to 0 if there is no correlated input W (see Figures 4.2F, 4.2H and 4.2J). However, when $W > 0$, the IG measures are more

strongly influenced (data not shown). The range of modulation for $W > 0$ was approximately on the order of 0.1, almost $10 - 10^3$ times larger than when $W = 0$. The values approach zero when the order of LLM k increases, suggesting that the IG measures calculated by higher-order LLM may be more robust to interferences from a background input h.

In summary, the analysis shows that the IG measures for three to five-neuron interactions are affected by a correlated input W in a highly non-linear manner. The influence by a background input h was insignificantly small if the correlated input did not exist, but it increased significantly when the correlated input was present.

3.3.4 The IG Measures for Six to Ten-Neuron Interactions, ($\boldsymbol{\theta}^{(k,10)}_{123456}$, $\boldsymbol{\theta}^{(k,10)}_{1234567}$, $\boldsymbol{\theta}^{(k,10)}_{12345678}$, $\boldsymbol{\theta}^{(k,10)}_{123456789}$, $\boldsymbol{\theta}^{(10,10)}_{12345678910}$)

The IG measures with this many neuronal interactions have not yet been used in data analysis. However, recent developments in recording technology should allow for the simultaneous recording of a large number of neurons in the near future. Therefore, it is important to investigate how these IG measures are influenced by correlated and background inputs. They are calculated as follows:

$$\theta_{123456}^{(10,10)}$$

$$= \log \frac{p_{111111\cdot 0000} \cdot p_{001111\cdot 0000}{}^{\binom{6}{2}} \cdot p_{000011\cdot 0000}{}^{\binom{6}{2}} \cdot p_{000000\cdot 0000}}{p_{011111\cdot 0000}{}^{\binom{6}{1}} \cdot p_{000111\cdot 0000}{}^{\binom{6}{3}} \cdot p_{000001\cdot 0000}{}^{\binom{6}{1}}}, (Full\ LLM) (3.49)$$

$$\theta_{123456}^{(k,10)} = \log \left(\frac{p_{111111\cdot \underbrace{0\ldots0}_{k-6}\cdot \underbrace{*\ldots*}_{10-k}} \cdot p_{001111\cdot \underbrace{0\ldots0}_{k-6}\cdot \underbrace{*\ldots*}_{10-k}}{}^{\binom{6}{2}}}{p_{011111\cdot \underbrace{0\ldots0}_{k-6}\cdot \underbrace{*\ldots*}_{10-k}}{}^{\binom{6}{1}} \cdot p_{000111\cdot \underbrace{0\ldots0}_{k-6}\cdot \underbrace{*\ldots*}_{10-k}}{}^{\binom{6}{3}}} \right.$$

$$\left. \times \frac{p_{000011\cdot \underbrace{0\ldots0}_{k-6}\cdot \underbrace{*\ldots*}_{10-k}}{}^{\binom{6}{2}} \cdot p_{000000\cdot \underbrace{0\ldots0}_{k-6}\cdot \underbrace{*\ldots*}_{10-k}}}{p_{000001\cdot \underbrace{0\ldots0}_{k-6}\cdot \underbrace{*\ldots*}_{10-k}}{}^{\binom{6}{1}}} \right). \quad (Partial\ LLM) (3.50)$$

$$\theta_{1234567}^{(10,10)} = \log \left(\frac{p_{1111111\cdot 000} \cdot p_{0011111\cdot 000}{}^{\binom{7}{2}}}{p_{0111111\cdot 000}{}^{\binom{7}{1}} \cdot p_{0001111\cdot 000}{}^{\binom{7}{3}}} \right.$$

$$\left. \times \frac{p_{0000111\cdot 000}{}^{\binom{7}{3}} \cdot p_{0000001\cdot 000}{}^{\binom{7}{1}}}{p_{0000011\cdot 000}{}^{\binom{7}{2}} \cdot p_{0000000\cdot 000}} \right), \quad (Full\ LLM)\ (3.51)$$

$$\theta_{1234567}^{(k,10)} = \log \left(\frac{p_{1111111\cdot \underbrace{0\ldots0}_{k-7}\cdot \underbrace{*\ldots*}_{10-k}} \cdot p_{0011111\cdot \underbrace{0\ldots0}_{k-7}\cdot \underbrace{*\ldots*}_{10-k}}{}^{\binom{7}{2}}}{p_{0111111\cdot \underbrace{0\ldots0}_{k-7}\cdot \underbrace{*\ldots*}_{10-k}}{}^{\binom{7}{1}} \cdot p_{0001111\cdot \underbrace{0\ldots0}_{k-7}\cdot \underbrace{*\ldots*}_{10-k}}{}^{\binom{7}{3}}} \right.$$

$$\left. \times \frac{p_{0000111\cdot \underbrace{0\ldots0}_{k-7}\cdot \underbrace{*\ldots*}_{10-k}}{}^{\binom{7}{3}} \cdot p_{0000001\cdot \underbrace{0\ldots0}_{k-7}\cdot \underbrace{*\ldots*}_{10-k}}{}^{\binom{7}{1}}}{p_{0000011\cdot \underbrace{0\ldots0}_{k-7}\cdot \underbrace{*\ldots*}_{10-k}}{}^{\binom{7}{2}} \cdot p_{0000000\cdot \underbrace{0\ldots0}_{k-7}\cdot \underbrace{*\ldots*}_{10-k}}} \right), \quad (Partial\ LLM)\ (3.52)$$

$$\theta_{12345678}^{(10,10)} = \log\left(\frac{p_{11111111\cdot 00}\cdot p_{00111111\cdot 00}^{\binom{8}{2}}\cdot p_{00001111\cdot 00}^{\binom{8}{4}}}{p_{01111111\cdot 00}^{\binom{8}{1}}\cdot p_{00011111\cdot 00}^{\binom{8}{3}}}\right.$$

$$\left.\times\frac{p_{00000011\cdot 00}^{\binom{8}{2}}\cdot p_{00000000\cdot 00}}{p_{00000111\cdot 00}^{\binom{8}{3}}\cdot p_{00000001\cdot 00}^{\binom{8}{1}}}\right), \qquad (Full\ LLM) \quad (3.53)$$

$$\theta_{12345678}^{(k,10)} = \log\left(\frac{p_{11111111\cdot\underbrace{0\dots0}_{k-8}\cdot\underbrace{*\dots*}_{10-k}}\cdot p_{00111111\cdot\underbrace{0\dots0}_{k-8}\cdot\underbrace{*\dots*}_{10-k}}^{\binom{8}{2}}\cdot p_{00001111\cdot\underbrace{0\dots0}_{k-8}\cdot\underbrace{*\dots*}_{10-k}}^{\binom{8}{4}}}{p_{01111111\cdot\underbrace{0\dots0}_{k-8}\cdot\underbrace{*\dots*}_{10-k}}^{\binom{8}{1}}\cdot p_{00011111\cdot\underbrace{0\dots0}_{k-8}\cdot\underbrace{*\dots*}_{10-k}}^{\binom{8}{3}}}\right.$$

$$\left.\times\frac{p_{00000011\cdot\underbrace{0\dots0}_{k-8}\cdot\underbrace{*\dots*}_{10-k}}^{\binom{8}{2}}\cdot p_{00000000\cdot\underbrace{0\dots0}_{k-8}\cdot\underbrace{*\dots*}_{10-k}}}{p_{00000111\cdot\underbrace{0\dots0}_{k-8}\cdot\underbrace{*\dots*}_{10-k}}^{\binom{8}{3}}\cdot p_{00000001\cdot\underbrace{0\dots0}_{k-8}\cdot\underbrace{*\dots*}_{10-k}}^{\binom{8}{1}}}\right), \quad (Partial\ LLM) \quad (3.54)$$

$$\theta_{123456789}^{(10,10)} = \log\left(\frac{p_{111111111\cdot 0}\cdot p_{001111111\cdot 0}^{\binom{9}{2}}\cdot p_{000011111\cdot 0}^{\binom{9}{4}}}{p_{011111111\cdot 0}^{\binom{9}{1}}\cdot p_{000111111\cdot 0}^{\binom{9}{3}}\cdot p_{000001111\cdot 0}^{\binom{9}{4}}}\right.$$

$$\left.\times\frac{p_{000000111\cdot 0}^{\binom{9}{3}}\cdot p_{000000001\cdot 0}^{\binom{9}{1}}}{p_{000000011\cdot 0}^{\binom{9}{2}}\cdot p_{000000000\cdot 0}}\right), \qquad (Full\ LLM) \quad (3.55)$$

$$\theta_{123456789}^{(9,10)} = \log\left(\frac{p_{111111111\cdot *}\cdot p_{001111111\cdot *}^{\binom{9}{2}}\cdot p_{000011111\cdot *}^{\binom{9}{4}}}{p_{011111111\cdot *}^{\binom{9}{1}}\cdot p_{000111111\cdot *}^{\binom{9}{3}}\cdot p_{000001111\cdot *}^{\binom{9}{4}}}\right.$$

$$\left.\times\frac{p_{000000111\cdot *}^{\binom{9}{3}}\cdot p_{000000001\cdot *}^{\binom{9}{1}}}{p_{000000011\cdot *}^{\binom{9}{2}}\cdot p_{000000000\cdot *}}\right), \qquad (Partial\ LLM) \quad (3.56)$$

$$\theta_{12345678910}^{(10,10)} = \log\left(\frac{p_{1111111111}\cdot p_{0011111111}^{\binom{10}{2}}\cdot p_{0000111111}^{\binom{10}{4}}}{p_{0111111111}^{\binom{10}{1}}\cdot p_{0001111111}^{\binom{10}{3}}\cdot p_{0000011111}^{\binom{10}{5}}}\right.$$

$$\times \frac{p_{0000001111}{}^{\binom{10}{4}} \cdot p_{0000000011}{}^{\binom{10}{2}} \cdot p_{0000000000}}{p_{0000000111}{}^{\binom{10}{3}} \cdot p_{0000000001}{}^{\binom{10}{1}}} \Bigg). \qquad (Full\ LLM) \qquad (3.57)$$

Please note that the IG measure for a nine-neuron interaction $\theta^{(k,10)}_{123456789}$ has only one partially expanded LLM ($k = 9$) and the IG measure for a ten-neuron interaction $\theta^{(10,10)}_{12345678910}$ has the full LLM ($k = 10$) only.

The analytical results for $\theta^{(k,10)}_{123456}$, $\theta^{(k,10)}_{1234567}$, $\theta^{(k,10)}_{12345678}$, $\theta^{(k,10)}_{123456789}$ and $\theta^{(10,10)}_{12345678910}$ are shown in Figure 3.3. The general trend of dependency of these measures on correlated and background inputs was similar to that of $\theta^{(k,10)}_{1234}$ and $\theta^{(k,10)}_{12345}$. When $W = 0$, all the measures are zero regardless of the existence of a background input h (see Figures 3.3A, 3.3C, 3.3E, 3.3G and 3.3I). However, when $W > 0$, especially when $W > 0.5\ (= 5J)$, the IG measures deviated from zero in a highly non-linear manner. The values tended to approach zero when the order of LLM k increased; although the trend was less obvious as compared to IG measures involving three to seven neurons. When a background input h is varied, the IG measures stay very close to zero if there is no correlated input W (see Figures 3.3B, 3.3D, 3.3F, 3.3H and 3.3J). When $W > 0$, the IG measures are more strongly influenced (data not shown). The range of modulation was almost $10^3 - 10^5$ fold larger than when $W = 0$. When the order of LLM k increased, the values became less variable.

In summary, this analysis shows that the IG measures for six to ten-neuron interactions are affected by a correlated input W in a highly non-linear manner. The influence by a background input h was insignificantly small if $W = 0$, but increased significantly for $W > 0$.

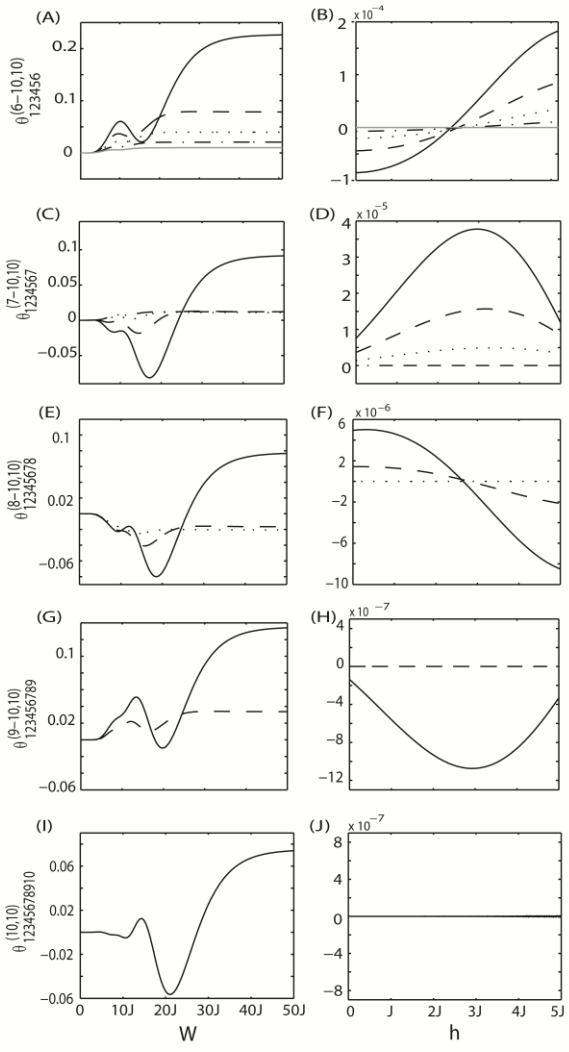

Figure 3

Figure 3.3: Relationship between the IG measures ($\theta^{(k,10)}_{123456}$, $\theta^{(k,10)}_{1234567}$, $\theta^{(k,10)}_{12345678}$, $\theta^{(k,10)}_{123456789}$, $\theta^{(10,10)}_{12345678910}$), a correlated input ($W$), and a background input (h) for a ten-neuron uniformly connected network.

The network parameters are set as $J = 1/10$ and $h_0 = 0.5$. W is modified in the range of $[0, 50J]$ and h is modified in the range of $[0, 5J]$. (A) $\theta_{123456}^{(k,10)}$ when a correlated input (W) is varied in the absence of a background input ($h = 0$). (B) $\theta_{123456}^{(k,10)}$ when background input (h) is varied in the absence of a correlated input ($W = 0$). $\theta_{123456}^{(6,10)}$, $\theta_{123456}^{(7,10)}$, $\theta_{123456}^{(8,10)}$, $\theta_{123456}^{(9,10)}$, and $\theta_{123456}^{(10,10)}$ are represented by a black solid line, a black dashed line, a black dotted line, a black dash-dot line, and a gray solid line. (C) $\theta_{1234567}^{(k,10)}$ when a correlated input (W) is varied in the absence of a background input ($h = 0$). (D) $\theta_{1234567}^{(k,10)}$ when a background input (h) is varied in the absence of a correlated input ($W = 0$). $\theta_{1234567}^{(7,10)}$, $\theta_{1234567}^{(8,10)}$, $\theta_{1234567}^{(9,10)}$, and $\theta_{1234567}^{(10,10)}$ are represented by a black solid line, a black dashed line, a black dotted line, and a black dash-dot line. (E) $\theta_{12345678}^{(k,10)}$ when a correlated input (W) is varied in the absence of a background input ($h = 0$). (F) $\theta_{12345678}^{(k,10)}$ when a background input (h) is varied in the absence of a correlated input ($W = 0$). $\theta_{12345678}^{(8,10)}$, $\theta_{12345678}^{(9,10)}$, and $\theta_{12345678}^{(10,10)}$ are represented by a black solid line, a black dashed line, and a black dotted line. (G) $\theta_{123456789}^{(k,10)}$ when a correlated input (W) is varied in the absence of a background input ($h = 0$). (H) $\theta_{123456789}^{(k,10)}$ when a background input (h) is varied in the absence of a correlated input ($W = 0$). $\theta_{123456789}^{(9,10)}$ and $\theta_{123456789}^{(10,10)}$ are represented by a black solid line and a black dashed line. (I) $\theta_{12345678910}^{(10,10)}$ when a correlated input (W) is varied in the absence of a background input ($h = 0$). (J) $\theta_{12345678910}^{(10,10)}$ when a background input (h) is varied in the absence of a correlated input ($W = 0$). $\theta_{12345678910}^{(10,10)}$ is represented by a black solid line.

3.4. Simulation Study of IG Measures with Asymmetric Connections

Although the analytical relationship between the IG measures and network parameters is useful, we had to apply a strong constraint of uniform connectivity between neurons. We also had to use a small network size of ten neurons to obtain the analytical solutions. These constraints made it difficult to obtain further insights into a more general situation such as asymmetric connections. Therefore, we extended our investigation by using computer simulation.

First, to demonstrate the accuracy of computer simulation, we numerically calculated the IG measures for a uniformly connected ten-neuron network and compared them with the analytical results that were obtained in the previous section. Second, we extended the connections from uniform to asymmetric. We investigated how external inputs (correlated input W and background input h) influenced the IG measures and how the network size affected the relationship. In addition, we also investigated how the magnitude of the asymmetry of connection weights influenced the IG measures.

3.4.1 Comparison between Computer Simulations and Analytical Results

We performed numerical simulations using ten uniformly connected Ginzburg and Sompolinsky neurons (1994). We computed the IG measures from one-neuron interaction ($\theta_1^{(k,10)}$) to ten-neuron interactions ($\theta_{12345678910}^{(10,10)}$) with all possible LLM orders k, corresponding to Figures 3.2 and 3.3. We calculated the IG measures by sampling a correlated input W from 0 to 50J with an increment of 5J. We also calculated the IG measures by sampling a background input h from 0 to 5J with an increment of 0.5J. At each value of W and h, we performed one-hundred simulation trials where each trial consisted of 10^6 updates. The parameter m that controls the firing probability of a model neuron in equation 3.24 was set to 1. The results are reported as the mean $\pm$ SEM.

Figure 3.4 shows the representative examples in which we compare the values of numerical simulations and the corresponding analytical results. For clarity, we showed the results only for the single IG measure $\theta_1^{(k,10)}$ (Figures 3.4A and 3.4B), the pairwise IG

measure $\theta_{12}^{(k,10)}$ (Figures 4C and 4D), the nine-neuron IG measure $\theta_{123456789}^{(k,10)}$ (Figures 3.4E and 3.4F), and the ten-neuron IG measure $\theta_{12345678910}^{(10,10)}$ (Figures 3.4G and 3.4H). We also plotted the results only for the lowest and highest LLM orders$\theta_{1}^{(1,10)}$; and $\theta_{1}^{(10,10)}$ for the single IG measure (Figures 3.4A and 3.4B), $\theta_{12}^{(2,10)}$ and $\theta_{12}^{(10,10)}$ for the pairwise IG measure (Figures 3.4C and 3.4D) , $\theta_{123456789}^{(9,10)}$ and $\theta_{123456789}^{(10,10)}$ for the nine-neuron IG measure (Figures 3.4E and 3.4F), and $\theta_{12345678910}^{(10,10)}$ the ten-neuron IG measure (Figures 4G and 4H). Figure 3.4 shows that the numerical simulations and analytical results strongly agree; all analytical results are included within the mean ± SEM of the values obtained with the numerical simulations. We also confirmed that the same relationship holds true for all the IG measures that were not included in Figure 3.4 and for all possible LLM orders. Taken together, these results demonstrate that the numerical simulation reproduces the analytical result accurately, and that it could be used for investigating the relationship between the IG measures and network parameters in more general settings such as asymmetric connections.

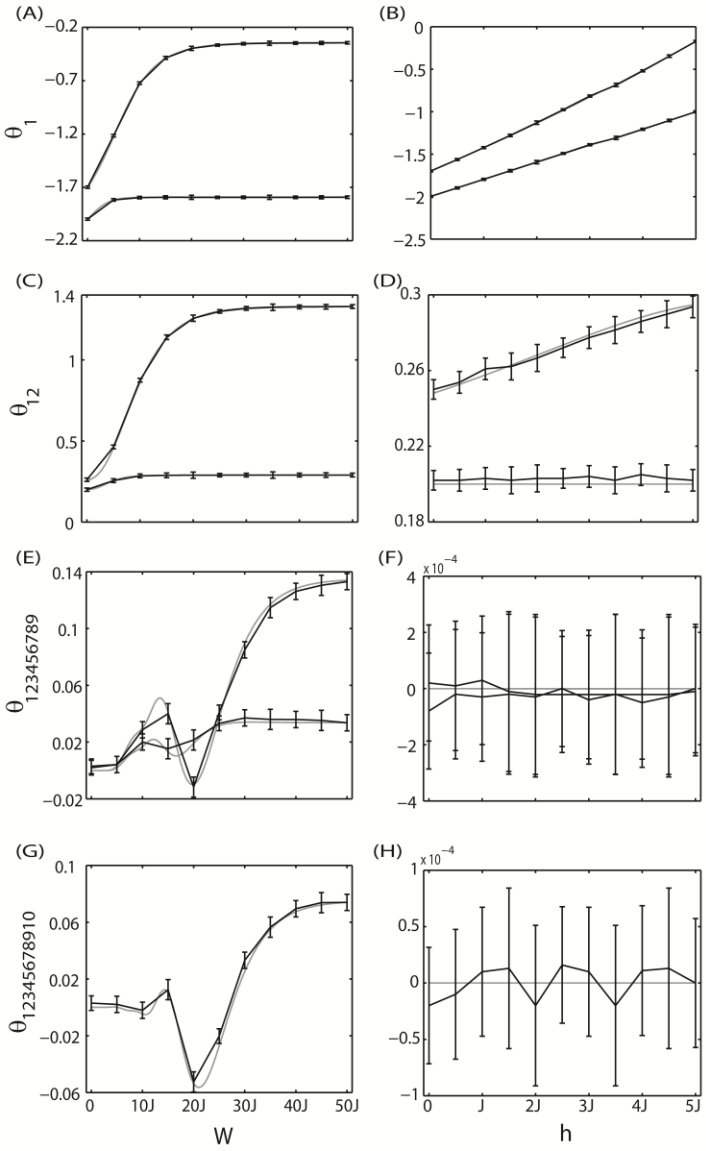

Figure 4

Figure 3.4: Comparison between a numerical simulation and an analytical solution.

The results of one-hundred simulation trials (mean $\pm$ SEM) are plotted against the theoretical calculation in Figures 2 and 3. The network parameters are set as $J = 1/10$ and $h_0 = 0.5$. W is modified in the range of $[0, 50J]$ and h is modified in the range of $[0, 5J]$. The numerical simulations are represented by solid lines with error bars. The analytical solutions are represented by gray lines. (A) Comparison for the single IG measures $\theta_1^{(1,10)}$ and $\theta_1^{(10,10)}$ when correlated input (W) is varied in the absence of a background input $(h = 0)$. (B) Comparison for the single IG measures $\theta_1^{(1,10)}$ and $\theta_1^{(10,10)}$ when background input (h) is varied in the absence of a correlated input $(W = 0)$. (C) Comparison for the pairwise IG

measures $\theta_{12}^{(1,10)}$ and $\theta_{12}^{(10,10)}$ when correlated input (W) is varied in the absence of a background input ($h = 0$). (D) Comparison for the pairwise IG measures $\theta_{12}^{(1,10)}$ and $\theta_{12}^{(10,10)}$ when background input (h) is varied in the absence of a correlated input ($W = 0$). (E) Comparison for the nine-neuron IG measures $\theta_{123456789}^{(1,10)}$ and $\theta_{123456789}^{(10,10)}$ when correlated input (W) is varied in the absence of a background input ($h = 0$). (F) Comparison for the nine-neuron IG measures $\theta_{123456789}^{(1,10)}$ and $\theta_{123456789}^{(10,10)}$ when background input (h) is varied in the absence of a correlated input ($W = 0$). (G) Comparison for the ten-neuron IG measures $\theta_{12345678910}^{(1,10)}$ and $\theta_{12345678910}^{(10,10)}$ when correlated input (W) is varied in the absence of a background input ($h = 0$). (H) Comparison for the ten-neuron IG measures $\theta_{12345678910}^{(1,10)}$ and $\theta_{12345678910}^{(10,10)}$ when background input (h) is varied in the absence of a correlated input ($W = 0$).

3.4.2 Relationship between the IG Measures and External Inputs for Asymmetrically Connected Networks

In this section, we extended a uniformly connected neural network to an asymmetrically connected one. We numerically calculated the IG measures up to ten-neuronal interactions with $N = 10$ and one-thousand neurons. Asymmetric connections were set as $J_{ij} = 1/N + \varepsilon_{ij}$ at each simulation trial, where ε_{ij} was a random number drawn from the normal distribution $\mathrm{N}(m, \sigma^2)$ with the mean $m = 0$ and variance $\sigma^2 = 1/N$, respectively. Without losing generality, we calculated the IG measures for a specific neuron group as follows. For the pairwise IG measure $\theta_{12}^{(k,N)}$, we selected the neurons 1 and 2, and set their connection weights to $J_{12} = 1/N + \varepsilon_{12}$ and $J_{21} = \frac{2}{N} - J_{12}$. In this way, the magnitude of their total connections was kept constant ($J_{12} + J_{21} = 2/N$). The rest of the connections were set following $J_{ij} = 1/N + \varepsilon_{ij}$. Similarly, for the three-neuron IG measure $\theta_{123}^{(k,N)}$, we selected the neurons 1, 2 and 3, and set their connection weights to ($J_{12} = 1/N + \varepsilon_{12}$ and $J_{21} = 2/\mathrm{N} - J_{12}$), ($J_{23} = 1/N + \varepsilon_{23}$ and $J_{32} = 2/N - J_{32}$), and ($J_{31} = 1/N + \varepsilon_{31}$

and $J_{13} = 2/\mathrm{N} - J_{31}$). The rest of the connections were set following $J_{ij} = 1/N + \varepsilon_{ij}$. We used the same procedure for all the other IG measures with four or more neuronal interactions. The influence of a common input W was investigated at two representative values *0* and *10J*. Similarly, the influence of a background input $h_i = h$ was investigated at *0* and *5J*. Each simulation trial consisted of 10^6 updates and one-hundred trials were performed at each W and h values. The parameter m that controls the firing probability of a model neuron in equation 2.24 was set to 1. The results are presented as the mean $\pm$ SEM.

3.4.2.1 The IG Measures for Single and Pairwise Interactions, ($\boldsymbol{\theta_1^{(k,N)}}$, $\boldsymbol{\theta_{12}^{(k,N)}}$)

Figures 3.5A and 3.5B show how the single IG measure $\theta_1^{(k,10)}$ is influenced by a common input W and a background input h, for an asymmetric network of ten neurons. For clarity, we showed the results for the lowest and highest LLM orders only ($k = 1$ (dashed line) and $k = 10$ (solid line)), but we confirmed that the IG measures with $k = 2$ to $k = 9$ reside between $k = 1$ and $k = 10$. The simulation showed that $\theta_1^{(1,10)}$ (dashed line, lowest LLM order) was affected by both the common input and the background input. However, $\theta_1^{(10,10)}$ (solid line, highest LLM order) was robust against the common input and was related to the background input only. Note the similarity between the simulation results in Figure 3.5 and the analytical results for a uniformly connected network in Figure 3.2; $\theta_1^{(1,10)}$ and $\theta_1^{(10,10)}$ at $W = 0$ and $W = 10J$ in Figure 3.5A and those at $W = 0$ and at $W = 1$ in Figure 3.2A are similar. Also, $\theta_1^{(1,10)}$ and $\theta_1^{(10,10)}$at $h = 0$ and $W = 5J$ in Figure 3.5B and those at $h = 0$ and at $h = 0.5$ in Figure 3.2B have

similar values. When the size of the network was increased to N=1000, the influence of a common input became significantly smaller (Figure 5C), even for $\theta_1^{(1,1000)}$ (dashed line, lowest LLM order). Note that the values of $\theta_1^{(10,10)}$ and $\theta_1^{(10,1000)}$ were more consistent than those of $\theta_1^{(1,10)}$ and $\theta_1^{(1,1000)}$, although their network size was one-hundred times different (Figures 3.5A-3.5D). Furthermore, we also confirmed that the values of $\theta_1^{(10,10)}$ and $\theta_1^{(10,1000)}$ were close to the values predicted from equation 3.1, even under the influence of both the common input and the background input (data not shown). This result suggests that $\theta_1^{(1,10)}$ and $\theta_1^{(10,1000)}$, the single IG measure with the highest LLM order in this study, was able to detect the background input correctly even under the influence of the common input.

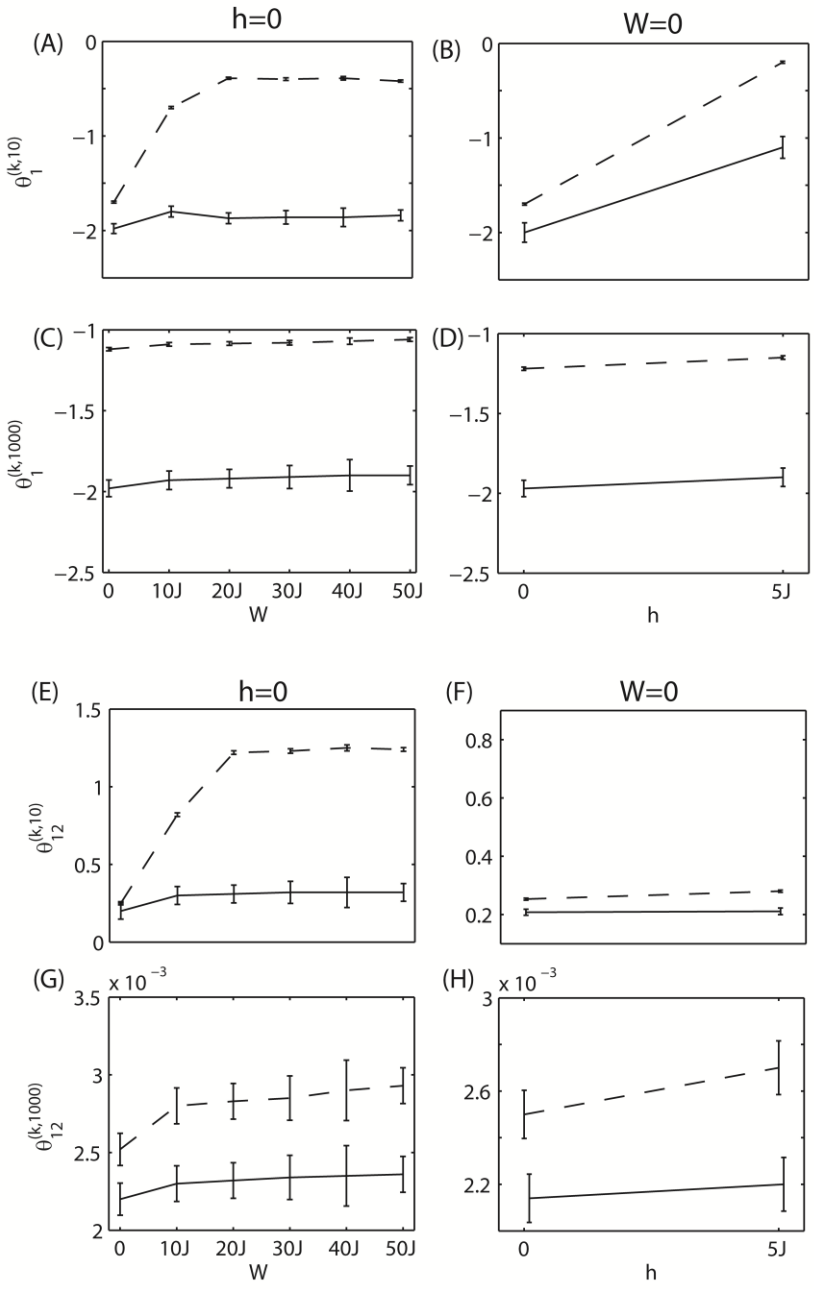

Figure 5

Figure 3.5: Relationship between the IG measures ($\boldsymbol{\theta_1^{(k,N)}}$, $\boldsymbol{\theta_{12}^{(k,N)}}$), a correlated input ($\boldsymbol{W}$), and a background input ($\boldsymbol{h}$) for an asymmetrically connected network.

For a ten-neuron network (N=10), the network parameters are set as $J = 1/10$ and $h_0 = 0.5$. For a one-thousand neuron network (N=1000), the network parameters are set as $J = 1/1000$ and $h_0 = 0.005$. W is sampled at 0 and $10J$ and h is sampled at 0 and $5J$. The IG measures with the lowest LLM order (e.g.,

$\theta_1^{(1,10)}$) are represented by a dashed line. The IG measures with the highest LLM order (e.g., $\theta_1^{(10,10)}$) are represented by a solid line. (A) The single IG measures for a ten-neuron network $\theta_1^{(1,10)}$ and $\theta_1^{(10,10)}$ when a correlated input (W) is varied in the absence of a background input ($h = 0$). (B) The single IG measures for a ten-neuron network $\theta_1^{(1,10)}$ and $\theta_1^{(10,10)}$ when background input (h) is varied in the absence of a correlated input ($W = 0$). (C) The single IG measures for a one-thousand neuron network $\theta_1^{(1,1000)}$ and $\theta_1^{(10,1000)}$ when a correlated input (W) is varied in the absence of a background input ($h = 0$). (D) The single IG measures for a 1000-neuron network $\theta_1^{(1,1000)}$ and $\theta_1^{(10,1000)}$ when background input (h) is varied in the absence of a correlated input ($W = 0$). (E) The pairwise IG measures for a ten-neuron network $\theta_{12}^{(2,10)}$ and $\theta_{12}^{(10,10)}$ when a correlated input (W) is varied in the absence of a background input ($h = 0$). (F) The pairwise IG measures for a ten-neuron network $\theta_{12}^{(2,10)}$ and $\theta_{12}^{(10,10)}$ when background input (h) is varied in the absence of a correlated input ($W = 0$). (G) The pairwise IG measures for a one-thousand neuron network $\theta_{12}^{(2,1000)}$ and $\theta_{12}^{(10,1000)}$ when a correlated input (W) is varied in the absence of a background input ($h = 0$). (H) The pairwise IG measures for a one-thousand neuron network $\theta_{12}^{(2,1000)}$ and $\theta_{12}^{(10,1000)}$ when background input (h) is varied in the absence of a correlated input ($W = 0$).

For the pairwise IG measure $\theta_{12}^{(k,N)}$, the results for an asymmetric network of ten neurons is shown in Figures 3.5E and 3.5F. The desired property of the pairwise IG measure is to detect the two-neuron interaction correctly; $\theta_{12} \sim J_{12} + J_{21} = 0.2$ for N=10.

We observed that $\theta_{12}^{(2,10)}$ (the measure with the lowest LLM order), was strongly influenced by a common input (Figure 3.5E, dashed line), but the influence of a background input was much weaker (Figure 3.5F, dashed line). In contrast, the influence of external inputs to $\theta_{12}^{(10,10)}$ (the measure with the highest LLM order), was much weaker, and $\theta_{12}^{(10,10)}$ was able to estimate the connection weight almost correctly (Figures 3.5E and 3.5F, solid lines). It is also important to note the similarity of $\theta_{12}^{(k,10)}$ values to the corresponding analytical results for a uniform connection (Figures 3.2C and 3.2D). When

the size of the network was increased to N=1000, we observed a similar tendency (Figures 3.5G and 3.5H); $\theta_{12}^{(10,1000)}$ (solid line) was more robust against the external inputs than $\theta_{12}^{(2,1000)}$ (dashed line). Also note that $\theta_{12}^{(10,1000)}$ estimated the connection weight almost correctly; $\theta_{12}^{(10,1000)} \sim J_{12} + J_{21} = 2 \times 10^{-3}$.

In summary, the numerical simulation demonstrated that the single IG measure $\theta_{1}^{(10,N)}$ and the pairwise IG measure $\theta_{12}^{(10,N)}$ (highest LLM order) were able to detect the background input and the sum of connection weights, for an asymmetrically connected network. We also found that the influence of external inputs became less significant for a larger network.

3.4.2.2 The IG Measures for Three to Six-Neuron Interactions, ($\boldsymbol{\theta_{123}^{(k,N)}}$, $\boldsymbol{\theta_{1234}^{(k,N)}}$, $\boldsymbol{\theta_{12345}^{(k,N)}}$, $\boldsymbol{\theta_{123456}^{(k,N)}}$, $\boldsymbol{\theta_{1234567}^{(k,N)}}$, $\boldsymbol{\theta_{12345678}^{(k,N)}}$, $\boldsymbol{\theta_{123456789}^{(k,N)}}$, $\boldsymbol{\theta_{12345678910}^{(k,N)}}$)

The influence of external inputs to the IG measures with intermediate neural interactional levels, $\theta_{123}^{(k,N)}$, $\theta_{1234}^{(k,N)}$, $\theta_{12345}^{(k,N)}$, $\theta_{123456}^{(k,N)}$, is summarized in Figure 3.6, and that with many neural interactional levels, $\theta_{1234567}^{(k,N)}$, $\theta_{12345678}^{(k,N)}$, $\theta_{123456789}^{(k,N)}$, $\theta_{12345678910}^{(k,N)}$, is summarized in Figure 3.7.

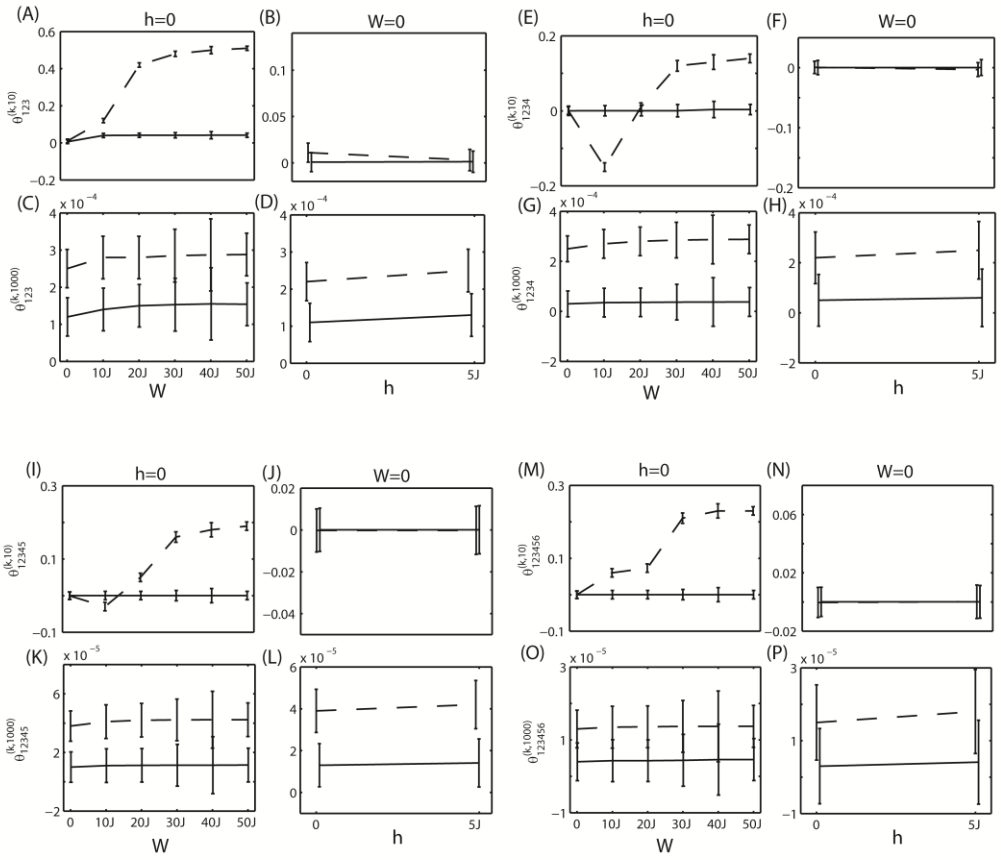

Figure 6

Figure 3.6: Relationship between the IG measures ($\boldsymbol{\theta}^{(\boldsymbol{k},\boldsymbol{N})}_{\mathbf{123}}$, $\boldsymbol{\theta}^{(\boldsymbol{k},\boldsymbol{N})}_{\mathbf{1234}}$, $\boldsymbol{\theta}^{(\boldsymbol{k},\boldsymbol{N})}_{\mathbf{12345}}$, $\boldsymbol{\theta}^{(\boldsymbol{k},\boldsymbol{N})}_{\mathbf{123456}}$), a correlated input ($\boldsymbol{W}$), and a background input ($\boldsymbol{h}$) for an asymmetrically connected network.

For a ten-neuron network (N=10), the network parameters are set as $J = 1/10$ and $h_0 = 0.5$. For a one-thousand neuron network (N=1000), the network parameters are set as $J = 1/1000$ and $h_0 = 0.005$. W is sampled at 0 and $10J$ and h is sampled at 0 and $5J$. The IG measures with the lowest LLM order (e.g., $\theta^{(3,10)}_{123}$) are represented by a dashed line. The IG measures with the highest LLM order (e.g., $\theta^{(10,10)}_{123}$) are represented by a solid line. (A) The three-neuron IG measures for a ten-neuron network $\theta^{(3,10)}_{123}$ and $\theta^{(10,10)}_{123}$ when a correlated input (W) is varied in the absence of a background input ($h = 0$). (B) The three-neuron IG measures for a ten-neuron network $\theta^{(3,10)}_{123}$ and $\theta^{(10,10)}_{123}$ when background input (h) is varied in the absence of a correlated input ($W = 0$). (C) The three-neuron IG measures for a one-thousand neuron network $\theta^{(3,1000)}_{123}$ and $\theta^{(10,1000)}_{123}$ when a correlated input (W) is varied in the absence of a background input ($h = 0$). (D) The three-neuron IG measures for a one-thousand neuron

network $\theta_{123}^{(3,1000)}$ and $\theta_{123}^{(10,1000)}$ when background input (h) is varied in the absence of a correlated input ($W = 0$). (E) The four-neuron IG measures for a ten-neuron network $\theta_{1234}^{(4,10)}$ and $\theta_{1234}^{(10,10)}$ when a correlated input (W) is varied in the absence of a background input ($h = 0$). (F) The four-neuron IG measures for a ten-neuron network $\theta_{1234}^{(4,10)}$ and $\theta_{1234}^{(10,10)}$ when background input (h) is varied in the absence of a correlated input ($W = 0$). (G) The four-neuron IG measures for a one-thousand neuron network $\theta_{1234}^{(4,1000)}$ and $\theta_{1234}^{(10,1000)}$ when a correlated input (W) is varied in the absence of a background input ($h = 0$). (H) The four-neuron IG measures for a one-thousand neuron network $\theta_{1234}^{(4,1000)}$ and $\theta_{1234}^{(10,1000)}$ when background input (h) is varied in the absence of a correlated input ($W = 0$). (I) The five-neuron IG measures for a ten-neuron network $\theta_{12345}^{(5,10)}$ and $\theta_{12345}^{(10,10)}$ when a correlated input (W) is varied in the absence of a background input ($h = 0$). (J) The five-neuron IG measures for a ten-neuron network $\theta_{12345}^{(5,10)}$ and $\theta_{12345}^{(10,10)}$ when background input (h) is varied in the absence of a correlated input ($W = 0$). (K) The five-neuron IG measures for a one-thousand neuron network $\theta_{12345}^{(5,1000)}$ and $\theta_{12345}^{(10,1000)}$ when a correlated input (W) is varied in the absence of a background input ($h = 0$). (L) The five-neuron IG measures for a one-thousand neuron network $\theta_{12345}^{(5,1000)}$ and $\theta_{12345}^{(10,1000)}$ when background input (h) is varied in the absence of a correlated input ($W = 0$). (M) The six-neuron IG measures for a ten-neuron network $\theta_{123456}^{(6,10)}$ and $\theta_{123456}^{(10,10)}$ when a correlated input (W) is varied in the absence of a background input ($h = 0$). (N) The six-neuron IG measures for a ten-neuron network $\theta_{123456}^{(6,10)}$ and $\theta_{123456}^{(10,10)}$ when background input (h) is varied in the absence of a correlated input ($W = 0$). (O) The six-neuron IG measures for a one-thousand neuron network $\theta_{123456}^{(6,1000)}$ and $\theta_{123456}^{(10,1000)}$ when a correlated input (W) is varied in the absence of a background input ($h = 0$). (P) The six-neuron IG measures for a one-thousand neuron network $\theta_{123456}^{(6,1000)}$ and $\theta_{123456}^{(10,1000)}$ when background input (h) is varied in the absence of a correlated input ($W = 0$).

For the three-neuron IG measure $\theta_{123}^{(k,10)}$ with a ten neuron network, $\theta_{123}^{(3,10)}$ (lowest LLM order) was strongly influenced by the common input (Figure 3.6A, dashed line) but the influence of the background input was much weaker (Figure 3.6B, dashed line). $\theta_{123}^{(10,10)}$ (highest LLM order) was more robust for both common and background inputs (Figures 3.6A and 3.6B, solid lines). Also, the $\theta_{123}^{(k,10)}$ values are similar to the corresponding

analytical values in Figures 3.2E and 3.2F. When the size of a network was increased to N=1000, the influence of external inputs on $\theta_{123}^{(k,1000)}$ almost disappeared and the values of $\theta_{123}^{(k,1000)}$ stayed around zero (Figures 3.6C and 3.6D). This result suggests that the three-neuron IG measure $\theta_{123}^{(k,N)}$ for an asymmetrically connected network is robust against external inputs, and that its value is likely to be found around zero if the size of the network is sufficiently large.

The results for the four-neuron IG measure $\theta_{1234}^{(k,10)}$ with a ten neuron network are summarized in Figures 3.6E and 3.6F. $\theta_{1234}^{(4,10)}$ (lowest LLM order) was strongly influenced by the common input (Figure 3.6E, dashed line) but the influence of the background input was much weaker (Figure 3.6F, dashed line). The influence of both external inputs $\theta_{1234}^{(10,10)}$ (highest LLM order) was negligibly small (Figures 6E and 6F, solid lines). The $\theta_{1234}^{(k,10)}$ values were similar to the corresponding analytical values in Figures 3.2G and 3.2H. For example, the downward change for $\theta_{1234}^{(4,10)}$ in Figure 3.6E corresponds to the bump where $W = 1$ in Figure 3.2G. When the size of the network was increased to N=1000, the influence of external inputs on $\theta_{1234}^{(k,1000)}$ disappeared (Figures 3.6G and 3.6H). These results suggest that the nonlinear relationship between $\theta_{1234}^{(k,N)}$ and the external inputs observed for a small asymmetric network is likely to disappear for a large asymmetric network.

The results for the five-neuron IG measure $\theta_{12345}^{(k,10)}$ with a ten neuron network are summarized in Figures 6I and 6J. We found that the results were very similar to the four-

neuron IG measure $\theta_{1234}^{(k,10)}$. Mainly, $\theta_{12345}^{(5,10)}$ (lowest LLM order) was strongly influenced by the common input (Figure 6I, dashed line), but the influence of the background input was much weaker (Figure 3.6J, dashed line). The influence of both external inputs to $\theta_{12345}^{(10,10)}$ (highest LLM order) was negligibly small (Figures 6I and 6J, solid lines). The downward change for $\theta_{12345}^{(5,10)}$ in Figure 6I corresponds to the bump where $W = 1$ in Figure 3.2I. For a network of N=1000, the influence of both external inputs on $\theta_{12345}^{(k,1000)}$ disappeared (Figures 3.6K and 3.6L). These results suggest that the nonlinear relationship between $\theta_{12345,}^{(k,N)}$ and the external inputs observed for a small asymmetric network is likely to disappear for a large asymmetric network.

The results for the six-neuron IG measure $\theta_{123456}^{(k,10)}$ with a ten neuron network are summarized in Figures 3.6M and 3.6N and those for $\theta_{123456}^{(k,1000)}$ with a one-thousand neuron network in Figures 3.6O and 3.6P. As with the other intermediate IG measures, we found that $\theta_{123456}^{(6,10)}$ (lowest LLM order) was strongly influenced by the common input (Figure 3.6M, dashed line), but the influence of the background input was much weaker (Figure 3.6N, dashed line). The influence of both external inputs to $\theta_{123456}^{(10,10)}$ (highest LLM order) was negligibly small (Figures 3.6M and 3.6N, solid lines). The $\theta_{123456}^{(k,10)}$ values were similar to the corresponding analytical values in Figures 3.3A and 3.3B. For a network of N=1000, the influence of both external inputs on $\theta_{123456}^{(k,1000)}$ disappeared (Figures 3.6O and 3.6P). These results suggest that the nonlinear relationship between $\theta_{123456}^{(k,N)}$ and the external inputs observed for a small asymmetric network is likely to disappear for a large asymmetric network.

In summary, the IG measures with intermediate neural interactional levels, $\theta_{123}^{(k,N)}$, $\theta_{1234}^{(k,N)}$, $\theta_{12345}^{(k,N)}$, $\theta_{123456}^{(k,N)}$, for a small asymmetrically connected network (N=10) are strongly influenced by a common input. This finding was similar to the analytical solution for a uniformly connected network. However, when the size of the network becomes large (e.g., N=1000), the influence by the external inputs becomes negligibly small, and these IG measures are likely to fluctuate around zero.

The influence of external inputs to the IG measures with many neural interactional levels, $\theta_{1234567}^{(k,N)}$, $\theta_{12345678}^{(k,N)}$, $\theta_{123456789}^{(k,N)}$, $\theta_{12345678910}^{(k,N)}$, is summarized in Figure 3.7. In short, the results were very similar to those found for the IG measures with intermediate interactional levels.

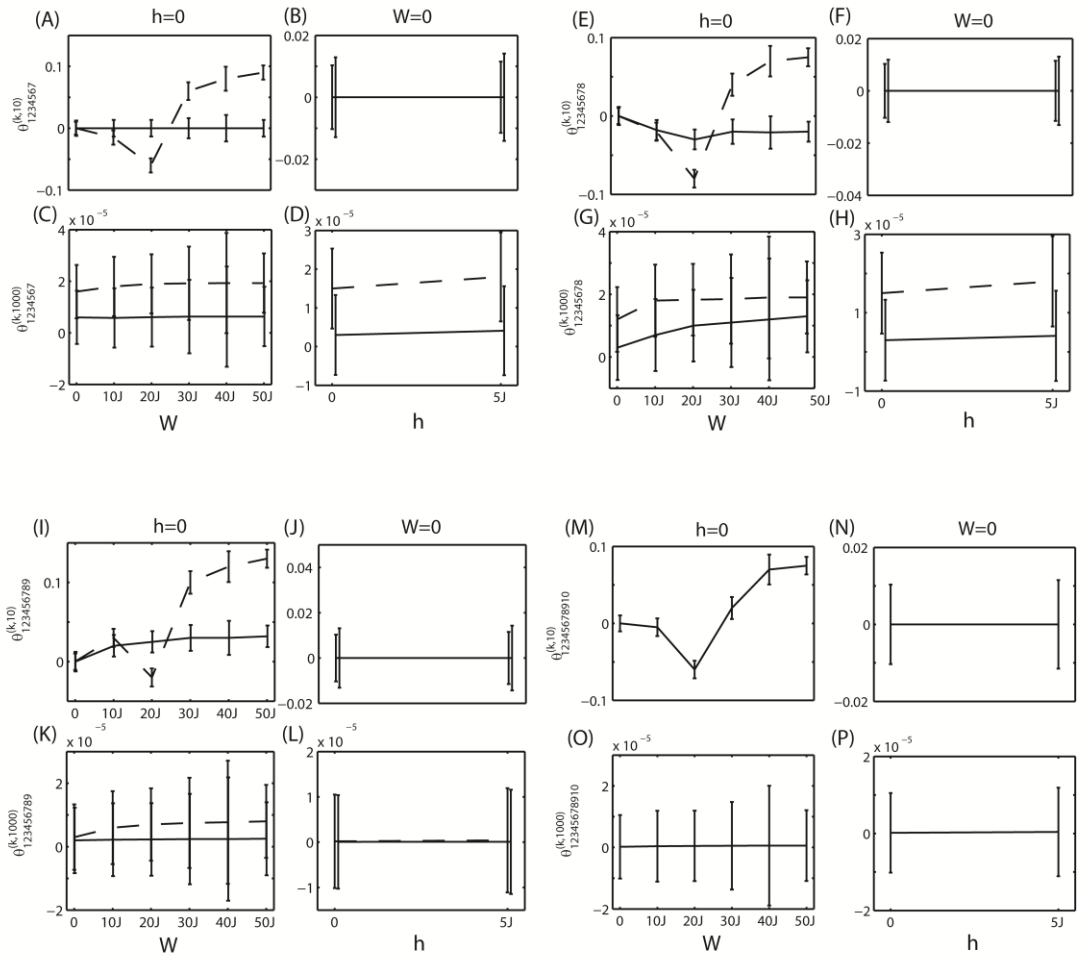

Figure 7

Figure 3.7: Relationship between the IG measures ($\boldsymbol{\theta_{1234567}^{(k,N)}}$, $\boldsymbol{\theta_{12345678}^{(k,N)}}$, $\boldsymbol{\theta_{123456789}^{(k,N)}}$, $\boldsymbol{\theta_{1234567890}^{(k,N)}}$), a correlated input ($\boldsymbol{W}$), and a background input ($\boldsymbol{h}$) for an asymmetrically connected network.

For a ten-neuron network (N=10), the network parameters are set as $J = 1/10$ and $h_0 = 0.5$. For a one-thousand neuron network (N=1000), the network parameters are set as $J = 1/1000$ and $h_0 = 0.005$. W is sampled at 0 and $10J$ and h is sampled at 0 and $5J$. The IG measures with the lowest LLM order (e.g., $\theta_{1234567}^{(7,10)}$) are represented by a dashed line. The IG measures with the highest LLM order (e.g., $\theta_{1234567}^{(10,10)}$) are represented by a solid line. (A) The seven-neuron IG measures for a ten-neuron network $\theta_{1234567}^{(7,10)}$ and $\theta_{1234567}^{(10,10)}$ when a correlated input (W) is varied in the absence of a background input ($h = 0$). (B) The seven-neuron IG measures for a ten-neuron network $\theta_{1234567}^{(7,10)}$ and $\theta_{1234567}^{(10,10)}$ when background input (h) is varied in the absence of a correlated input ($W = 0$). (C) The seven-neuron IG measures for a one-thousand neuron network $\theta_{1234567}^{(7,1000)}$ and $\theta_{1234567}^{(10,1000)}$ when a correlated input (W) is varied in the absence of a background

input ($h = 0$). (D) The seven-neuron IG measures for a one-thousand neuron network $\theta_{1234567}^{(7,1000)}$ and $\theta_{1234567}^{(10,1000)}$ when background input (h) is varied in the absence of a correlated input ($W = 0$). (E) The eight-neuron IG measures for a ten-neuron network $\theta_{12345678}^{(8,10)}$ and $\theta_{12345678}^{(10,10)}$ when a correlated input (W) is varied in the absence of a background input ($h = 0$). (F) The eight-neuron IG measures for a ten-neuron network $\theta_{12345678}^{(8,10)}$ and $\theta_{12345678}^{(10,10)}$ when background input (h) is varied in the absence of a correlated input ($W = 0$). (G) The eight-neuron IG measures for a one-thousand neuron network $\theta_{12345678}^{(8,1000)}$ and $\theta_{12345678}^{(10,1000)}$ when a correlated input (W) is varied in the absence of a background input ($h = 0$). (H) The eight-neuron IG measures for a one-thousand neuron network $\theta_{12345678}^{(8,1000)}$ and $\theta_{12345678}^{(10,1000)}$ when background input (h) is varied in the absence of a correlated input ($W = 0$). (I) The nine-neuron IG measures for a ten-neuron network $\theta_{123456789}^{(9,10)}$ and $\theta_{123456789}^{(10,10)}$ when a correlated input (W) is varied in the absence of a background input ($h = 0$). (J) The nine-neuron IG measures for a ten-neuron network $\theta_{123456789}^{(9,10)}$ and $\theta_{123456789}^{(10,10)}$ when background input (h) is varied in the absence of a correlated input ($W = 0$). (K) The nine-neuron IG measures for a one-thousand neuron network $\theta_{123456789}^{(9,1000)}$ and $\theta_{123456789}^{(10,1000)}$ when a correlated input (W) is varied in the absence of a background input ($h = 0$). (L) The nine-neuron IG measures for a one-thousand neuron network $\theta_{123456789}^{(9,1000)}$ and $\theta_{123456789}^{(10,1000)}$ when background input (h) is varied in the absence of a correlated input ($W = 0$). (M) The ten-neuron IG measure for a ten-neuron network $\theta_{12345678910}^{(10,10)}$ when a correlated input (W) is varied in the absence of a background input ($h = 0$). (N) The ten-neuron IG measure for a ten-neuron network $\theta_{12345678910}^{(10,10)}$ when background input (h) is varied in the absence of a correlated input ($W = 0$). (O) The ten-neuron IG measure for a one-thousand neuron network $\theta_{12345678910}^{(10,1000)}$ when a correlated input (W) is varied in the absence of a background input ($h = 0$). (P) The ten-neuron IG measure for a one-thousand neuron network $\theta_{12345678910}^{(10,1000)}$ when background input (h) is varied in the absence of a correlated input ($W = 0$).

The IG measures with the lowest LLM orders ($\theta_{1234567}^{(7,10)}$, $\theta_{12345678}^{(8,10)}$, $\theta_{123456789}^{(9,10)}$, $\theta_{12345678910}^{(10,10)}$) were strongly influenced by a common input (Dashed line in Figures 3.7A, 3.7E, 3.7I, and solid line in Figure 3.7M), but the influence of a background input was negligible (Dashed line in Figures 3.7A, 3.7E, 3.7I, and solid line in Figure 3.7M). The

influence of both external inputs to the highest order IG measures ($\theta^{(10,10)}_{1234567}$, $\theta^{(10,10)}_{12345678}$, $\theta^{(10,10)}_{123456789}$) were negligibly small (Figures 3.7A,3.7B, 3.7E, 3.7F, 3.7I and 3.7J, solid lines). When the size of a network was increased to N=1000, the influence of both external inputs on the IG measures disappeared (Figures 3.7C, 3.7D, 3.7G, 3.7H, 3.7K, 3.7L, 3.7O and 3.7P). These results suggest that the nonlinear relationship between the IG measures with many neuronal interactions, $\theta^{(k,N)}_{1234567}$, $\theta^{(k,N)}_{12345678}$, $\theta^{(k,N)}_{123456789}$, $\theta^{(k,N)}_{12345678910}$, and the external inputs observed for a small asymmetric network is likely to disappear for a large asymmetric network.

In summary, the numerical simulation demonstrated that if the size of network is sufficiently large (e.g., N=1000), the influence of common and background inputs to the IG measures with three or more neuronal interactions becomes negligible even for an asymmetrically connected network. For the simulations in this section, we used $J_{ij} = 1/N + \varepsilon_{ij}$ where ε_{ij} is a random number drawn from the normal distribution $\mathrm{N}(m, \sigma^2)$ with the mean $m = 0$ and variance $\sigma^2 = 1/N$. These results suggest that the single and pairwise IG measures provide sufficient information for the network property as long as the asymmetry of connections is moderate.

3.4.3 Relationship between the IG Measures and Asymmetry of Connections

In this section, we investigate if the IG measures are influenced by higher asymmetry of connections.

To modify the level of asymmetry of connections, we introduced a parameter λ; asymmetric connections were set as $J_{ij} = 1/N + \lambda\varepsilon_{ij}$ where ε_{ij} is a random number drawn from the normal distribution $\mathrm{N}(m, \sigma^2)$ with the mean $m = 0$ and variance $\sigma^2 = 1/N$, respectively, and λ is an integer between 1 and 5. Note that $\lambda = 1$ corresponds to the connection setting in the previous section. Similar to the procedure in Section 4.2, without losing generality, we calculated the IG measures for a specific neuron group as follows. For the pairwise IG measure $\theta_{12}^{(k,N)}$, we selected neurons 1 and 2, and set their connection weights to $J_{12} = 1/N + \lambda\varepsilon_{12}$ and $J_{21} = \frac{2}{N} - J_{12}$. In this way, the asymmetry of connections between neurons 1 and 2 was controlled by the parameter λ, but the magnitude of their total connections was kept constant ($J_{12} + J_{21} = 2/N$). The rest of the connections were set following $J_{ij} = 1/N + \lambda\varepsilon_{ij}$. Similarly, for the three-neuron IG measure $\theta_{123}^{(k,N)}$, we selected neurons 1, 2, and 3, and set their connection weights to ($J_{12} = 1/N + \lambda\varepsilon_{12}$ and $J_{21} = 2/\mathrm{N} - J_{12}$), ($J_{23} = 1/N + \lambda\varepsilon_{23}$ and $J_{32} = 2/\mathrm{N} - J_{32}$), and ($J_{31} = 1/N + \lambda\varepsilon_{31}$ and $J_{13} = 2/\mathrm{N} - J_{31}$). The rest of the connections were set following $J_{ij} = 1/N + \lambda\varepsilon_{ij}$. We used the same procedure for all the other IG measures with four or more neuronal interactions. We set N=1000 because we are interested in the behavior of networks in a biologically realistic size. To investigate the behavior under the influence of both common and background inputs, we used the magnitude of a common input as $W = 10J = 0.01$, and the magnitude of a background input as $h = 5J = 0.005$. The parameter m controlling the firing probability of a model neuron in equation 2.24 was set to 1. For each λ value, we performed one-hundred simulation trials where each trial consisted of 10^6 updates. For clarity, we show the results for the lowest

and highest LLM orders only. For example, $\theta_1^{(1,1000)}$ and $\theta_1^{(10,1000)}$ for the single IG measure and $\theta_{12}^{(2,1000)}$ and $\theta_{12}^{(10,1000)}$ for the pairwise IG measure. However, we confirmed that the IG measures for all other LLM orders fell between the IG measures with the lowest and highest LLM orders. The results are reported as the mean $\pm$ SEM.

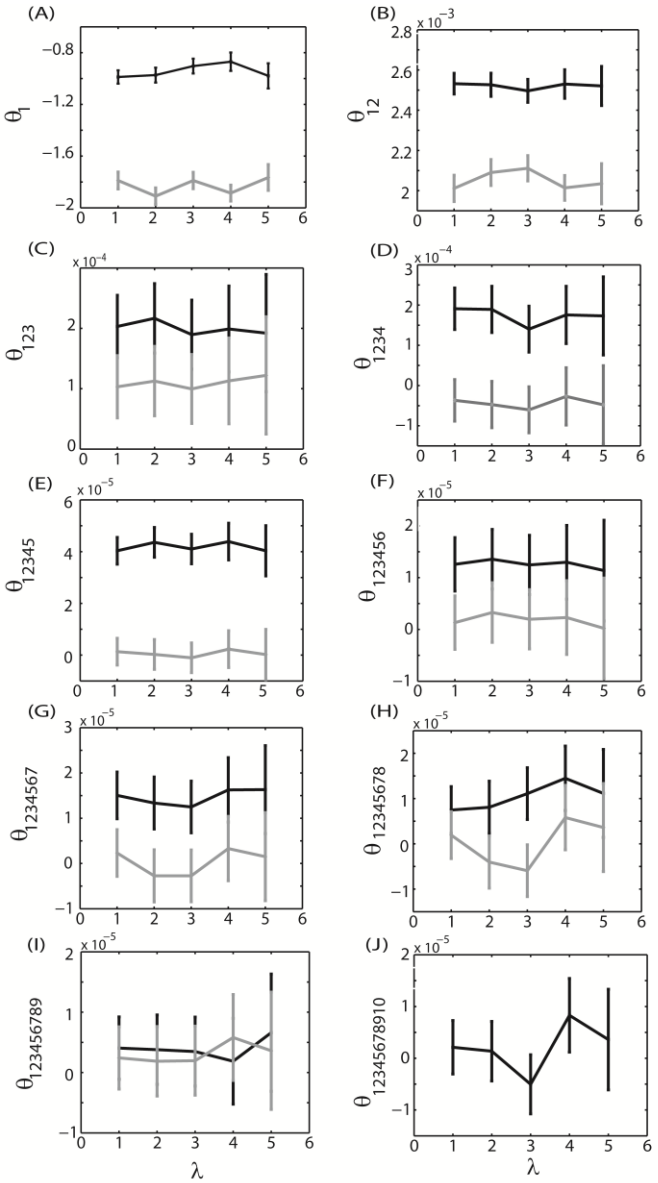

Figure 8

Figure 3.8: Relationship between the IG measures and asymmetry of connections.

An integer parameter λ that controls the level of asymmetry of connections is modified between 1 and 5. The number of neurons is set to $N = 1000$, a common input is set to $W = 10J = 0.01$ and the magnitude of a background input is set to $h = 5J = 0.005$.
The IG measures with the lowest LLM order (e.g., $\theta_1^{(1,1000)}$) are represented by a dashed line. The IG measures with the highest LLM order (e.g., $\theta_1^{(10,1000)}$) are represented by a solid line. (A) The single IG measures $\theta_1^{(1,1000)}$ and $\theta_1^{(10,1000)}$ when the asymmetry parameter (λ) is varied. (B) The pairwise IG measures $\theta_{12}^{(2,1000)}$ and $\theta_{12}^{(10,1000)}$ when the asymmetry parameter (λ) is varied. (C) The three-neuron IG measures $\theta_{123}^{(3,1000)}$ and $\theta_{123}^{(10,1000)}$ when the asymmetry parameter (λ) is varied. (D) The four-neuron IG measures $\theta_{1234}^{(4,1000)}$ and $\theta_{1234}^{(10,1000)}$ when the asymmetry parameter (λ) is varied. (E) The five-neuron IG measures $\theta_{12345}^{(5,1000)}$ and $\theta_{12345}^{(10,1000)}$ when the asymmetry parameter (λ) is varied. (F) The six-neuron IG measures $\theta_{123456}^{(6,1000)}$ and $\theta_{123456}^{(10,1000)}$ when the asymmetry parameter (λ) is varied. (G) The seven-neuron IG measures $\theta_{1234567}^{(7,1000)}$ and $\theta_{1234567}^{(10,1000)}$ when the asymmetry parameter (λ) is varied. (H) The eight-neuron IG measures $\theta_{12345678}^{(8,1000)}$ and $\theta_{12345678}^{(10,1000)}$ when the asymmetry parameter (λ) is varied. (I) The nine-neuron IG measures $\theta_{123456789}^{(9,1000)}$ and $\theta_{123456789}^{(10,1000)}$ when the asymmetry parameter (λ) is varied. (J) The ten-neuron IG measure $\theta_{12345678910}^{(10,1000)}$ when the asymmetry parameter (λ) is varied.

Figure 3.8 shows how the IG measures are influenced by the level of asymmetry of connections. The figure is organized in ascending order; the result for $\theta_1^{(k,1000)}$ is in Figure 8A and the result for $\theta_{12345678910}^{(10,1000)}$ is in Figure 3.8J. Solid and gray lines represent the results for the IG measures with the lowest and highest LLM orders, respectively. We found that all the IG measures were robust against the change of asymmetry of connections in the range from $\lambda = 1$ to $\lambda = 5$ (Figures 3.8A-3.8J). We also found that the IG measures with the highest LLM order provided the best result; for the single IG measure, $\theta_1^{(10,1000)}$ fluctuated between -2 and -1.8 (Figure 3.8A, gray line). According to

equation 3.1, a predicted value of $\theta_1^{(k,1000)}$ is -1.99. Figure 3.8A shows that $\theta_1^{(10,1000)}$ has a strong agreement with the theoretical prediction, even under a strong asymmetry of connections. Similarly, for the pairwise IG measure, $\theta_{12}^{(10,1000)}$ fluctuated around 2×10^{-3} (Figure 3.8B, gray line). According to equation 3.4, the predicted value of $\theta_{12}^{(10,1000)}$ is 2×10^{-3}, which was exactly the value we found in Figure 3.8B. For the IG measures with three or more neuronal interactions, the IG measures with the highest LLM order ($\theta_{123}^{(10,1000)}$ to $\theta_{12345678910}^{(10,1000)}$) fluctuated around zero.

In summary, the main findings in this section are that all the IG measures are robust against the increased asymmetry of connections, and that the IG measures with the highest LLM order provides the best results because they have a strong agreement with the theoretical predictions. These results suggest that the IG measures provide useful insights into the network parameters, even for strongly asymmetric connections. The single IG measure $\theta_1^{(k,N)}$ is linearly related to a background input and the pairwise IG measure $\theta_{12}^{(k,N)}$ is linearly related to the sum of connection weights. Furthermore, the fact that the IG measures with three or more neuronal interactions fluctuates around zero indicates that the single and pairwise IG measures contain the majority of information for the asymmetric network investigated in this paper.

3.5 Discussion

In this study, we investigated the influence of external inputs (a correlated input and an uncorrelated background input), and the asymmetry of connections to the IG measures

beyond pairwise interactions. Our goal was two-fold. First, we aimed at finding the analytical relationships between the IG measures for up to ten neuronal interactions and external inputs. For mathematical clarity, we investigated the dynamics of a network of ten uniformly connected binary model neurons. By investigating the relationships in the equilibrium limit, we obtained the explicit relationship between the IG measures and the strength of correlated input W and the background input h. We confirmed that the single and pairwise IG measures were good estimators of the background input and of the sum of connection weights, respectively. In contrast, for the IG measures with three or more neuronal interactions, the influence of a correlated input was stronger than a background input, and it was highly non-linear. Second, we aimed at extending the findings for a uniformly connected small network to an asymmetrically connected network. By numerical simulation, we found that the influence of external inputs, that was evident for a small-sized asymmetric network, became much weaker for a larger network (e.g., one-thousand neurons). We also found that all the IG measures from one-neuron to ten-neuron interactions were robust against the increased asymmetry of connections, and that the IG measures with the highest LLM order provided the best result. Taken together, this investigation demonstrated that the single and pairwise IG measures were good estimators of a background input and of the sum of connection weights, even under a strong asymmetry of connections. Our study also showed that the IG measures with three and more neuronal interactions were not influenced by the network parameters if a network was sufficiently large. All these findings support the usefulness of the IG approach and provide further insights when the IG method is used for neural data analysis.

One of the important claims of the information-geometric approach is that the single- and pairwise-IG measures are good estimators of the background input and of the sum of connection weights, respectively. In other words, the coefficients in the log-linear model can be related to the network parameters in the model. From a neuroscientific point of view, the relationship between the pairwise IG measure and the connection weights would be particularly interesting (Schneidman, et al., 2006; Tang, et al., 2008; Tyler, et al., 2012). However, we have to be careful as to whether the coefficients in the log-linear model actually reflect the real neuronal interaction strength. We also need to be cautious about whether the obtained complicated analytical relationship between the IG measures and external inputs is due to an oversimplified or inappropriate neural network model. We have previously investigated these questions using the Hodgkin-Huxley model (Hodgkin and Huxley, 1952). Using the NEURON simulator, we constructed a small network of cortical neurons in which each neuron was driven by an uncorrelated noisy input. The neurons were asymmetrically connected by conductance-based AMPA receptors (Hines and Carnevale, 1997; Lipa, et al., 2006; Lipa, et al., 2007). We were able to show that the pairwise IG measure was linearly related to the sum of the AMPA receptor's connection weights between the neurons. In addition, we also found that the single IG measure was linearly related to the mean amplitude of noisy input. Recently, we have also conducted numerical simulations using a spiking neuron model (Izhikevich, 2003). One-thousand cortical pyramidal neurons and two-hundred-and-fifty inhibitory neurons were connected and driven by oscillatory external inputs. We found again that the pairwise IG measure was linearly related to the sum of the connection weights (Nie et al., under review). These studies, which were conducted using more realistic neuron models and synaptic connections, suggested that the coefficients in the log-linear model

may be able to extract information about the real neuronal interaction strength. However, further investigation is necessary to clarify the relationship.

In addition, neural firing exhibits non-stationary changes in real electrophysiological experiments. The extension of the present research to a time-dependent domain would be a necessary step for the analysis of real neural data (Shimazaki, et al., 2012). Toward this end, we have recently investigated the property of IG measures under oscillatory inputs and found that the pairwise IG measure could estimate neural interactions (Nie et al., 2014). Finally, the proposed IG measures rely on the successful binary representation by binning spike trains. As previously discussed in (Nie and Tatsuno, 2012), the problem of binning needs to be treated with caution.

Despite these limitations, the present study is the first attempt to provide an analytical relationship between the IG measures involving up to ten neuronal interactions and external inputs for a uniformly connected small network. It also demonstrates numerically that the IG measures are robust against the influence of external inputs and the asymmetry of connection weights if the size of the network is sufficiently large. These findings further support that the single and pairwise IG measures are robust estimators of a background input and the sum of the connection weights. We believe that this study provides useful information for the future use of IG measures. We also hope that the development of theoretical analyses including information-geometric approaches could lead to further insights into neural information processing.

Appendix

For a ten-neuron system, we solved twenty-one equations for twenty-one marginal and coincident firing variables. Below is an equation for the first-order marginal $\langle x_1 \rangle$. The equation corresponds to equation 3.28 for a two-neuron system. Equations for other marginal and coincident firings can be written in a similar manner.

$$
\begin{aligned}
\langle x_1 \rangle = \langle x_0 x_1 x_2 x_3 x_4 x_5 x_6 x_7 x_8 x_9 \rangle \Big\{ & g(9J+W+h) - \binom{9}{1} g(8J+W+h) + \binom{9}{2} g(7J+W+h) \\
& - \binom{9}{3} g(6J+W+h) + \binom{9}{4} g(5J+W+h) - \binom{9}{5} g(4J+W+h) + \binom{9}{6} g(3J+W+h) \\
& - \binom{9}{7} g(2J+W+h) + \binom{9}{8} g(J+W+h) - \binom{9}{9} g(W+h) - \Big(g(9J+h) - \binom{9}{1} g(8J+h) \\
& + \binom{9}{2} g(7J+h) - \binom{9}{3} g(6J+h) + \binom{9}{4} g(5J+h) - \binom{9}{5} g(4J+h) + \binom{9}{6} g(3J+h) \\
& - \binom{9}{7} g(2J+h) + \binom{9}{8} g(J+h) - \binom{9}{9} g(h) \Big) \Big\} \\
+ \binom{9}{0} \langle x_1 x_2 x_3 x_4 x_5 x_6 x_7 x_8 x_9 \rangle \Big\{ & g(9J+h) - \binom{9}{1} g(8J+h) + \binom{9}{2} g(7J+h) - \binom{9}{3} g(6J+h) \\
& + \binom{9}{4} g(5J+h) - \binom{9}{5} g(4J+h) + \binom{9}{6} g(3J+h) - \binom{9}{7} g(2J+h) + \binom{9}{8} g(J+h) - \binom{9}{9} g(h) \Big\} \\
+ \binom{9}{1} \langle x_0 x_1 x_2 x_3 x_4 x_5 x_6 x_7 x_8 \rangle \Big\{ & g(8J+W+h) - \binom{8}{1} g(7J+W+h) + \binom{8}{2} g(6J+W+h) \\
& - \binom{8}{3} g(5J+W+h) + \binom{8}{4} g(4J+W+h) - \binom{8}{5} g(3J+W+h) + \binom{8}{6} g(2J+W+h) \\
& - \binom{8}{7} g(J+W+h) + \binom{8}{8} g(W+h) - \Big(g(8J+h) - \binom{8}{1} g(7J+h) + \binom{8}{2} g(6J+h) \\
& - \binom{8}{3} g(5J+h) + \binom{8}{4} g(4J+h) - \binom{8}{5} g(3J+h) + \binom{8}{6} g(2J+h) - \binom{8}{7} g(J+h) + \binom{8}{8} g(W+h) \Big) \Big\}
\end{aligned}
$$

$$+\binom{9}{1}\langle x_1x_2x_3x_4x_5x_6x_7x_8\rangle\Big\{g(8J+h)-\binom{8}{1}g(7J+h)+\binom{8}{2}g(6J+h)-\binom{8}{3}g(5J+h)$$
$$+\binom{8}{4}g(4J+h)-\binom{8}{5}g(3J+h)+\binom{8}{6}g(2J+h)-\binom{8}{7}g(J+h)+\binom{8}{8}g(h)\Big\}$$
$$+\binom{9}{2}\langle x_0x_1x_2x_3x_4x_5x_6x_7\rangle\Big\{g(7J+W+h)-\binom{7}{1}g(6J+W+h)+\binom{7}{2}g(5J+W+h)$$
$$-\binom{7}{3}g(4J+W+h)+\binom{7}{4}g(3J+W+h)-\binom{7}{5}g(2J+W+h)+\binom{7}{6}g(J+W+h)$$
$$-\binom{7}{7}g(W+h)-\Big(g(7J+h)-\binom{7}{1}g(6J+h)+\binom{7}{2}g(5J+h)-\binom{7}{3}g(4J+h)$$
$$+\binom{7}{4}g(3J+h)-\binom{7}{5}g(2J+h)+\binom{7}{6}g(J+h)-\binom{7}{7}g(h)\Big)\Big\}$$
$$+\binom{9}{2}\langle x_1x_2x_3x_4x_5x_6x_7\rangle\Big\{g(7J+h)-\binom{7}{1}g(6J+h)+\binom{7}{2}g(5J+h)-\binom{7}{3}g(4J+h)$$
$$+\binom{7}{4}g(3J+h)-\binom{7}{5}g(2J+h)+\binom{7}{6}g(J+h)-\binom{7}{7}g(h)\Big\}$$
$$+\binom{9}{3}\langle x_0x_1x_2x_3x_4x_5x_6\rangle\Big\{g(6J+W+h)-\binom{6}{1}g(5J+W+h)+\binom{6}{2}g(4J+W+h)$$
$$-\binom{6}{3}g(3J+W+h)+\binom{6}{4}g(2J+W+h)-\binom{6}{5}g(J+W+h)+\binom{6}{6}g(W+h)$$
$$-\Big(g(6J+h)-\binom{6}{1}g(5J+h)+\binom{6}{2}g(4J+h)-\binom{6}{3}g(3J+h)+\binom{6}{4}g(2J+h)$$
$$-\binom{6}{5}g(J+h)+\binom{6}{6}g(h)\Big)\Big\}$$

$$+\binom{9}{3}\langle x_1x_2x_3x_4x_5x_6\rangle\Big\{g(6J+h)-\binom{6}{1}g(5J+h)+\binom{6}{2}g(4J+h)-\binom{6}{3}g(3J+h)$$
$$+\binom{6}{4}g(2J+h)-\binom{6}{5}g(J+h)+\binom{6}{6}g(h)\Big\}$$
$$+\binom{9}{4}\langle x_0x_1x_2x_3x_4x_5\rangle\Big\{g(5J+W+h)-\binom{5}{1}g(4J+W+h)+\binom{5}{2}g(3J+W+h)$$
$$-\binom{5}{3}g(2J+W+h)+\binom{5}{4}g(J+W+h)-\binom{5}{5}g(W+h)$$
$$-\Big(g(5J+h)-\binom{5}{1}g(5J+h)+\binom{5}{2}g(4J+h)-\binom{5}{3}g(3J+h)+\binom{5}{4}g(2J+h)$$
$$-\binom{5}{5}g(J+h)\Big)\Big\}$$
$$+\binom{9}{4}\langle x_1x_2x_3x_4x_5\rangle\Big\{g(5J+h)-\binom{5}{1}g(4J+h)+\binom{5}{2}g(3J+h)-\binom{5}{3}g(2J+h)$$
$$+\binom{5}{4}g(J+h)-\binom{5}{5}g(h)\Big\}$$
$$+\binom{9}{5}\langle x_0x_1x_2x_3x_4\rangle\Big\{g(4J+W+h)-\binom{4}{1}g(3J+W+h)+\binom{4}{2}g(2J+W+h)$$
$$-\binom{4}{3}g(J+W+h)+\binom{4}{4}g(W+h)$$
$$-\Big(g(4J+h)-\binom{4}{1}g(3J+h)+\binom{4}{2}g(2J+h)-\binom{4}{3}g(J+h)+\binom{4}{4}g(h)\Big)\Big\}$$

$$+\binom{9}{5}\langle x_1x_2x_3x_4\rangle\left\{g(4J+h)-\binom{4}{1}g(3J+h)+\binom{4}{2}g(2J+h)-\binom{4}{3}g(J+h)+\binom{4}{4}g(h)\right\}$$

$$+\binom{9}{6}\langle x_0x_1x_2x_3\rangle\left\{g(3J+W+h)-\binom{3}{1}g(2J+W+h)+\binom{3}{2}g(J+W+h)-\binom{3}{3}g(W+h)\right.$$

$$\left.-\left(g(3J+h)-\binom{3}{1}g(2J+h)+\binom{3}{2}g(J+h)-\binom{3}{3}g(h)\right)\right\}$$

$$+\binom{9}{6}\langle x_1x_2x_3\rangle\left\{g(3J+h)-\binom{3}{1}g(2J+h)+\binom{3}{2}g(J+h)-\binom{3}{3}g(h)\right\}$$

$$+\binom{9}{7}\langle x_0x_1x_2\rangle\left\{g(2J+W+h)-\binom{2}{1}g(J+W+h)+\binom{2}{2}g(W+h)\right.$$

$$\left.-\left(g(2J+h)-\binom{2}{1}g(J+h)+\binom{2}{2}g(h)\right)\right\}$$

$$+\binom{9}{7}\langle x_1x_2\rangle\left\{g(2J+h)-\binom{2}{1}g(J+h)+\binom{2}{2}g(h)\right\}$$

$$+\binom{9}{8}\langle x_0x_1\rangle\{g(J+W+h)-g(W+h)-(g(J+h)-g(h))\}$$

$$+\binom{9}{8}\langle x_1\rangle\{g(J+h)-g(h)\}+\binom{9}{9}\langle x_0\rangle\{g(W+h)-g(h)\}+g(h)$$

Chapter 4 Information-geometric measures estimate neural interactions during oscillatory brain states

Preface

This chapter refers the publication *Nie,Y. Fellous J.M., and Tatsuno. M. Information-geometric measures estimate neural interactions during oscillatory brain states. Frontiers in Neural Circuits (2014).* This work investigated how IG measures are related to the structure of a network with different oscillatory frequencies. We show that the IG measures provide robust estimation for the connection weights and single neuronal firing even if the neuronal firing is non-stationary.

Abstract

The characterization of functional network structures among multiple neurons is essential to understanding neural information processing. Information geometry (IG), a theory developed for investigating a space of probability distributions has recently been applied to spike-train analysis and has provided robust estimations of neural interactions. Although neural firing in the equilibrium state is often assumed in these studies, in reality, neural activity is non-stationary. The brain exhibits various oscillations depending on cognitive demands or when an animal is asleep. Therefore, the investigation of the IG measures during oscillatory network states is important for testing how the IG method can be applied to real neural data. Using model networks of binary neurons or more realistic spiking neurons, we studied how the single- and pairwise-IG measures were influenced by oscillatory neural activity. Two general oscillatory mechanisms, externally driven oscillations and internally induced oscillations, were considered. In both mechanisms, we

found that the single-IG measure was linearly related to the magnitude of the external input, and that the pairwise-IG measure was linearly related to the sum of connection strengths between two neurons. We also observed that the pairwise-IG measure was not dependent on the oscillation frequency. These results are consistent with the previous findings that were obtained under the equilibrium conditions. Therefore, we demonstrate that the IG method provides useful insights into neural interactions under the oscillatory condition that can often be observed in the real brain.

4.1 Introduction

The dynamics of neural interactions have been conjectured to play an important role in neural information processing. One way to investigate the neural interactions is to record multi-neuronal firing activity from a freely behaving animal, and analyze the correlations between individual units. In past decades, electrophysiological studies have significantly been advanced by the use of multi-electrode recording techniques (Buzsaki, 2004; Chapin, et al., 1999; Davidson, et al., 2009; Dragoi and Tonegawa; Dragoi and Tonegawa, 2013; Euston, et al., 2007; Hoffman and McNaughton, 2002; Kudrimoti, et al., 1999; Laubach, et al., 2000; Peyrache, et al., 2009; Tatsuno, et al., 2006; Wilson and McNaughton, 1993). In order to analyze such high-dimensional multi-neuronal datasets, a number of statistical methods have also been developed (Abeles and Gerstein, 1988; Aertsen, et al., 1989; Amari, 2009; Brown, et al., 2004; Czanner, et al., 2005; Fellous, et al., 2004; Gerstein and Perkel, 1969; Grun, et al., 2002; Grun, et al., 2002; Lopes-dos-Santos, et al., 2011; Panzeri and Schultz, 2001; Peyrache, et al., 2009; Shimazaki, et al., 2012; Shimazaki and

Shinomoto, 2007; Shimokawa and Shinomoto, 2009; Zhang, et al., 1998). Recently, a method based on information geometry (IG) has been applied to the analysis of neural data (Amari, 2001; Amari and Nagaoka, 2000; Amari, et al., 2003; Brown, et al., 2011; Eleuteri, et al., 2005; Ikeda, 2005; Ince, et al., 2010; Miura, et al., 2006; Nakahara and Amari, 2002; Nakahara, et al., 2006; Ohiorhenuan and Victor, 2011; Shimazaki, et al., 2012; Tatsuno, et al., 2009; Tatsuno and Okada, 2004). It has been demonstrated that IG provides a powerful statistical tool for analyzing spiking data. Some of the advantages of IG approach include the orthogonal decomposition of neural interactions (Amari, 2001; Nakahara and Amari, 2002), and its direct relationship to underlying connections (Brown, et al., 2011; Tatsuno, et al., 2009; Tatsuno and Okada, 2004); the single-IG measure is related to the amount of external inputs and the pairwise-IG measure is related to the amount of direct neural interactions between two neurons.

These IG properties were often investigated under the assumption that the network is in an equilibrium state. However, in the brain, the equilibrium assumption does not hold true. Instead, the brain undergoes a variety of non-equilibrium states such as oscillations. For example, the slow-wave oscillation (~1Hz) was discovered during non-REM sleep (Crunelli and Hughes, 2010; Steriade, et al., 1993), and evidence suggests that it plays an important role in memory consolidation (Diekelmann and Born, 2010; Huber, et al., 2004; Stickgold, 2005). The theta (6-10 Hz) rhythm is a prominent coherent oscillation observed in the hippocampus, and its surrounding area during rat spatial navigation (Bland, 1986; Buzsaki, 2002; Vanderwolf, 1969). The theta rhythm has also been observed in various human neocortical areas during the delay period of working memory tasks (Meltzer, et al., 2008; Raghavachari, et al., 2001). The beta (15-30Hz) oscillation is

conjectured to play a key role in action preparation and inhibitory control in the motor system (Baker, et al., 1997). The gamma (30-80Hz) oscillation has been shown to play a role in the integration of sensory information (Gray, et al., 1989; Singer and Gray, 1995). The fast hippocampal sharp wave ripples (100-200 Hz) were also reported during an animal's awake immobility and slow-wave sleep (Buzsaki, et al., 1992). Therefore, it is important to investigate if the IG measures can be applied to neural data under oscillatory conditions.

In this study, we investigated how the single- and pairwise-IG measures are influenced by a network oscillation. Under an equilibrium assumption, previous studies have shown that the single- and pairwise-IG measures provide a robust estimation of the magnitude of external input and direct neural interactions (Brown, et al., 2011; Tatsuno, et al., 2009). We also focused on these IG measures in this study because the external inputs and intrinsic neural interactions are the two main factors for characterizing network dynamics. For the oscillation mechanisms, we have considered two representative cases; one is an external driven oscillation where a network is influenced by external oscillatory inputs. The other is an internally induced oscillation where interactions between excitatory and inhibitory neuron populations produce an oscillation. By computer simulations using simple binary model neurons or more biologically plausible spiking neurons, we investigated whether the properties of the IG measures that were established with the equilibrium condition still hold true under oscillatory network states.

In Section 2, we briefly introduce an information-geometric analysis of neural spikes. In Section 3, we describe the model and network structure used in the numerical simulation.

In Section 4, the simulation results for both externally driven and internally induced oscillations are described in detail. In Section 5, we summarize our findings and discuss future directions of research on this topic.

4.2 Methods

4.2.1 Information-geometric method

We briefly introduce the information-geometric method for spiking data analysis (for details see (Amari and Nagaoka, 2000)). Generally, in an N-neuron system, the state of i-th ($i = 1, \dots, N$) neuron is represented by a binary random variable x_i , where $x_i = 1$ or 0 representing neuronal firing or silence, respectively. The joint probability distribution of the N-neuron system can be described by a fully expanded N-th order log-linear model (LLM)

$$\log p_{x_1 x_2 \dots x_N} = \sum_i \theta_i^{(N,N)} x_i + \sum_{i<j} \theta_{ij}^{(N,N)} x_i x_j + \cdots + \theta_{12,\dots N}^{(N,N)} x_1 x_2 \dots x_N - \psi(\boldsymbol{\theta})^{(N,N)}, \quad (4.1)$$

where $\theta_{ij,\dots m}^{(N,N)} (1 \le m \le N)$ represents the m-neuron interaction and $\psi(\boldsymbol{\theta})^{(N,N)}$ with $\boldsymbol{\theta} = \left\{\theta_i^{(N,N)}, \theta_{ij}^{(N,N)}, \dots, \theta_{12,\dots N}^{(N,N)}\right\}$ is a normalization constant such that $\sum p_{x_1 x_2 \dots x_N} = 1$. The first and the second superscripts in $\theta_{ij,\dots m}^{(N,N)}$ represent the order of the LLM and the number of neurons in the system. We use $\theta_i^{(N,N)}$, $\theta_{ij}^{(N,N)}$, and $\theta_{ij,\dots m}^{(N,N)}$ to describe the single-IG measure, the pairwise-IG measure and the m-neuron IG measure with the N-th order LLM for a N-neuron system, respectively (Nie and Tatsuno, 2012). The joint probability of N neurons is calculated by

$$p_{x_1 x_2,\ldots,x_N} = \frac{c_{x_1 x_2,\ldots,x_\mathrm{N}}}{\sum_{x_1 x_2,\ldots,x_\mathrm{N}} c_{x_1 x_2,\ldots,x_\mathrm{N}}}, \tag{4.2}$$

where $c_{x_1 x_2,\ldots,x_\mathrm{N}}$ is the count of events $(X_1 = x_1, X_2 = x_2, \ldots, X_\mathrm{N} = x_\mathrm{N})$ that occur.

However, in reality, it is difficult to calculate the statistical information from all neurons in a large network. Therefore, the partially expanded LLM is often used for the estimation of neuronal interactions. The partially expanded k-th order LLM in an N-neuron network is given by

$$\log p_{x_1 x_2 \ldots x_{k,*\ldots*}} = \sum_i \theta_i^{(k,N)} x_i + \sum_{i<j} \theta_{ij}^{(k,N)} x_i x_j + \cdots + \theta_{12,\ldots k}^{(k,N)} x_1 x_2 \ldots x_k - \psi(\boldsymbol{\theta})^{(k,N)} \tag{4.3}$$

where $\boldsymbol{\theta} = \left\{\theta_i^{(k,N)}, \theta_{ij}^{(k,N)}, \ldots, \theta_{12,\ldots k}^{(k,N)}\right\}$. The first few terms of $\boldsymbol{\theta}$ and normalization factor are given as follows:

$$\theta_i^{(k,N)} = \log \frac{p_{x_1=0,\ldots,x_i=1,\ldots,x_k=0,*\ldots*}}{p_{x_1=0,\ldots,x_k=0,*\ldots*}},$$

$$\theta_{ij}^{(k,N)} = \log \frac{p_{x_1=0,\ldots,x_i=1,\ldots,x_j=1,\ldots,x_k=0,*\ldots*} p_{x_1=0,\ldots,x_k=0,*\ldots*}}{p_{x_1=0,\ldots,x_i=1,\ldots,x_j=0,\ldots,x_k=0,*\ldots*} p_{x_1=0,\ldots,x_i=0,\ldots,x_j=1,\ldots,x_k=0,*\ldots*}},$$

$$\ldots \ldots \ldots$$

$$\psi^{(k,N)} = -\log p_{x_1=0,\ldots,x_k=0,*\ldots*}, \tag{4.4}$$

where $'*...*'$ represents the marginalization over the $(N-k)$ neurons.

The single-IG measure $\theta_i^{(k,N)}$ and the pairwise-IG measure $\theta_{ij}^{(k,N)}$ are the two main focuses in this study because $\theta_i^{(k,N)}$ is related to the amount of external inputs and $\theta_{ij}^{(k,N)}$ is related to the amount of direct neural interactions between two neurons (Brown, et al., 2011; Tatsuno, et al., 2009; Tatsuno and Okada, 2004). Using a network of simple binary neurons, and the assumption of an equilibrium state, the previous study has shown that the single-IG measure $\theta_i^{(2,N)}$ and the pairwise-IG measure $\theta_{ij}^{(2,N)}$ with the 2nd-order LLM are related to the network parameters as

$$\theta_i^{(2,N)} \propto 2h_i + O\left(\frac{1}{N}\right), \qquad \theta_{ij}^{(2,N)} \propto \left(J_{ij} + J_{ji}\right) + O\left(\frac{1}{N}\right), \tag{4.5}$$

where h_i represents the magnitude of constant external input to a neuron i, and J_{ij} (J_{ji}) is the connection weight from a neuron j to i (from a neuron i to j), respectively (Tatsuno, et al., 2009). If a network receives correlated inputs, the relationship for $\theta_{ij}^{(2,N)}$ in Equation 5 does not hold true anymore. However, we have also shown that $\theta_{ij}^{(k,N)}$ with the higher k-th order LLM provides a better estimation of neural interactions (Nie and Tatsuno, 2012). For example, $\theta_{ij}^{(4,N)}$ was shown to have the relationship

$$\theta_{ij}^{(4,N)} \propto \left(J_{ij} + J_{ji}\right), \tag{4.6}$$

within approximately a 10% error if the number of neurons N is $\sim 10^3$ or larger; a typical size of network in a cortical column (Braitenberg and Schuz, 1999). We have also confirmed that the relationship $\theta_i^{(4,N)} \propto 2h_i$ holds true within approximately a 10% error (unpublished data).

These properties could be useful for the field of neuroscience because the IG measures can estimate the changes of underlying network parameters (h_i and J_{ij}) separately, while other correlation measures have not yet been shown to have such a property (Amari, 2009). However, these results were derived under the equilibrium limit, and little is known if the similar relationship holds under the oscillatory condition.

4.2.2 Neuron model and network structure

4.2.2.1 Neuron model

We investigated the influence of oscillations using a network of simple binary neurons with stochastic dynamics (Ginzburg and Sompolinsky, 1994) and biologically plausible spiking neurons (Izhikevich, 2003). Using simple binary model neurons, we first investigated whether the property of the IG measures that were shown under the equilibrium condition also held true for the oscillatory condition. We then extended our investigation to more realistic spiking neurons.

For a binary model neuron, the transition between the binary states is given by the transition rate w as

$$w(x_i = 0 \rightarrow x_i = 1) = \frac{g(u_i)}{\tau_0},$$

$$w(x_i = 1 \rightarrow x_i = 0) = \frac{1 - g(u_i)}{\tau_0},$$

$$w(x_i = 0 \rightarrow x_i = 0) = 1 - w(0 \rightarrow 1),$$

$$w(x_i = 1 \rightarrow x_i = 1) = 1 - w(1 \rightarrow 0), \qquad (4.7)$$

where τ_0 is a microscopic characteristic time and u_i represents the total input to the i-th neuron.

$$g(u_i) = \frac{1 + \tanh(u_i - m)}{2} \qquad (4.8)$$

is the sigmoidal function in the bounded interval [0,1] where m is a parameter controlling the firing probability of a model neuron.

For a biologically more plausible neuron model, we adopted the Izhikevich model because it is known to be computationally efficient and biologically plausible (Izhikevich, 2003). The Izhikevich model reduced the complex dynamics of the Hodgkin-Huxley (HH) neuronal models to two coupled differential equations as

$$\frac{dV_i}{dt} = 0.04V_i^2 + 5V_i + 140 - U_i + I_i, \qquad \frac{dU_i}{dt} = a_i(b_iV_i - U_i). \qquad (4.9)$$

Here the variable V_i represents the membrane potential of neuron i, and U_i represents a membrane recovery variable which correlates with the activation of K^+ ionic currents and inactivation of Na^+ (for detail see (Izhikevich, 2003)). U_i and V_i are reset after a spike: if $V_i \geq 30\text{mV}$, then $V_i \leftarrow c_i,\ U_i \leftarrow U_i + d_i.$ I_i represents a total input to neuron i; a_i, b_i, c_i, d_i are dimensionless adjustable parameters which are usually taken as $(a_i, b_i) = (0.02, 0.2)$ and $(c_i, d_i) = (-65, 8) + (15, -6)r_i^2$ for excitatory neurons, $(a_i, b_i) = (0.02, 0.25) + (0.08, -0.05r_i)$ and $(c_i, d_i) = (-65, 2)$ for inhibitory neurons. r_i is a uniformly distributed random variable on the interval [0, 1] (Izhikevich, 2003).

4.2.2.2 Network structure

We considered two mechanisms for generating oscillatory network states; one is the oscillation driven by external inputs (Figure 4.1A), and the other is the oscillation induced by the intrinsic interaction between excitatory and inhibitory neuron populations (Figure 4.1B). The former mechanism can be a model for hippocampal theta oscillation in which the projections from the medial septum to the hippocampus play a central role (Dragoi, et al., 1999). The latter structure where excitatory and inhibitory neuron pools interact is widely observed in cortical areas (Buzsaki and Wang, 2012). It can be a model for cortical oscillations (such as in a gamma-range) that rely on the interplay between excitatory and inhibitory neuron pools.

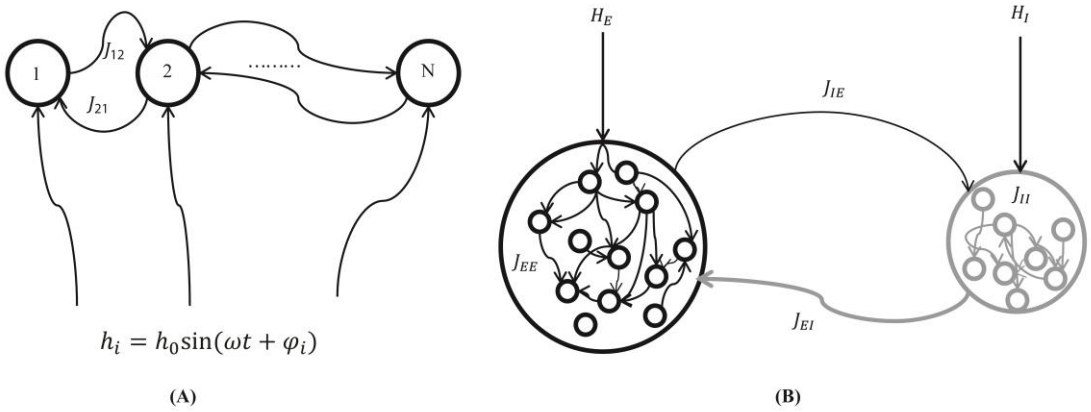

Figure 1

Figure 4.1: A schematic of two mechanisms for generating network oscillations.

(A) Oscillation is generated by an external oscillatory input (externally driven oscillation). A neuron i in the network of N neurons with recurrent connections J_{ij} receives a sinusoidal external input $h_i = h_0 \sin(\omega t + \varphi_i)$ where h_0, ω, and φ_i represent the amplitude, angular speed, and phase of the sinusoidal input, respectively. (B) Oscillation is generated by the interaction between excitatory and inhibitory neuron pools (internally induced oscillation). Excitatory neurons are connected by positive connections J_{EE}, inhibitory neurons are connected by negative connections J_{II}, inhibitory neurons receive positive connections J_{IE} from excitatory neurons, and excitatory neurons receive negative connections J_{EI} from inhibitory neurons. In addition, excitatory and inhibitory neurons receive external constant input H_i^E and H_k^I, respectively.

In the first scenario (externally driven oscillation, Figure 4.1A), a sinusoidal external input $h_i(t) = h_0 \sin(\omega t + \varphi_i)$ for the i-th neuron was used to generate oscillatory states

in a network, where h_0, ω, and φ_i represent the amplitude, angular speed, and phase of sinusoidal signals, respectively. Note that h_0 and ω are common to all neurons, but φ_i can be different for individual neurons. The explicit expression of an input signal allows one to produce different network oscillations systematically. For the binary neuron model, the total input to the *i*-th neuron is written as,

$$u_i(t) = \sum_j J_{ij} x_j(t) + h_i(t). \tag{4.10}$$

where J_{ij} represents a connection weight from the *j*-th neuron to the *i*-th neuron. The neuronal state $x_i(t)$ was then updated following the transition rate w in Equation 4.7. Note that model neurons are identical, whether they are excitatory or inhibitory.

For the Izhikevich model in the first scenario, we considered a population of excitatory neurons. Although it has been demonstrated that a network of excitatory neurons can synchronize, a network of Izhikevich neurons that were connected in this particular way cannot produce an intrinsic oscillation (Han, et al., 2008; Miri, et al., 2011). This allows us to investigate the relationship between the IG measures and an externally driven oscillation in a more realistic setting. The total input to an Izhikevich neuron i is given by,

$$I_i^E(t) = \sum_j J_{ij}^{EE} s_j^E(t) + h_i(t), \tag{4.11}$$

where J^{EE} represent positive weights between excitatory neurons and $s_j^E = \delta(t - t_j^f)$ is the delta function representing the existence of a spike emitted from an excitatory neuron j at time t_j^f. The neuronal state was then updated by Equation 4.9 and the associated reset dynamics. In the numerical simulation, we used a small bin width of one millisecond so that it would contain no more than one spike.

Figures 4.2A, 4.2B, and 4.2C show example spike trains and multi-unit activity of binary model neurons driven by external sinusoidal inputs of 1 Hz, 6 Hz, and 100 Hz oscillations, respectively. Izhikevich neurons also exhibited very similar activity (data not shown). It can be clearly seen that neural activity is entrained to external input. Using these two models, we investigated how the IG measures are affected by externally driven oscillations.

In the second scenario (internally induced oscillation, Figure 4.1B), interaction between excitatory and inhibitory neuron pools generates an oscillation. For the binary neuron model, the total input to the *i*-th excitatory neuron and the *k*-th inhibitory neuron are written as,

$$u_i^E(t) = \sum_j J_{ij}^{EE} x_j^E(t) + \sum_j J_{ij}^{EI} x_j^E(t) + H_i^E,$$

$$u_k^I(t) = \sum_j J_{kj}^{II} x_j^I(t) + \sum_j J_{kj}^{IE} x_j^I(t) + H_k^I, \qquad (4.12)$$

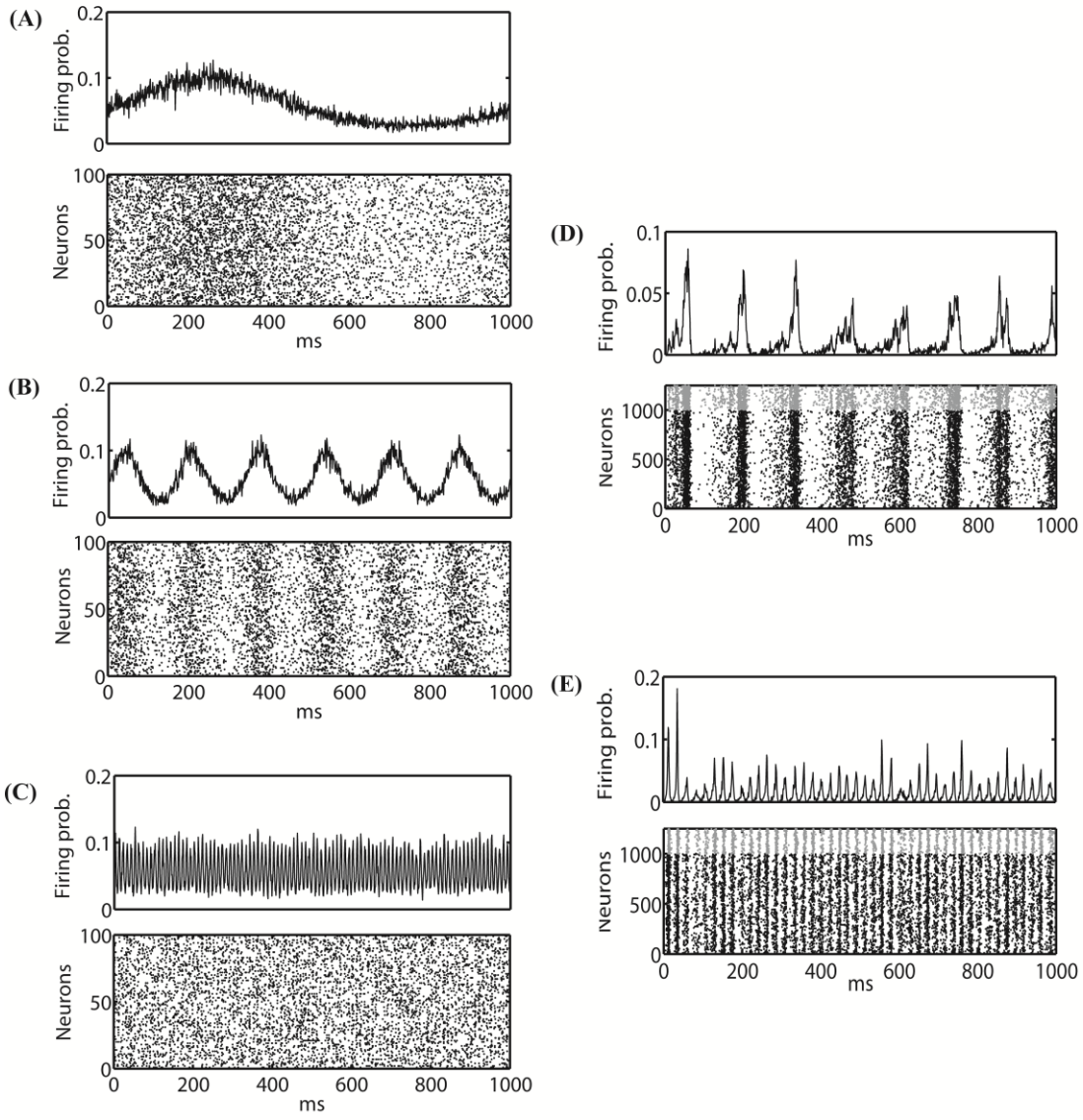

Figure 2

Figure 4.2: Average firing probability and raster plot of representative oscillatory activity.

(A) Average firing probability of 1,000 binary neurons (top panel) and a raster plot of one-hundred randomly sampled neurons (bottom panel) over one-thousand milliseconds under the influence of an external sinusoidal input of 1 Hz (slow oscillation) are shown. (B) Average firing probability of 1,000 binary neurons (top panel) and a raster plot of one-hundred randomly sampled neurons (bottom panel) for an external sinusoidal input of 6 Hz (theta oscillation) are shown. (C) Average firing probability of 1,000 binary neurons (top panel) and a raster plot of one-hundred randomly sampled neurons (bottom panel) for an external sinusoidal input of 100 Hz (ripple oscillation) are shown. (D) One-thousand milliseconds of average firing probability of 1,250 Izhikevich neurons (top panel) and a raster plot

(bottom panel) with approximately a 6-Hz oscillation are shown. In the top panel, spikes from an excitatory neuron and an inhibitory neuron are represented by a black dot and a grey dot, respectively. (E) One-thousand milliseconds of average firing probability of 1,250 Izhikevich neurons (top panel) and a raster plot (bottom panel) with approximately a 40-Hz oscillation are shown.

where J^{II}, J^{IE}, and J^{EI} represent negative weights between inhibitory neurons, positive weights from excitatory neurons to inhibitory neurons, and negative weights from inhibitory neurons to excitatory neurons, respectively. The excitatory and inhibitory neurons receive constant external inputs H_i^E and H_i^I, and maintain sustained oscillatory activity. The neuronal state was updated following the transition rate *w* in Equation 4.7.

For the Izhikevich model in the second scenario, a similar relationship exists for the total inputs for the *i*-th excitatory neuron and the *k*-th inhibitory neuron,

$$I_i^E(t) = \sum_j J_{ij}^{EE} s_j^E(t) + \sum_j J_{ij}^{EI} s_j^E(t) + H_i^E,$$

$$I_k^I(t) = \sum_j J_{kj}^{II} s_j^I(t) + \sum_j J_{kj}^{IE} s_j^I(t) + H_k^I. \qquad (4.13)$$

The neuronal state was then updated following Equation 4.9 and the associated reset dynamics. Figures 4.2D and 4.2E provide examples of spike trains and multi-unit activity of Izhikevich neurons that exhibited approximately 6 Hz and 40 Hz oscillations, respectively. Binary neurons also exhibited a very similar activity (data not shown).

Neural activity was synchronized, but the degree of entrainment was weaker than the externally driven mechanisms. Using these two models, we investigated how the IG measures were influenced by the internally induced oscillation.

4.3 Results

4.3.1 Externally driven oscillation

We investigated the relationship between the IG measures, $\theta_i^{(4,N)}$ and $\theta_{ij}^{(4,N)}$, and the connection weights, $(J_{ij} + J_{ji})$, using a network of 1,000 binary neurons and 1,000 Izhikevich neurons. We focused on the IG measures with 4th-order LLM because they have been shown to estimate connection weights (Nie and Tatsuno, 2012) and external inputs (unpublished data) within a 10% error under an equilibrium assumption. In the simulation, we kept the amplitude of external input at a value such that the overall network firing probability is relatively low (p_{x_i}~0.1). Connection weights were set to the order of $1/N$ to prevent saturation of neuronal activity. For a binary neuron model, we used $J_{ij} = 1/N + \varepsilon_{ij}$ where ε_{ij} is a random variable from a normal distribution $N(0,1/N)$ with a mean of 0 and the standard deviation of $1/\sqrt{N}$. For the Izhikevich model, we restricted the simulations to a pool of only excitatory neurons to ensure that no internally induced oscillation occurred. The connection weights were assigned as $J_{Ij}^{EE} = 1/N + \varepsilon'_{ij}$ where ε'_{ij} is a random variable following uniform distribution $U(0, 1/N)$ within the interval of $[0, 1/N]$. $\theta_i^{(4,N)}$ and $\theta_{ij}^{(4,N)}$were calculated by 10^6 updates of the network. With the time resolution of one millisecond, the simulation corresponds to approximately

fifteen minutes of recordings. To obtain the mean and variances of the IG measures, we performed one-hundred independent simulations. Error bars in the figure represent the standard error of mean (SEM).

We investigated the oscillation frequencies that have often been observed in the brain; slow oscillation (~1 Hz), theta oscillation (6-10 Hz), and ripple oscillation (100-200 Hz). The left column of Figure 4.3 (Panels A, D and G) shows the results for the slow oscillation. The multi-unit activity of the binary neurons exhibits a slow oscillation of the frequency of external input (Figure 4.3A) and the neurons were entrained to this frequency (Figure 4.2A). The spiking activity of Izhikevich neurons also showed almost identical activity (data not shown). To investigate how $\theta_i^{(4,N)}$ and $\theta_{ij}^{(4,N)}$ are related to the change of connection weights, we systematically modified the sum of connection weights between two neurons (1 and 2) from $-9/N$ to $9/N$. Due to the randomness of the connectivity, focusing the neurons (1 and 2) did not affect the generality. We found that $\theta_{12}^{(4,N)}$ was linearly related to the sum of the connection weights, and that the values of $\theta_{12}^{(4,N)}$ for both the binary and Izhikevich models were very close (Figure 4.3D, black line for a binary model and grey line for the Izhikevich model). On the other hand, $\theta_1^{(4,N)}$ (and $\theta_2^{(4,N)}$) were independent from the change of synaptic weights (Figure 4.3G). These

results

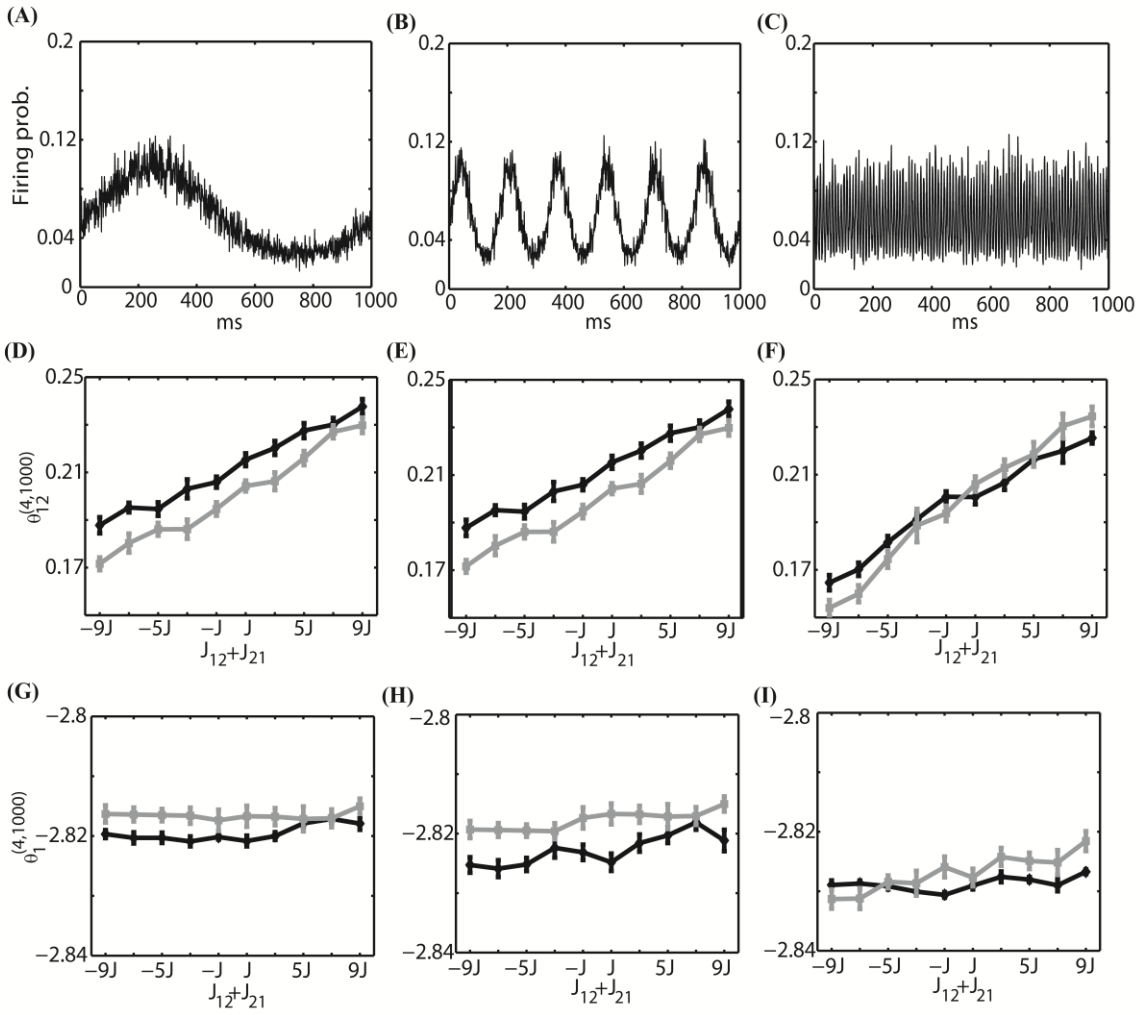

Figure 3

Figure 4.3: Relationship between the IG measures and the sum of connection weights for an externally driven oscillation.

(A) Average firing probability of 1,000 binary neurons with a 1-Hz oscillatory modulation is shown. (B) Average firing probability of 1,000 binary neurons with a 6-Hz oscillatory modulation is shown. (C) Average firing probability of 1,000 binary neurons with a 100-Hz oscillatory modulation is shown. (D) Relationship between the pairwise IG measure ($\theta_{12}^{(4,1000)}$) and the sum of connection weights ($J_{12}+J_{21}$) under a 1-Hz oscillation. Black and grey lines represent the simulation results by binary neurons and Izhikevich neurons, respectively. (E) Relationship between the pairwise IG measure ($\theta_{12}^{(4,1000)}$) and the sum of connection weights ($J_{12}+J_{21}$) under a 6-Hz oscillation. (F) Relationship between the pairwise IG measure ($\theta_{12}^{(4,1000)}$) and the sum of connection weights ($J_{12}+J_{21}$) under a 100-Hz

oscillation. (G) Relationship between the single IG measure $(\theta_1^{(4,1000)})$ and the sum of connection weights $(J_{12} + J_{21})$ under a 1-Hz oscillation. Black and grey lines represent the simulation results by binary neurons and Izhikevich neurons, respectively. (H) Relationship between the single IG measure($\theta_1^{(4,1000)}$) and the sum of connection weights $(J_{12} + J_{21})$ under a 6-Hz oscillation. (I) Relationship between the single IG measure ($\theta_1^{(4,1000)}$) and the sum of connection weights $(J_{12} + J_{21})$ under a 100-Hz oscillation.

are consistent with the previous findings under the equilibrium assumption; showing that IG measures can also provide useful insights in conditions where the network oscillates. The middle and right columns of Figure 4.3 show the results for theta oscillations (Figures 4.3B, 4.3E and 4.3H) and ripple oscillations (Figures 4.3C, 4.3F and 4.3I), respectively. We found that the relationship between the IG measures and connection weights was robust against a different frequency of external inputs. This confirmed that the IG measures can also provide useful information for externally driven theta and ripple oscillations.

To further investigate if the robust property of the IG measures for slow, theta, and ripple oscillations holds true for other frequencies, we varied the frequency over 1 Hz to 200 Hz, the range that can be typically observed in the brain. We set $(J_{12} + J_{21}) = 2J$. Figure 4.4 shows that $\theta_{12}^{(4,N)}$ and $\theta_1^{(4,N)}$ did not depend on oscillation frequencies (Figures 4.4A and 4.4B for a binary model, and Figures 4.6C and 4.6D for Izhikevich model). The results confirmed that the IG measures would be useful for neural data analysis when the brain exhibits a variety of oscillations depending on cognitive demands and the sleep stages.

The previous analyses (Figures 4.3 and 4.4) were performed under the zero relative phase difference between two neurons i and j, namely $\delta\varphi_{ij} = \left|\varphi_i - \varphi_j\right| = 0$. This corresponds to the synchronous neural firings that were depicted in Figures 4.2A, 4.2B, and 4.2C. Neurons can, however, exhibit phase differences. For instance, sequential neural activity was observed in the natural and anesthetized brain states (Dombeck, et al., 2010; Euston, et al., 2007; Lee and Wilson, 2002; Luczak, et al., 2007). Therefore, we calculated IG measures with phase differences. Figure 4.5 shows the results of the 6-Hz simulations in which the phase difference between sinusoidal inputs to the neurons 1 and 2 was set to $\pi/6$ (Figures 4.5A and 4.5C) and $\pi/2$ (Figures 4.5B and 4.5D). The rest of the neuron pairs have random phases in the range of $[0, 2\pi]$. Figures 4.5A and 4.5B show that $\theta_{12}^{(4,1000)}$ is linearly related to the sum of synaptic weights, suggesting that the relationship observed in zero phase difference condition also holds for the non-zero phase difference condition. Similarly, Figures 4.5C and 4.5D show that $\theta_1^{(4,1000)}$ does not depend on the connection weights, even when neurons fire with phase differences. By comparing these results with Figures 4.3E and 4.3H where there was no phase difference, we also found that phase difference produced the shift of the actual values of IG measures. This suggests that if the phase relationship drastically changes between the two recording epochs, the values of the IG measures cannot be directly comparable. However, if their

difference is not large or if phase difference can

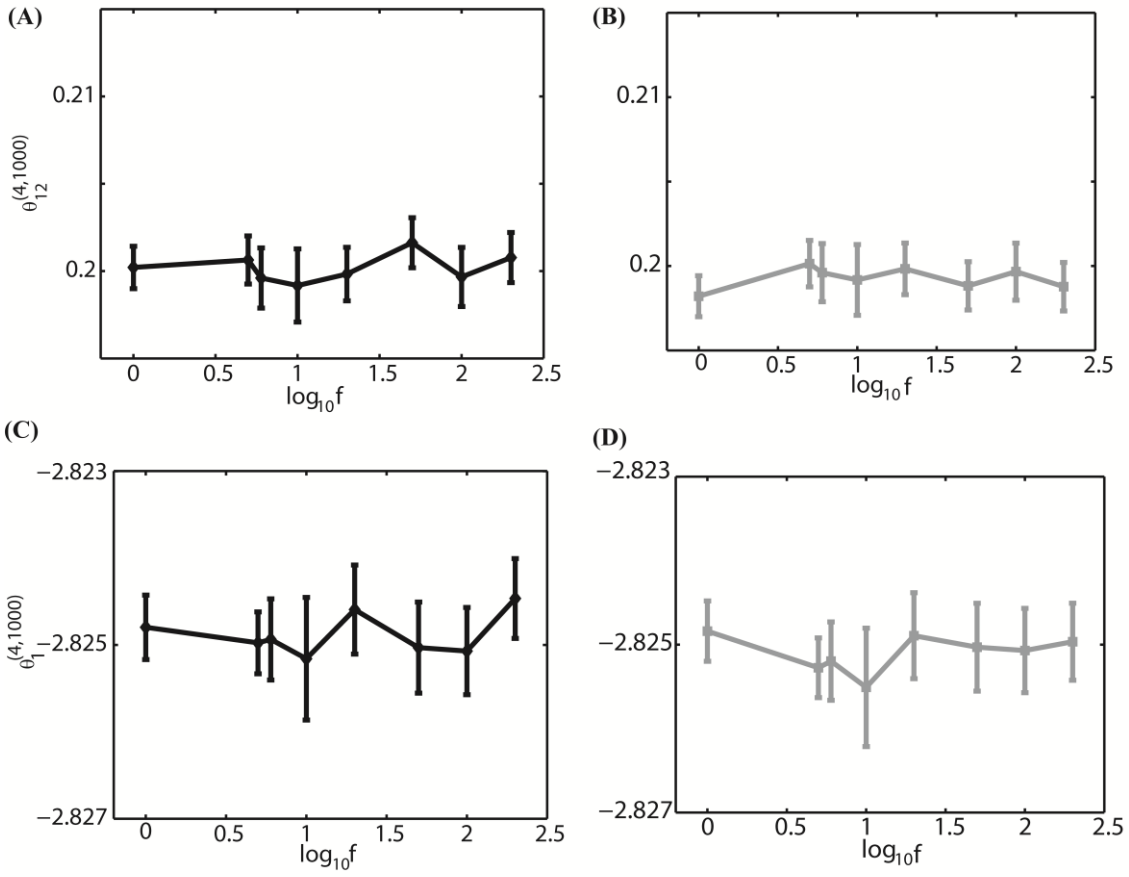

Figure 4

Figure 4.4: Dependency of the IG measures for an oscillation frequency for an external drive oscillation.

The values of the single-IG measure $\theta_1^{(4,1000)}$and the pairwise-IG measure $\theta_{12}^{(4,1000)}$ were calculated for different oscillatory frequencies (1, 5, 6, 10, 20, 50, 100, and 200 Hz). Parameters were set as $J_{12} + J_{21} = 2J,\ h_0 = 0.05$, and $\varphi_i = 0$. (A) The relationship between $\theta_{12}^{(4,1000)}$and the oscillation frequency by binary model neurons. (B) The relationship between $\theta_{12}^{(4,1000)}$and the oscillation frequency by Izhikevich neurons. (C) The relationship between $\theta_1^{(4,1000)}$and the oscillation frequency by binary model neurons. (D) The relationship between $\theta_1^{(4,1000)}$and the oscillation frequency by Izhikevich neurons.

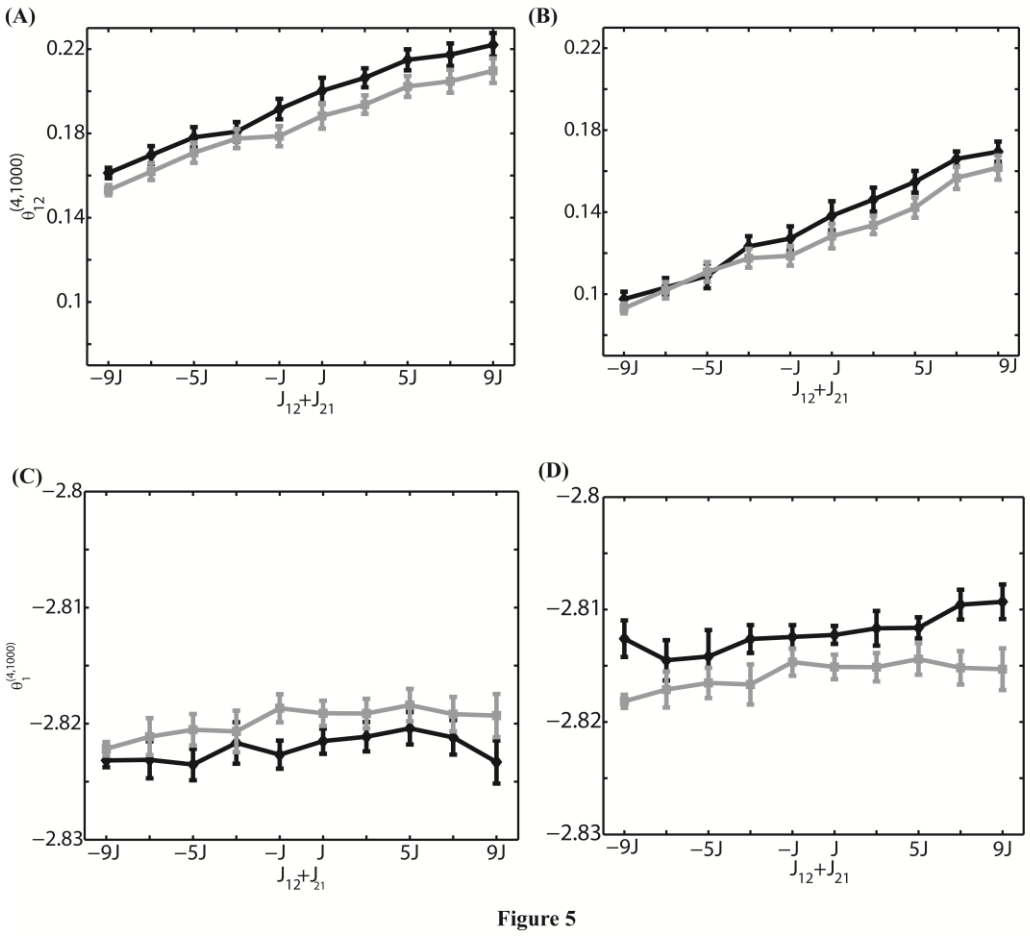

Figure 5

Figure 4.5: Relationship between the IG measures and the sum of connection weights for non-zero phase differences.

An external oscillation mechanism was used, and the oscillation frequency was set to 6 Hz. (A) Relationship between the pairwise IG measure ($\theta_{12}^{(4,1000)}$) and the sum of connection weights ($J_{12}+J_{21}$) for the phase difference of $\delta\varphi_{12} = \pi/6$. Black and grey curves represent the simulation by binary neurons and Izhikevich neurons, respectively. (B) Relationship between the pairwise IG measure ($\theta_{12}^{(4,1000)}$) and the sum of connection weights, $(J_{12}+J_{21})$ for the phase difference of $\delta\varphi_{12} = 2$. (C) Relationship between the single-IG measure ($\theta_{1}^{(4,1000)}$) and the sum of connection weights ($J_{12}+J_{21}$) for the phase difference of $\delta\varphi_{12} = \pi/6$. (D) Relationship between the single-IG measure ($\theta_{1}^{(4,1000)}$) and the sum of connection weights ($J_{12}+J_{21}$) for the phase difference of $\delta\varphi_{12} = \pi/2$.

be estimated beforehand, we could use the information for adjusting the IG values. We also confirmed that these relationships held true for slow (1 Hz) and ripple (100 Hz) frequencies (data not shown).

So far we have focused on the relationship between the IG measures and the connection weights. Another important parameter is the magnitude of sinusoidal input h_0. Therefore, we have analyzed how $\theta_1^{(4,1000)}$ and $\theta_{12}^{(4,1000)}$ are related to h_0. Figure 4.6 shows the result when the external sinusoidal input has a frequency of 6 Hz (theta oscillation). We found that $\theta_{12}^{(4,1000)}$ was nearly independent from the change of h_0 (Figure 4.6A), but $\theta_1^{(4,1000)}$ was almost linearly related to it (Figure 4.6B). We also confirmed that almost identical relationship holds true for other frequencies such as slow oscillation and ripple oscillation if there is no phase difference. For non-zero phases between neurons, we observed that the IG values were shifted, like the case for the IG values and connection weights, but that the same linear and independent relationship in Figure 4.6 was sustained. The results under the oscillatory condition are consistent with the previous findings under the equilibrium condition; $\theta_i^{(4,N)}$ was linearly related to the magnitude of the constant input and that $\theta_{ij}^{(4,N)}$ was almost independent from it (Nie and Tatsuno, 2012). The investigation here provides further evidence that $\theta_i^{(4,N)}$is useful for the estimation of the magnitude of external input.

In summary, we investigated how the IG measures were influenced by an externally driven oscillation. Using a simple binary neuron model, and a more realistic Izhikevich

model, we found that $\theta_{ij}^{(4,N)}$ had a linear relationship with the sum of the connection weights, and that it was almost independent from the magnitude of a sinusoidal input. In contrast, $\theta_{i}^{(4,N)}$ was almost independent from the connection weights, but was linearly related to the magnitude of the sinusoidal input. These properties were not affected by the frequency of the oscillations or the relative phase differences between neurons.

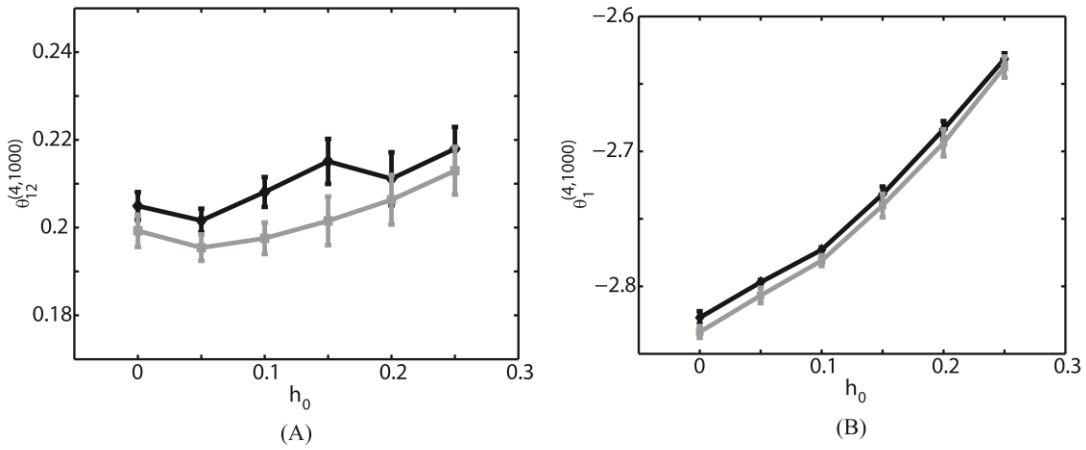

Figure 6

Figure 4.6: Relationship between the IG measures and the amplitude of an external sinusoidal input for an externally driven oscillation.

Oscillation frequency was set to 6 Hz and phase difference was $\delta\varphi_{12} = 0$. (A) Relationship between the pairwise-IG measure, $\theta_{12}^{(4,1000)}$, and the amplitude of a sinusoidal input, h_0. Black and grey lines represent the simulation results by binary neurons and Izhikevich neurons, respectively. (B) Relationship between the single-IG measure, $\theta_{1}^{(4,1000)}$, and the amplitude of a sinusoidal input, h_0.

4.3.2 Internally induced oscillation

As another mechanism for generating an oscillatory network behavior, we also investigated the interactions between excitatory and inhibitory neuron pools. We analyzed the network structure in Figure 4.1B by simple binary model neurons and Izhikevich neurons. Unlike the first oscillation mechanism, where an oscillation

frequency and phase differences could be explicitly controlled, it was not easy to generate an oscillation with desired parameters. However, we were able to generate two examples that were often observed in the brain. Figures 4.7A and 4.7B show multi-unit activity corresponding to theta frequency (approximately 8 Hz) and gamma frequency (approximately 40 Hz), respectively. The same examples with a raster plot were also depicted in Figures 4.2D and 4.2E. To avoid saturation in neural activity, we have set the connection weights to the order of $1/N$. For a theta oscillation, we set the connection as $J_{ij}^{EE} = J_1 \cdot \epsilon'_{ij}$, $J_{ij}^{IE} = 5J_1 \cdot \epsilon'_{ij}$, $J_{ij}^{II} = -J_2 \cdot \epsilon'_{ij}$ and $J_{ij}^{EI} = -J_2 \cdot \epsilon'_{ij}$ where $J_1 = 1/N_e$, $J_2 = 1/N_i$, and ϵ'_{ij} is a random variable following a uniform distribution $U(0,1)$ within the interval [0,1]. For a gamma oscillation, we used $J_{ij}^{EE} = J_1 \cdot \epsilon'_{ij}$, $J_{ij}^{IE} = 6J_1 \cdot \epsilon'_{ij}$, $J_{ij}^{II} = -J_2 \cdot \epsilon'_{ij}$ and $J_{ij}^{EI} = -2J_2 \cdot \epsilon'_{ij}$. The stronger J^{IE} was necessary to induce oscillation (Adini, et al., 1997). The external constant inputs to excitatory and inhibitory neurons were set as $H_i^E = 0.05$ and $H_i^I = 0.02$, respectively. The simulation of 10^6 update was performed with $N_e = 1000$ excitatory neurons and $N_i = 250$ inhibitory neurons. The mean and variance was estimated using one-hundred independent simulations.

To investigate the relationship between the IG measures and the sum of connection weights, without losing the generality, we modified $(J_{12} + J_{21})$ between the neurons (1 and 2) in the range of $[-9J, 9J]$. Firstly, we focused on the connections within the excitatory neuron population and within the inhibitory neuron population. In other words, both connections, J_{12} and J_{21}, were positive for the range of $(J_{12} + J_{21}) \geq 0$ and both were negative for $(J_{12} + J_{21}) < 0$. Figures 4.7C and 4.7E show the relationship between

$\theta_{12}^{(4,1250)}$ and $\theta_{1}^{(4,1250)}$, and the sum of connection strengths ($J_{12} + J_{21}$) under the theta oscillation. The results clearly show that $\theta_{12}^{(4,1250)}$ is linearly related to the sum of the connection weights and that $\theta_{1}^{(4,1250)}$ was independent from the modulation of the connection weights. Furthermore, the dependency of the IG measures on the connection weights was continuous in both positive and negative ranges. This suggests that IG measures can be applicable to both positive and negative connections. Figures 4.7D and 4.7F show results for gamma oscillation. Similar results were obtained for both $\theta_{12}^{(4,1250)}$ and $\theta_{1}^{(4,1250)}$.

Secondly, we investigated the interaction between excitatory and inhibitory neurons. Namely, we selected the neuron 1 from the excitatory neuron pool and the neuron 2 from the inhibitory neuron pool. The sum of connection weights was modified from -9J to 9J. Figures 4.8A and 4.8B are the same with Figures 4.7A and 4.7B, showing the multi-unit activity for theta and gamma oscillation, respectively. Figures 4.8C and 4.8E show the relationship between the IG measures and the sum of the connection weights under the theta oscillation. Similarly, Figures 4.8D and 4.8F are for gamma oscillation. The results show that the linear dependency of $\theta_{12}^{(4,1250)}$ on the sum of the connection weights holds

true for an excitatory and inhibitory neuron pair. We also found that

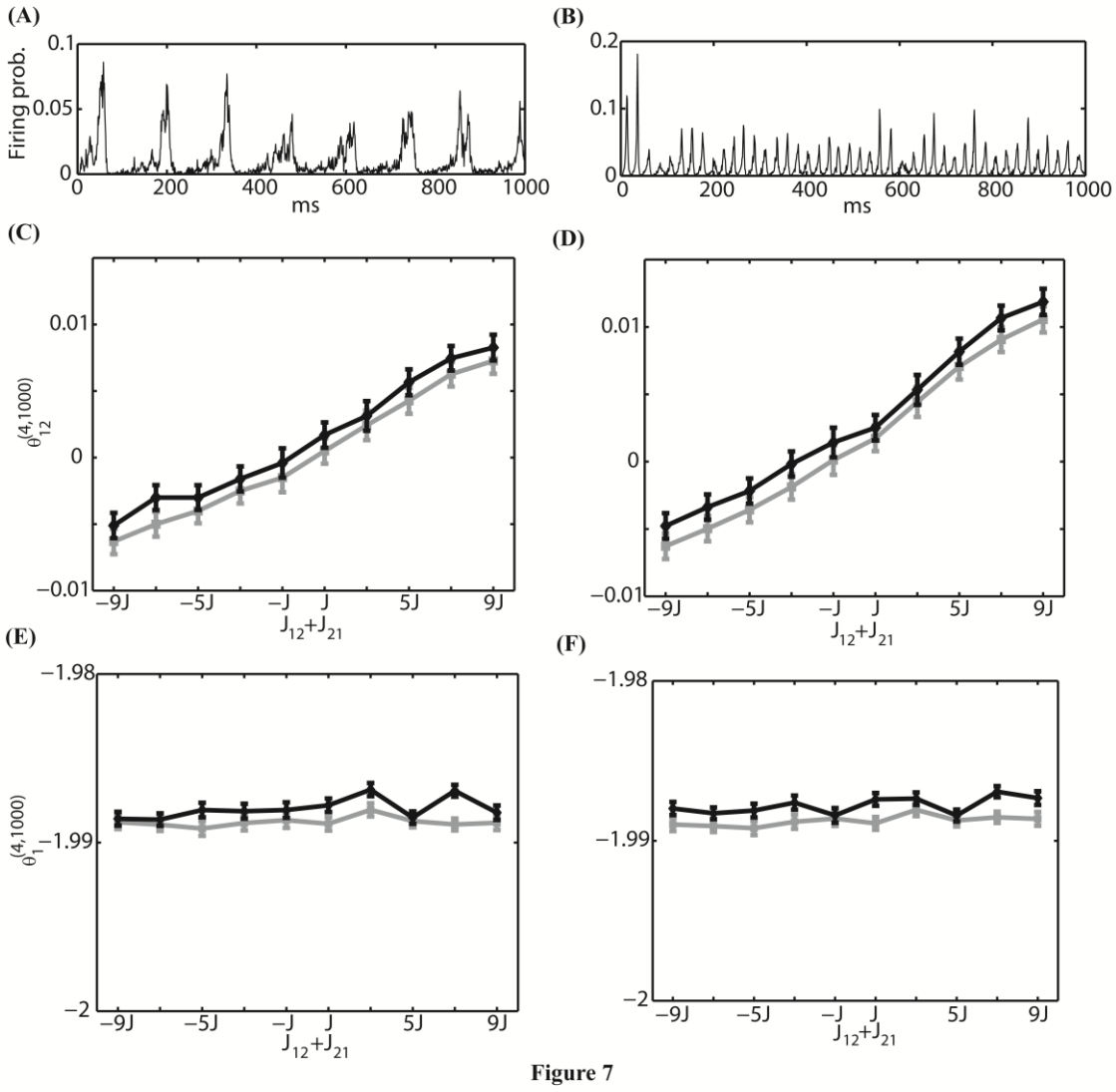

Figure 7

Figure 4.7: Relationship between the IG measures and the sum of connection weights for an internally induced oscillation.

Both connections, J_{12} and J_{21}, were positive for the range of $(J_{12}+J_{21}) \geq 0$ and they were negative for $(J_{12}+J_{21}) < 0$. (A) Average firing probability of 1,250 Izhikevich neurons with approximately a 6-Hz oscillatory oscillation is shown. (B) Average firing probability of 1,250 Izhikevich neurons with approximately a 40-Hz oscillatory oscillation is shown. (C) Relationship between the pairwise-IG measure ($\theta_{12}^{(4,1000)}$) and the sum of connection weights ($J_{12}+J_{21}$) under a 6-Hz oscillation. Black and grey lines represent the simulation results by binary neurons and Izhikevich neurons, respectively. (D) Relationship between the pairwise-IG measure ($\theta_{12}^{(4,1000)}$) and the sum of connection weights ($J_{12}+J_{21}$) under a 6-Hz oscillation. (E) Relationship between the single-IG

measure($\theta_1^{(4,1000)}$) and the sum of connection weights ($J_{12}+J_{21}$) under a 6-Hz oscillation. (F) Relationship between the single-IG measure ($\theta_1^{(4,1000)}$) and the sum of connection weights ($J_{12}+J_{21}$) under a 40-Hz oscillation.

$\theta_1^{(4,1250)}$ had almost no relationship with the sum of connection weight. For the relationship between the IG measures and the magnitude of constant input H_i^E and H_i^I, we confirmed that $\theta_1^{(4,1250)}$ was linearly related to their magnitude, but $\theta_{12}^{(4,1250)}$ was independent from them (data not shown).

In summary, for internally generated oscillations, we demonstrated that the relationship between the IG measures and the connection weights that were found under equilibrium assumption also held true.

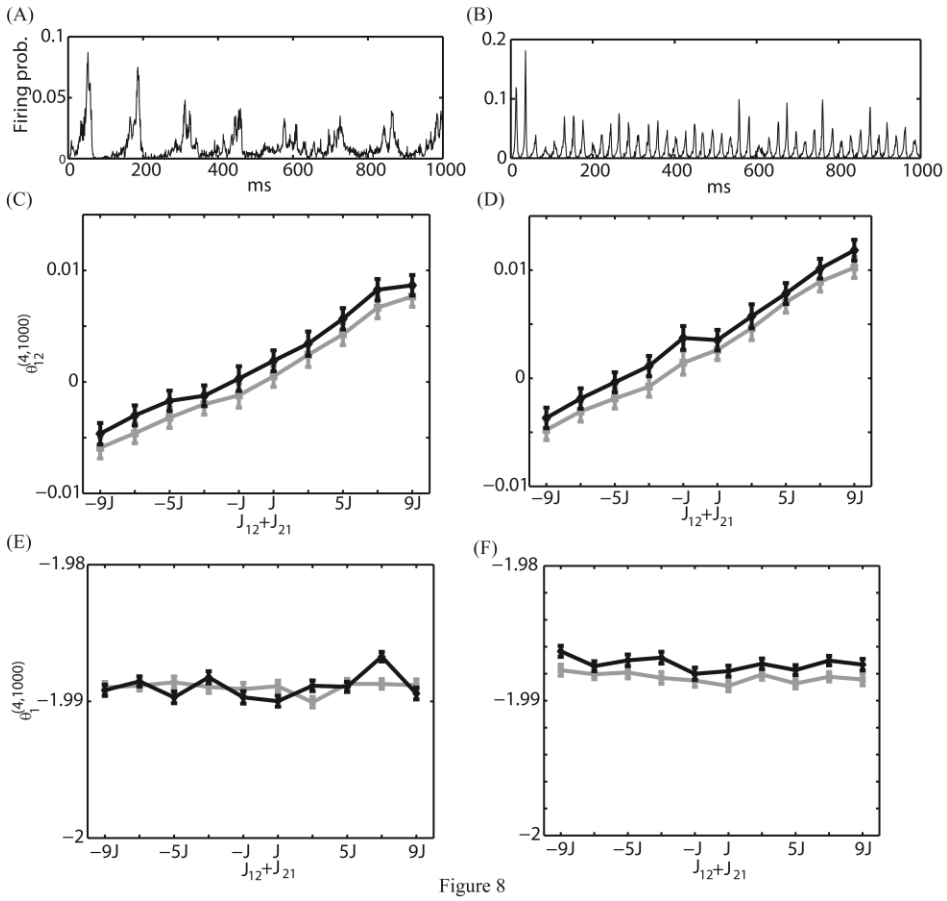

Figure 8

Figure 4.8: Relationship between the IG measures and the sum of connection weights for an internally induced oscillation.

Neuron 1 was selected from the excitatory neuron pool and Neuron 2 was selected from the inhibitory neuron pool. In other words, one of the connections in $J_{12} + J_{21}$ was positive and the other was negative. (A) Average firing probability of 1,250 Izhikevich neurons with approximately a 6-Hz oscillatory oscillation is shown. (B) Average firing probability of 1,250 Izhikevich neurons with approximately a 40-Hz oscillatory oscillation is shown. (C) Relationship between the pairwise-IG measure ($\theta_{12}^{(4,1000)}$) and the sum of connection weights ($J_{12} + J_{21}$) under a 6-Hz oscillation. Black and grey lines represent the simulation results by binary neurons and Izhikevich neurons, respectively. (D) Relationship between the pairwise-IG measure ($\theta_{12}^{(4,1000)}$) and the sum of connection weights ($J_{12} + J_{21}$) under a 6-Hz oscillation. (E) Relationship between the single-IG measure ($\theta_{1}^{(4,1000)}$) and the sum of connection weights ($J_{12} + J_{21}$) under a 6-Hz oscillation. (F) Relationship between the single-IG measure ($\theta_{1}^{(4,1000)}$) and the sum of connection weights ($J_{12} + J_{21}$) under a 40-Hz oscillation.

4.4 Discussion

Previous studies have shown that the IG measures provided useful information about network structures (Brown, et al., 2011; Tatsuno, et al., 2009; Tatsuno and Okada, 2004). Specifically, the single-IG measure $\theta_i^{(4,N)}$ was related to the magnitude of external constant input, and the pairwise-IG measure $\theta_{ij}^{(4,N)}$ was related to the sum of the connection strengths. Although these studies were conducted under the equilibrium assumption, the real neural signals exhibit various oscillations depending on cognitive demand of the task or the state of the brain. Therefore, we studied the relationship between the IG measures and the neural network parameters under oscillatory network states.

We have considered two general oscillation mechanisms; one was the oscillation driven by external input, and the other was the oscillation induced internally due to interactions

between excitatory and inhibitory neuron pools. Numerical simulation was performed by the network of a simple binary neuron model and the Izhikevich neuron model. The former model was used so as to compare the results with that of previous studies, and the latter was used to investigate the relationship with more realistic model neurons.

For the external oscillation, our investigation showed that $\theta_{ij}^{(4,N)}$ was linearly related to the sum of the connection strengths, and that $\theta_{i}^{(4,N)}$ was independent from it over a wide range of frequency from 1 Hz to 200 Hz. We also showed that the relationship holds true when there are phase differences between neurons. In addition, we demonstrated that $\theta_{i}^{(4,N)}$ was almost linearly related to the magnitude of sinusoidal input, but that $\theta_{ij}^{(4,N)}$ was almost independent from it. For the internally induced oscillation, we have also confirmed that $\theta_{ij}^{(4,N)}$ was linearly related to the sum of the connection strengths, and that $\theta_{i}^{(4,N)}$ was independent from it. We have also shown that the same relationship holds true for any neuron pairs (within excitatory population, within inhibitory population, and across excitatory and inhibitory populations).

In summary, this study and previous studies have demonstrated that the IG measure provides useful information for analyzing neural circuits; not only for the equilibrium condition, but also for the oscillatory condition. The single-IG measure is useful for estimating the relative strength of external inputs. In addition, the single-IG measure is better than using the change in firing rate because the firing rate can be modulated both by the change in synaptic coupling strength and the magnitude of external inputs. Studies show that the appropriately selected single-IG measure is capable of estimating the

external inputs with relatively small influence from synaptic interactions. Similarly, the pairwise-IG measure can provide more direct information about the synaptic interactions between neurons than other correlation measures (Amari, 2009). It has been also shown that the pairwise-IG measure is statistically independent from the change in firing rate and that it provides pure neural interactions (Amari, 2001; Nakahara and Amari, 2002). Together with the findings in this study, the pairwise-IG measure is a very useful measure to study direct neural interactions between neurons.

This study suggests that the actual values of the IG measures depend on the mechanisms of oscillation. For an externally driven oscillation, $\theta_{12}^{(4,N)} \sim 0.2$ was obtained for $(J_{12} + J_{21}) \sim 1/N$. For an internally induced oscillation, the same connection strength produced $\theta_{12}^{(4,N)} \sim 0.002$. Within the same oscillation mechanism, the selection of model neurons (binary model or Izhikevich model), or a small difference in network parameters such as phase differences also produced a difference in the actual value of the IG measures. Nonetheless, as long as the network is in one of the oscillation mechanisms, and the phase difference is kept the same, the IG measures can provide useful insights into network structures regardless of the oscillation frequencies.

In the study of memory consolidation, one of the key questions is to understand how the changes in synaptic connections are related to learning and memory formation. Evidence suggests that neural activity during slow-wave sleep plays an important role in learning (Diekelmann and Born, 2010). Specifically, there is increasing evidence supporting the hypothesis that replay of neural activity during subsequent sleep is positively correlated

with memory formation (Euston, et al., 2007; Girardeau, et al., 2009; Kudrimoti, et al., 1999; Lee and Wilson, 2002; Pavlides and Winson, 1989; Peyrache, et al., 2009; Ponticorvo and Miglino; Wilson and McNaughton, 1994). However, the direct information about synaptic change is not available from multi-unit recordings of a freely behaving animal because spikes and local field potentials are the two main observables. In this study, we showed that $\theta_{ij}^{(4,N)}$ was linearly related to the sum of the connection weights, and that $\theta_{i}^{(4,N)}$ was linearly related to the magnitude of external inputs, even under the oscillatory conditions. We have also verified these relationships not only with a simple binary model neuron, but also with a more realistic spiking model neuron. This finding would allow us to analyze neural activity during slow-wave sleep before and after the task; $\theta_{ij}^{(4,N)}$ would be a good measure for the change of connection weight, and $\theta_{i}^{(4,N)}$ for the magnitude of background input that would be influenced by local field potentials. By comparing the relative change of $\theta_{ij}^{(4,N)}$ between slow-wave sleeps before and after the task, and the strength of memory replay/improvement of behavior performance, the IG measure may provide a way to estimate the relationship between the synaptic modification and memory formation without having direct access to information of synaptic change.

As a related approach to the IG method, the maximum entropy (MaxEnt) has attracted much attention recently (Schneidman, et al., 2006; Szuts, et al., 2011; Tang, et al., 2008). The philosophy of the MaxEnt approach is not to assume anything other than what we know from the data. For example, if firing rate and pairwise correlation are the only

information we have, the distribution with maximum entropy is given as the Boltzmann distribution,

$$P^{(2)}\{x\} = \frac{1}{Z}\exp\left(\sum_i h'_i x_i + \sum_{i<j} J'_{ij} x_i x_j\right), \tag{4.14}$$

where h'_i is a bias term for the neuron i, J'_{ij} is the symmetric coupling strength between neurons i and j, and the partition function Z is given by,

$$Z = \sum_{\{x\}} \exp\left(\sum_i h'_i x_i + \sum_{i<j} J'_{ij} x_i x_j\right). \tag{4.15}$$

We see that the MaxEnt is equivalent to the IG with the 2nd-order LLM,

$$\log p_{x_1 x_2 * \ldots *} = \sum_i \theta_i^{(2,N)} x_i + \sum_{i<j} \theta_{ij}^{(2,N)} x_i x_j - \psi(\boldsymbol{\theta})^{(2,N)}, \tag{4.16}$$

where the relationship between the parameters are given as,

$$\theta_i^{(2,N)} = h'_i, \;\; \theta_{ij}^{(2,N)} = J'_{ij}, \;\; \psi(\boldsymbol{\theta})^{(2,N)} = \log Z. \tag{4.17}$$

As was discussed in Tatsuno and Okada (2004) and in Tatsuno et al. (2009), it is possible to relate these IG measures, $\theta_i^{(2,N)}$ and $\theta_{ij}^{(2,N)}$, to the network structure even for a network

with asymmetric connections (Equation 4.5). However, under the influence of correlated inputs, we have also shown that the relationship in Equation 4.5 broke down, and that it was necessary to use the IG measures with the higher-order LLM such as the 4th-order (Equation 4.6) (Nie and Tatsuno, 2012). In other words, it was necessary to take into account neural activity of two additional neurons to estimate the direct neural interaction between neuron i and j. In summary, we see that the MaxEnt approach and the IG method are closely related. In addition, we also see that the MaxEnt can be considered a part of the IG method that provides a more general analysis framework for the space of the probability distributions.

In this study, we used the synchronous neural activity for estimating the direct neural interaction as the form of $(J_{ij} + J_{ji})$. However, in the real learning processes such as sequential learning, it is possible that synaptic modification occurs differently for each direction; e.g., J_{ij} increases, while J_{ji} decreases. The proposed method is not able to estimate the directed synaptic change. As one possible remedy for this difficulty, calculation of the pairwise-IG measure using the time-lagged spiking activity between neurons was suggested (Brown, et al., 2011; Tatsuno and Okada, 2004). Another limitation of the present study is not including the effect of delay; e.g., axonal conduction delay or synaptic transmission delay. It is possible that these delays dramatically change the firing patterns as well as increase a variety of coexisting patterns (Izhikevich, 2006). Little is known about the relationship between the IG measures and direct neural interactions with conduction delay. In addition, it has not been clear how IG measures with more neuronal interactions such as triplewise-IG measures $\theta_{ijk}^{(k,N)}$ or quadruple-IG

measures $\theta_{ijkl}^{(k,N)}$ behave under oscillatory conditions. It would be interesting to extend the current study to include more neuronal interactions.

Despite these limitations, the IG method is one of the most promising statistical tools for spike train analysis (Amari, 2001; Nakahara and Amari, 2002). Its direct relationship with the network parameters would provide useful information for the estimation of structural changes (Tatsuno and Okada, 2004; Tatsuno et al., 2009; Nie and Tatsuno, 2012). We hope that an advancement of novel analysis methods including information geometry will lead to a break-through finding in neuroscience.

Chapter 5 Conclusion, discussion and future work

5.1 Novel findings

The primary goal of the present work was to extend the previous studies on IG approach to more realistic and complex cases, and develop applicable neuronal spike data analysis methodology based on theoretical and numerical investigation. To this end, we systematically investigated the properties of IG method on the measurement of single neuronal firing rate, pair-wise correlation (synaptic connection weights), and higher-order (triple-wise, fourth-order, etc.) neuronal interactions by studying small and large recurrent neural networks. To make our findings solid, we started from the mathematical analysis for a symmetrically connected small neural network (10-neuron) using simplified model neurons—binary neuron, which only has 0 or 1 states. The advantage of this model is that we are able to derive the detailed analytical results for the relationship between IG measures and multiple network parameters, including the external uncorrelated inputs h, recurrent connection weights J from the same layer, and the correlated background inputs W projected from neurons in another layer. By detailed mathematical analysis, we obtained the insights of how IG measures are affected by these parameters. The range of the parameters is adjustable such that we are capable of observing the behavior of the IG measures. In the realistic brain network, however, neurons are connected asymmetrically. The detailed mathematical solution for such a complicated system becomes impossible. Therefore, computer simulations for IG measures were carried out in both symmetrically and asymmetrically connected network (10- and 1000-neuron network). By comparing out simulation results with the theoretical calculations using small network (10-neuron

network), we confirmed the validity and correctness of our simulation strategy. By the large network simulations (1000-neuron network), we confirmed the robustness of IG measures on the estimation of synaptic connection weights and external inputs.

Specifically, by numerical simulations of large asymmetric network, we found that 4th and 5th log-linear expansions of IG measure $\theta_{ij}^{(4,N)}$ or $\theta_{ij}^{(5,N)}$ in a *N*-neuron network receiving correlated inputs provide a robust estimation of the sum of the connection weights $J_{ij} + J_{ji}$ with approximately a ten percent error (for detail, see the Fig.8 in chapter 2). In contrast, the previous studies for IG method showed that 2-th order log-linear expansion $\theta_{ij}^{(2,N)}$ is sufficient to estimate $J_{ij} + J_{ji}$ in an *N*-neuron network that only receives uncorrelated external inputs *h*. The existence of correlated background inputs *W*, therefore, violates the correct estimation of $J_{ij} + J_{ji}$ using $\theta_{ij}^{(2,N)}$. Our novel analysis suggests that higher-order log-linear expansion could offset this estimation error. This finding indicates that in realistic neuronal data sets, we can estimate the change of synaptic connection weight between neuron pair *i* and *j* by taking into account the spiking data from additional 2 or 3 neurons, together with the spike data from neuron *i* and *j*. This solution makes it possible to analyze massive neuronal data set in reasonable time and space.

Since the IG theory proposes hierarchical structure of neuronal interactions, we further extended the study of IG methods to higher order neuronal interactions. In chapter 3, we thoroughly studied the relationship between external inputs (correlated and uncorrelated) and the asymmetry of connections on IG measures involving up to ten neuronal interactions. In this chapter, we again performed analytical and numerical calculations.

We aimed to obtain how measures of up to ten neuronal interactions are characterized by external inputs. We not only confirmed the single and pair-wise IG measures were good estimators of the background input and of the synaptic connection weights, but also confirmed that for higher order IG measures, the influence of external inputs was highly nonlinear. In addition, by introducing a new parameter λ, which characterizes the asymmetry of a network, we also found that all the IG measures from the single-neuron IG to the ten-neuron IG measures were robust against the increased asymmetry of connection weights, and the IG measures with the higher log-linear model provide a better result. The single-neuron IG θ_i and the two-neuron IG θ_{ij} always are good estimators of external input *h* and the sum of the connection weights $J_{ij} + J_{ji}$ even under a strong asymmetrically connected network (λ is large). The simulation results also indicate that higher-order neuronal interactions (triple-wise IG θ_{ijk}, 4-neuron IG θ_{ijkl}, etc.) are trivial comparing to the 1-and 2-neuron IG measures. These results are consistent with those which are derived from information theory such as maximum entropy analysis for neuronal spike data (see section 1.2.4).

To summarize, chapter 2 and 3 showed that IG measures provide useful information on network structure. We demonstrated that the single-IG (1-neuron IG) measure $\theta_{\mathrm{i}}^{(4,\mathrm{N})}$ is related to the amplitude of external constant input, while the pair-wise (2-neuron) IG $\theta_{\mathrm{ij}}^{(4,\mathrm{N})}$ gives the robust measure of the connection weights. These findings are important and attractive to neuroscientist, because in the neuroscience point of view, estimating the single neuronal firing rate and the synaptic change play a key role in understanding the brain functions. Nevertheless, these extensive studies of IG methods were mainly based on the assumption of stationarity. That is, we assume that the network firing exhibits a

stable feature, which is not always true in realistic brain unfortunately. Instead, neural firing exhibits non-stationary changes in real electrophysiological experiments. The real neuronal signals observed from experiments contain various oscillations depending on cognitive demand of animals' behaving tasks. Therefore, it is natural to ask the question of whether and how IG methods proposed here provide the measure for network parameters in an oscillatory network. To answer this question, chapter 4 studied the single-neuron IG $\theta_i^{(4,N)}$ and two-neuron IG $\theta_{ij}^{(4,N)}$ by considering two general network oscillation mechanisms: the oscillation driven by external fluctuating inputs and the oscillation induced by the interplay between excitatory and inhibitory neuronal pool in a network. For the nonstationary network, we only performed numerical simulations by the network of a binary neuron and Izhikevich neuron. Using binary neuron, it is easy to set up a sinusoidal external input and change the input frequencies, and phases of oscilations , it is again less realistic. By using Izhikevich neuron, which can produce more biologically plausible neuronal firing patterns, it is convincing to visualize how IG measures behave in oscillatory networks. From both scenarios, we found that the two-neuron IG $\theta_{ij}^{(4,N)}$ keeps the linearity to the sum of connection weights, and the single-neuron IG $\theta_i^{(4,N)}$ was almost linearly related to the magnitude of external input, and these characters are independent from the network oscillation frequencies. These findings indicate that the properties of IG measure found under stationary assumption still hold true under oscillatory network states.

5.2 Future studies in multiple spike data analysis

The advanced recording techniques of multiple spike trains from freely behaving animals offer a way to record the neuronal population activity from as many neurons as possible. As the development of these techniques, it is impossible to quantitatively analyze the neuronal activity from the massive spiking data without substantial statistical methods. The study of IG measures discussed in the present thesis provides one way of estimating both pair-wise and higher-order neuronal interactions. Nevertheless, this method has not been verified by large number of real experiments. The future challenge, therefore, is still to verify the validity of IG methods that truly allow neuroscientists to extract the useful information from the real experimental data.

In practice, cross correlation approach is still a widely accepted method for the analysis of neuronal interactions. One of the most recent studies using cross correlation was the analysis of weak connection between excitatory cortical neurons (Schwindel et al., 2014). In this study, due to the weakness of excitatory neuronal interactions, a long-time recorded data (~25h) from rat prefrontal cortex was analyzed to improve the poor sampling. The limitation of cross correlation approach, however, is that the method assumes the stationarity of spike trains. In addition, cross correlations are affected by firing rate differences between neurons (de la Rocha et al., 2007; Amari, 2009). Comparing to cross correlation method, IG method might overcome these difficulties in practice. In the present thesis, we have shown that IG approach may not need the assumption of stationarity. In chapter 3, our modeling study indicates that the linear relationship between 2-neuron IG measures holds under different network oscillations.

This property is useful for real spike data analysis, because the stability of IG measures allows us to treat segments of spike data from different oscillation periods as an integrated set. For instance, in the study of memory consolidation during sleep, rats are trained to perform reaching tasks in the pre-learning period. After the sleeping period, the rats will be trained to take the same reaching actions again in the post-learning period. This procedure will be repeated many days until the rats learn a skilled reaching task, and neuronal activity in the motor cortex will be recorded each day. The main purpose of this experiment is to find whether memory in the motor cortex is consolidated during non-REM sleep. It is believed that the corresponding neuronal synaptic plasticity during learning is a slow and asymptotic process. During the learning procedure, evident plasticity has not occurred in the first several training days. Instead, there would be a remarkable synaptic plasticity during the last several training days. In both pre and post-learning phases, the rats might experience multiple brain oscillation states. It is because the rats take not only reaching actions, but also other behaviors such as walking and resting during the entire recording. Based on the study in chapter 3, it is possible to treat data segments recorded from pre-learning phase as one set, and the data from post-learning phase as another set. The calculations of IG measures for the two big data sets provide us with reliable information, indicating whether synaptic plasticity occurs or not during the training. Therefore, in real spike data analysis using IG method, we might be able to divide spike data in terms of learning stages. A preliminary study has been conducted for rat's parietal cortex using IG approach (unpublished work). 38 neurons from parietal cortical area are recorded for rat's sequential learning and memory consolidation during sleep. We tested the computational efficiency on IG approach. For example, one calculation using 4^{th} order IG measures for 30min spike data of 38 neurons

(703 neuronal pairs) requires about 20 minutes computational time. Although the average computational time by IG approach is longer than the time by cross correlation analysis in a single CPU, we are capable of completing 3h spike data through six CPUs simultaneously in 20 minutes with the help of parallel computing techniques. Thus, parallel computing techniques might allow neuroscientists to apply IG approach in a more efficient way for multi spike data analysis under different brain states.The present study of IG measures focused on coincident firings only, which corresponds to the zero time-lagged bin of a cross correlation function. The most appealing property of IG method is that the two-neuron IG measure θ_{ij} is only linearly related to the sum of the connection weights $J_{ij} + J_{ji}$. This property indicates that the calculation of θ_{ij} can estimate the change of total synaptic connection weights between neuron pairs in current study. Recent behavioral experiments show the evidence of directional plasticity during animals' sequential learning in rat's hippocampal place cells (Zenata, 2012). When a rat is placed in an open field environment, the firing of place cells is statistically independent of the direction of traverse through the place field. However, if the rat's path is strict on a track, the firing rates in the two directions substantially diverged. This directionality also developed in an open environment when rats learned to run along a specified path. The study indicated that the effect is almost due to positive and negative changes in direction-specific firing rates of the neurons. This evidence suggests the importance of estimating the directional plasticity of synaptic connection change. The IG method developed here has limitation of calculating the directional change of synaptic connections. The current studies on IG measures only showed the relationship between θ_{ij} and $J_{ij} + J_{ji}$. That is, θ_{ij} is incapable of calculating J_{ij} and J_{ji} individually. The IG measure was calculated by

the time bins with zero time delay. For instance, the IG measure in a two-neuron system is calculated by

$$\theta_{12}(t,0) = \log \frac{\langle S_1(t)S_2(t)\rangle(1 - \langle S_1(t)\rangle - \langle S_2(t)\rangle + \langle S_1(t)S_2(t)\rangle)}{(\langle S_1(t)\rangle - \langle S_1(t)S_2(t)\rangle)(\langle S_2(t)\rangle - \langle S_1(t)S_2(t)\rangle)} \tag{5.1}$$

A time-lagged IG measure can be defined by $\theta_{12}(t,\tau)$, τ represents the delayed time relative to *t*. Here $\theta_{12}(t,0)$ represents zero-legged IG measure. The state S_1 and S_2 for neuron 1 and 2 are calculated within the same time bin *t* with a zero delay time. To extend this method, the non-zero time lagged IG measure $\theta_{12}(t,\tau)$ ($\tau \neq 0$) could be one future research direction so that a directed connection can be estimated more directly. Tatsuno et al. (Tatsuno, 2004) has conducted a preliminary study on the time-delayed IG measure. They calculated $\theta_{12}(t,\tau)$ for the analysis in a two-neuron system. This study showed that the asymmetry of connection weights cannot be determined when using only the information at time lag zero, whereas this ill-posed nature can be reduced by taking into account a time-delayed IG measure $\theta_{12}(\tau)$ (Tatsuno, 2004). Therefore, we speculate that a future investigation and extension of the time-delayed IG could be the study of higher order IG $\theta_{ij}(t,\tau), \theta_{ijk}(t,\tau), \theta_{ijkl}(t,\tau)$, ... mathematically and numerically. Interestingly, the simulations of neural networks with time delay is a necessary step not only for verifying a theoretical calculation of time delayed IG, but also for uncovering more attractive properties related to IG measures. It is because a network with neuronal axonal time delay plays an important role for neuronal synchronization, brain rhythm generation, and pattern formation in the brain (Izhikevich, 2006) . We expect that these future

exciting computational modeling studies give insight into how IG measures can be applied in a dynamic neural network.

Another limitation of IG method is that it is applicable only for discrete signals (0 and 1 spike data). For example, in a 2-neuron system, IG methods only compute four different patterns $p_{11}, p_{10}, p_{01}, p_{00}$ for all-or-none (0 or 1) neuronal firing states. Therefore, it is an interesting theoretical change that how IG measures might be applied to provide measures for continuous patterns p_{xy} with continuous values x and y. Inspired by quantum field theory, we speculate that one possible way could be quantization of probability space. More specifically, one can expand the continuous pattern p_{xy} by basic patterns $p_{11}, p_{10}, p_{01}, p_{00}$ with multiple quantization factors. Since IG measures for discrete patterns are solved, one might be able to solve the issue under continuous patterns. Admittedly, the detailed theory needs to be intensively studied in the future theoretical research of IG measures.

We currently performed numerical simulation study for IG method using simplified neural network in which the synaptic dynamics is ignored. It has been shown that conductance-based neuronal receptors such as AMPA and NMDA play a key role in network properties. Therefore, from modeling point of view, it is necessary to investigate how IG measures are influenced by these biological parameters by simulating more complex networks. NEURON simulator would be a good candidate tool for this purpose (Lipa et al., 2006, 2007). Furthermore, we currently only consider a single layer neural network simulations. It is interesting to investigate IG method by the simulation of multi-layered feedforward and feedback networks.

Graphic models recently attract neuroscientists for neuronal modeling and data analysis. The graph, a mathematical representation of a set of variables with vertices and edges, play a key role in analysis of railroads, airlines, web, social networks, and neural networks. A combination of graphic theory and information-geometric measures was proposed to identify the intrinsic network structures (Atsushi, et al. 2013). Thus, one future advanced algorithm for neural data analysis might come from the combination of advanced machine learning techniques and IG methods.

As multivariate point processes, analysis methods for multiple spike trains is far from being well developed. Therefore, as the improvement of spike sorting algorithms, it is critical for neuroscientists to further develop novel methodologies for multiple spiking data analysis. Whatever the approach, the objective must be to design tractable methods for estimating high-dimensional neuronal interactions from their spike trains. Furthermore, due to the high nonstationality of neuronal dynamics, it is important to develop explicit adaptive algorithms for estimation of the neuronal activity through highly dynamic time-series processes.

In summary, the current work of IG method covers the study of the single-neuron, pair-wise, and higher-order interactions under network with stationary firing and oscillatory firing. The methodologies used here involve mathematical analysis, nonlinear analysis, statistical analysis and numerical estimations. We show that IG measures provide promising estimation for network structure from its multiple neuronal spike data. IG measures root deeply in the differential geometry and information theory, and can be calculated directly from the calculation of probability of spike events. The hierarchical property of IG measures separates the single-neuron firing, pair-wise firing, and other

higher-order interactions, providing an advanced data analysis methodology. Despite some limitations in current method, the IG method is one of the advanced statistical tools for multiple spike data analysis. Its direct relationship with the network parameters provides useful information for the estimation of structural changes. We expect that an advancement of novel analysis methods combining information geometry and other statistical methods will lead to a break-through finding in the future.

References

Abeles, M. (1982) Quantification, smoothing, and confidence limits for single-unit histograms, *J Neurosci. Methods*, **5**, 317-325.

Abeles, M. and Gerstein, G.L. (1988) Detecting spatiotemporal firing patterns among simultaneously recorded single neurons, *J Neurophysiol*, **60**, 909-924.

Abeles, M., Gerstein, G.L. (1988) Detecting spatiotemporal firing patterns among simultaneously recorded single neurons, *J Neurophysiol*, **60**, 16.

Adini, Y., Sagi, D. and Tsodyks, M. (1997) Excitatory-inhibitory network in the visual cortex: psychophysical evidence, *Proc Natl Acad Sci U S A*, **94**, 10426-10431.

Aertsen, A.M.*, et al.* (1989) Dynamics of neuronal firing correlation: modulation of "effective connectivity", *J Neurophysiol*, **61**, 900-917.

Aertsen, A.M., Gerstein, G.L., Habib,M.K., & Palm,G. (1989) Dynamics of neuronal firing correlation:modulation of "effective connectivity", *J Neurophysiol*, **61**, 18.

Amari, S. (2001) Information Geometry on Hierarchy of Probability Distributions, *IEEE Transactions on Information Theory*, **47**, 1701 - 1711.

Amari, S. (2001) Information Geometry on Hierarchy of Probability Distributions, *IEEE Transactions on Information Theory*, **47**, 12.

Amari, S. (2009) Measure of correlation orthogonal to change in firing rate, *Neural Comput*, **21**, 960-972.

Amari, S., & Nagaoka,H. (2000) *Methods of information geometry*. Oxford University Press, New York.

Amari, S., Kawanabe, M. (1997) Information geometry of estimating functions in semi parametric statistical models, *Bernoulli*, **3**, 29-54.

Amari, S., Kurata, Nagaoka, H. (1992) Information geometry of Boltzman machines, *IEEE Trans. Neural Networks*, **3**.

Amari, S. and Nagaoka, H. (2000) *Methods of information geometry*. Oxford University Press, New York.

Amari, S.*, et al.* (2003) Synchronous firing and higher-order interactions in neuron pool, *Neural Comput*, **15**, 127-142.

Amari, S.I., S, Shimokawa,H. (2000) Information geometry of alpha-projection in mean-field approximation, *Recent Development of Mean Field Approximation*.

Baker, S.N., Olivier, E. and Lemon, R.N. (1997) Coherent oscillations in monkey motor cortex and hand muscle EMG show task-dependent modulation, *The Journal of physiology*, **501 (Pt 1)**, 225-241.

Bar-Gad, I., et al. (2001) Failure in identification of overlapping spikes from multiple neuron activity causes artificial correlations, *J. Neurosci. Methods*, **107**, 1-13.

Bhattacharyya, C., Keerthi, S.S. (2001) Mean-Field methods for stochastic connnections networks, *Physical Review A*.

Bland, B.H. (1986) The physiology and pharmacology of hippocampal formation theta rhythms, *Prog Neurobiol*, **26**, 1-54.

Braitenberg, V. and Schuz, A. (1999) *Cortex: Statistics and Geometry of Neuronal Connectivity*. Springer, Berlin.

Brillinger, D.R. (1978) Comparative aspects of the study of ordinary time series and of point processes, *in Developments in Statistics*, **1**, 33-129.

Brillinger, D.R. (1981) Time Series.

Brillinger, D.R. (1992) Nerve cell spike train data analysis: a progression of techniques, *J.Amer.Stat.Assoc.*, **87**, 260-271.

Brody, C.D. (1999) Correlations without synchrony, *Neural Comput*, **11**, 153-1551.

Brown, A.R*., et al.* (2011) High frequency stimulation of the subthalamic nucleus acutely rescues motor deficits and neocortical movement representations following 6-hydroxydopamine administration in rats, *Exp Neurol*, **231**, 82-90.

Brown, E.N., Kass, R.E. and Mitra, P.P. (2004) Multiple neural spike train data analysis: state-of-the-art and future challenges, *Nat Neurosci*, **7**, 456-461.

Brown, E.N., Kass, R.E., &Mitra, P.P. (2004) Multiple neural spike train data analysis: state-of-the-art and future challenges, *Nat Neurosci*, **7**, 6.

Buzsaki, G. (2002) Theta oscillations in the hippocampus, *Neuron*, **33**, 325-340.

Buzsaki, G. (2004) Large-scale recording of neuronal ensembles, *Nat Neurosci*, **7**, 446-451.

Buzsaki, G*., et al.* (1992) High-frequency network oscillation in the hippocampus, *Science*, **256**, 1025-1027.

Buzsaki, G. and Wang, X.J. (2012) Mechanisms of gamma oscillations, *Annual review of neuroscience*, **35**, 203-225.

Campbell, L.L. (1985) The relation between information theory and the differential geometric approach to statistics, *Inform.Sci.*, **35**, 199-210.

Chapin, J.K.*, et al.* (1999) Real-time control of a robot arm using simultaneously recorded neurons in the motor cortex, *Nat Neurosci*, **2**, 664-670.

Chentsnov, N.N. (1982) Statistical Decision Rules and Optimal Inference (in Russian), *Moscow, U.S.S.R.: Nauka*.

Courchesne, E. (1975) Stimulus novelty,task relevance and the visual evoked potential in man, *Electroencephalogr Clin Neurophysiol*, **39**, 131-143.

Crunelli, V. and Hughes, S.W. (2010) The slow (<1 Hz) rhythm of non-REM sleep: a dialogue between three cardinal oscillators, *Nature Neuroscience*, **13**, 9-17.

Czanner, G., Grun, S. and Iyengar, S. (2005) Theory of the snowflake plot and its relations to higher-order analysis methods, *Neural Comput*, **17**, 1456-1479.

Davidson, T.J., Kloosterman, F. and Wilson, M.A. (2009) Hippocampal replay of extended experience, *Neuron*, **63**, 497-507.

Daw, N.D.e.a. (2005) Uncertainty-based competition between prefrontal and dorsallateral striatal systems for behavioral control, *Nat Neurosci*, **8**, 1704-1711.

Daw, N.D.e.a. (2011) Model-Based Influences on Human's Choices and Striatal Prediction Errors, *Neuron*, **69**, 1204-1215.

Denk, W., Strickler, J., Webb,. W. (1990) Two-photon laser scanning fluorescence microscopy, *Science*, **248**, 73-76.

Diekelmann, S. and Born, J. (2010) The memory function of sleep, *Nat Rev Neurosci*, **11**, 114-126.

Dombeck, D.A.*, et al.* (2010) Functional imaging of hippocampal place cells at cellular resolution during virtual navigation, *Nature Neuroscience*, **13**, 1433-1440.

Dragoi, G.*, et al.* (1999) Interactions between hippocampus and medial septum during sharp waves and theta oscillation in the behaving rat, *The Journal of neuroscience : the official journal of the Society for Neuroscience*, **19**, 6191-6199.

Dragoi, G. and Tonegawa, S. (2011) Preplay of future place cell sequences by hippocampal cellular assemblies, *Nature*, **469**, 397-401.

Dragoi, G. and Tonegawa, S. (2013) Distinct preplay of multiple novel spatial experiences in the rat, *Proc Natl Acad Sci U S A*, **110**, 9100-9105.

Eleuteri, A., Tagliaferri, R. and Milano, L. (2005) A novel information geometric approach to variable selection in MLP networks, *Neural Netw*, **18**, 1309-1318.

Euston, D.R., Tatsuno, M. and McNaughton, B.L. (2007) Fast-forward playback of recent memory sequences in prefrontal cortex during sleep, *Science*, **318**, 1147-1150.

Fellous, J.M.*, et al.* (2004) Discovering spike patterns in neuronal responses, *J Neurosci*, **24**, 2989-3001.

Ganmor, E., Segev, R. and Schneidman, E. (2011) Sparse low-order interaction network underlies a highly correlated and learnable neural population code, *Proc Natl Acad Sci U S A*, **108**, 9679-9684.

Gerstein, G.L., & Perkel, D.H. (1969) Simultaneously recorded trains of action potentials: analysis and functional interpretation, *Science*, **164**, 3.

Gerstein, G.L. and Perkel, D.H. (1969) Simultaneously recorded trains of action potentials: analysis and functional interpretation, *Science*, **164**, 828-830.

Ginzburg, I.I. and Sompolinsky, H. (1994) Theory of correlations in stochastic neural networks, *Physical Review. E. Statistical Physics, Plasmas, Fluids, and Related Interdisciplinary Topics*, **50**, 3171-3191.

Girardeau, G.*, et al.* (2009) Selective suppression of hippocampal ripples impairs spatial memory, *Nat Neurosci*, **12**, 1222-1223.

Gray, C.M.*, et al.* (1989) Oscillatory responses in cat visual cortex exhibit inter-columnar synchronization which reflects global stimulus properties, *Nature*, **338**, 334-337.

Grun, S. (2010) *Analysis of parallel spike trains*. Springer.

Grun, S., Diesmann, M. and Aertsen, A. (2002) Unitary events in multiple single-neuron spiking activity: I. Detection and significance, *Neural Comput*, **14**, 43-80.

Grun, S., Diesmann, M. and Aertsen, A. (2002) Unitary events in multiple single-neuron spiking activity: II. Nonstationary data, *Neural Comput*, **14**, 81-119.

Hampson, R.E., Simeral, J.D. and Deadwyler, S.A. (1999) Distribution of spatial and nonspatial information in dorsal hippocampus, *Nature*, **402**, 610-614.

Han, F., Caporale, N. and Dan, Y. (2008) Reverberation of recent visual experience in spontaneous cortical waves, *Neuron*, **60**, 321-327.

Han, T.S., Amari, S. (1998) Statistical inference under multiterminal data compression, *IEEE Transactions on Information Theory*, **44**, 2300-2324.

Harris, K.D., Henze, D.A.,Hirase, H., Buzsaki,G. (2000) Accuracy of tetrode spike separation as determined by simultaneous intracellular and extracellular measurements, *J.Neurophysiology*, 401-414.

Hines, M.L. and Carnevale, N.T. (1997) The NEURON simulation environment, *Neural Comput*, **9**, 1179-1209.

Hodgkin, A.L. and Huxley, A.F. (1952) A quantitative description of membrane current and its application to conduction and excitation in nerve, *J Physiol*, **117**, 500-544.

Hoffman, K.L. and McNaughton, B.L. (2002) Coordinated reactivation of distributed memory traces in primate neocortex, *Science*, **297**, 2070-2073.

Huber, R.*, et al.* (2004) Local sleep and learning, *Nature*, **430**, 78-81.

Ikeda, K. (2005) Information geometry of interspike intervals in spiking neurons, *Neural Comput*, **17**, 2719-2735.

Ince, R.A.*, et al.* (2010) Information-theoretic methods for studying population codes, *Neural Netw*, **23**, 713-727.

Izhikevich, E.M. (2003) Simple model of spiking neurons, *IEEE Trans Neural Netw*, **14**, 1569-1572.

Izhikevich, E.M. (2006) Polychronization: Computation with spikes, *Neural Comput*, **18**, 245-282.

Kass, R.E., Ventura, V., Cai C. (2003) Statistical smoothing of neuronal data, *Network: Computation in Neural Systems*, **14**, 5-15.

Kass, R.E., Vos, P.W. (1997) *Geometrical Foundations of Asymptotic Inference*. New York:Wiley.

Knutson, B.e.a. (2005) Distributed neural representation of expected value, *J Neurosci*, **25**, 4806-4812.

Kudrimoti, H.S., Barnes, C.A. and McNaughton, B.L. (1999) Reactivation of hippocampal cell assemblies: effects of behavioral state, experience, and EEG dynamics, *J Neurosci*, **19**, 4090-4101.

Laubach, M., Wessberg, J. and Nicolelis, M.A. (2000) Cortical ensemble activity increasingly predicts behaviour outcomes during learning of a motor task, *Nature*, **405**, 567-571.

Lee, A.K. and Wilson, M.A. (2002) Memory of sequential experience in the hippocampus during slow wave sleep, *Neuron*, **36**, 1183-1194.

Lipa, P.*, et al.* (2006) A novel analysis framework for characterizing ensemble spike patterns using spike train clustering and information geometry, *Soc Neurosci Abstr*, **36:371**, 6.

Lipa, P.*, et al.* (2007) Dynamics of neural assemblies involved in memory-trace replay, *Soc Neurosci Abstr*, **37.308**, 13.

Lopes-dos-Santos, V.*, et al.* (2011) Neuronal assembly detection and cell membership specification by principal component analysis, *PLoS One*, **6**, e20996.

Luczak, A.*, et al.* (2007) Sequential structure of neocortical spontaneous activity in vivo, *Proc Natl Acad Sci U S A*, **104**, 347-352.

Meltzer J, Z.H., Goncharoval I, Distasio M. (2008) Effects of working memory load on oscillatory power in human intracranial EEG, *Cereb Cortex*, **18**, 1843-1855.

Meltzer, J.A.*, et al.* (2008) Effects of working memory load on oscillatory power in human intracranial EEG, *Cerebral cortex*, **18**, 1843-1855.

Miri, A.*, et al.* (2011) Regression-based identification of behavior-encoding neurons during large-scale optical imaging of neural activity at cellular resolution, *J Neurophysiol*, **105**, 964-980.

Miura, K., Okada, M. and Amari, S. (2006) Estimating spiking irregularities under changing environments, *Neural Comput*, **18**, 2359-2386.

Nakahara, H., & Amari,S. (2002) Information-geometric measure for neural spikes, *Neural Comput*, **14**, 48.

Nakahara, H. and Amari, S. (2002) Information-geometric measure for neural spikes, *Neural Comput*, **14**, 2269-2316.

Nakahara, H., Amari, S. and Richmond, B.J. (2006) A comparison of descriptive models of a single spike train by information-geometric measure, *Neural Comput*, **18**, 545-568.

Nguyen, D.F., L.M., Brown,E.N. (2003) An application of reversible-jump MCMC to spike classification of multiunit extracellular recordings, *Network Comput. Neural Syst*, **14**, 61-82.

Nie, Y. and Tatsuno, M. (2012) Information-Geometric Measures for Estimation of Connection Weight Under Correlated Inputs, *Neural Comput*.

Ohara, A., Suda, N., Amari, S. (1996) Dualistic differential geometry of positive definite matrices and its applications to related problems, *Linear Alg. its Applic.*, **247**, 31-53.

Ohiorhenuan, I.E.*, et al.* (2010) Sparse coding and high-order correlations in fine-scale cortical networks, *Nature*, **466**, 617-621.

Ohiorhenuan, I.E. and Victor, J.D. (2011) Information-geometric measure of 3-neuron firing patterns characterizes scale-dependence in cortical networks, *J Comput Neurosci*, **30**, 125-141.

Panzeri, S. and Schultz, S.R. (2001) A unified approach to the study of temporal, correlational, and rate coding, *Neural Comput*, **13**, 1311-1349.

Pavlides, C. and Winson, J. (1989) Influences of hippocampal place cell firing in the awake state on the activity of these cells during subsequent sleep episodes, *J Neurosci*, **9**, 2907-2918.

Percival, D.B., Walden, A. T. (2002) Spectral Analysis for Physical Applications:Multitaper and Conventional Univariate Techniques, *Cambridge Univ. Press*.

Pesaran, B., Pezaris, J.S., Sahani,M., Mitra,P.P.,Anderson,R.A. (2002) Temporal structure in neural activity during working memory in macaque parietal cortex, *Nat Neurosci*, **5**, 805-811.

Peyrache, A.*, et al.* (2009) Principal component analysis of ensemble recordings reveals cell assemblies at high temporal resolution, *J Comput Neurosci*.

Peyrache, A.*, et al.* (2009) Replay of rule-learning related neural patterns in the prefrontal cortex during sleep, *Nat Neurosci*, **12**, 919-926.

Pola. G., T.A., Hoffmann,K.P., Panzeri, S. (2003) An extract method to quantify the information transimission by different mechanisms of correlation coding, *Network: Computation in Neural Systems*, **14**, 35-60.

Ponticorvo, M. and Miglino, O. Encoding geometric and non-geometric information: a study with evolved agents, *Anim Cogn*, **13**, 157-174.

Raghavachari, S.*, et al.* (2001) Gating of human theta oscillations by a working memory task, *The Journal of neuroscience : the official journal of the Society for Neuroscience*, **21**, 3175-3183.

Rao., C.R. (1945) Information and accuracy attainable in the estimation of statistical parameters, *Bull. Calcutta.Math.Soc.*, **37**, 81-91.

Riehle, A.*, et al.* (1997) Spike synchronization and rate modulation differentially involved in motor cortical function, *Science*, **278**, 1950-1953.

Schneidman, E.*, et al.* (2006) Weak pairwise correlations imply strongly correlated network states in a neural population, *Nature*, **440**, 1007-1012.

Shimazaki, H., & Shinomoto, S. (2007) A method for selecting the bin size of a time histogram, *Neural Comput*, **19**, 25.

Shimazaki, H.*, et al.* (2012) State-space analysis of time-varying higher-order spike correlation for multiple neural spike train data, *PLoS computational biology*, **8**, e1002385.

Shimazaki, H., Amari, S. I., Brown, E. N. & Grun, S (2009) Detection of non-stationary higher-order spike correlation. *COSYNE*. Salt Lake CIty.

Shimazaki, H. and Shinomoto, S. (2007) A method for selecting the bin size of a time histogram, *Neural Comput*, **19**, 1503-1527.

Shimokawa, T., & Shinomoto, S. (2009) Estimating instantaneous irregularity of neuronal firing, *Neural Comput*, **21**, 21.

Shimokawa, T. and Shinomoto, S. (2009) Estimating instantaneous irregularity of neuronal firing, *Neural Comput*, **21**, 1931-1951.

Singer, W. and Gray, C.M. (1995) Visual feature integration and the temporal correlation hypothesis, *Annual review of neuroscience*, **18**, 555-586.

Steriade, M., Nunez, A. and Amzica, F. (1993) A novel slow (< 1 Hz) oscillation of neocortical neurons in vivo: depolarizing and hyperpolarizing components, *The Journal of neuroscience : the official journal of the Society for Neuroscience*, **13**, 3252-3265.

Stickgold, R. (2005) Sleep-dependent memory consolidation, *Nature*, **437**, 1272-1278.

Strobel, A. (2008) Novelty and target processing during an auditory novelty oddball: a simulaneous event-related potential and functional magnetic resonance imaging study, *Neuroimage*, **40**, 869-883.

Szuts, T.A*., et al.* (2011) A wireless multi-channel neural amplifier for freely moving animals, *Nature Neuroscience*, **14**, 263-269.

Tanaka.T. (2000) Information geometry of mean field approximation, *Neural Comput*, **12**, 1951-1968.

Tang, A*., et al.* (2008) A maximum entropy model applied to spatial and temporal correlations from cortical networks in vitro, *J Neurosci*, **28**, 505-518.

Tatsuno, M., Fellous, J.M. and Amari, S.I. (2009) Information-Geometric Measures as Robust Estimators of Connection Strengths and External Inputs, *Neural Comput*, **21**, 2309-2335.

Tatsuno, M., Fellous, J. M., & Amari, S. I. (2009) Information-Geometric Measures as Robust Estimators of Connection Strengths and External Inputs, *Neural Comput*, **21**, 2309-2335.

Tatsuno, M., Lipa, P. and McNaughton, B.L. (2006) Methodological considerations on the use of template matching to study long-lasting memory trace replay, *J Neurosci*, **26**, 10727-10742.

Tatsuno, M. and Okada, M. (2004) Investigation of possible neural architectures underlying information-geometric measures, *Neural Comput*, **16**, 737-765.

Tatsuno, M., Okada, M. (2004) Investigation of possible neural architectures underlying information-geometric measures, *Neural Comput*, **16**, 29.

Thomson, D.J., Chave,A.D., (1991) Jackknifed error estimates for spectra, coherences, and transfer functions., *in Advances in Spectrum Analysis and Array Processing*, 58-113.

Tyler, A.L*., et al.* (2012) Functional network changes in hippocampal CA1 after status epilepticus predict spatial memory deficits in rats, *The Journal of neuroscience : the official journal of the Society for Neuroscience*, **32**, 11365-11376.

Urban, N.N., Henze, D.A. and Barrionuevo, G. (2001) Revisiting the role of the hippocampal mossy fiber synapse, *Hippocampus*, **11**, 408-417.

Vanderwolf, C.H. (1969) Hippocampal electrical activity and voluntary movement in the rat, *Electroencephalogr Clin Neurophysiol*, **26**, 407-418.

Wang, X.-J. (2008) Decision making in recurrent neuronal circuits *Neuron*, **60**, 215-234.

Wilson, M.A. and McNaughton, B.L. (1993) Dynamics of the hippocampal ensemble code for space, *Science*, **261**, 1055-1058.

Wilson, M.A. and McNaughton, B.L. (1994) Reactivation of hippocampal ensemble memories during sleep, *Science*, **265**, 676-679.

Zenata, N.e.a. (2012) Experience-dependent firing rate remapping generates directional selectivity in hippocampal place cells, *Front.Neural.Circuits*.

Zhang, K.*, et al.* (1998) Interpreting neuronal population activity by reconstruction: unified framework with application to hippocampal place cells, *J Neurophysiol*, **79**, 1017-1044.